AFRRI REPORTS

First Quarter
1991

Defense Nuclear Agency
Armed Forces Radiobiology Research Institute
Bethesda, Maryland 20889-5145

REPORT DOCUMENTATION PAGE

Form Approved
OMB No. 0704-0188

1. AGENCY USE ONLY *(Leave blank)*	2. REPORT DATE	3. REPORT TYPE AND DATES COVERED
	1991 April	Reprints/Technical

4. TITLE AND SUBTITLE

AFRRI Reports, Jan-Mar 1991

5. FUNDING NUMBERS

NWED QAXM

6. AUTHOR(S)

7. PERFORMING ORGANIZATION NAME(S) AND ADDRESS(ES)

Armed Forces Radiobiology Research Institute
Bethesda, MD 20889-5145

8. PERFORMING ORGANIZATION REPORT NUMBER

SR91-1 - SR91-21

9. SPONSORING/MONITORING AGENCY NAME(S) AND ADDRESS(ES)

Defense Nuclear Agency
Washington, DC 20305

10. SPONSORING/MONITORING AGENCY REPORT NUMBER

11. SUPPLEMENTARY NOTES

12a. DISTRIBUTION/AVAILABILITY STATEMENT

Approved for public release; distribution unlimited.

12b. DISTRIBUTION CODE

13. ABSTRACT *(Maximum 200 words)*

This volume contains AFRRI Scientific Reports SR91-1 through SR91-21 for Jan-Mar 1991.

14. SUBJECT TERMS

15. NUMBER OF PAGES
139

16. PRICE CODE

17. SECURITY CLASSIFICATION OF REPORT	18. SECURITY CLASSIFICATION OF THIS PAGE	19. SECURITY CLASSIFICATION OF ABSTRACT	20. LIMITATION OF ABSTRACT
UNCLASSIFIED	UNCLASSIFIED	UNCLASSIFIED	same as report

CLASSIFIED BY:

DECLASSIFY ON:

CONTENTS

SR91-15: Maier, D. M., Landauer, M. R., Davis, H. D., and Walden, T. L. Effect of electron radiation on aggressive behavior, activity, and hemopoiesis in mice.

SR91-16: McCarthy, K. F., and Hale, M. L. Further enrichment and analysis of rat CFU-s.

SR91-17: McClain, D. E., Trypus, C. A., and May, L. Effect of γ radiation on membrane fluidity of MOLT-4 nuclei.

SR91-18: McKinney, L. C., and Gallin, E. K. Effect of adherence, cell morphology, and lipopolysaccharide on potassium conductance and passive membrane properties of murine macrophage J774.1 cells.

SR91-19: Murphy, P. M., Gallin, E. K., Tiffany, H. L., and Malech, H. L. The formyl peptide chemoattractant receptor is encoded by a 2 kilobase messenger RNA. Expression in *Xenopus* oocytes.

SR91-20: Pellmar, T. C., Neel, K. L., and Lee, K. H. Free radicals mediate peroxidative damage in guinea pig hippocampus *in vitro*.

SR91-21: Schwartz, G. N., Patchen, M. L., Neta, R., and MacVittie, T. J. Radioprotection of mice with interleukin-1: relationship to the number of erythroid and granulocyte-macrophage colony-forming cells.

RADIATION RESEARCH 122, 215–217 (1990)

SHORT COMMUNICATION

Quinolone Therapy of *Klebsiella pneumoniae* Sepsis following Irradiation: Comparison of Pefloxacin, Ciprofloxacin, and Ofloxacin

ITZHAK BROOK,[1] THOMAS B. ELLIOTT, AND G. DAVID LEDNEY

Wound Infection Management Program, Experimental Hematology Department, Armed Forces Radiobiology Research Institute, Bethesda, Maryland 20814-5145

BROOK, I., ELLIOTT, T. B., AND LEDNEY, G. D. Quinolone Therapy of *Klebsiella pneumoniae* Sepsis following Irradiation: Comparison of Pefloxacin, Ciprofloxacin, and Ofloxacin. *Radiat. Res.* 122, 215–217 (1990).

Exposure to whole-body irradiation is associated with fatal gram-negative sepsis. The effect of oral therapy with three quinolones, pefloxacin, ciprofloxacin, and ofloxacin, for orally acquired *Klebsiella pneumoniae* infection was tested in B6D2F1 mice exposed to 8.0 Gy whole-body irradiation from bilaterally positioned ^{60}Co sources. A dose of 10^8 organisms was given orally 2 days after irradiation, and therapy was started 1 day later. Quinolones reduced colonization of the ileum with *K. pneumoniae:* 16 of 28 (57%) untreated mice harbored the organisms, compared to only 12 of 90 (13%) mice treated with quinolones ($P < 0.005$). *K. pneumoniae* was isolated from the livers of 6 of 28 untreated mice, compared to only 1 of 90 treated mice ($P < 0.001$). Only 5 of 20 (25%) untreated mice survived for at least 30 days compared with 17 of 20 (85%) mice treated with ofloxacin, 15 of 20 (75%) mice treated with pefloxacin, and 14 of 20 (70%) treated with ciprofloxacin ($P < 0.05$). These data illustrate the efficacy of quinolones for oral therapy of orally acquired *K. pneumoniae* infection in irradiated hosts.

INTRODUCTION

Ionizing radiation reduces the host's defenses to infection (*1*) and enhances its susceptibility to systemic infection due to endogenous and exogenous organisms (*2, 3*). *Klebsiella pneumoniae* is one of the most frequent causes of gram-negative bacteremia (*4, 5*) and is especially prevalent in immunocompromised patients (*6*).

Therapy for severe systemic infection due to gram-negative bacteria generally involves the use of aminoglycosides in combination with β-lactam antibiotics (*7*). However, several recently developed quinolone compounds have exhibited high *in vitro* bactericidal activity against most gram-negative bacteria, including *K. pneumoniae* (*8*).

In this study, we evaluated the efficacy of oral therapy with several quinolones in a model of experimental septicemia due to orally ingested *K. pneumoniae* in irradiated mice.

MATERIALS AND METHODS

Animals

Female B6D2F1 mice approximately 10 weeks of age were obtained from Jackson Laboratories (Bar Harbor, ME). All animals were kept in quarantine for about 2 weeks before being transferred to a room with a 12-h light–dark cycle. Representative samples were examined to ensure the absence of specific bacteria and common murine diseases. Animals were maintained at an AAALAC accredited facility in microisolator cages on hardwood chip bedding and provided commercial rodent chow and acidified water (pH 2.2) that was changed to tap water 48 h before irradiation. All experimental procedures were done in compliance with National Institute of Health and Armed Forces Radiobiology Research Institute (AFRRI) guidelines regarding animal use and care.

Cobalt-60 Irradiation

Mice were placed in Plexiglas restrainers and exposed to 8.0 Gy whole-body irradiation at 0.4 Gy/min from bilaterally positioned ^{60}Co sources. Dose determinations were made using a 50-ml AFRRI-designed tissue-equivalent ionization chamber calibrated against a National Institute of Standards and Technology ionization chamber. The dose within the exposure field varied by 3%, as determined by thermal luminescence dosimetry conducted within tissue-equivalent mouse phantoms.

Bacteria

The strain used in this study was a clinical isolate of *K. pneumoniae* with a capsule type 5 (AFRRI No. 7). We have used this strain in previous animal studies (*9*). The organisms were harvested in the logarithmic phase of growth in brain heart infusion (BBL) media. A concentration of 10^9 organisms per 1 ml saline was prepared, and a volume of 0.1 ml was fed to each animal by gavage using a blunt syringe. This number of organisms was used since ingestion of lower number of bacteria did not produce a high mortality rate in the animals.

Antimicrobials

Pefloxacin (Rhone-Poulenc-Sante, Anthony Cedex, France), ciprofloxacin (Miles Inc., West Haven, CT), and ofloxacin (Ortho Pharmaceutical Corp., Raritan, NJ) were obtained from their manufacturers. Standard powder formulations with known potencies were used for *in vitro* and *in vivo* studies. Pefloxacin and ciprofloxacin (25 mg/kg) were administered

[1] To whom reprint requests should be addressed.

0033-7587/90 $3.00

every 12 h in 0.1 ml of water by gavage. In the case of ofloxacin 40 mg/kg was given once every day.

Antimicrobial Serum Concentration

Serum concentrations of the antimicrobials were measured in six mice 1 and 11½ h after oral administration of pefloxacin and ciprofloxacin and 1 and 23½ h after oral administration of ofloxacin on the fifth day of therapy. *Bacillus subtilis* ATCC 6633 was used as a test organism, and Mueller-Hinton agar (pH 7.4) was used as a test agar.

In Vitro Susceptibility

Minimal inhibitory concentrations and minimal bactericidal concentrations were determined in Mueller-Hinton broth that was inoculated with an inoculum of 1.5×10^5 organisms per milliliter from an overnight culture. The values for minimal inhibitory concentration/minimal bactericidal concentration for *K. pneumoniae* used in this study were as follows: pefloxacin, 0.06/0.06 μg/ml; ciprofloxacin, 0.03/0.03 μg/ml; and ofloxacin, 0.06/0.12 μg/ml.

Microbial Methods

Animals challenged with bacteria were observed for mortality and signs of disease for 30 days. Five animals were selected at random for each group on Days 4, 6, 8, 10, and 12 following irradiation. Cultures were also obtained from another group of mice whenever the animals showed signs of serious illness and were moribund. Animals were killed by cervical dislocation. Specimens of livers were processed for microbial cultures. No other organs were processed and no blood samples were obtained, since previous studies showed that liver cultures correlated best with the presence of sepsis (*3*). The livers were removed aseptically and homogenized immediately. The ileum was opened, and ileal content samples were obtained using a swab. The liver and stool specimens were swabbed onto blood and MacConkey agars, and the organisms were identified using conventional methods (*10*).

Experimental Design

Forty-eight hours following irradiation, each mouse was fed 10^8 organisms. This time of feeding was chosen after preliminary data indicated that the animals became susceptible to *K. pneumoniae* sepsis when they were fed gram-negative bacteria 48 h after irradiation (Brook, Elliott, Ledney, unpublished data). The increased susceptibility to sepsis as a result of oral feeding 48 h after irradiation with gram-negative bacteria is similar to what we observed with *Pseudomonas aeruginosa* (*11*). Antimicrobial therapy was initiated 24 h later and was administered for 7 days. A total of 240 mice were included in each of the experiments, and each experiment was done three times. However, since the microbiological and mortality data were consistent, only the data from one experiment are reported. Each experiment was composed of the three antibiotic therapy groups and the untreated control group. Each therapy or control group consisted of 60 mice: 20 were observed for mortality, 30 were used for cultures of liver on the designated days, and 10 were used for cultures of livers of morbid animals.

Statistical Methods

Statistical analyses were done using the Cox-Mantel Test (*12*).

RESULTS

Mortality

Mortality in the groups that received each of the quinolones was significantly less ($P < 0.05$) than that of the untreated mice, but the groups were not different from each other (Fig. 1). Only 25% of the untreated mice survived, compared with 85% of those treated with ofloxacin, 75% of those treated with pefloxacin, and 70% of those treated with ciprofloxacin.

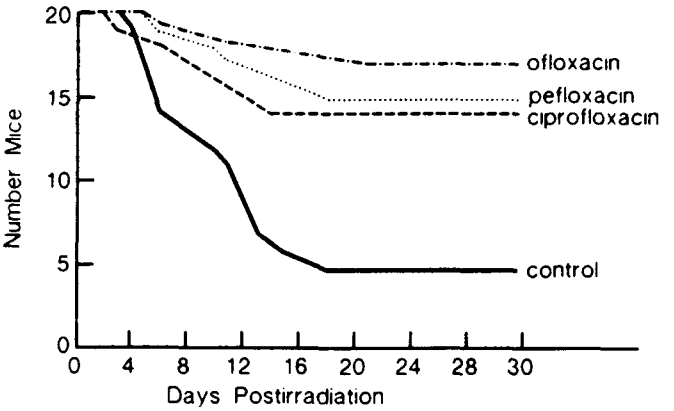

FIG. 1. Survival of γ-irradiated mice B6D2F1 (8.0 Gy) fed 10^8 *K. pneumoniae* and treated orally with three quinolones. The data shown are from one experiment. Two repeated experiments yielded similar results.

Isolation of Organisms in Liver

Klebsiella pneumoniae was isolated in 6 of the 28 (21%) randomly selected untreated animals. There was no correlation between the time following irradiation and the isolation of *K. pneumoniae*. *Klebsiella pneumoniae* was recovered in only 1 of 30 (3%) animals treated with pefloxacin and in none of those treated with ciprofloxacin or ofloxacin ($P < 0.05$). However, *K. pneumoniae* was recovered from 95% of moribund animals of all therapy or control groups.

Isolation of Organisms in Ileal Contents

Klebsiella pneumoniae was isolated in ileal content specimens of 16 of 28 (57%) untreated mice, compared to only 12 of 90 (13%) treated with quinolones ($P < 0.005$). The rate of isolation of *K. pneumoniae* in quinolone-treated mice was 4 of 30 (13%) mice treated with pefloxacin, 5 of 30 (17%) mice treated with ciprofloxacin, and 3 of 30 (10%) mice treated with ofloxacin ($P < 0.005$).

Antibiotic Serum Concentration

Mean serum concentrations of pefloxacin were as follows: 2.4 (±0.3 μg/ml) at 1 h and 0.2 (±0.1 μg/ml) at 11½ h after administration of the antimicrobial. Mean concentrations of ciprofloxacin were 2.8 (±0.5 μg/ml) at 1 h and 0.2 (±0.1 μg/ml) at 11½ h. Mean concentrations of ofloxacin were 2.6 (±0.4 μg/ml) at 1 h and 0.4 (±0.2 μg/ml) at 23½ h.

DISCUSSION

This study demonstrates that the three quinolones, pefloxacin, ciprofloxacin, and ofloxacin, can reduce the col-

onization of the ileum and the development of subsequent septicemia with *K. pneumoniae* in irradiated mice. It supports the findings of Trautmann *et al.* (*13*), who observed the efficacy of ciprofloxacin in the management of systemic *K. pneumoniae* infection in neutropenic mice.

We have developed a model of acquired *K. pneumoniae* infection in irradiated mice that may represent the mode of acquisition of external pathogens into an irradiated host. We have previously shown that irradiated animals develop fatal septicemia due to orally administered *P. aeruginosa* (*11*). We have also observed that the number of the endogenous aerobic and anerobic bacteria in the gastrointestinal tract declined 24 h following irradiation and the decline was maximal at 7 days (*14*). The decrease in the number of that endogenous bacterial flora may make the host more susceptible to the acquisition of external pathogens such as *K. pneumoniae*.

The ability of *K. pneumoniae* to cause systemic infection in irradiated mice may be due to the following factors: the bacterial void created in the gut following the decline in the number of other organisms, the increased permeability of the mucosal cells damaged by irradiation, and the decrease in the local and systemic immune defenses.

The effectiveness of quinolones in the therapy of *K. pneumoniae* infection may be attributed to their local inhibition of the organism's growth within the gut lumen, while preserving the anaerobic gut flora (*15*), and to their systemic antibacterial activity against the organisms that spread to other body sites. The duration of quinolone therapy is yet to be determined. Although minimal mortality occurred following termination of therapy at Day 11, longer therapy might have prevented the mortality noticed after that day. Further studies are underway to determine the optimal duration of therapy.

Selective decontamination of the gut with orally administered quinolones is used to prevent sepsis in immunocompromised hosts (*15, 16*). These agents were also found to be effective in the management of septic episodes in neutropenic patients.[2] The availability of an oral route of administration, the advantage of achieving selective inhibition of potential pathogens in the gut, and the ability to treat systemic infection make the quinolones promising agents for the therapy of irradiated hosts.

ACKNOWLEDGMENTS

The authors acknowledge the secretarial assistance of Mrs. Gloria Contreras. This research was supported by the Armed Forces Radiobiology Research Institute, Defense Nuclear Agency, under work unit 4440-00129. Views presented in this paper are those of the authors; no endorsement by the Defense Nuclear Agency has been given or should be inferred. Research was conducted according to the principles enunciated in the "Guide of the Care and Use of Laboratory Animals" prepared by the Institute of Animal Resources, National Research Council.

RECEIVED: June 2, 1989; ACCEPTED: November 28, 1989

[2] S. Segeve, S. D. Pitlick, and E. Reubenstein. Pefloxacin for gram negative infections in compromised patients. Abstract, 15th International Congress of Chemotherapy, Istanbul, Turkey, 1987.

REFERENCES

1. G. MATHE, Total body irradiation injury: A review of the disorders of the blood and hematopoietic tissues and their therapy. In *Nuclear Hematology* (E. Eszirami, Ed.), pp. 275–338. Academic Press, New York, 1965.
2. H. W. KAPLAN, R. S. SPECK, and F. JAWETZ, Impairment of antimicrobial defenses following total body irradiation of mice. *J. Lab. Clin. Med.* **40**, 682–691 (1985).
3. I. BROOK, T. J. MACVITTIE, and R. I. WALKER, Recovery of aerobic and anaerobic bacteria from irradiated mice. *Infect. Immun.* **46**, 270–271 (1984).
4. D. G. MAKI, Nosocomial bacteremia. An epidemiologic overview. *Am. J. Med.* **70**, 719–732 (1981).
5. M. P. WEINSTEIN, L. B. RELLER, J. R. MURPHY, and K. A. LICHTENSTEIN, The significance of positive blood cultures: A comprehensive analysis of 500 episodes of bacteremia and fungemia in adults. I. Laboratory and epidemiologic observations. *Rev. Infect. Dis.* **5**, 35–53 (1983).
6. T. UMSAWASDI, E. A. MIDDLEMAN, M. LUNA, and G. P. BODEY, Klebsiella bacteremia in cancer patients. *Am. J. Med. Sci.* **165**, 473–482 (1973).
7. J. W. HATHORN, M. RUBIN, and P. A. PIZZO, Empiric antibiotic therapy in the febrile neutropenic cancer patient: Clinical efficacy and impact of monotherapy. *Antimicrob. Agents Chemother.* **31**, 971–977 (1987).
8. M. P. WESTLAND and J. B. CORNETT, Quinolone antibacterial agents. *Annu. Rep. Med. Chem.* **20**, 145–154 (1985).
9. G. S. MADONNA, G. D. LEDNEY, T. B. ELLIOTT, I. BROOK, J. T. ULRICH, K. P. MYERS, M. L. PATCHEN, and R. I. WALKER, Trehalose dimycolate enhances resistance to infection in neutropenic animals. *Infect. Immun.* **57**, 2495–2501 (1989).
10. E. H. LENNETTE, A. BALOWS, W. HAUSLER, and J. H. SHADOMY, Eds. *Manual of Clinical Microbiology*, 4th ed. American Society for Microbiology, Washington, DC, 1985.
11. R. I. WALKER, I. BROOK, J. W. COSTERTON, T. J. MACVITTIE, and M. L. MYHAL, Possible association of mucous blanket integrity with post-irradiation colonization resistance. *Radiat. Res.* **104**, 346–357 (1985).
12. T. E. LEE, *Statistical Methods for Survival Data Analysis*, pp. 127–129. Lifetime Learning Publications, Belmont, CA, 1980.
13. M. TRAUTMANN, O. BRUCKNER, R. MARRE, and H. HAHN, Comparative efficacy of ciprofloxacin, ceftizoxime, and gentamicin, given alone or in combination, in a model of experimental septicemia due to *Klebsiella pneumoniae* in neutropenic mice. *Infection* **16**, 49–53 (1988).
14. I. BROOK, R. I. WALKER, and T. J. MACVITTIE, Effect of antimicrobial therapy on the gut flora and bacterial infection in irradiated mice. *Int. J. Radiat. Biol.* **53**, 709–716 (1988).
15. S. PECQUET, A. ANDERMONT, and C. TANACREDE, Selective antimicrobial modulation of the intestinal tract by norfloxacin in human volunteers and in gnotobiotic mice associated with a human fecal flora. *Antimicrob. Agents Chemother.* **29**, 1047–1052 (1986).
16. M. ROZENBERG-ARSKA, A. W. DEKKER, and J. VERHOEF, Ciprofloxacin for selective decontamination of the alimentary tract in patients with acute leukemia during remission induction treatment. The effect in fecal flora. *J. Infect. Dis.* **142**, 104–107 (1985).

Biomedical Lessons From the Chernobyl Nuclear Power Plant Accident

Lt Col Doris Browne, MC*

The Chernobyl nuclear accident afforded the treating physicians a chance to observe clinical ARS in man, defining the degree of severity according to average radiation dose exposure, and to make prognoses for the individual patients on the course of the ARS, based on biological criteria. The author gives a detailed account of the clinical cause of the disease including all available laboratory values. She provides valuable data that can be utilized in handling similar accidents in the future.

The world's worst radiation accident occurred at the Chernobyl nuclear power plant in the USSR during the early hours of April 26, 1986. This accident unleashed megacuries of radioactive contamination into the atmosphere, generated an explosive blast that knocked the thousand-ton lid off the top of the reactor, and sent burning graphite and heat in a plume about three miles high. The aftermath and significance of this disaster are still being realized in the USSR and neighboring countries.

Details of the accident were reported at the International Atomic Energy Agency (IAEA) meeting held in Vienna, Austria, in August 1986, and summarized in IAEA Safety Series Technical Report No. 75.[1,2] This report summarizes the basic information on casualties, triage, and treatment, and the radionuclides released into the atmosphere. The immediate casualties included only plant personnel, firemen, and auxiliary staff present at, or in the vicinity of the accident site.

These casualties were all subject to the combined effects of the following: short-term beta/gamma radiation released in the emission cloud; external beta/gamma radiation from fragments of the damaged reactor core scattered through the accident site; inhalation of gaseous and aerosolized dust composed primarily of radioisotopes of cesium, plutonium, and iodine; and beta/gamma particles deposited on the skin and mucous membranes from the molten steam and dust. Wet clothing contaminated by the steam and dust provided another source of contamination.

Within 15 minutes of the acident, first aid was provided by middle level medical personnel and emergency team members. Individuals with acute symptoms were transported to the hospital in Pripyat, where the initial screening took place; others in satisfactory condition were instructed to go to the hospital for examination. The initial care consisted of antiemetics, symptomatic medication, and stable saturated potassium iodide. The specialized emergency team of radiation accident specialists arrived at the accident site within 12 hours and, with the on-site medical personnel, screened and triaged more than 350 persons within the first 36 hours. During the first 24 hours, 132 persons were hospitalized; one individual died from severe thermal burns during the first hour, and another worker (a reactor operator) was unaccounted for and believed to be buried under the collapsed debris.

The triage officer, a physician, made decisions based on the initial symptoms and lymphocyte counts. Persons with severe symptoms were hospitalized with clinical complaints of acute radiation sickness (ARS). Three hundred of these patients were sent to a specialized treatment center in Moscow and another 200 were sent to a hospital in Kiev. The 237 hospitalized individuals received significant combined radiation effects from the extensive beta/gamma exposure, which was generally external and relatively uniform over the whole body, as well as with the intake of additional radionuclides through inhalation. These patients were diagnosed as having ARS resulting from extensive beta radiation burns to the skin and significant whole-body gamma radiation exposure.

The diagnostic criteria used to assess the presence of ARS was the presence, intensity, and duration of symptoms ie, nausea, vomiting, and erythema of the skin and mucosa); time of onset; and the peripheral lymphocyte count, which decreased to less than 10^9/L during the first 24 hours following radiation exposure in patients with ARS. During the first 36 hours after the accident, the 237 hospitalized

***Lt Col Doris Browne, MC**, is Chief, Medical Operations Division, Military Requirements and Applications Department (MRA), Armed Forces Radiobiology Research Institute (AFRRI). She is a licensed physician in hematology-oncology. Dr. Browne attended medical school at Georgetown University, and completed an internship and residency in internal medicine at Walter Reed Army Medical Center. She was a fellow in hematology and oncology at Walter Reed Army Medical Center. She joined the staff of William Beaumont Army Medical Center, El Paso, Texas as the Assistant Director of the Hematology-Oncology Clinic, Department of Medicine. She joined the staff of the AFRRI as Chief of the Medical Operations Division and is responsible for the Medical Effects of the Nuclear Weapons (MENW) Course and all technology transfer activities at the institute. She is the Officer-in-Charge of the Medical Radiobiology Advisory Team (MRAT) that recently sponsored the First Consensus Development Conference on the Treatment of Radiation Injuries. A summary report of this conference was published in an international journal and the proceedings of the conference are in press. She is a member of the American Society of Clinical Oncology, American College of Physicians, and the National Medical Association.*

*Chief, Medical Operations Division, Military Requirements and Applications Department, Armed Forces Radiobiology Research Institute, Bethesda, MD 20814.

Supported by the Armed Forces Radiobiology Research Institute, Defense Nuclear Agency. Views presented in this paper are those of the author; no endorsement by the Defense Nuclear Agency has been given or should be inferred.

persons were diagnosed as having a clinical pattern consistent with first degree through fourth degree ARS. After admission to the hospital, they were monitored again for contamination and, when necessary, decontaminated with soap, water, and a clothing change. Routine samples of urine and blood were drawn for analysis, and thyroid scanning was performed. The radiation dose received was estimated by counting the number of aberrant chromosomes (dicentrics) in cultured lymphocytes (cytogenetic analysis). The diagnosis of ARS was confirmed during the first five days for persons admitted to the Moscow Hospital. Approximately seven days after the accident, the radiation dose was estimated and the patients were categorized into four groups according to prognosis and severity of hematopoietic syndrome (Table I). Twenty-two injured persons were classified as having fourth degree (extremely severe) ARS; 23 as having third degree (severe) ARS; 53 as having second degree (moderate) ARS; and 139 as having first degree (mild) ARS.[3]

Neutrophil count was used to determine finally the magnitude of radiation dose. The parameter used was the time required for the neutrophils to decrease to 0.5×10^9/L, based on data collected over a period of up to three months in cases that exhibited typical postirradiation platelet and/or neutrophil counts with distinct depletion and restoration phases. Complete blood counts were performed two to three times per week for two to three months. This data was used to definitively confirm the diagnosis and prognosis of ARS. Hyperamylasemia was used as a supplementary diagnostic tool.

Treatment consisted of supportive therapy, which included selective antimicrobial intestinal decontamination, reverse isolation, empiric systemic antibiotic administration, and transfusion replacement of blood and blood products. Definitive treatment of allogeneic bone marrow transplantation (BMT) and human embryonic liver cell transplantation (LCT) was performed on patients with irreversible myelosuppression. A sterile environment was maintained through strict observance of hand washing by all attending personnel upon entering and leaving the room; mandatory use of disposable gowns, masks, and caps; antiseptic decontamination of footwear; changing of patient undergarments daily; antiseptic washing of walls, floors and items used in the room; and individually assigned antiseptically treated nursing items. Isolation rooms provided air sterilization with ultraviolet lamps. The microorganism population was maintained at less than $500 m^{-3}$ in the room air. Raw fruits and vegetables and canned products were eliminated from the patients' diet.[4]

The decision was made early to perform BMT on patients with third and fourth degree ARS and possible irreversible myelosuppression.[5] These patients vomited within the first half-hour, suffered from diarrhea during the first one to two hours, and from swelling of the parotid gland during the first 24 to 36 hours of exposure, in addition to myelosuppression.

Infections, manifested by the onset of fever and neutropenia, were treated with intravenous administration of triple broad-spectrum antibiotics, including aminoglycoside, cephalosporin and semi-synthetic penicillin. If this regimen did not reduce the fever within 48 hours, three or four doses of gamma globulin were administered. An intravenous antifungal (amphotericin B) was administered if the neutropenic fever persisted for seven days, along with the antibiotics and gamma globulin. Patients with herpes simplex were given acyclovir. Approximately one third of the patients with third and fourth degree ARS had the herpes virus. Viral skin lesions were treated with topical acyclovir. No deaths were attributed to bacterial infection alone in patients with hematopoietic syndrome. However, infectious complication was the primary cause of death in patients with ARS complicated by thermal burns, radiation-induced enteritis, or acute graft-versus-host disease from BMT. The etiology of terminal septicemia, documented by surveillance cultures, was most often from *Staphylococcus epidermidis*

The hematopoietic syndrome was treated with prophylactic and therapeutic fresh random donor platelets when the platelet count dropped to 20×10^9/L or lower, or with the first sign of bleeding. Transfusions usually were required every one to three days. To inactivate the immunocompetent cells from the donor, all blood components were irradiated with 1,500 cGy of gamma radiation before transfusion. Only one person received single donor platelets. While the majority of patients showed no evidence of overt bleeding, autopsy results disclosed micro-circulatory failure and very porous capillaries in several organs. In some situations, cryo-preserved autologous platelets, as well as allogeneic platelets, were used successfully. Autologous platelets were taken from patients with second and third degree ARS on the first day post-irradiation. Platelet transfusions prevented life-threatening bleeding. Three to eight transfusions of 250 cc per

Table I. Diagnostic Categories for Acute Radiation Sickness (ARS)

Degree of ARS	Dose (cGy)	Severity of ARS	Prognosis
I	100-200	Mild	Very favorable
II	200-400	Moderate	Relatively favorable
III	400-600	Severe	Doubtful
IV	≥ 600	Extremely severe	Poor

person were used to treat patients with second and third degree ARS. No evidence of refractoriness developed. A considerable number of packed red blood cells were transfused in patients with second and third degree ARS accompanied by severe radiation burns.

Allogeneic BMT taken from 113 random related donors was performed on 13 patients with third and fourth degree ARS. Additionally, six patients with fourth degree ARS received embryonic LCT, which contained stem cells and few immunocompetent cells to decrease the risk of developing acute graft-versus-host disease (Table II). Fifty percent (seven patients) of the BMT patients died within 17 days of transplantation (15 to 25 days following radiation exposure) from acute radiation injury to lung, intestine, and/or skin. The remaining six patients did not have severe skin burns or intestinal injuries but received a total radiation dose estimated to be between 440 and 1,020 cGy. Two of the six patients survived BMT (having received 560 cGy and 870 cGy doses, respectively) from haplo-identical female (sisters) donors. Both experienced transient partial engraftment of the transplanted marrow before rejection 32 and 35 days after BMT, respectively, with restoration of their own myelopoiesis after 28 days. These two patients are still alive at more than three and one half years after the accident.[5] A 62-year-old female patient who received LCT lived for 30 days; postmortem findings showed evidence of regeneration of her own myelopoiesis, indicated by female cell karyotype. She had received a male donor transplant.[4,6]

The effectiveness of BMT in an emergency situation may be limited to patients receiving less than 300 cGy of gamma radiation with at least 1% of marrow stem cells remaining, no skin or intestinal radiation injuries, and no combined injury.[7] Seven of the 13 BMT patients died of skin and intestinal injuries before the transplanted marrow engrafted. While recovery of autologous myelopoiesis may occur following large doses of radiation exposures, such as experienced by those patients with third and fourth degree ARS, it is unknown if this occurred due to transient engraftment of transplanted stem cells.

Table II. Transplantation Cases, Estimated Radiation Dose, and Outcome.

Degree of ARS	Dose (cGy)	Treatment	Day of Death	Cause of Death
IV	920	BMT	15	Skin; pneumonitis
IV	1200	BMT	17	Skin; GI injury
IV	1180	BMT	18	Skin; GI injury
IV	1000	BMT	18	Skin; GI injury
III	550	BMT	21	Hemorrhage[1]
IV	830	BMT	24	Pneumonitis
IV	660	BMT	25	ARDS; toxicity
III	440	BMT[2]	34	Mixed infection; GVH
IV	640	BMT[3]	48	Mixed infection; GVH
IV	750	BMT[3]	86	Mixed infection; GVH
IV	1020	BMT[4]	91	Mixed infection; GVH
III	560	BMT[5]	Alive	
IV	870	BMT[5]	Alive	
IV	1110	LCT	14	Skin; GI injury
IV	> 1000	LCT	14	Skin; GI injury
IV	1370	LCT	15	Skin; GI injury
IV	1240	LCT	17	Skin; GI injury
IV	1090	LCT	18	Skin; GI injury
IV	830	LCT[6]	30	Toxicity; ARDS

Note: BMT = bone marrow transplantation; LCT = liver cell transplantation; GI = gastrointestinal injury; GVH = graft-versus-host; ARDS = acute respiratory distress syndrome (respiratory insufficiency).

[1]Hemorrhage from mechanical trauma during catheterization.

[2]BMT from haplo + 1 identical donor but own myelopoiesis restored.

[3]BMT from HLA-identical donor.

[4]BMT from haplo-identical donor but own myelopoiesis restored.

[5]BMT from haplo-identical donor rejected, own myelopoiesis restored.

[6]LCT from male, postmortem evidence of own myelopoiesis being restored.

Radiation-induced skin injuries (beta radiation burns) were seen only in combination with hematopoietic syndrome radiation injury. Skin doses of radiation were estimated to be 10 to 20 times greater than bone marrow or whole-body doses, confirming the uncontrolled, nonuniform nature of radiation accident exposure. These skin injuries, according to their severity, duration, and recurrence, contributed significantly to the overall pathophysiology and outcome of the patient. Severe skin injuries were manifested by diffuse hyperemia; secondary erythema; dry and wet desquamation with blistering, ulceration, and necrotic dermatitis; recurrent waves of erythema; and after evidence of healing of the primary lesions, edema, fever, and a worsening of the patient's clinical picture.[4] Topical treatment was necessary, with glucocorticoids and analgesia in the more severe cases. Pain control was relatively ineffective, especially topical anesthesia, which seems to be typical for radiation injuries.

Burns were fatal in the 19 of 56 patients with radiation burns on > 40% to 100% of body surface area.[6] If early secondary erythema over > 40% body surface area was present, a clinical picture of febrile-toxemia, followed by hepatorenal insufficiency, encephalopathy with cerebral edema, coma, and death resulted 14 to 48 days postirradiation. Plasmapheresis was used to control the hepatorenal insufficiency.[1,4] This treatment prolonged survival slightly but did not prevent death from encephalopathic coma. The burns may have been the primary cause of death in some cases; however, in most cases, the burns were associated with severe hematopoietic syndrome and severe acute gastrointestinal syndrome (enteritis).

In ten patients, the gastrointestinal syndrome was the life-threatening manifestation of ARS, with severe diarrhea suggesting a radiation dose greater than 1,000 cGy. All of these patients died within three weeks of irradiation. When the enteritis persisted in spite of supportive fluid and electrolyte therapy, death may have been caused solely by the gastrointestinal syndrome.

Large amounts of thick rubber-like mucous formed in the oropharyngeal area of about 82 patients and in some cases resulted in respiratory difficulty. Initially, some patients showed benign acute radiation-induced inflammation of cheeks, tongue, and gums. Those having third and fourth degree ARS had, in addition to the rubbery mucous plugs, painful erosions and ulcers of oral mucosa, which required sterile saline irrigation and frequent debridement. In a significant number of patients this radiation-induced inflammation was complicated by secondary bacterical and viral infections.

In one third of the patients with severe hematopoietic syndrome, herpetic lesions formed massive crusts on the lips and face about three to four days postirradiation. Patients with fourth degree ARS and herpetic lesions also developed radiation-induced parotitis, inability to salivate, and resulting hyperamylasemia.[8] No treatment was indicated for the parotitis, which gradually resolved; salivation, however, recurred very slowly.

Rapidly intense dyspnea with acute respiratory insufficiency (adult respiratory distress-like syndrome) was seen in seven patients with third and fourth degree ARS. This condition rapidly progressed for two to three days leading to death. Postmortem examination revealed enlarged blue lungs with interstitial edema but no destruction of mucous membranes of the trachea and bronchi. These patients also had severe skin and intestinal radiation injuries.

Beta radiation caused early damage to the eye tissues; erythema of the eyelid, with increased vasculature of the lid, and conjunctiva. Cutaneous changes were manifested by waves of erythema, hyperpigmentation, and scaling. Partial epilation of the eyebrows was transient, and all patients retained their eyelashes. (Scalp hair growth recovered fully.) Other eye changes noted were decreased corneal sensitivity and superficial radiation-induced keratitis, which regressed over one to two months without corneal opacification. Treatment for the eye changes included topical ointments to the eyelid skin and eyedrops of 20% albucid, sophradex, and vitamin solutions into the conjunctival cavity.[4] One severely ill patient with fourth degree ARS, who survived the acute phase, developed angioretinopathy with hemorrhage and plasma discharges about five months postirradiation. He also had persistent low diastolic pressure in the central retinal artery. He is one of the two surviving BMT patients. No radiation-induced lens changes were observed one year postirradiation.

Convalescence of three to four months was required for those patients with first and second degree ARS; a much longer period was necessary for those having third and fourth degree ARS. The majority of the patients have resumed work but cannot work with radiation sources. Periodic follow-up examinations were made during the first year after the accident. Patients usually had dystrophic and ulcerative skin lesions, some with subcutaneous edema primarily over the knees and feet. Skin lesions were treated with agents that improved local blood circulation and tissue trophism. Five patients suffered deep ulcers which required repeated plastic surgery.

The immunologic status of patients with second, third, and fourth degree ARS, tested 1 to 1.5 years after the accident showed a persistent decrease in T-helper lymphocytes with an increase in T-suppressor lymphocyte activity and a significant decrease in the helper-suppressor ratio. However, there was no evidence of a decrease in the absolute lymphocyte level or in the T- and B-subpopulations. These changes in lymphocyte helper and suppressor populations were not seen in patients with first degree ARS. During the follow-up period, no severe or life-threatening infections were noted. Immunocorrective therapy was attempted using T- and B-activin in several cases. Respiratory infections occurred in three of eight patients with third and fourth degree ARS and only one of 22 patients with second degree ARS. A competent immune system remains critical in enhancing microbial and viral resistance during convalescence of the irradiated patient. A plan of long-term follow-up observation remains in effect.

Conclusion

The consequences of the Chernobyl radiation accident provide data on a large group of critically ill patients who received uniform whole-body irradiation and required treatment of ARS in a massive casualty situation. The event afforded the opportunity to learn many lessons regarding the biomedical effects of ionizing radiation and to clarify many aspects about the early radiobiological effects in humans. The accident also provided data on severe and extensive beta radiation skin injuries, which com-

plicated the course of illness and played a significant role in the death of 19 of the 31 patients. Combined injuries consisting of trauma, thermal burns, and radiation were the cause of death in two patients very early in the course of ARS. Clinical ARS was observed in man, the degrees of severity defined according to average radiation dose exposure, and prognosis made for the course of ARS based on biological criteria. Information for biological dosimetry was obtained from karyotypical analysis, lymphocyte counts, and symptoms during the early stages of illness; later the granulocyte count proved to be a useful dosimetric tool. While continuous data and follow-up assessment is necessary, this information should prove useful in responding to radiation accidents and providing effective medical care to the resulting casualties.

REFERENCES

1. USSR State Commission on the Utilization of Atomic Energy. *The accident at the Chernobyl nuclear power plant and its consequences.* Information complied for the Post-Accident Review Meeting, part II, Annex 7, Vienna, Austria, August 25-29, 1986.
2. International Nuclear Safety Advisory Group. *Summary report on the post-accident review meeting on the Chernobyl accident.* Vienna, Austria: International Atomic Energy Agency (IAEA), 1986. (Safety Series No. 75-INSAG-1).
3. Bair WJ: Radiological impacts of the Chernobyl accident. *Health Physics Society Newsletter.* February, 1987.
4. Guskova AK, Barabanova AV, Baranov AE, et al: Acute radiation effects in victims of the Chernobyl nuclear power plant accident. Appendix to *Sources, Effects and Risks of Ionizing Radiation.* United Nations Scientific Committee on the Effects of Atomic Radiation. New York, 1988, pp 613-647.
5. Baranov AE, Gale RP, Guskova AK, et al: Bone marrow transplantation after the Chernobyl nuclear accident. *N Engl J Med* **321(4)**:205-212, 1989.
6. Young RW: Chernobyl in retrospect. *Pharmac Ther* **39**:27-32, 1988.
7. Browne D, Weiss JF, MacVittie TJ, et al: Conference report: The first consensus development conference on the treatment of radiation injuries. *Int J Radiat Biol* **57(2)**:437-442, 1990.
8. Guskova AK, Nadezhina NM, Barabanova AV, et al: Acute effects of radiation exposure following the Chernobyl accident: Immediate results of radiation sickness and outcome of treatment. In *Treatment of Radiation Injuries.* Browne D, Weiss JF, Mac Vittie TJ, et al (eds). Plenum, New York, 1990. ●

Microecology and Therapy
Mikroökologie und Therapie
Vol. 19, 105 108 (1989)
ISSN 0720-0536

Edited by
Institut für Mikroökologie
D 6348 Herborn-Dill
Federal Republic of Germany

COMBINED THERAPY FOR POSTIRRADIATION INFECTION

KOMBINIERTE THERAPIE VON INFEKTIONEN NACH BESTRAHLUNG

THOMAS B. ELLIOTT, GARY S. MADONNA, G. DAVID LEDNEY, and ITZHAK BROOK

SUMMARY

Increased susceptibility to bacterial infection, probably by translocation from the intestinal flora, can be a lethal complication for 2-3 weeks after exposure to ionizing radiation. Antibiotics alone do not provide adequate therapy for induced infections in neutropenic mice. Because some substances that are derived from bacterial cell walls activate macrophages and stimulate nonspecific resistance to infection, such agents might be used to prevent or treat postirradiation infections. In this study, a cell-wall glycolipid, trehalose dimycolate (TDM), was evaluated together with a third-generation cephalosporin, ceftriaxone, for their separate and combined effects on survival of B6D2F1 female mice that were exposed to the sublethal dose of 7.0 Gy ^{60}Co radiation and challenged s.c. with lethal doses of *Klebsiella pneumoniae*. A single injection of TDM (100 μg in 2% oil emulsion) inoculated i. p. 1 hr postirradiation increased 30-day survival to 80% after a lethal challenge by *K. pneumoniae* (10 $LD_{50/30}$) 4 days later. When the challenge dose of *K. pneumoniae* was increased to 5000 $LD_{50/30}$ on Day 4, all mice died. Ceftriaxone (75 mg/kg) injected i. m. from days 5 to 14 postirradiation increased survival to 70% after a lethal challenge by *K. pneumoniae* of 5000 $LD_{50/30}$ on Day 4. However, when TDM and ceftriaxone were combined, survival was enhanced synergistically to 100% even when the dose of *K. pneumoniae* injected on Day 4 was 5000 $LD_{50/30}$. These results indicate that a combination of an immunomodulator and an antimicrobial agent will be more effective for treating postirradiation bacterial infections than either treatment alone in immunocompromised, neutropenic mice.

ZUSAMMENFASSUNG

Die erhöhte Empfindlichkeit gegenüber bakteriellen Infektionen kann 2-3 Wochen nach Aussetzung gegenüber radioaktiver Bestrahlung zu tödlichen Komplikationen führen, möglicherweise beeinflußt durch die Translokation von Mikroorganismen aus der Intestinalflora. Als Therapie für induzierte Infektionen von Mäusen mit einem Mangel an neutrophilen Zellen sind Antibiotika alleine nicht ausreichend. Da bekannt ist, daß einige, in Zellwänden von Bakterien enthaltene Substanzen Makrophagen aktivieren und die unspezifische Resistenz gegenüber Infektionen stimulieren, besteht die Möglichkeit, mit Hilfe solcher Agentien Infektionen nach Bestrahlung zu verhüten oder zu behandeln. Bei dieser Studie wurde Trehalose-Dimycolat (TDM), ein zellwandständiges Glycolipid, zusammen mit einem Cephalosporin der dritten Generation, Ceftriaxon, auf ihre Einzel- und Kombinationswirkung auf das Überleben von B6D2F1 Mäusen weiblichen Geschlechts untersucht, die der sublethalen Dosis von 7,0 Gy Kobalt-60-Bestrahlung ausgesetzt und mit subkutan applizierten, lethalen Dosen von *Klebsiella pneumoniae* infiziert wurden. Eine ein-

zelne Injektion von TDM (100 µg in 2% Öl-Emulsion), die intraperitoneal eine Stunde nach Bestrahlung gegeben wurde, erhöhte das 30 Tage-Überleben auf 80% nach der lethalen Infektion mit *Klebsiella pneumoniae* (10 $LD_{50/30}$) 4 Tage später. Bei Erhöhung der Infektionsdosis von *Klebsiella pneumoniae* auf 5000 $LD_{50/30}$ an Tag 4 starben alle Mäuse. Die intramuskuläre Injektion von Ceftriaxon (25 mg/kg) in den Tagen 5 bis 14 nach Bestrahlung erhöhte das Überleben auf 70% nach lethaler Infektion mit *Klebsiella pneumoniae* von 5000 $LD_{50/30}$ an Tag 4. Durch die synergistische Wirkung kombinierten TDM's und Ceftriaxon's wurde die Überlebensrate jedoch auf 100% gesteigert, selbst bei der Injektion einer Dosis von *Klebsiella pneumoniae* von 5000 $LD_{50/30}$ an Tag 4. Diese Resultate belegen, daß die Kombination eines immunmodulierenden und eines antimikrobiellen Agens in der Behandlung von bakteriellen Infektionen nach Bestrahlung immunkompromittierter Mäuse mit einem Mangel an neutrophilen Zellen effektiver sind, als die Behandlung mit jeweils einem dieser Mittel alleine.

INTRODUCTION

Ionizing radiation causes an hematopoietic syndrome in mice that induces prolonged neutropenia and increased susceptibility to bacterial infections (SCHECHMEISTER, 1954). Antibiotics alone do not assure cure of infections or survival of irradiated animals (BROOK and ELLIOTT, 1989; BROOK et al., 1989; MADONNA et al., 1989a; MADONNA et al., 1989b). Consequently, there is a practical need to develop effective therapeutic modalities for infections following radiation injury.

Ceftriaxone is a third-generation semisynthetic cephalosporin that has a broad spectrum of activity against bacteria and a long elimination half-life (6-9 hr), which allows a once-daily administration i.v. or i.m. Trehalose dimycolate (TDM) is a bacterial cell-wall glycolipid (LEMAIRE et al., 1986), which has potentially beneficial properties, including enhanced resistance to bacterial infections (YARKONI and BEKIERKUNST, 1976), activation of macrophages with production of mediators, such as interleukin-1, colony-stimulating factors, and interferons (MADONNA et al., 1986; RIBI, 1986; TENU et al., 1980; YARKONI et al., 1977).

We evaluated the separate and combined effects of TDM and ceftriaxone on survival in mice that were made neutropenic by irradiation and then challenged with *Klebsiella pneumoniae*. The data showed that the combination of TDM and ceftriaxone protected irradiated mice from a fatal infection.

METHODS

The animals, bacteria, radiation dose and dosimetry, therapeutic agents, and statistical evaluation were described (MADONNA et al., 1989; STEWART et al., 1982).

Mice were given TDM in 2% squalene oil-0.2% Tween 80 emulsion (TDM/o), TDM in 0.9% NaCl-0.2% Tween 80 solution (TDM/s), saline solution, or oil emulsion i.p. 1 hr after 7.0 Gy irradiation from ^{60}Co. To determine the effect of TDM against different challenge doses of *K. pneumoniae*, 10, 100, 1000, and 5000 $LD_{50/30}$ of the bacteria were injected s. c. four days after irradiation, when the mice were neutropenic (1 $LD_{50/30}$ = 1.2×10^3 CFU). Another group of mice were given 5000 $LD_{50/30}$ *K. pneumoniae* and treated for ten days with either ceftriaxone or water beginning one day after challenge with bacteria.

RESULTS

Either trehalose dimycolate or ceftriaxone alone enhanced survival of mice that were lethally challenged with *K. pneumoniae* 4 days after sublethal radiation. Combined therapy with TDM and ceftriaxone synergistically protected mice from lethal challenge with *K. pneumoniae* (Table 1).

Mean survival times for all treatments were greater than for saline control for each inoculum ($p < 0.001$) and TDM/o enhanced survival time more than TDM/s ($p < 0.001$), except with 1.2×10^4 CFU/mouse ($p = 0.0835$). Mean survival times were greater for combined therapies than for single therapies: TDM/o-ceftriaxone vs. ceftriaxone, $p = 0.0165$, TDM/o-ceftriaxone vs. TDM/o-water, $p < 0.001$, and TDM/s-ceftriaxone vs. ceftriaxone, $p > 0.05$.

Serum Concentration of Ceftriaxone.

Sera of a separate group of mice that received 10.0 Gy gamma radiation contained an average 142.6 (± 2.2) µg ceftriaxone/ml 1.3 hr after injection and 2.3 (± 0.6) µg/ml 25.9 hr after injection.

TABLE 1

Survival of Mice Challenged with *Klebsiella pneumoniae* and Treated with Combined Therapy of TDM and Ceftriaxone.

$LD_{50/30}$	Antibiotic	% Survival[a]			
K. pneumoniae	Therapy	TDM/o	TDM/s	Saline	Oil
5000	ceftriaxone	100	88	69	nd[d]
	water	0	0	0[b]	nd
1000	ceftriaxone	100	94	88	nd
	water	13	0	0[b]	0[c]
100	nd	69	20	0	nd
10	nd	90	60	0	nd

[a]N = 16, except [b] n = 10 and [c] n = 12; [d] nd = not done

DISCUSSION

Our results with the combination of TDM and ceftriaxone lead to a new method to improve the treatment for bacterial infections in irradiated hosts and the prognosis for survival. Other combinations of an immunomodulator and an antibiotic synergistically enhance survival of irradiated mice. Pefloxacin, and other quinolones, given orally, prolonged survival of lethally irradiated mice (BROOK, I., et al.,1989) and was synergistic with glucan F (PATCHEN, M., BROOK, I., and ELLIOTT, T. B., unpublished data). Although the mechanism of action of TDM is unclear, it may involve the release of specific cytokines from macrophages. We are examining the application of interleukin-1 in irradiated mice.

MADONNA and colleagues (1989a) used the number of bacteria in livers of lethally irradiated mice as an indicator of septicemia caused by translocated endogenous bacteria. The number remained low in mice treated with TDM from 7 to 11 days after irradiation, but bacteria increased in mice treated with saline solution. Similarly, both the incidence and the mean numbers of streptomycin-resistant *Escherichia coli* in mesenteric lymph nodes decreased in specific-pathogen-free mice that were treated with killed *Propionibacterium acnes* (FULLER and BERG, 1985).

These observations support the principle that the nonspecific host defences must be enhanced in neutropenic and immunosuppressed animals in addition to use of antibiotics in order to prevent death from bacterial infections.

ACKNOWLEDGEMENTS

We are grateful to *William E. Jackson*, III, for analysis of data on survival of mice. This research was supported by Work Unit No. 4420-00129 of the Armed Forces Radiobiology Research Institute, Defense Nuclear Agency. The views presented in this paper are those of the authors. No endorsement by the Defense Nuclear Agency has been given or should be inferred. Research was conducted according to the principles enunciated in the „Guide for the Care and Use of Laboratory Animals" prepared by the Institute of Laboratory Animal Resources, National Research Council.

Thomas B. Elliott, Ph. D., Gary S. Madonna, G. David Ledney, and Itzhak Brook Ph. D., Department of Experimental Hematology, Armed Forces Radiobiology Research Institute, Building 42, National Naval Medical Center, Bethesda, Maryland 20814-5145, USA.

Paper presented as poster by Dr. Elliott at the XIV. International Symposium on Microbial Ecology and Disease, September 21-23, 1989, San Antonio, Texas, USA.

LITERATURE

BROOK, I., and ELLIOTT, T. B.: Treatment of Wound Sepsis in Irradiated Mice. Int. J. Radiat. Biol. *56*, 75-82 (1989).

BROOK, I., ELLIOTT, T. B., and LEDNEY, G. D.: Therapy of *Klebsiella pneumoniae*

Sepsis Following Irradiation: Comparison of Pefloxacin, Ciprofloxacin, and Ofloxacin. Microecology and Therapy *19* (1989).

FULLER, K. G., and BERG, R. D.: Inhibition of Bacterial Translocation from the Gastrointestinal Tract by Nonspecific Immunostimulation. In: Germfree Research: Microflora Control and Its Application to the Biomedical Sciences (Editor: WOSTMANN, B. S.). Alan R. Liss, Inc., New York, 195-198 (1985).

LEMAIRE, G., TENU, J. P., PETIT, J. F., and LEDERER, E.: Natural and Synthetic Trehalose Diesters as Immunomodulators. Med. Res. Rev. *6*, 243-274 (1986).

MADONNA, G. S., PETERSON, J. E., RIBI, E. E., and VOGEL, S. N.: Early-phase Endotoxin Tolerance: Induction by a Detoxified Lipid A Derivative, Monophosphoryl Lipid A. Infect. Immun. *52*, 6-11 (1986).

MADONNA, G. S., LEDNEY, G. D., ELLIOTT, T. B., BROOK, I., ULRICH, J. T., MYERS, K. R., PATCHEN, M. L., and WALKER, R. I.: Trehalose Dimycolate Enhances Resistance to Infection in Neutropenic Animals. Infect. Immun. *57*, 2495-2501 (1989a).

MADONNA, G. S., MOORE, M. M., LEDNEY, G. D., ELLIOTT, T. B., and BROOK, I.: Combined Therapy of Septicemia in Irradiated, Wounded Mice with Ofloxacin, Gentamicin, Oxacillin and/or Synthetic Trehalose Dimycolate (s-TDM). Microecology and Therapy *19* (1989b).

RIBI, E.: Structure-function Relationship of Bacterial Adjuvants. In: Advances in Carriers and Adjuvants for Veterinary Biologics (Editors: NERVIG, R., GOUGH, P., KAEBERLE, M., and WHETSTONE, C.) Iowa State University Press, Ames, 35-49 (1986).

SCHECHMEISTER, I. L.: Susceptibility of Irradiated Animals to Infection. Radiat. Res. *1*, 401-409 (1954).

STEWART, D. A., LEDNEY, G. D. BAKER, W. H., DAXON, E. G., and SHEEHY, P. A.: Bone Marrow Transplantation of Mice Exposed to a Modified Fission Neutron (N/G – 30:1) Field. Radiat. Res. *92*, 268-279 (1982).

TENU, J. P., LEDERER, E., and PETIT, J. F.: Stimulation of Thymocyte Mitogenic Protein Secretion and of Cytostatic Activity of Mouse Peritoneal Macrophages by Trehalose Dimycolate and Muramyl-dipeptide. Eur. J. Immunol. *10*, 647-653 (1980).

YARKONI, E., and BEKIERKUNST, A.: Nonspecific Resistance against Infection with *Salmonella typhi* and *Salmonella typhimurium* Induced in Mice by Cord Factor (Trehalose-6-6'-dimycolate) and Its Analogues. Infect. Immun. *14*, 1125-1129 (1976).

YARKONI, E., WANG, L., and BEKIERKUNST, A.: Stimulation of Macrophages by Cord Factor and by Heat-killed and Living BCG. Infect. Immun. *16*, 1-8 (1977).

INTERACTION OF LEUKOTRIENE C_4 AND CHINESE HAMSTER LUNG FIBROBLASTS (V79A03 CELLS). 1. CHARACTERIZATION OF BINDING

T.A. Fitz[1,4], D.F. Contois[1], Y.X. Liu[1], D.S. Watt[2], T.L. Walden, Jr.[3]

[1]Department of Obstetrics and Gynecology, Uniformed Services University of the Health Sciences, Bethesda, Maryland 20889-4799, [2] Department of Chemistry and Division of Medicinal Chemistry, Lucille Parker Markey Cancer Research Center, University of Kentucky, Lexington, Kentucky 40506-0055, [3]Radiation Biochemistry Department, Armed Forces Radiobiology Research Institute, Bethesda, Maryland 20889-5145, [4]Correspondence

Abstract

A novel, specific, and potent biological action of leukotriene C_4 (LTC_4) was demonstrated in the Chinese hamster lung fibroblast cell line V79A03 (V79 cells), namely the conferment of protection against subsequent γ-irradiation. Consequently, studies were conducted to determine whether LTC_4-conferred radioprotection could be attributed to a receptor-mediated phenomenon. Specific binding sites for leukotriene C_4 (LTC_4) were identified and characterized using intact V79 cells incubated at 4°C in the presence of serine-borate, during which time conversion of LTC_4 to LTD_4 or LTE_4 was undetectable. Binding was maximal in a broad region between pH 6.2 and 8.8. Ca^{2+}, Mg^{2+}, and Na^+ were not required for binding, and binding was not altered by GTP, ATP, or cAMP, by leukotrienes B_4, D_4, or E_4, or by the leukotriene end point antagonists LY 171883, FPL 55712, or Revlon 5901-5. Scatchard analyses and kinetic experiments indicated the presence of high-affinity [Kd = 2.5 ± 0.63 nM, approximately 9.9 x 10^5 sites/cell] and low-affinity [Kd = 350 ± 211 nM, approximately 2.7 x 10^6 sites/cell] binding sites. The observed binding characteristics of LTC_4 to V79 cells are consistent with a receptor-mediated phenomenon. In a companion communication which follows this report, we report the subcellular distribution of LTC_4 binding to V79 cells and demonstrate that this binding is unlikely to be attributed principally to interaction with glutathione-S-transferase.

Introduction

Eicosanoids have come under increasing scrutiny as possible agents to alleviate the damaging effects of ionizing radiation and because elevated eicosanoid synthesis by certain tumors is associated with their resistance to chemotherapy and radiation therapy (1). An in vitro model system was recently described (2) to evaluate the radioprotective effects of eicosanoids in the Chinese hamster lung fibroblast cell line V79A03 (V79 cells). In this system, pretreatment of V79 cells with leukotriene C_4 (LTC_4) elevated the cellular rate of postirradiation survival. The radioprotective effects of LTC_4 on V79 cells were attenuated if the cells to be treated were harvested from culture flasks by trypsin preincubation (unpublished data), suggesting that the radioprotective effect of LTC_4 depends on the presence of a proteinaceous factor present on the V79 cell surface.

In addition to its effect in V79 cells, pretreatment with LTC_4 was radioprotective in murine hematopoietic stem cells in vivo (3) and

enhanced animal survival following otherwise lethal radiation exposure (4). The mechanism(s) by which LTC_4 induced this protection has not been elucidated. The magnitude of the protection in vivo (3) was greater than the protection observed in vitro (4), indicating that specific cellular activities as well as physiological processes at the tissue and organ level may be important in vivo. The V79 cell provides a controlled model system in which to specifically study the cellular responses to LTC_4 that are important in the radioprotective response. In view of the observation that trypsinization attenuated LTC_4-induced radioprotection in the V79 model, studies were conducted to assess the possibility that LTC_4 receptors could be detected on V79 cells. The properties of LTC_4 interaction with V79 cells are described in this communication. In the companion communication that follows this report (5), we describe additional studies that determine the subcellular localization of LTC_4 binding by V79 cells and demonstrate that this binding site is distinct from that of glutathione-S-transferase, which is known to bind LTC_4.

Methods

Materials. Leukotrienes were a gift from Dr. J. Rokach (Merck Frosst Canada, Inc., Pointe Claire-Dorval, Quebec). Prostaglandin D_2 was a gift from Dr. D. Morton (Upjohn, Kalamazoo, MI). Other unlabeled eicosanoids were obtained from Cayman Chemical (Ann Arbor, MI). Tritiated eicosanoids and Aquasol-2 were obtained from New England Nuclear (Boston, MA). The leukotriene end point antagonists FPL 55712, LY 171883, and Revlon 5901-5 were gifts from Dr. A. Taub (Fison Corp., Bedford, MA), Mr. W. Fields (Lilly Research Laboratories, Indianapolis, IN), and Dr. T. P. Pruss (Rorer Group, Inc., Tuckahoe, NY), respectively. Nucleotides, trypsin, neuraminidase, hyaluronidase, glutathione-S-transferase, and 1-chlor-2,4-dinitrobenzene were obtained from Sigma (St. Louis, MO); Whatman glass-fiber filters (GF/B) from Fisher Scientific (Pittsburgh, PA); Iscove's Modified Dulbecco's Medium (IMDM), Medium 199 (M199), Hank's buffered salt solution (HBSS) and Ca^{2+},Mg^{2+}-free HBSS from MA Bioproducts (Walkersville, MD); α-minimal essential medium (MEM) with Earl's salts and fetal bovine serum (FBS) from Gibco (Grand Island, NY); and KINETIC-LIGAND program from Elsevier-Biosoft (Cambridge, U.K.).

Cell Culture. Cells were grown either in MEM or IMDM supplemented with 10% FBS and maintained as monolayers in both culture flasks and roller bottles at 37°C under humidified 95% air:5% CO_2. Cells were harvested by exposure for 10 min to 0.002% EDTA in phosphate-buffered saline at pH 7.35. Harvested cells were washed, resuspended in HBSS, and counted using a hemocytometer. All cells used in these experiments were harvested during the log growth phase.

Binding Assays. Binding assays were conducted in a reaction buffer composed of HBSS containing 25 mM HEPES and 10 mM serine-borate. Serine-borate was added to block metabolism of LTC_4 (6). After completion of studies to optimize time, pH, and temperature, incubations were conducted in pH 7.35 reaction buffer at 4°C, in a shaking water bath for 30 min. Assay tubes contained 10^5-10^7 cells, 20-70 fmol [^{3}H]-LTC_4 (specific activity 40 Ci/mmol) and reaction buffer in a total volume of 50-100 μl. Nonspecific binding was assessed by determining the binding of [^{3}H]-LTC_4 in the presence of excess unlabeled LTC_4 (16 μM). All binding assays were conducted in triplicate or quadruplicate.

Binding assays were terminated by dilution with 3 ml of ice-cold HBSS. The cell-bound radioactivity was recovered either by centrifugation at 2000 x g for 5 min to pellet the cells followed by aspiration of the supernatant or by filtration through Whatman GF/B filters on a Yeda filtration manifold. Retentates were solubilized in scintillation fluid (Aquasol-2), and bound radioactivity was assessed on a Tracor Analytic Mark III scintillation counter. The centrifugation and filtration methods yielded similar recoveries of tritiated ligand. Scatchard analyses were performed by incubating aliquots of cells with tritiated ligand and graded levels of unlabeled ligand from 0 to 16 μM/assay tube. The resulting displacement curves were transformed to Scatchard plots using LIGAND. All experiments reported herein were replicated at least once, and results are presented as means ± SEM unless otherwise indicated. Kinetic data were evaluated using KINETIC.

Binding Specificity: Eicosanoids and Leukotriene Antagonists. Specificity of LTC_4 binding was assessed by adding 1 μg of selected eicosanoids (100 μl total volume) to assay tubes. The following eicosanoids were individually tested: LTC_4, LTA_4, LTB_4, LTD_4, LTE_4, PGA_2, PGB_2, PGD_2, PGE_2, $PGF_{2\alpha}$, 5-HETE, and 12-HETE. Additional binding assays were conducted in the presence of varying concentrations of the putative leukotriene receptor antagonists LY 171883, FPL 55712, or REV 5901-5 and using graded concentrations of the isomer 14,15-LTC_4.

Cationic and Nucleotide Requirements. Cells were harvested in Ca^{2+},Mg^{2+}-free HBSS that contained 0.002% EDTA. The pelleted cells were washed twice in Ca^{2+},Mg^{2+}-free HBSS and aliquoted into four groups for binding assays. Group (a) binding assays were conducted in 100 μl of Ca^{2+},Mg^{2+}-free HBSS containing 0.02% EDTA; group (b) contained Ca^{2+},Mg^{2+}-free HBSS; group (c) contained complete HBSS (9.5×10^{-4} M Ca^{2+} and 9.0×10^{-4} M Mg^{2+}); and group (d) contained M199. Nucleotide requirements were assessed by modifying the standard ligand assay to include 1 μg/tube of cAMP, ATP, or GTP.

Examination of Other Eicosanoid Receptors on V79 Cells. Specific binding to V79 cells by PGD_2, PGE_2, $PGF_{2\alpha}$, LTD_4, LTE_4, and LTB_4 was examined by a modification of the standard LTC_4 ligand assay replacing the [^{3}H]-LTC_4 with the other [^{3}H]-labeled eicosanoids. Nonspecific binding was determined by adding a 100-fold molar excess of the respective unlabeled eicosanoid.

High-Performance Liquid Chromatography. Purity of leukotrienes was routinely monitored by high-performance liquid chromatography (HPLC) prior to use in binding assays. Reversed-phase HPLC was conducted as previously described (2,7) using either a Beckman or LKB GTi system with an Ultrasphere (Beckman Inc., Columbia, MD) C-18 column, 4.6 x 250 mm, packed with 5-μm particles. Leukotrienes were eluted using 35% (v/v) acetonitrile/water containing 0.1% acetic acid at a pH adjusted to 5.8 with ammonium hydroxide and at a flow rate of 1.0 ml/min. Unlabeled leukotrienes were detected by absorbance at 280 nm. Tritiated leukotrienes were located on chromatographs by collecting fractions and assessing radioactivity with liquid scintillation counting or with an HPLC flow-through radiation monitor (RAMONA-D; IN/US, Inc.).

Metabolism of [^{3}H]-LTC_4 was assessed by incubating 10^6 cells with 112 fmol

[^{3}H]-LTC_4 at 4°C for periods of up to 1 hr. Following incubation, labeled material was extracted from the assay mixture containing cells and medium as described (2). Briefly, the pH of the medium was adjusted to 3.0 with HCl, followed by addition of 100 µl of isopropyl alcohol and 2.0 ml of ethyl acetate. This mixture was sonicated to maximize dissolution of the cellular membrane and centrifuged at 1000 x g for 5 min. More than 98% of the radiolabel was extracted. The extract was evaporated to dryness, resuspended in HPLC mobile phase buffer, and analyzed by HPLC. Radioactivity in the eluate was identified by coelution with known standards.

Statistical Analyses. All experiments were replicated at least once, with equivalent results. Scatchard analyses were derived from displacement curves in duplicate. Other determinations were conducted in triplicate. Differences between treatments were assessed by student's t-test.

Results

Optimization of Binding Assay. The pH dependence of [^{3}H]-LTC_4 binding was examined using whole cells. Cells were pelleted by centrifugation, and then resuspended in medium in which the pH of the reaction buffer was adjusted with NaOH or HCl to 6.2, 6.8, 7.35, 8.0, 8.4, 8.8, or 9.2. Binding assays were conducted as described in Methods. Binding plateaued between pH 6.2 and 8.0 (Fig. 1) and decreased at higher pH values (>8.0). Subsequent binding assays were conducted at pH 7.35.

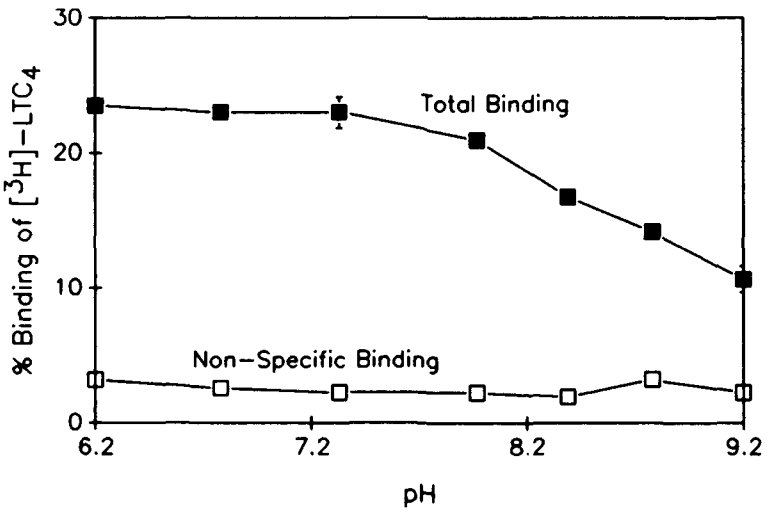

Fig. 1. Optimum pH for Binding of [^{3}H]-LTC_4 to V79 Cells. Total binding (■) was determined in assay tubes containing 10^6 cells and 1.3 nM [^{3}H]-LTC_4, incubated in 50 µl assay buffer in which pH was adjusted with either NaOH or HCl. Nonspecific binding (□) was assessed in parallel tubes containing 16 µM unlabeled LTC_4. Mean ± S.D.

Binding assays were optimized for incubation time and temperature. Parallel sets of tubes with or without 1 μM unlabeled LTC_4 were incubated for 0, 15, 30, 45, or 60 min at 4°, 22° and 37°C. This experiment was conducted in the absence of serine-borate to assess the contribution of cellular levels of γ-glutamyl transpeptidase to binding. Radiolabeled LTC_4 was rapidly bound by cells (Fig. 2) and binding approached maximal levels within 15 min at either 4°C or 22°C. Binding at 37°C was lower and more variable than at lower temperatures (data not shown). HPLC analyses (reported in reference 2) confirmed catabolism of [^{3}H]-LTC_4 at the higher temperatures. Parallel groups of tubes were incubated in the absence of cells (cell blanks) at both 4°C and 22°C. Because binding at 4°C and 22°C in both the nonspecific and cell blank groups were similar, for clarity only the data from the 4°C incubation for these two groups are included in Fig. 2. A better estimate of nonspecific binding was obtained by increasing unlabeled LTC_4 from 1 μM to 16 μM. This reduced nonspecifically bound radioactivity to levels not different from bound radioactivity in the absence of cells (data not shown). On the basis of these results, subsequent binding assays were conducted in triplicate at 4°C for 30 min, and nonspecific binding was assessed in the presence of 16 μM LTC_4.

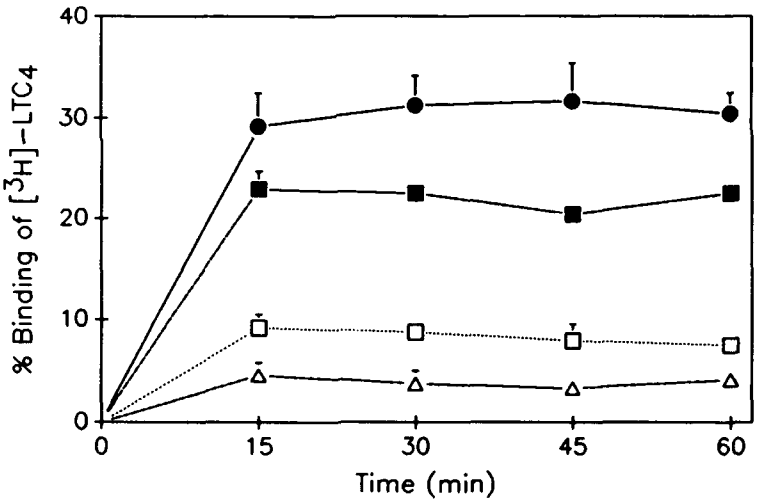

Fig. 2. Time and Temperature Dependence of [^{3}H]-LTC_4 Binding to V79 Cells. Assay tubes containing 5 x 10^5 cells and 1.3 nM [^{3}H]-LTC_4 in 50 μl assay buffer were incubated for the indicated times at 4°C (●) or 24°C (■). Parallel series of tubes were incubated at 4°C containing 1 μM unlabeled LTC_4 (□) or lacking cells (Δ). Mean ± S.D.

Association and Dissociation of [^{3}H]-LTC_4. To determine the rate of association of [^{3}H]-LTC_4 with the receptor, aliquots of the cells were incubated for 2, 4, 6, 10, 20, 30, and 60 min (Fig. 3). To determine the dissociation rate, 10 min after the incubations were initiated, 16 μM of unlabeled LTC_4 was added to a parallel set, and those incubations were terminated at the indicated times (Fig. 4). KINETIC was used to generate lines that best fit the data.

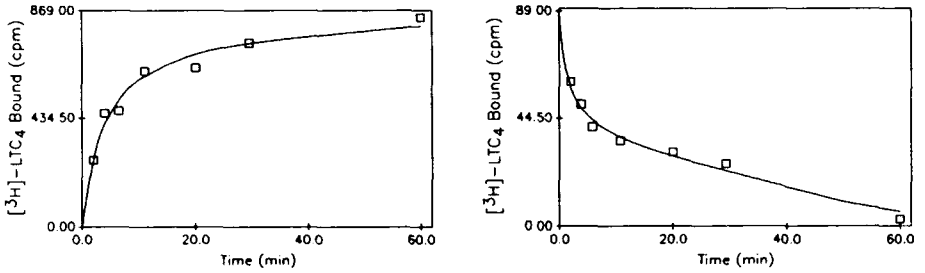

Association (**Fig. 3**) and Dissociation (**Fig. 4**) of [^{3}H]-LTC_4 by Intact V79 Cells. 10^6 cells/tube were incubated at 4°C with 1.3 nM [^{3}H]-LTC_4 in 50 µl assay buffer. Dissociation rate was monitored in tubes to which 10 µl unlabeled LTC_4 (16 µM final concentration) was added after an initial incubation of 10 min. All incubations were terminated by filtration at indicated times. Curves were generated using KINETIC and a two-site model (Association: 54% K_{ass1} = 0.032 ± 0.028; 46% K_{ass2} = 0.86 ± 0.23. Dissociation: 41% K_{dss1} = 0.032 ± 0.013; 59% K_{dss2} = 0.77 ± 1.25).

Identification of Binding Products. V79 cells metabolize LTC_4 to LTD_4 and LTE_4 when incubations are conducted at 37°C (2). Therefore, reversed phase HPLC was used to assess radiolabeled products obtained after incubation of V79 cells with [^{3}H]-LTC_4. No metabolism of LTC_4 was detected during incubations at 4°C for up to 1 hr (Fig. 5), demonstrating that binding was attributable to LTC_4 and not a metabolic product such as LTD_4 or LTE_4. This also suggested that the binding process did not alter the ligand, and that when released from the binding site LTC_4 could bind again.

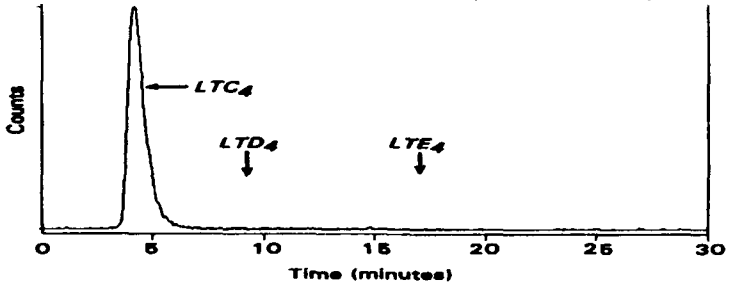

Fig. 5. High Performance Liquid Chromatrography (HPLC) Analysis of [^{3}H]-LTC_4 Binding Products. V79 cells were incubated with [^{3}H]-LTC_4, then extracts were analyzed by HPLC as described in Methods. Units of radioactivity are not provided on the abscissa, because area under the LTC_4 peak (10,000 dpm) accounts for all labeled material recovered. Arrows indicate regions of elution of authentic standards of LTD_4 and LTE_4.

Binding Specificity. V79 cells were incubated with selected tritiated eicosanoids to determine the presence of other classes of eicosanoid receptors or specific binding sites. Incubations with tritiated PGD_2, PGE_2, and $PGF_{2\alpha}$ did not result in tracer binding that was displaceable by 100-fold molar excess of the respective unlabeled ligand. Incubations

with tritiated LTD_4 resulted in minimal and inconsistent levels of specific binding (data not shown). Glutathione at concentrations of up to 3 μM had no effect on [^{3}H]-LTC_4 binding (data not shown).

Table 1. Specificity of [^{3}H]-LTC_4 Binding.[a]

Eicosanoid	Control Binding (%)[b]
LTC_4	16.6 ± 1.9[c]
LTA_4	98.4 ± 5.2
LTB_4	105.4 ± 8.5
LTD_4	107.3 ± 15.9
LTE_4	94.5 ± 8.7
PGA_2	79.8 ± 8.5[c]
PGB_2	107.5 ± 5.1
PGD_2	95.6 ± 3.7
PGE_2	106.9 ± 3.5
$PGF_{2\alpha}$	126.3 ± 11.9
5-HETE	100.1 ± 4.8
12-HETE	116.3 ± 13.6

[a] 10^6 cells/tube in 50 μl buffer were incubated at 4°C for 30 min with 30 fmol [^{3}H]-LTC_4 and 1 μg of each eicosanoid.
[b] ($\bar{x}$ ± SEM)
[c] P<.001 by t-test

Table 1 shows the capacity of various eicosanoids to displace [^{3}H]-LTC_4. Only LTC_4 and PGA_2 competed with [^{3}H]-LTC_4 for binding to V79 cells. The isomer of LTC_4 14,15-LTC_4 competed with [^{3}H]-LTC_4 for binding, although the displacement curve for 14,15-LTC_4 was displaced appreciably to the right of that by LTC_4 (Fig. 6).

To assess further the specificity of LTC_4 binding, V79 cells were incubated with compounds that have reported leukotriene antagonist activity. The compounds LY 171883, FPL 55712, or REV 5901-5 did not affect LTC_4 binding (Fig. 7). Interestingly, binding actually tended to be higher in the presence of LY171883 or REV5901-5.

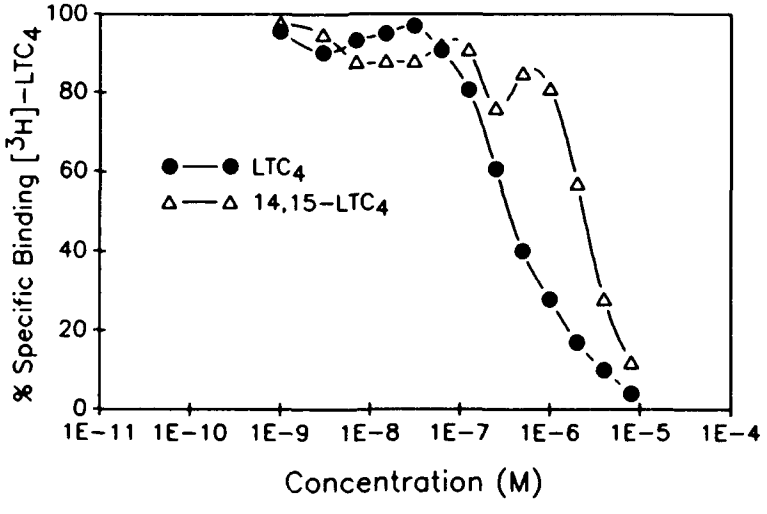

Fig. 6. Competition by 14,15-LTC_4 for Binding to V79 Cells. Parallel displacement curves were conducted using LTC_4 (•) or the 14,15 isomer of LTC_4 (Δ).

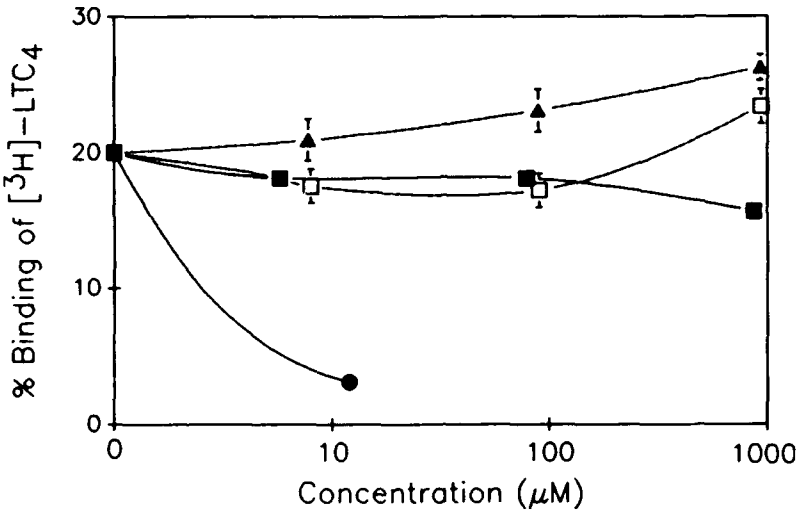

Fig. 7. Effect of Leukotriene Antagonists on LTC_4 Binding. 10^6 V79 cells were incubated at 4°C for 30 min with 1 nM [^{3}H]-LTC_4 and differing concentrations of either LTC_4 (•), LY 171883 (□), FPL 55712 (■), or REV 5901-5 ( ).

LTC_4 and LTD_4 binding to tissues may be influenced by monovalent and divalent cations (8,9,10), and nucleotides (10,11). To determine if media components influence the binding of LTC_4, V79 cells were incubated with [^{3}H]-LTC_4 in media of differing compositions. No difference in binding was detected when assays were conducted in M199, HBSS, Ca^{2+}/Mg^{2+}-free HBSS, Ca^{2+}/Mg^{2+}-free HBSS containing 0.01% EDTA, or 25 mM Tris-1 mM $CaCl_2$ (pH 7.35 in all buffers). Also, binding of [^{3}H]-LTC_4 was not significantly altered by inclusion of 1 μg/100 μl of cAMP, ATP, or GTP in HBSS (data not shown).

Scatchard Analyses. Scatchard analyses were conducted using either live cells or cells that were previously frozen and stored in pellets at -80°C. To determine if freezing affected Scatchard analyses, pools of V79 cells were divided into two aliquots. One aliquot was placed on ice for 12 hr, while the other was pelleted, frozen, and stored for 12 hr at -80°C. Subsequent Scatchard analyses revealed no differences in LTC_4 binding abundance or affinities (data not shown). A summary of Scatchard analyses conducted on eight separate pools of cells was curvilinear, having high-affinity [Kd = 2.5 ± 0.63 nM; 9.9 x 10^5 sites/cell) and low-affinity [Kd = 350 ± 211 nM; 2.7 x 10^6 sites/cell] binding sites (Fig. 8).

Discussion

LTC_4 plays a role in controlling the lungs (12,13,14,15), cardiovascular system (12,16) and smooth muscle (12). LTC_4-immunoreactive neurons identified in the hypothalamic median eminence (17), in which LTC_4 has been demonstrated as a potent mediator of gonadotropin-releasing hormone (18) and LTC_4 in very small amounts induces gonadotropin release from anterior pituitary cells in vitro (17). Binding of LTC_4 to rat lung fibroblasts was

correlated with stimulation of collagen by the treated cells (19). However, the contribution of LTC_4 in regulation of some physiologic processes has proven controversial because a number of cell and tissue types contain "binding sites" for LTC_4 without demonstrable biologic responsiveness to LTC_4 (20).

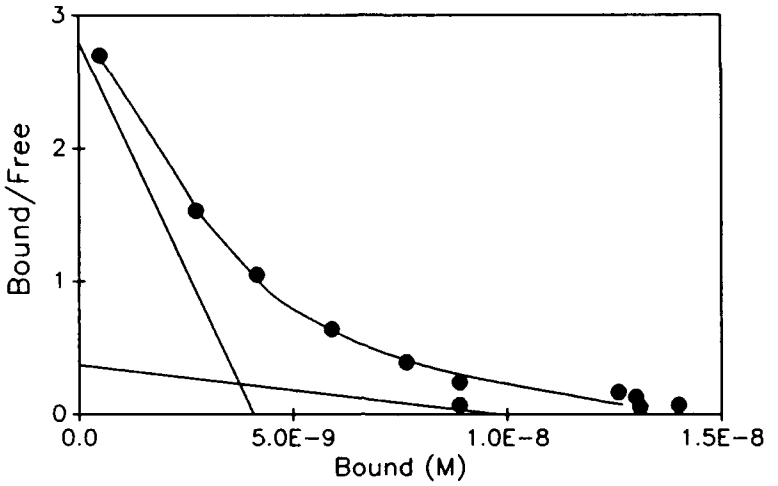

Fig. 8. Scatchard Analysis of [^{3}H]-LTC_4 Binding Sites on V79 Cells. Incubations were conducted at 4°C for 30 min using 10^6 cells and 1.3 nM of [^{3}H]-LTC_4 per tube, while concentrations of unlabeled LTC_4 ranged from 0-16 μM. Displacement curves were transformed to Scatchard plots using LIGAND, which revealed high-affinity (Kd = 2.5 ± 0.63 nM) and low-affinity (Kd = 350 ± 211 nM) binding sites.

A series of criteria has been established for distinguishing receptor-mediated events from events of a less specific nature. One summarization of the events that classically elevate the events of a tissue-ligand interaction to a receptor-mediated event (21) included the criteria of drug displacement, correlation between drug affinity in vitro and pharmacological potency, regional distribution, subcellular distribution, stereospecificity, saturability, reversibility and high affinity. Our studies indicate that the interaction of LTC_4 with V79 cells satisfies most, but not all, of the criteria describing a classical "receptor": our studies demonstrate reasonable levels of saturability, reversibility, stereospecificity, pharmacologic potency, and high affinity. Regional distribution of binding is not applicable in our studies using a cell line. The issue of subcellular distribution is assessed in the companion communication (5), and the issue of drug displacement is addressed below.

As outlined in Table 1, competition with [^{3}H]-LTC_4 for binding to the intact V79 cell was specific for LTC_4 and was not displaceable to a significant degree by other classes of leukotrienes or by a molecular component of LTC_4, glutathione. The 14,15-isomer of LTC_4 exhibited approximately 10% potency. LTC_4 binding was not displaceable by a number of structurally similar and pharmacologically similar compounds, including

a long list of prostaglandins (Table 1). The inhibition of binding by PGA_2 was unusual but repeatable and it is not known whether this was a direct or indirect effect on the receptor protein. Specific antagonists for LTC_4 are not presently available. There are several antagonists for LTD_4 and LTE_4, including FPL 77512 (9,22), LY 171883 (23), and REV 5901-5 (24), but these compounds do not antagonize LTC_4 effects or binding to a great degree (9,22,24). Therefore, it was not surprising that they were ineffective antagonists to LTC_4 binding by the V79 cell, but they indicate common specificity patterns among LTC_4 receptors. The specificity of the receptor was further confirmed when these LTD_4 and LTE_4 antagonists did not compete for the LTC_4 binding sites.

The curvilinear Scatchard plots describing LTC_4 binding to intact V79 cells suggested either multiple classes of binding sites or negative cooperativity in LTC_4 binding. Because the curvilinear Scatchard plots were not demonstrable in binding assays using plasma membrane or nuclear V79 cell preparations (5), it seems most likely that multiple classes of binding sites were revealed in binding assays using intact V79 cells. While the low-affinity binding sites on V79 cells were more abundant than the high-affinity sites (low-affinity binding was approximately 70% of total specific binding), the high-affinity sites on V79 cells were relatively abundant in comparison with reported abundance in other cell lines. For example, the cumulative binding site abundance using intact V79 cells was approximately tenfold higher than that reported for the DDT1M2F hamster smooth muscle cell line (25).

The binding affinities of LTC_4 to V79 cells correlated with doses of LTC_4 that decreased the radiosensitivity of this cell line. In radioprotection studies, pretreatment with 0.5×10^{-6} M LTC_4 was minimally effective, while 2.5×10^{-6} M LTC_4 conferred greater radioprotection (2). Thus LTC_4-conferred radioprotection in the V79 cell line, while not a usual physiologic event, nevertheless provides a correlation of pharmacological potency with the affinity range determined for LTC_4 binding.

V79 cells metabolize LTC_4 to LTD_4 and LTE_4 when cultured at 37°C, and both cells and tissue culture medium possess γ-glutamyl transpeptidase activity (2). Enhanced degradation of LTC_4 may explain the decrease in binding observed with increasing incubation temperature (Fig. 2). The addition of serine-borate, a transition state inhibitor of γ-glutamyl transpeptidase (6), decreased the possibility of LTC_4 degradation in later experiments. HPLC analysis of products from the binding assay suggested that LTC_4 was not decomposed or metabolized during binding studies conducted at 4°C.

The LTC_4 binding site in V79 cells, like the rat glomeruli binding site (26), did not appear to require Na^+, Ca^{2+}, or Mg^{2+} for binding activity. Guanine nucleotides were reported to regulate the binding of LTD_4 to guinea pig lung membranes (10), but appeared to have no effect on LTC_4 receptors in either the guinea pig myocardium (8) or in V79 cells. The V79 cell was reportedly responsive to agents that stimulate cyclic AMP, including prostaglandins (27). The latter is interesting in light of our inability to demonstrate specific binding of several tritiated prostaglandins by this cell line. In particular, we did not observe specific binding of PGE_2 by V79 cells. It was reported in a prior study that pretreatment with PGE_2 did not confer radioprotection of V79 cells (28), which is not

inconsistent with the hypothesis that eicosanoid-induced radioprotection is receptor mediated.

The mechanism by which LTC_4 confers radioprotection to the V79 cell is unknown, although leukotrienes may induce synthesis of cAMP (29), cGMP (29), or other eicosanoids (30), which may in turn have protective effects. Further studies are needed to clarify the mechanism by which LTC_4 protects V79 cells from the deleterious effects of irradiation, although our studies suggest that LTC_4 may interact with V79 cells through a receptor-mediated event. In view of its abundant LTC_4 binding capacity, the V79 cell line may provide both an excellent source for leukotriene receptor purification and a model for defining certain cellular responses to leukotrienes.

Acknowledgements

The authors gratefully acknowledge gifts of V79 cells from Dr. E. V. Holahan, leukotrienes from Dr. J. Rokach, prostaglandins from Dr. D. Morton, and leukotriene antagonists from Dr. A. Taub, Mr. W. Fields and Dr. T. P. Pruss. Valuable technical assistance was provided by C. Hollies. J. Koeser and M. Waldbillig provided skilled secretarial assistance. This work was supported by NIH HD20780, USUHS Protocol C08517, and Defense Nuclear Agency Work Unit #B2152. The views presented in this paper are those of the authors. No endorsement by the Defense Nuclear Agency or the Department of Defense has been given or should be inferred.

References

1. Furuta Y., E.R. Hall, S. Sanduja, T. Barkley Jr., and L. Miles. Prostaglandin Production by Murine Tumors as a Predictor for Therapeutic Response to Indomethacin. *Cancer Res.* 48:3002. 1988.
2. Walden, T.L., E.V. Holahan, and G.N. Catravas. Development of a Model System to Study Leukotriene-Induced Modification of Radiation Sensitivity in Mammalian Cells. *Prog. Lipid Res.* 25:587. 1986.
3. Walden Jr, T.L., M.L. Patchen, and T.J. MacVittie. Leukotriene-Induced Radioprotection of Hematopoietic Stem Cells in Mice. *Radiat. Res.* 113:388. 1988.
4. Walden Jr, T.L. Pretreatment with Leukotriene C_4 Enhances the Whole-Animal Survival of Mice Exposed to Ionizing Radiation. *Ann. N.Y. Acad. Sci.* 524:431. 1988.
5. Liu, Y.X., D.S. Watt, T.L. Walden Jr, and T.A. Fitz. Interaction of Leukotriene C_4 and Chinese Hamster Lung Fibroblasts (V79A03 Cells). 2. Subcellular Distribution of Binding and Unlikely Role of Glutathione-S-Transferase. *Prostaglandins*, this volume.
6. Tate, S.S., and A. Meister. Serine-Borate Complex as a Transition State Inhibitor of Gamma-Glutamyl Transpeptidase. *Proc. Natl. Acad. Sci. USA* 75:4806. 1978.
7. Borgeat, P., and B. Samuelsson. Arachidonic Acid Metabolism in Polymorphonuclear Leukocytes: Effects of Ionophore A23187. *Proc. Natl. Acad. Sci. USA* 76:2148. 1979.
8. Hogaboom, G.K., S. Mong, J.M. Stadel, and S.T. Crooke. Characterization of Guinea Pig Myocardial Leukotriene C_4 Binding Sites: Regulation by Cations and Sulfhydryl-Directed Reagents. *Mol. Pharmacol.* 27:236. 1985.

9. Rovati, G.E., D. Oliva, L. Sautebin, G.C. Folco, A.F. Welton, and S. Nicosia. Identification of Specific Binding Sites for Leukotriene C_4 in Membranes from Human Lung. *Biochem. Pharmacol.* 34:2831. 1985.
10. Mong, S., H.-L. Wu, G.K. Hogaboom, M.A. Clark, J.M. Stadel, and S.T. Crooke. Regulation of Ligand Binding to Leukotriene D_4 Receptors: Effects of Cations and Guanine Nucleotides. *Eur. J. Pharmacol.* 106:241. 1984.
11. Hogaboom, G.K., S. Mong, H.-L. Wu, and S.T. Crooke. Peptidoleukotrienes: Distinct Receptors for Leukotriene C_4 and D_4 in the Guinea Pig Lung. *Biochem. Biophys. Res. Commun.* 116:1136. 1983.
12. Sirois, P. Pharmacology of the Leukotrienes. *Adv. Lipid Res.* 21:79. 1985.
13. Samhoun, N.M., and P.J. Piper. In: *Leukotrienes and Other Lipoxygenase Products.* (P.J. Piper, ed.) Research Studies Press, New York, 1982, p. 161.
14. Dahlen, S.-E. Pulmonary Effects of Leukotrienes. *Acta Physiol. Scand. Suppl.* 512:1. 1983.
15. Dahlen, S.-E., G. Hansson, P. Hedqvist, T. Bjorck, E. Granstrom, and B. Dahlen. Allergen Challenge of Lung Tissue from Asthmatics Elicits Bronchial Contraction That Correlates With the Release of Leukotrienes C_4, D_4, and E_4. *Proc. Natl. Acad. Sci. USA* 80:1712. 1983.
16. Feuerstein, G., Z. Zukowska-Grojec, and I.J. Kopin. Cardiovascular Effects of Leukotriene D_4 in SHR and WKY Rats. *Eur. J. Pharmacol.* 76:107. 1981.
17. Hulting, A.L., J.A. Lindgren, T. Hokfellt, P. Eneroth, S. Werner, C. Patrono, and B. Samuelsson. Leukotriene C_4 as a Mediator of Luteinizing Hormone Release From Rat Anterior Pituitary Cells. *Proc. Natl. Acad. Sci. USA* 82:3834. 1985.
18. Wisner-Provost, A., K. Gerozissis, M.C. Bommelaer, C.A. Renard, C. Rougeot, F.A. Levi, and F. Dray. Eicosanoids in Relation With LHRH Secretion. *Adv. Prostaglandin Thromboxane Leukotriene Res.* 16:235. 1986.
19. Phan S.H., B.M. McGarry, K.M. Loeffler, and S.L. Kunkel. Binding of Leukotriene C_4 to Rat Lung Fibroblasts and Stimulation of Collagen Synthesis In Vitro. *Biochemistry* 27:2846. 1988.
20. Sun, F.F., L.Y. Chau, and K.F. Austen. Binding of Leukotriene C_4 by Glutathione Transferase: A Reassessment of Biochemical and Functional Criteria for Leukotriene Receptors. *Federation Proceedings* 46:204. 1987.
21. Laduron, P.M. Criteria for Receptor Sites in Binding Studies. *Biochem. Pharmacol.* 33:833. 1984.
22. Drazen, J.M., K.F. Austen, R.A. Lewis, D.A. Clark, G. Goto, A. Marfat, and E.J. Corey. Comparative Airway and Vascular Activities of Leukotrienes C_4 and D_4 In Vivo and In Vitro. *Proc. Natl. Acad. Sci. USA* 77:4351. 1980.
23. Fleisch, J.H., L.E. Rinkema, and W.S. Marshall. Commentary: Pharmacological Receptors for the Leukotrienes. *Biochem. Pharmacol.* 33:3919. 1984.
24. Gordon, R.J., J. Travis, H.R. Godfrey, D. Sweeny, P.S. Wolf, T.P. Pruss, E. Neiss, J. Musser, U. Chakraborty, H. Jones, and M. Leibowitz. In Vivo Activity of a Lipoxygenase Inhibitor and Leukotriene Antagonist. Abstract #261 in *Prostaglandins and Leukotrienes '84*, Washington, D.C. 1984.
25. Clark, M.A., M. Cook, S. Mong, G.K. Hogaboom, R. Shorr, J. Stadel, and S.T. Crooke. Leukotriene C_4 ($[^3H]LTC_4$) Binding to Membranes Isolated From a Hamster Smooth Muscle Cell Line (DDT1MF2). *Life Sci.* 35:441. 1984.

26. Ballerman, B.J., R.A. Lewis, E.J. Corey, K.F. Austin, and B.M. Brenner. Identification and Characterization of Leukotriene C_4 Receptors in Isolated Rat Renal Glomeruli. *Circ. Res.* 56:324. 1985.
27. Lehnert, S. Modification of Postirradiation Survival of Mammalian Cells by Intracellular Cyclic AMP. *Radiat. Res.* 62:107. 1975.
28. Holahan, E.V., W.F. Blakely, and T.L. Walden. In: *Prostaglandin and Lipid Metabolism in Radiation Injury* (T.L. Walden and H.N. Hughes, eds.) Plenum Press, New York, 1982, p. 253.
29. Vesin, M.F., S. Bourgoin, D. Leiber, and S. Harbon. Lipoxygenase and Cyclooxygenase Products of Arachidonic Acid in Uterus. Selective Interaction With cGMP and cAMP Systems. *Prost. Leuko. Med.* 13:75. 1984.
30. Feuerstein, N., M. Foegh, and P.W. Ramwell. Leukotrienes C_4 and D_4 Induce Prostaglandin and Thromboxane Release Rrom Rat Peritoneal Macrophages. *Br. J. Pharmacol.* 72:389. 1981.

Editor: P. Ramwell Received: 5-18-87 Accepted 8-16-90

JOURNAL OF NEUROPHYSIOLOGY
Vol. 62, No. 4, October 1989. Printed in U.S.A.

Membrane Current Underlying Muscarinic Cholinergic Excitation of Motoneurons in Lobster Cardiac Ganglion

JOSEPH E. FRESCHI AND DAVID R. LIVENGOOD
Department of Neurology, Emory University School of Medicine, Atlanta, Georgia 30322

SUMMARY AND CONCLUSIONS

1. We studied the effect of cholinergic agonists on motoneurons of the lobster cardiac ganglion under voltage clamp.

2. In unclamped neurons, acetylcholine (ACh) caused a depolarization and increase in burst potential frequency. By the use of nicotinic and muscarinic agonists, we determined that both types of receptors are present on the neurons. We therefore used specific muscarinic agonists to further study ionic mechanisms underlying the muscarinic cholinergic current (I_{mch}).

3. Muscarinic agonists produced detectable inward current at doses above 10^{-6} M, and maximum effect was seen at doses above 10^{-3} M.

4. I_{mch} was voltage-dependent. When the membrane holding potential was shifted to levels negative to the resting potential, the response declined, nulling but not reversing at −80 to −100 mV. The response enlarged with membrane depolarization, reaching a maximum at between −30 and −10 mV. With further depolarization, the response declined and then reversed at potentials around +20 mV.

5. The muscarinic response varied as a function of extracellular Na^+ concentration and was completely blocked in Na^+-free solutions. The relationship between response amplitude and external Na^+ was well described by the electrodiffusion equation for Na^+ driving force.

6. I_{mch} amplitude also varied as a function of extracellular potassium concentration, becoming larger with low external K^+ and smaller at higher concentrations. Shifting the Cl^- equilibrium potential did not affect the properties of the I_{mch}.

7. Tetrodotoxin (TTX) had no effect on I_{mch}. In concentrations of 1–10 mM, such K^+-channel blocking agents as Ba^{2+}, Cs^+, 4-aminopyridine (4-AP), or tetraethylammonium (TEA), and such Ca^{2+}-channel blockers as Co^{2+} or Mn^{2+}, when applied externally, did not suppress I_{mch}. Above 30 mM, TEA did inhibit the response, and combinations of K^+-channel blocking agents, each at concentrations insufficient alone to block the current, also inhibited I_{mch}.

8. Current-voltage (*I-V*) curves obtained during muscarinic agonist perfusion consistently crossed the control *I-V* curves at a mean membrane potential of +24 mV. The reversal potential shifted to a more negative value in low extracellular Na^+.

9. Although no reversal of I_{mch} was seen when agonists were applied to cells clamped at negative holding potentials, the averaged curve of I_{mch}, obtained by subtracting control ramp *I-V* curves from those obtained in the presence of agonist, did show a small net outward current at membrane potentials negative to −100 mV.

10. We conclude that ACh, acting at muscarinic receptors, causes an inward current predominantly by activating a voltage-dependent cation current that is largely carried by Na^+. The current is also dependent on extracellular K^+ concentration.

INTRODUCTION

Acetylcholine (ACh) acts at both nicotinic and muscarinic receptors in crustacean nervous systems (Florey 1963; Gerschenfeld 1973; Marder et al. 1985, 1986). The electrophysiological responses coupled to activation of cholinergic receptors are similar to those found in vertebrates. In the stomatogastric ganglion of lobsters, for example, cholinergic agonists cause a fast nicotinic depolarization, a slow muscarinic hyperpolarization, and a slow muscarinic depolarization (Marder et al. 1978, 1986). These responses, and an additional peptidergic slow depolarization (Hooper and Marder 1987), resemble the electrophysiology of vertebrate sympathetic ganglia (Kuba and Koketsu 1978).

In many crustacean species, ACh causes acceleration of the neurogenic heartbeat (Davenport 1942; Maynard 1955; Smith 1947; Welsh 1939; Wiersma and Novitski 1942). Previous studies by others suggested that the response to ACh in the crustacean cardiac ganglion is mediated by muscarinic receptors (Florey and Rathmayer 1980; Sullivan and Miller 1982; and M. W. Miller, personal communication). Barker and coworkers (1986) recently showed the presence of L-[^{3}H]quinuclidinyl benzilate binding sites in membranes from central ganglia of crab. These sites closely resembled muscarinic receptors in vertebrate central and peripheral nervous systems. There is preliminary evidence that muscarinic depolarization of certain lobster neurons may be because of a reduction in a resting K^+ conductance [cardiac ganglion (Sullivan and Miller 1982; M. W. Miller, personal communication) and stomatogastric ganglion (Nagy et al. 1985)]. We therefore wished to study in more detail the action of cholinergic agonists on cardiac ganglion motoneurons under voltage clamp.

In the experiments described here, we first examined the extent to which nicotinic responses might contribute to the total response to ACh. We then confined our studies on ionic mechanisms to those responses elicited by muscarinic agonists. We found that, although previous studies using current-clamp technique emphasized a reduction of a K^+ conductance, muscarinic agonists cause a slow, voltage-dependent inward current (I_{mch}) that is predominantly dependent on extracellular Na^+ concentration ($[Na]_o$). Furthermore, the response is also dependent on extracellular K^+ concentration ($[K]_o$), so that the ligand- and voltage-activated channel may be significantly permeable to K^+. Alternatively, or in addition, at negative membrane potentials the agonists may suppress a separate K^+ conductance.

METHODS

Preparation

We obtained specimens of lobster *Homarus americanus* (0.65–0.9 kg) from local food markets and kept them in a tank containing filtered, aerated, and cooled artificial seawater for up to 4 wk. We have previously reported the methods of dissection and descriptions of the recording chamber (Livengood et al. 1972, 1983). Following the methods of Tazaki and Cooke (1983, 1986), we ligated the axons of the anteriorly located motoneurons (*cells 1* and *2*) [for description of cardiac ganglion anatomy and terminology see Hartline (1967, 1979)]. We teased out a single strand of silk surgical suture and tied this around the ganglion trunk within 300 μm of the soma. In some experiments, where only comparative qualitative results were required, we studied unligated neurons, including *cells 3, 4*, and *5*. The amplitude of the cholinergic response was not diminished by proximal ligatures compared with responses from preparations unligated or ligated more distally (1–1.5 mm). Thus proximal ligation apparently did not exclude a significant fraction of cholinoreceptors.

We studied >100 neurons from >80 animals during a period of 18 mos. Although many of the figures show results from single experiments, we confirmed each observation in at least three repeated experiments. We required a membrane potential negative to −40 mV and an input resistance >1 MΩ before accepting a neuron for further study. Current-voltage curves were acceptable only if they returned to control values after muscarinic agonist washout.

Solutions and drugs

Normal saline was a modification of Cole lobster physiological saline and had the following composition (in mM): 440 NaCl, 15 KCl, 4 $MgSO_4$, 4 $MgCl_2$, 25 $CaCl_2$, 10 HEPES (*N*-2-hydroxyethylpiprazine-*N'*-2-ethanesulphonic acid), pH 7.4, adjusted with NaOH. We added drugs up to 50 mM without adjusting osmolality. We changed K^+ concentrations by adding or subtracting equal concentrations of Na^+. We substituted for Na^+ by replacing equal concentrations of Na^+ with either *N*-methyl-D-glucamine or Tris (tris[hydroxymethyl] aminomethane). We obtained all drugs from Sigma except 4-aminopyridine (4-AP) (Aldrich), $BaCl_2$ (Mallincrodt), and CsCl (Fisher). We diluted tetrodotoxin (TTX) from frozen aliquots of 1 mM stock and muscarine from 100 mM stock kept at 4° for <2 wk. We made up all other drug solutions on the day of the experiment. Dr. John Sarvey kindly donated dihydro-β-erythroidine.

Voltage-clamp recording

We used two microelectrodes, with tip resistances of 5–15 MΩ when filled with 3 M-KCl, to voltage clamp individual motoneurons. To reduce capacitative coupling, we placed a grounded copper shield between the two electrodes. The reference electrode was a saline-agar bridge, which, together with the voltage-clamp electrodes, we connected to the system electronics by means of a 3 M KCl/Ag/AgCl junction (WPI half-cell). We used a commercial voltage-clamp amplifier (Axoclamp-2, Axon Instruments, Burlingame, CA, USA) with the gain setting at the maximum value of 10,000 volt/volt, at which the maximum current that could be passed was 600 nA. We routinely filtered high-frequency noise at 1 KHz with an 8-pole Bessel filter and then recorded the voltage and current signals on a storage oscilloscope and penwriter. For penwriter recordings, the unfiltered frequency response was 140 Hz. For slow currents at high gain, the signal was low-pass filtered at 5 or 15 Hz. In most experiments we used a digital computer (PDP 11/23+, INDEC Systems, Sunnyvale, CA, USA) to generate families of command voltages and to store the evoked currents. The sampling rate was typically 2 ms for voltage steps of 440-ms duration and 200 ms for voltage ramps of 44-s duration.

The validity of voltage-clamping ligated cardiac ganglion motoneurons is discussed in detail in the paper by Tazaki and Cooke (1986). These authors have previously shown, by recording from both axon and soma, that there is little decline in evoked voltage changes along the axon for >300 μm. Tazaki and Cooke have estimated the resting neuron space constant to be 3 mm. Their data indicate that when current loss to the axon is prevented by ligation, current loss to remaining dendritic processes is minimal. Nevertheless, as noted by Tazaki and Cooke, even in ligated neurons there is inadequate clamp control of inward Ca^{2+} currents, as evidenced by variable delay in time to peak. We have verified, by the use of three independent microelectrodes, that imposed voltage changes in the soma are equally recorded in all electrodes. Such intracellular homogeneity, however, does not exclude the possibility that infoldings of the soma membrane may lead to imperfect voltage control of the membrane. Several other observations seem relevant. First, we have previously shown that the post-burst hyperpolarization can be reversed near the estimated K^+ equilibrium potential (E_K) in different $[K]_o$ (Livengood and Kusano 1972). Second, in both ligated and unligated neurons, by changing the holding potential, the current produced by γ-aminobutyric acid (GABA) can be reversed over the range expected by shifts in E_{Cl} (see RESULTS below). Third, as shown in the RESULTS, the inward current produced by muscarinic agonists can be reversed at positive membrane potentials, and we have found no difference in the reversal potentials (E_r) determined in ligated and unligated neurons. These observation suggest that the physiological events of interest in this paper occur within a spatially compact somatodendritic area wherein voltage control is adequate. Because our observations are essentially qualitative, and we have undertaken no kinetic studies, uncertainty about the adequacy of voltage-controlled membrane does not substantially affect the results of this study.

Curve fitting

To fit the averaged current-voltage data to a model equation, we used a commercial computer program (RS/Explore, BBN Software Products, Cambridge, MA) that uses the Marquardt-Levenberg iteration method for least-squares estimation of nonlinear parameters.

RESULTS

Effects of nicotinic and muscarinic cholinergic drugs on motoneurons

In unligated, unclamped motoneurons ACh caused a depolarization and increase in burst frequency (Fig. 1A_1). Both nicotine and muscarinic agonists mimicked the effect of ACh (Fig. 1, A_2 and A_3). The effect of nicotine was blocked by 0.1–1 mM (+)-tubocurarine (TC) and by 0.1 mM dihydro-β-erythroidine (not shown). The effect of muscarinic agonists was blocked by 10 μM-atropine and unaffected by TC at concentrations sufficient to block the response to nicotine (Fig. 1*B*). The response to muscarinic agonists was present on virtually all healthy neurons studied. On the other hand, responses to nicotine were variable. In some cases, such as that shown in Fig. 1*A*, nicotine

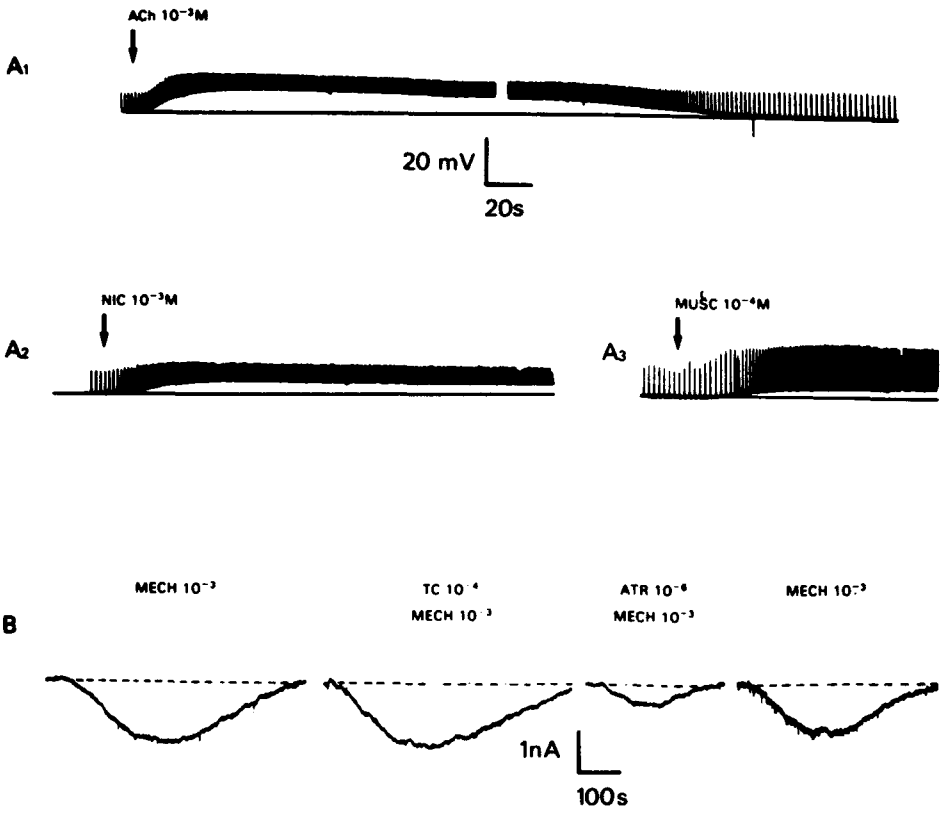

FIG. 1. Effect of cholinergic drugs on lobster motoneurons. *A*: effect of agonists on unligated *neuron* C_1 (for terminology see METHODS) under current clamp. A_1: effect of ACh on membrane potential and pacemaker burst frequency. Gap in record represents 7 min. Washout of ACh began after gap. A_2: effect of nicotine on same cell. Washout not shown. A_3: effect of muscarine on same cell. Washout not shown. *B*: effect of cholinergic antagonists on I_{mch} evoked by 1 mM MeCh. I_{mch} (control, *far left*) is unchanged in presence of 0.1 mM TC (*middle left*), but is reduced to 30% of control in presence of 10 μM atropine (*middle right*). After 10-min washout of atropine, response has returned to 80% of control (*far right*).

produced a response with an amplitude up to 50% of that caused by ACh; but in most cells the nicotinic response was small and accounted for no more than 10% of the total ACh amplitude. We were not interested in studying this in a detailed or systematic way. Nevertheless, our preliminary data suggested that ACh may activate both nicotinic and muscarinic receptors. Therefore, to study the muscarinic response in more detail, we used muscarinic agonists and not ACh. As shown in Fig. 1*B*, at the doses used in these experiments, muscarinic agonists such as methacholine (MeCh) had no nicotinic activity. Fig. 2 shows a representative dose-response curve for a voltage-clamped motoneuron exposed to increasing doses of MeCh. Half-maximal responses were obtained with doses of ~0.25 mM. Equal doses of muscarine, pilocarpine, and MeCh produced similar response amplitudes (data not shown).

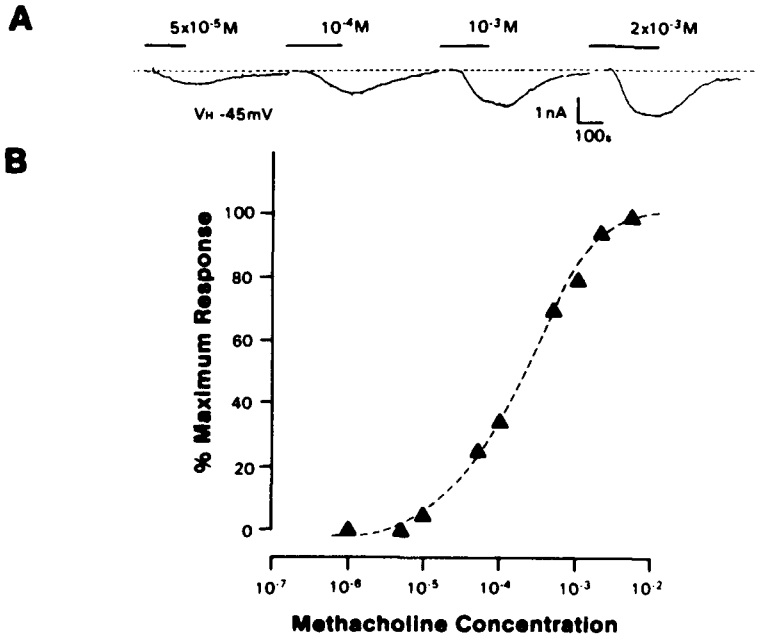

FIG. 2. Relationship between dose of MeCh and response amplitude in voltage-clamped ligated cardiac ganglion neuron. *A*: individual current records. Horizontal bar in this and subsequent figures indicates the duration of agonist perfusion. Dose of MeCh is indicated above each current trace. *B*, dose-response curve from the same neuron as in *A*. Although data are from 1 neuron, in all cells studied 1 mM represented a near-saturating dose of muscarinic agonist and was the routine dose used in all experiments.

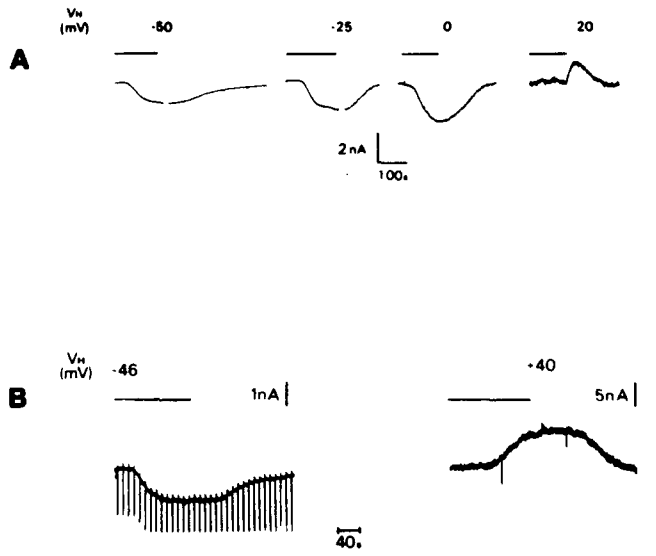

FIG. 3. Relationship between membrane potential and MeCh-induced current. Motoneurons were held at various membrane potentials by changing the voltage-clamp holding potential. Selected current traces are shown at the indicated holding potentials. *A* and *B* are from different cells. *A*: ligated C_1 neuron. *B*: unligated C_4 neuron. Note that in *B*, at −46 mV, large burst currents (cut off by chart recorder filter) generated from a remote area of the axon are inward. At +40 mV, the burst currents are small and outward. Note the different current scales in *B*.

Relationship between agonist-induced current and membrane potential

To determine the ionic basis of the muscarinic current (I_{mch}), we examined the response at various holding potentials (Figs. 3 and 4). In Fig. 4, data from five different neurons are plotted together against clamp-holding potential. Selected current traces from two of the neurons are shown in Fig. 3. In these and other experiments, in normal saline, the response amplitude enlarged at more depolarized potentials and diminished at hyperpolarized potentials. The potential at which the response was nulled was between −80 and −100 mV. Using this protocol, we have not seen a reversal of the response at negative potentials, even when E_K had been shifted positively by changes in $[K]_o$ (see below). On the other hand, when the membrane potential was held at positive membrane potentials (a condition often difficult to achieve), we were able to see a reversal of I_{mch}. Despite the expected decrease in driving force, these outward-going currents were considerably larger than those obtained at negative membrane potentials, suggesting a voltage dependence for I_{mch}.

Effects of changing the extracellular sodium concentration

The relationship between I_{mch} and membrane potential suggested the activation of an inward current chiefly mediated by ions with positive equilibrium potentials, such as Na^+ or Ca^{2+}. When Na_o was replaced by Tris or *N*-methyl-D-glucamine, the response was blocked (Fig. 5, *A* and *B*). The inhibitory effect of low $[Na]_o$ was not because of blocking the electrogenic Na^+-K^+ pump, because blocking the pump by 30 min exposure to K^+-free saline (not shown) or ouabain (Fig. 5*B*) did not inhibit I_{mch}. The relationship between I_{mch} amplitude and $[Na]_o$ (Fig. 5*C*) was well fit by a curve obtained by plotting the Na^+ current driving force (V_H-E_{Na}) as a function of $[Na]_o$.

Relationship between muscarinic current and extracellular potassium concentration

We examined the effect of different extracellular K^+ concentrations on I_{mch}. As shown in Fig. 6, the response amplitude changed as a function of $[K]_o$. The response amplitude was largest in reduced $[K]_o$ and became smaller as $[K]_o$ was increased. The data in Fig. 6*B* were plotted on a semilogarithmic scale along with a line representing the electrodiffusion equation for K^+-driving force, from which electrodiffusion theory predicts deviation at low $[K]_o$ (Marmor 1975). The data, even at high $[K]_o$, is not well fit by the equation.

If part of the ionic mechanism of I_{mch} were because of voltage-dependent closure of agonist-sensitive K^+ channels at negative potentials, then it may be possible to shift E_K to a more positive potential so that reversal of the current can be studied in a voltage range in which channel closure has not occurred (Brown and Adams 1980). After shifting E_K to more positive potentials by raising $[K]_o$ (from −71 mV in 15 mM K_o to −53 mV in 30 mM K_o to −36 mV in 60 mM K_o), in five separate experiments, we were unable to demonstrate an unequivocal shift in the potential where I_{mch} is null. Instead, as demonstrated in Figs. 3, 4, and 6, an inward current was evoked at holding potentials negative to the expected value of E_K at various concentrations of K_o.

Effect of K^+-channel blockers on the muscarinic current

We tested a number of cations and drugs known to inhibit various voltage- and ligand-activated K^+ conduc-

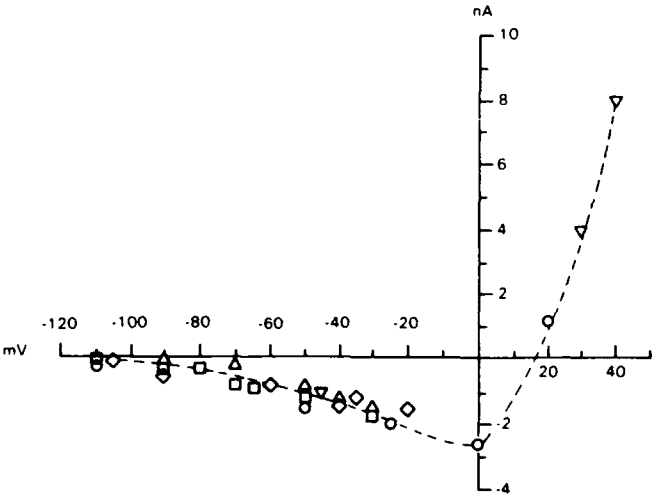

FIG. 4. I_{mch} amplitude plotted against voltage-clamped membrane potential for 5 different neurons. Cell in Fig. 3*A* is represented by circles. Cell in Fig. 3*B* is represented by down-pointing triangles. Dashed line was drawn by eye.

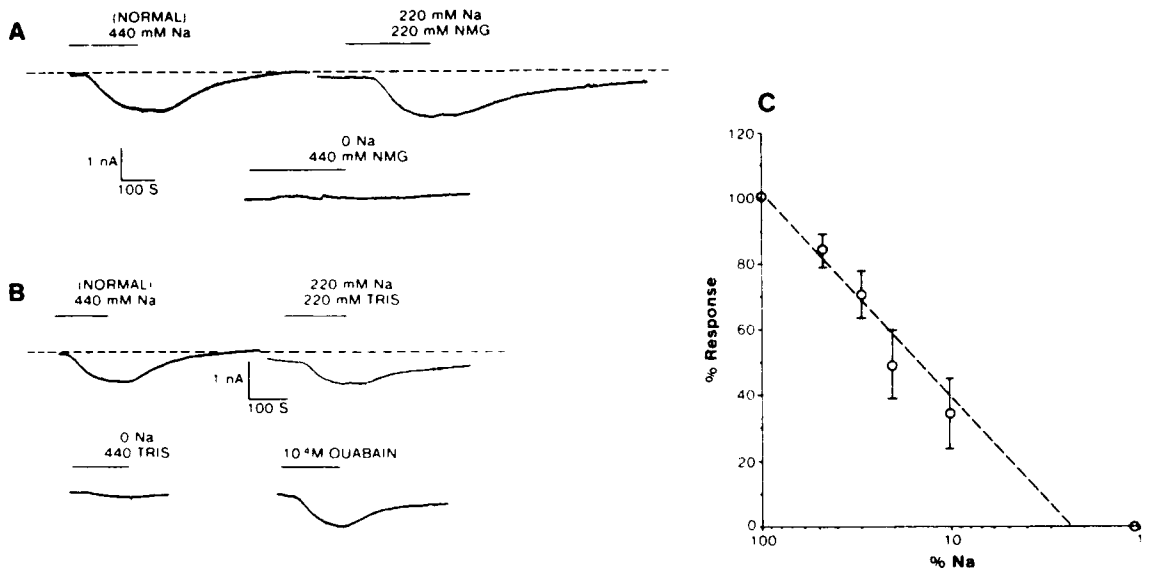

FIG. 5. I_{mch} as a function of $[Na]_o$. *A*: current traces from same ligated voltage-clamped neuron in solutions of varying $[Na]_o$ (V_H, −45 mV). *N*-methyl-D-glucamine was used as the Na^+ substitute. *B*: current traces from another ligated neuron perfused in salines of varying $[Na]_o$ for which Tris was used as the Na^+ substitute. *Bottom right* trace is from a different cell that had been bathed in normal saline + 0.1 mM ouabain for 20 min before perfusion with MeCh. Note that for both Na^+ substitutes, the trace in 220 mM Na^+ (50%) is little changed from control. Response, however, is totally abolished in Na^+-free saline. *C*: I_{mch} amplitude plotted against $[Na]_o$ shown as percent of normal (440 mM). Responses were normalized as a percent of that response obtained in normal $[Na]_o$, and the results from 4 experiments were averaged (±SE). Dashed line is derived from the calculated driving force (V-E_{Na}), where voltage-clamped V was −40 mV and $[Na]_i$ was assumed to be 50 mM.

tances in other preparations. Added to the extracellular bath solution, neither Ba^{2+}, Cs^+, 4-AP, nor TEA, in doses of 1–10 mM, were effective blockers of I_{mch} (Figs. 7 and 8). TEA at doses of 30–50 mM, however, consistently inhibited I_{mch} (Fig. 7). Furthermore, these blockers, in concentrations insufficient alone, could inhibit the current when combined. An example is shown in Fig. 8. TEA, 10 mM, did not reduce I_{mch}. Neither 10 mM Cs, 10 mM 4-AP, nor the two combined were sufficient to inhibit the current. When 10 mM TEA, however, was added to 10 mM Cs and 10 mM 4-AP, I_{mch} was considerably reduced. The inhibitory effect of these agents was more noticeable at membrane potentials around the resting potential, e.g., −60 mV to −40 mV. At depolarized potentials the I_{mch} was still prominent (see below, Fig. 10).

Effects of altering the chloride equilibrium potential

We examined the effects of changing E_{Cl} on the muscarinic agonist-induced current. Over time, during recording with 3 M-KCl-filled electrodes, sufficient Cl^- leaks into the neurons to shift E_{Cl} to more positive potentials. When GABA was perfused onto a neuron impaled with two KCl-filled electrodes, the membrane potential depolarized and bursts were inhibited (Fig. 9*A*). In contrast, GABA caused membrane potential hyperpolarization when perfused onto cells in which recording was made with electrodes filled with K^+-acetate (Fig. 9*C*). In neurons voltage-clamped with KCl electrodes, GABA caused an inward current at holding potentials near normal resting values, and an outward current at depolarized potentials (Fig. 9*B*). In the same cells where reversal of the chloride-dependent GABA current was achieved, the muscarinic current remained inward over this same voltage range (Fig. 9*B*). Thus, under these conditions of varying E_{Cl}, neither the amplitude nor the voltage dependence of the response to muscarinic agonists was altered.

Effect of calcium-channel blockers

In many experiments (e.g., Figs. 7, 8, and 10), we included TTX and a calcium-channel blocker, such as Co^{2+} or Mn^{2+}, to inhibit large inward currents during command voltage steps. These divalent cations, in sufficient concentrations to inhibit the voltage-dependent inward calcium current, had no effect on I_{mch}.

Current-voltage relationship

Another way to examine the ionic nature of I_{mch} is to examine the steady-state I-V relationship before and during exposure of the neuron to agonist. By using command voltage steps one can also determine whether specific voltage- and time-dependent currents are affected by the agonist. In most of our cells, the leakage and voltage-activated currents were so much larger than the muscarinic current, small changes in conductance were difficult to appreciate when comparing I-V curves near the resting potential. We found that the most effective way to study I-V relationships over a wide voltage range was by imposing command voltage ramps. Figure 10*A* shows ramp I-V curves obtained

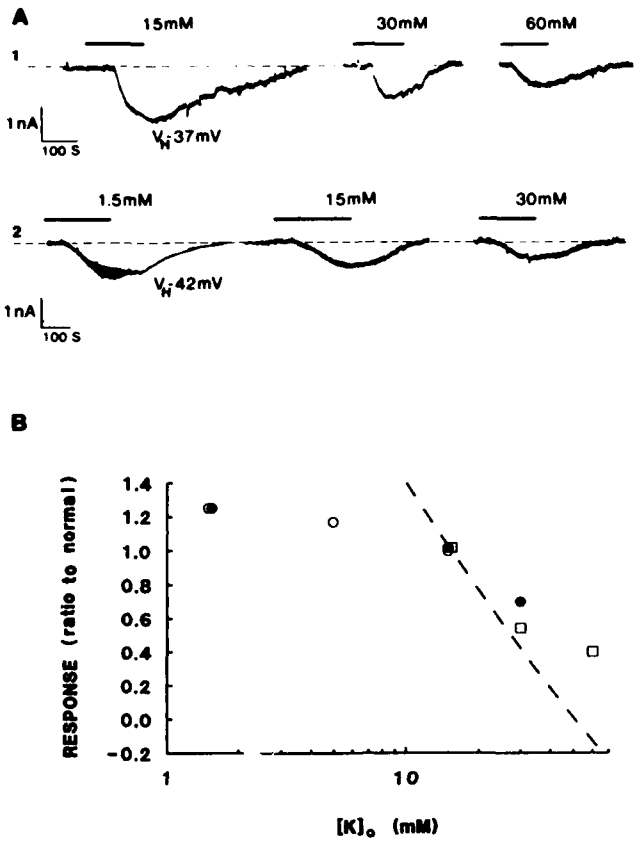

FIG. 6. I_{mch} as a function of $[K]_o$. *A*: representative MeCh-induced current traces in various concentrations of K_o for 2 different neurons (cell in *A2* was unligated). *B*: I_{mch} amplitude plotted against $[K]_o$ for 3 different neurons. Response amplitudes are expressed as a ratio to the amplitude in normal (15 mM) K_o. Dashed line was derived from the calculated driving force for a K^+ current, V-E_K, where the voltage-clamped V was −40 mV and $[K]_i$ was assumed to be 254 mM.

before and during perfusion of 1 mM methacholine. The difference between the two curves, shown in Fig. 10*B*, represents I_{mch} as a function of voltage. Two sets of curves are shown; one set (*A, curves 1* and *2; B, curve 2-1*) was obtained in normal lobster saline, and the other (*A, curves 3* and *4; B, curve 4-3*) in saline containing Ca^{2+}- and K^+-channel blockers. In normal saline, outward rectification produced large outward currents at depolarized membrane potentials (*A, curve 1*). MeCh (1 mM) caused an inward or downward shift in the curve (*A, curve 2*). The curve in MeCh converged with and then crossed over the control curve at positive potentials (*B, curve 2-1*). In the solution-containing channel blockers, outward rectification was reduced (*A, curve 3*). MeCh no longer caused an inward shift at membrane potentials around the resting potential, but did cause an inward shift at more depolarized voltages (*A, curve 4*). As in normal saline, the curve in MeCh crossed the control curve at a positive membrane potential (*B, curve 4-3*). As noted above (*Effect of K^+-channel blockers on the muscarinic current*), the inhibitory effect of combinations of K^+-channel blockers was most evident near the resting potential, but not at depolarized potentials. As shown in Fig. 10*B*, at −50 mV there was a measurable I_{mch} in normal saline, which disappeared in the solution containing channel blockers. At −10 mV, however, I_{mch} was of similar amplitude in both solutions.

We combined the results from six experiments in normal saline and plotted the mean value of the normalized I_{mch} for each 10-mV interval of membrane potential over the entire 180-mV range of the ramp (Fig. 11). These results show that there is often a small amount of outward agonist-induced current at membrane potentials negative to −100 mV. Because this current is rather small in amplitude (typically <1 nA), and because there is always increased electrode noise and drift when the membrane is held in this negative potential range, it would be difficult to see an unequivocal outward current when agonist is applied (see sections above). The averaged current-voltage curve shows the voltage dependence of I_{mch}. The inward current was activated in the range of −80 to −90 mV and reached a peak at a potential between −10 and −30 mV. The current amplitude then declined with further depolarization, and reversed at +24 mV (23.7 ± 5.1 mV, mean ± SE). The E_r was shifted to more negative values by lowering $[Na]_o$. In Fig. 12, E_r shifted 42 mV, from +20 mV to −22 mV after $[Na]_o$ was lowered to 132 mM (30% of normal). The expected change from the Nernst equation is 30 mV. A negative shift of E_r in lowered $[Na]_o$ was a consistent finding, but the degree of change was not often close to that predicted by theory. A complication that contributed to vari-

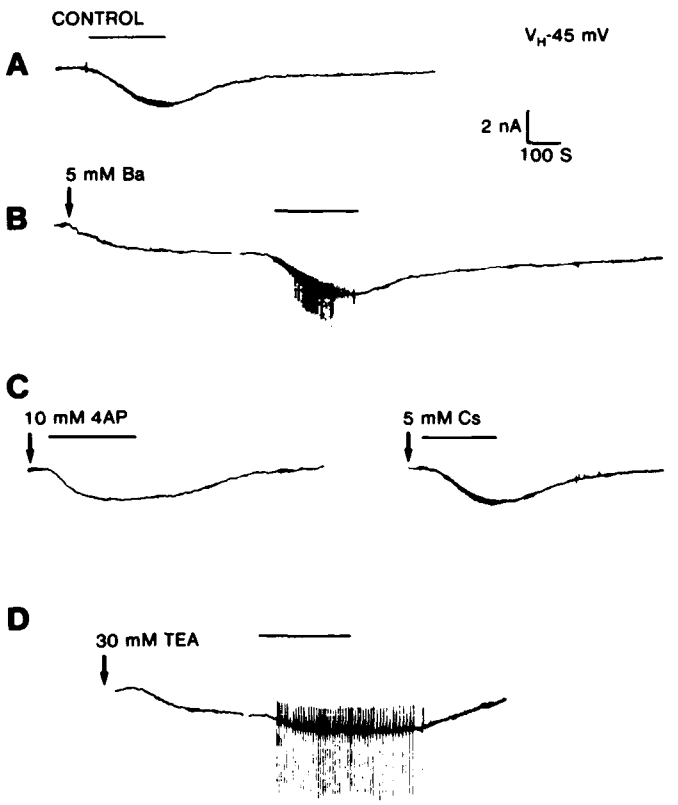

FIG. 7. Effect of K^+-channel blockers on I_{mch}. For each trace the horizontal bar represents the duration of perfusion of 1 mM MeCh. Onset of perfusion of K^+ blockers is indicated by the vertical arrow. Note that Ba^{2+} and TEA caused an inward current. *Neuron C*, unligated. Control solution contained 0.3 μM TTX and 10 mM Mn^{2+}, to which the various K^+-channel blockers were added.

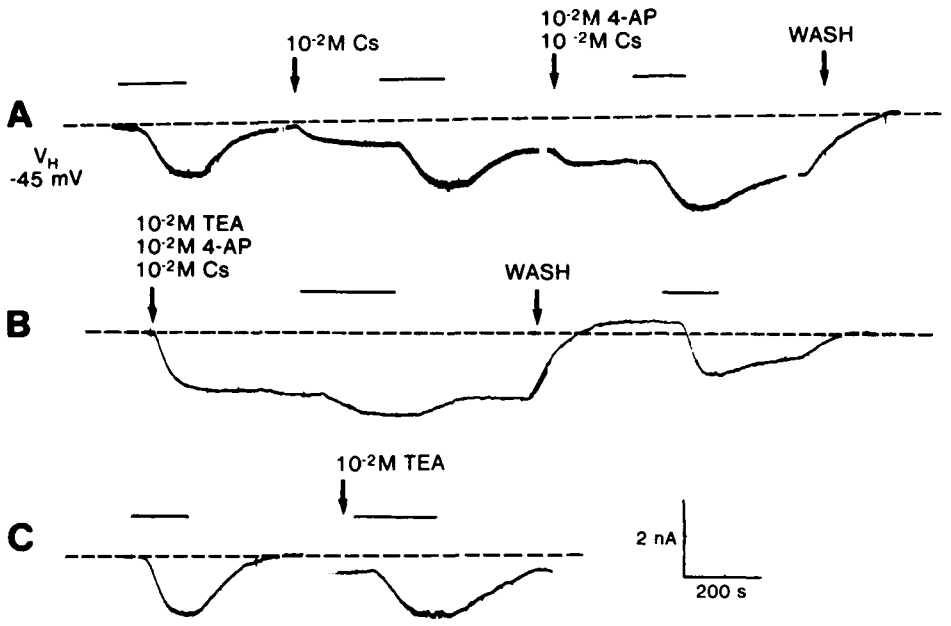

FIG. 8. Effect of combinations of K^+-channel blockers on I_{mch}. Traces were obtained sequentially in 1 neuron. Protocol as in Fig. 8. Note that all combinations of blockers caused inward current, but the degree of inward current produced did not correlate with the ability to inhibit the response to MeCh. *Neuron* C_2, ligated. Control solution as in Fig. 8.

ability was a slow, progressive increase in resting membrane conductance in the presence of low-$[Na]_o$ solutions. This increase in resting leak current, assuming E_{leak} to be zero, would add to the negative shift. Others have noted a similar deleterious effect of Na^+-free solutions (Gola and Selverston 1981). The possible contribution of K^+ permeation is discussed below.

Tazaki and Cooke (1986) analyzed voltage- and time-dependent currents in lobster cardiac ganglion neurons. Inward currents included a rapid, transient, TTX-sensitive Na^+ current and a slower transient inward Ca^{2+} current (I_{Ca}). They found no evidence of slow, TTX-resistant, voltage-dependent Na^+ currents and no negative slope resistance region after Ca^{2+} current was blocked. Outward currents included a transient outward current (I_A) sensitive to 4-AP, a delayed outward current (I_K) blocked by TEA, and a Ca^{2+}-dependent outward current (I_C) blocked by Cd^{2+} or Mn^{2+}. Tazaki and Cooke (1986) found that responses to hyperpolarizing clamp commands were not perfectly ohmic but rapidly declined about 15% from their initial value to reach steady state. We found that none of these voltage- and time-dependent currents appeared specifically affected by muscarinic agonists, yet there was a general depression of chord conductance as assessed by the ampli-

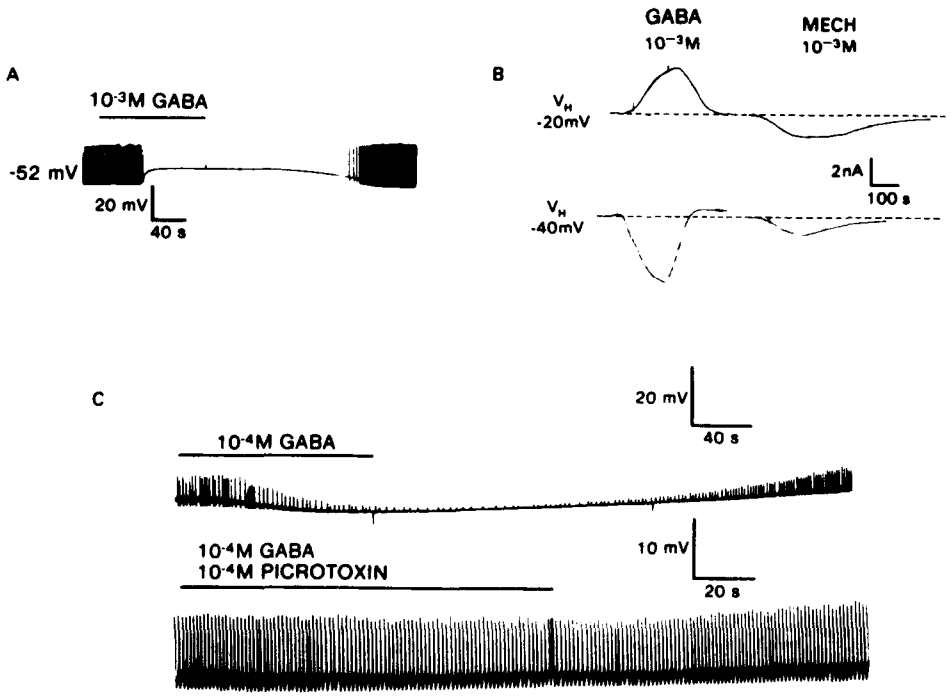

FIG. 9. Effect of changing E_{Cl} on GABA response. *A*: in a neuron (unligated C_3) impaled with 2 3-M KCl-filled microelectrodes, 1 mM GABA caused a depolarization of the cell under current clamp. *B*: in another unligated C_3 neuron, GABA caused an inward current when the cell was held at −40 mV and an outward current at −20 mV; but MeCh caused an inward current at both membrane potentials. *C*: in a different neuron (unligated C_4), impaled with a 4 M-K^+ acetate-filled electrode, 0.1 mM GABA caused a hyperpolarization from the resting membrane potential of −47 mV (*top*). Response was abolished by 0.1 mM picrotoxin (*bottom*).

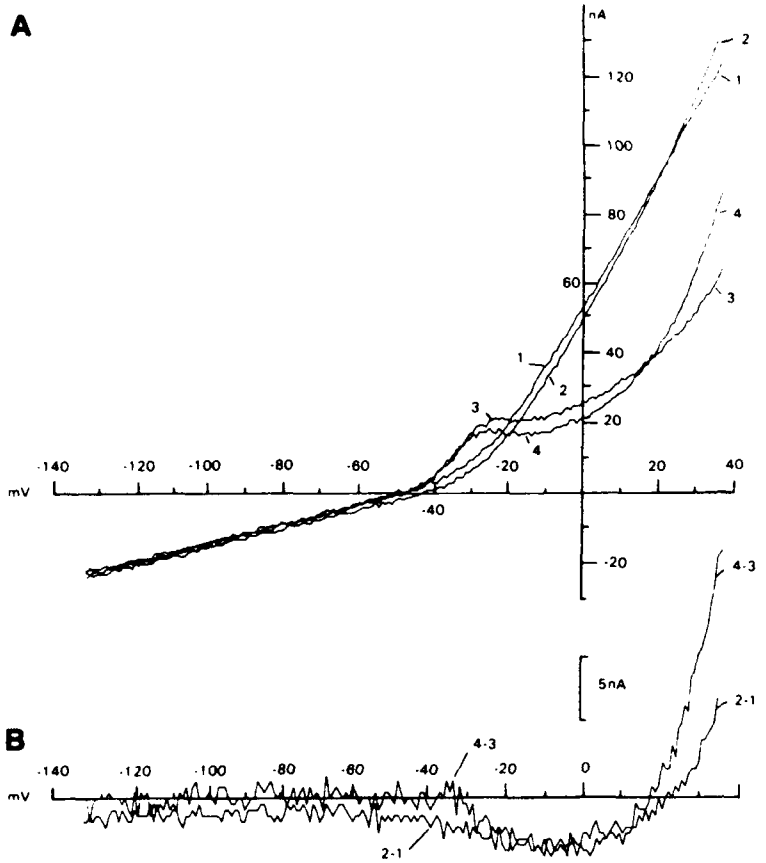

FIG. 10. Effect of muscarinic agonist on the *I-V* relationship for a motoneuron in normal saline and in saline containing Ca^{2+}- and K^+-channel blockers. *A*: a command voltage ramp (from −140 mV to +40 mV over 44 s) was applied to a ligated voltage-clamped C_2 neuron in normal saline before (*curve 1*) and during (*curve 2*) perfusion with 1 mM MeCh. Same clamp protocol was applied to the same cell after the control solution was changed to saline containing (in mM) 30 TEA, 4 4-AP, 10 Mn^{2+}, and 15 Ca^{2+}, before (*curve 3*), and during (*curve 4*) perfusion with 1 mM MeCh. *B*: computer-subtracted *I-V* curves. *Curve 2-1* is the resultant current after computer-subtracting *curve 1* from *curve 2* in *A* (normal saline). *Curve 4-3* is the resultant current after computer-subtraction of *curve 3* from *curve 4* in *A* (saline with blockers). Resultant currents are the actual MeCh-induced current as a function of membrane potential.

tudes of the instantaneous current jumps. An example is shown in Fig. 13. In this ligated C_1 neuron in TTX, depolarizing voltage steps evoked an inward-going current (I_{Ca}) (although not *net* inward) followed by a slow outward current ($I_K + I_C$). At the end of the step a slow tail current can be seen. Hyperpolarizing steps evoked a nearly ohmic inward current, although a rapid outward relaxation can be differentiated from the capacitative transient. At the end of the step, a transient outward current (I_A) was elicited. Muscarine caused an inward current during which the voltage- and time-dependent currents appeared unchanged. There

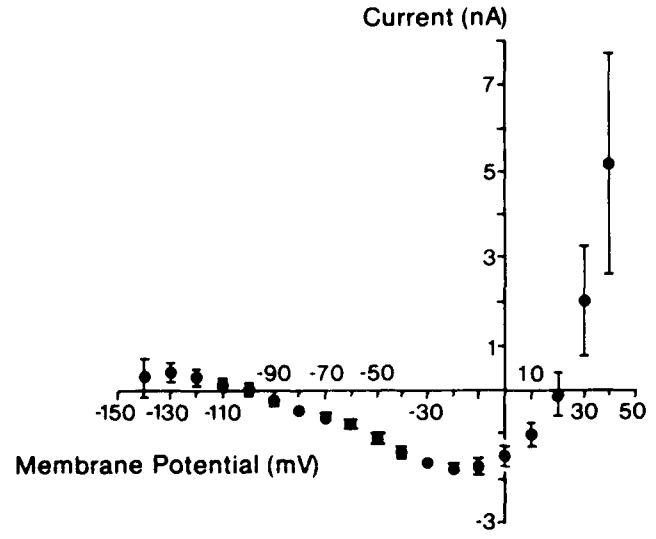

FIG. 11. Relationship between averaged I_{mch} and membrane potential. Each data point represents the mean ± SE of 6 measurements, except for $n = 3$ at −140 mV and $n = 5$ at 40 mV. I_{mch}, from computer-subtraction of *I-V* curves (as in Fig. 9*B*), was measured at 10-mV intervals between −140 mV and 40 mV. Current was normalized to the average maximum inward current. Where error bars are not visible, they were smaller than the diameter of the data symbol.

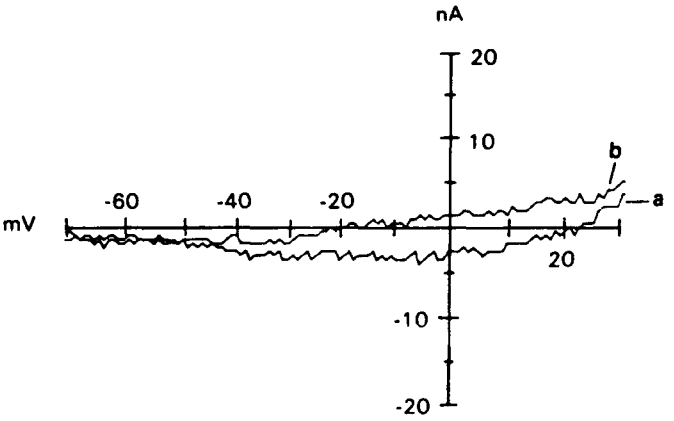

FIG. 12. I_{mch} plotted against clamped membrane potential in different Na_o^+ concentrations. Command voltage ramps were applied and computer-subtracted currents obtained, as described in Fig. 9, in 440 mM (*curve a*) and in 132 mM (*curve b*) Na_o. E_r is +20 mV for *curve a* and −22 mV for *curve b*, a shift of 42 mV. Nernst equation under these conditions predicts a shift of 30 mV, from +60 mV to +30 mV.

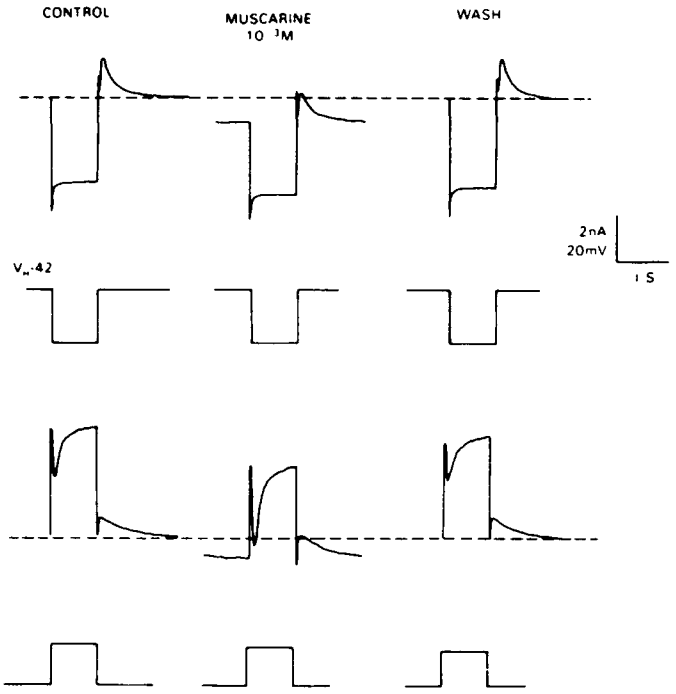

FIG. 13. Voltage- and time-dependent currents are unaffected by muscarinic agonists. Shown are representative current traces evoked by command voltage steps during perfusion with control (0.3 μM TTX) saline and during perfusion with 1 mM muscarine onto a ligated C_2 neuron. *Top traces*: currents evoked by hyperpolarizing steps shown beneath each current sample. *Bottom traces*: currents evoked by depolarizing command voltage steps. Inward current produced by muscarine is shown by the downward displacement of current traces below the dashed line representing the base-line current at V_H.

was, however, a reduction in the size of the ohmic or "instantaneous" current jumps, indicating a decrease in conductance. This caused the depolarization-evoked inward-going current to become net inward. The decrease in chord conductance can be understood in terms of the *I-V* curves. The activation of a voltage-dependent inward current contributes a region of negative slope resistance (Fig. 10). Therefore, although a specific conductance is increased, the total membrane conductance appears decreased (Adams et al. 1980). This is seen in Fig. 10*A*, in *curves 3* and *4*, where, in the presence of Ca^{2+}- and K^+-channel blockers, the remaining outward rectification was interrupted by downward depression of the *I-V* curves beginning at about −30 mV. This effect was accentuated by MeCh.

Models of the conductances involved in the agonist-induced current

Because E_r was +24 mV rather than the expected +60 mV for a pure Na^+ conductance, the slow inward Na^+ channel may not be selective for Na^+ alone, but may also allow K^+ to pass through. Assuming the conditions of the constant field equation (Edwards 1982; Goldman 1943; Hodgkin and Katz 1949) apply, we can use our measured value of E_r to estimate the ratio of permeabilities of K^+ and Na^+ (P_K/P_{Na}) by the use of the equation

$$P_K/P_{Na} = \frac{[Na]_i e^{FE_r/RT} - [Na]_o}{[K]_o - [K]_i e^{FE_r/RT}}, \qquad (1)$$

where $[Na]_i$ = 40 mM, $[Na]_o$ = 440 mM, $[K]_i$ = 253 mM, $[K]_o$ = 15 mM, the constants RT/F = 25 mV, and E_r is our measured mean value of +24 mV. This gives a calculated value of P_K/P_{Na} of 0.52. Thus this slow, voltage-dependent Na^+ channel would appear less Na^+-selective than the TTX-sensitive action potential Na^+ channel (P_K/P_{Na} = 0.086) but more Na^+-selective than other well-studied ligand-activated cation channels (e.g., P_K/P_{Na} = 1.1 for ACh-activated nicotinic channel in frog) (Edwards 1982). We note, however, that if adequate voltage- and space-clamp control is not achieved, the estimate of E_r, and hence permeability ratios, may be substantially in error.

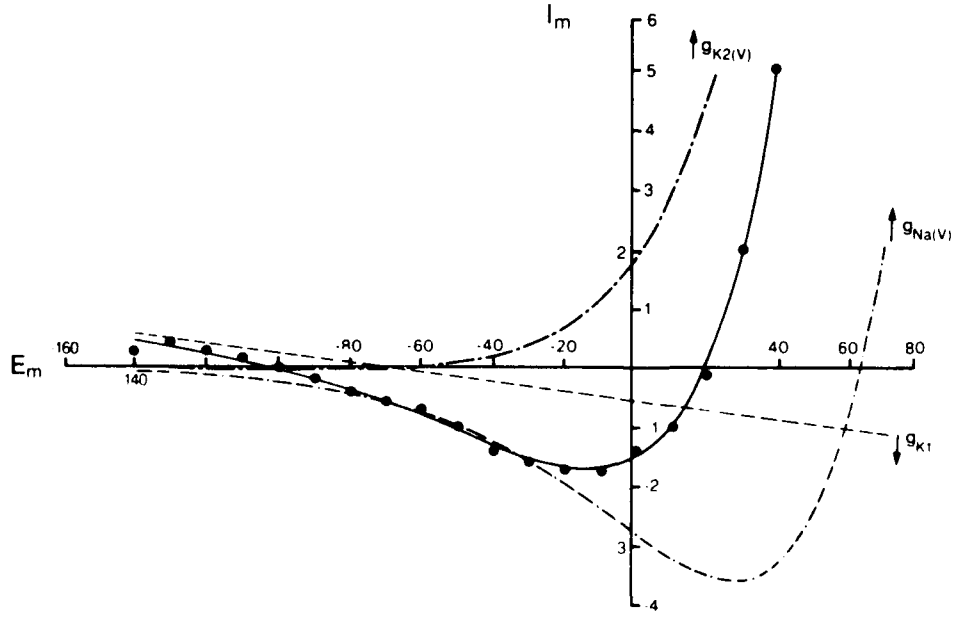

FIG. 14. Descriptive model of the muscarinic agonist-induced current. Solid line, filled circles: the mean values of the averaged data shown in Fig. 10 were fit by a least-squares method to the equation

$$I_{mch} = \Delta g_{K1}(E_m - E_K) + \{1 + \exp(ze/kT)(E_r - E_m)\}^{-1} \times [(g_{K2})(E_m - E_K) + (g_{Na})(E_m - E_{Na})]$$

Other curves represent the individual component conductances of the equation: dashed line, decrease in g_{K1}; dotted line, increase in $g_{Na(V)}$; dashed-dotted line, increase in $g_{K2(V)}$. Details in text.

The averaged *I-V* data in Fig. 11 was well fit by a model equation that included a term for a decrease in a resting K^+ conductance and an increase in a voltage-dependent conductance to Na^+ and K^+ (Fig. 14). The model assumes that the voltage-dependent channel has only open and closed states, whose rate constants vary exponentially with voltage. The general form of the equation is:

$$I_{mch} = \Delta g_{K1}(E_m - E_K) + [1 + \exp(ze/kT)(E_o - E_m)]^{-1} \cdot [(g_{K2})(E_m - E_K) + (g_{Na})(E_m - E_{Na})], \quad (2)$$

where Δg_{K1} is the change in the separate K^+ conductance; $E_K = -70$ mV; $E_{Na} = +63$; the constants kT/e = 25 mV; E_o is the membrane potential where the voltage-dependent conductance is one-half activated; z is the valence of the equivalent gating charge; and g_{K2} and g_{Na}, treated separately, are the contributions of, respectively, K^+ conductance and Na^+ conductance to the total voltage-dependent cation conductance. The computed values for best fit of the experimental data under the constraints of *Eq. 2* were: $\Delta g_{K1} = -8$ nS, $z = 0.85$, $E_o = 76$ mV, $g_{K2} = 372$ nS, and $g_{Na} = 644$ nS ($R^2 = 0.99$). Although some of the parameter values of the equation seem well determined by the data, we do not assume that they are necessarily unique. The ratio g_{K2}/g_{Na} of 0.58 is comparable to the P_K/P_{Na} ratio of 0.52 calculated with *Eq. 1*.

Also shown in Fig. 14 are curves for the individual currents constituting the total agonist-induced current as predicted by *Eq. 2*: the current from a decrease in a nonvoltage-dependent K^+ conductance; the current from an increase in K^+, but not Na^+, conductance of the voltage-dependent channel; and the current from an increase in a voltage-dependent Na^+ conductance alone.

DISCUSSION

From these results it is apparent that the current induced by muscarinic agonist is more complex than earlier current-clamp studies predicted. The amplitude of I_{mch} depends primarily on $[Na]_o$ but is also affected by changes in $[K]_o$.

This is the first example of which we are aware of a muscarinic ACh receptor linked to a slow, voltage-dependent Na^+ conductance. In vertebrates, muscarinic slow depolarizations have generally been found to be caused by suppression of K^+ currents (Brown and Adams 1980; Hartzell 1981; Kuba and Koketsu 1978; Madison et al. 1987; North 1986). In bullfrog sympathetic neurons, Kuba and Koketsu (1974) found that, in addition to suppression of K^+ conductance, muscarinic stimulation also caused a concomitant increase in conductance to Na^+ and Ca^{2+}. In those neurons, depending on the ratio of decreased K^+ conductance to increased Na^+ and Ca^{2+} conductances, the *I-V* curves before and during muscarinic agonist could either cross, remain parallel, or even diverge at hyperpolarized potentials. This was further verified by Jones (1985), who found that at more hyperpolarized potentials, at which muscarinic voltage-sensitive K^+ channels are closed, the agonists can produce an inward current because of an increased conductance, which appears to be mainly a voltage-insensitive Na^+ conductance.

Neurotransmitter and neurohormonal alteration of a voltage-dependent, slow inward Na^+ current has been noted in a number of invertebrate studies (Barker and Smith 1976; Ichinose and McAdoo 1988; Kirk et al. 1988; Ruben et al. 1984). The current we studied seems similar to the Na^+ current induced by injection of cyclic nucleotides into gastropod neurons (Aldenhoff et al. 1983; Connor and Hockberger 1984; Green and Gillette 1983; Kononenko et al. 1986). In *Aplysia* neurons Connor and Hockberger (1984) found a relationship between the cyclic AMP-induced current and the membrane holding potential similar to that which we report here. We explain our data by invoking the same mechanism that they hypothesized: the increase in Na^+-electrochemical driving force accompanying membrane hyperpolarization may be offset by a decrease in the fraction of voltage-activated channels. Because of the frequent association between the slow inward Na^+ current and intracellular cAMP levels, we hypothesize that this second messenger likely mediates the muscarinic agonist-induced current in lobster cardiac ganglion motoneurons. Preliminary experiments (our unpublished observations) with the use of inhibitors of phosphodiesterase support this view.

Although we consider the predominant ionic mechanism of muscarinic excitation to be activation of a voltage-dependent Na^+ conductance, we cannot exclude an additional involvement of a K^+ conductance. There are several observations that suggest this additional mechanism. First, the response is dependent on $[K]_o$. Second, I_{mch}, when determined from *I-V* curves, frequently appears to be outward-going at negative membrane potentials; and the best fit to our averaged experimental data is obtained using an equation that contains a term for a decrease in K^+ conductance. Third, the response is inhibited by combinations of agents that are typically classed as K^+ channel blockers. On the other hand, a number of results fail to support the involvement of a separate K^+ conductance. Despite the small outward current seen at negative potentials in the subtracted *I-V* curves, we were never able to show an outward current when agonist was applied to a neuron in which the steady holding potential had been shifted to potentials as negative as −120 mV. Furthermore, in low-Na^+ or Na^+-free solutions, there was no residual current that reversed around E_K. Instead of, or in addition to, a separate ionic channel, it is possible that the dependence on $[K]_o$ may mainly reflect a significant permeability of the ligand- and voltage-activated channel to K^+. The value of E_r that we found, 35 mV negative to E_{Na}, would support this idea (Ruben et al. 1984). Furthermore, the somewhat weak blocking effect of combinations of agents such as TEA and Cs^+ could also be viewed as arising from their permeation in a cation channel of this selectivity. The curves from the model in Fig. 14 predict that the effects of a decrease in a K^+ conductance plus the increase in K^+ conductance of the voltage-sensitive cation channel would tend to cancel each other over a broad voltage range.

We did not study the kinetics of this voltage-dependent Na/K conductance, but our experimental findings suggest that its activation may be rapid, since it appears operationally as an "instantaneous" current.

We accepted the results of Na^+-substitution experiments with caution because of the many biological effects these solutions can have, which are not primarily related to the neurotransmitter action. Wilson et al. (1977) showed that Tris buffer is a potent inhibitor of cholinergic responses in *Aplysia*. Glucosamine appears to interact with ACh channels in *Aplysia* (Marchais and Marty 1980). In some cases, the ionic strength or osmolality of the solution is affected by the Na^+ substitute. Low-Na^+ solutions may affect Na-dependent or Na-coupled processes, such as the Na^+-K^+ pump (Thomas 1972), Na^+-Ca^{2+} exchange (Requena et al. 1977), or Na^+-H^+ transport (Thomas 1977).

The action of muscarinic cholinergic agonists on these neurons appears similar to that produced by proctolin. Studying lobster neurons under current clamp, Sullivan and Miller (1984) concluded that proctolin appears to reduce a resting K^+ conductance. The response was not blocked by TEA, 4-AP, Cs, or quinine, but was reduced in low-Na^+ solution. In preliminary experiments, we have found that proctolin, like cholinergic agonists, also excites motoneurons by activating a slow inward Na^+ current (Freschi 1989). It appears likely that proctolin and ACh, acting at different receptors, share the same ionic mechanisms (Sullivan and Miller 1984). In this way the lobster cardiac ganglion resembles the vertebrate sympathetic ganglion, in which luteinizing hormone-releasing hormone and ACh, through different receptors, affect the same conductance mechanisms (Adams and Brown 1980; Jones 1985).

We thank Dr. Mark W. Miller for providing us with an unpublished manuscript on cholinergic effects in lobster cardiac ganglion.

This work was supported by National Institute of Neurological and Communicative Disorders and Stroke Grant NS-22628.

Present address of D. Livengood: Physiology Department, Armed Forces Radiobiology Research Institute, Bethesda, MD 20814.

Address for reprint requests: J. E. Freschi, Dept. of Neurology, Drawer V, 401 Woodruff Memorial Research Bldg., Emory University School of Medicine, Atlanta, GA 30322.

Received 4 August 1988; accepted in final form 18 May 1989.

REFERENCES

ADAMS, P. R. AND BROWN, D. A. Luteinizing hormone-releasing factor and muscarinic agonists act on the same voltage-sensitive K^+-current in bullfrog sympathetic neurones. *Br. J. Pharmacol.* 68: 353–355, 1980.

ADAMS, W. B., PARNAS, I., AND LEVITAN, I. B. Mechanisms of long-lasting synaptic inhibition in *Aplysia* neuron R15. *J. Neurophysiol.* 44: 1148–1160, 1980.

ALDENHOFF, J. B., HOFMEIER, G., LUX, H. D., AND SWANDULLA, D. Stimulation of a sodium influx by cAMP in *Helix* neurons. *Brain Res.* 276: 289–296, 1983.

BARKER, D. L., MURRAY, T. F., SIEBENALLER, J. F., AND MPITSOS, G. J. Characterization of muscarinic cholinergic receptors in the crab nervous system. *J. Neurochem.* 46: 583–588, 1986.

BARKER, J. L. AND SMITH, T. G. Peptide regulation of neuronal membrane properties. *Brain Res.* 103: 167–170, 1976.

BROWN, D. A. AND ADAMS, P. R. Muscarinic suppression of a novel voltage-sensitive K^+ current in a vertebrate neurone. *Nature Lond.* 283: 673–676, 1980.

CONNOR, J. A. AND HOCKBERGER, P. A novel membrane sodium current induced by injection of cyclic nucleotides into gastropod neurones. *J. Physiol. Lond.* 354: 139–162, 1984.

DAVENPORT, D. Further studies on the pharmacology of the heart of *Cancer magister* Dana. *Biol. Bull. Woods Hole* 82: 255–260, 1942.

EDWARDS, C. The selectivity of ion channels in nerve and muscle. *Neuroscience* 7: 1335–1366, 1982.

FLOREY, E. Acetylcholine in invertebrate nervous systems. *Can. J. Biochem. Physiol.* 41: 2619–2626, 1963.

FLOREY, E. AND RATHMAYER, M. Pharmacological characterization of cholinoreceptors of cardiac ganglion cells of crustaceans. *Gen. Pharmacol.* 11: 47–53, 1980.

FRESCHI, J. E. Proctolin activates a slow, voltage-dependent sodium current in motoneurons of the lobster cardiac ganglion. *Neurosci. Lett.* In Press.

GERSCHENFELD, H. M. Chemical transmission in invertebrate central nervous systems and neuromuscular junctions. *Physiol. Rev.* 53: 1–119, 1973.

GOLA, M. AND SELVERSTON, A. Ionic requirements for bursting activity in lobsters stomatogastric neurons. *J. Comp. Physiol.* 145: 191–207, 1981.

GOLDMAN, D. E. Potential, impedance, and rectification in membranes. *J. Gen. Physiol.* 27: 37–60, 1943.

GREEN, D. J. AND GILLETTE, R. Patch- and voltage-clamp analysis of cyclic AMP-stimulated inward current underlying neurone bursting. *Nature* 306: 22–29, 1983.

HARTLINE, D. K. Impulse identification and axon mapping of the nine neurons in the cardiac ganglion of the lobster, *Homarus americanus*. *J. Exp. Biol.* 47: 327–346, 1967.

HARTLINE, D. K. Integrative neurophysiology of the lobster cardiac ganglion. *Am. Zool.* 19: 53–65, 1979.

HARTZELL, H. C. Mechanisms of slow postsynaptic potentials. *Nature* 291: 539–544, 1981.

HODGKIN, A. L. AND KATZ, B. The effect of sodium ions on the electrical activity of the giant axon of the squid. *J. Physiol. Lond.* 108: 37–77, 1949.

HOOPER, S. L. AND MARDER, E. Modulation of the lobster pyloric rhythm by the peptide proctolin. *J. Neurosci.* 7: 2097–2112, 1987.

JONES, S. W. Muscarinic and peptidergic excitation of bull-frog sympathetic neurones. *J. Physiol. Lond.* 366: 63–87, 1985.

ICHINOSE, M. AND MCADOO, D. J. The voltage-dependent, slow inward current induced by the neuropeptide FMRFamide in Aplysia neuron R14. *J. Neurosci.* 8: 3891–3900, 1988.

KIRK, M. D., TAUSSIG, R., AND SCHELLER, R. H. Egg-laying hormone, serotonin, and cyclic nucleotide modulation of ionic currents in the identified motoneuron B16 of *Aplysia*. *J. Neurosci.* 8: 1181–1193, 1988.

KONONENKO, N. I., KOSTYUK, P. G., AND SHCHERBATKO, A. D. Properties of cAMP-induced transmembrane current in mollusc neurons. *Brain Res.* 376: 239–245, 1986.

KUBA, K. AND KOKETSU, K. Ionic mechanism of the slow excitatory postsynaptic potential in bullfrog sympathetic ganglion cells. *Brain Res.* 81: 338–342, 1974.

KUBA, K. AND KOKETSU, K. Synaptic events in sympathetic ganglia. *Prog. Neurobiol.* 11: 77–169, 1978.

LIEBERMAN, E. M. AND LANE, T. G. The influence of cardioactive steroids, metabolic inhibitors, temperature, and sodium on membrane conductance and potential of crayfish giant axons. *Pfluegers Arch.* 366: 189–193, 1976.

LIVENGOOD, D. R. Coupling ratio of the Na-K pump in the lobster cardiac ganglion. *J. Gen. Physiol.* 82: 853–874, 1983.

LIVENGOOD, D. R. AND KUSANO, K. Evidence for an electrogenic sodium pump in follower cells of the lobster cardiac ganglion. *J. Neurophysiol.* 35: 170–186, 1972.

MADISON, D. V., LANCASTER, B., AND NICOLL, R. A. Voltage clamp analysis of cholinergic action in the hippocampus. *J. Neurosci.* 7: 733–741, 1987.

MARCHAIS, D. AND MARTY, A. Action of glucosamine on acetylcholine-sensitive channels. *J. Membr. Biol.* 56: 43–48, 1980.

MARDER, E. Neurotransmitters and neuromodulators. In: *The Crustacean Stomatogastric Nervous System: A Model for the Study of Central Nervous Systems*, edited by A. I. Selverston and M. Moulins. New York: Springer-Verlag, 1986, p. 263–300.

MARDER, E. AND HOOPER, S. L. Neurotransmitter modulation of the stomatogastric ganglion of decapod crustaceans. In: *Model Neural Networks and Behavior*, edited by A. I. Selverston. New York: Plenum, 1985, p. 319–337.

MARDER, E. AND PAUPARDIN-TRITSCH, D. The pharmacological properties of some crustacean neuronal acetylcholine, γ-aminobutyric acid, and L-glutamate responses. *J. Physiol.* 280: 213–236, 1978.

MARMOR, M. F. The membrane of giant molluscan neurons: electrophysiological properties and the origin of the resting potential. *Prog. Neurobiol.* 5: 167–195, 1975.

MAYNARD, D. M. Activity in a crustacean ganglion. II. Pattern and interaction in burst formation. *Biol. Bull. Woods Hole* 109: 420–436, 1955.

NAGY, F., BENSON, J. A., AND MOULIN, M. Cholinergic inputs reduce a steady outward K^+ current allowing activation of a Ca^+ conductance which underlies the burst-generating oscillations in lobster pyloric neurons. *Soc. Neurosci. Abstr.* 11: 1022, 1985.

NORTH, R. A. Muscarinic receptors and membrane ion conductances. *Trends Pharmacol. Sci. 9, Suppl.* II: 19–22, 1986.

O'SHEA, M. Neuropeptide function: the invertebrate contribution. *Annu. Rev. Neurosci* 8: 171–198, 1985.

REQUENA, J., DIPOLO, R., BRINLEY, JR., F. J., AND MULLINS, L. J. The control of ionized calcium in squid axons. *J. Gen. Physiol.* 70: 329–353, 1977.

RUBEN, P., JOHNSON, J. W., AND THOMPSON, S. Analysis of FMRF-amide effects on *Aplysia* bursting neurons. *J. Neurosci.* 6: 252–259, 1984.

SMITH, R. I. The action of electrical stimulation and certain drugs on cardiac nerves of the crab, *Cancer irroratus*. *Biol. Bull. Woods Hole* 93: 72–88, 1947.

SULLIVAN, R. E. AND MILLER, M. W. Actions of acetylcholine on the rhythmic burst activity of cardiac ganglion. *Soc. Neurosci. Abstr.* 8: 162, 1982.

SULLIVAN, R. E. AND MILLER, M. W. Dual effects of proctolin on the rhythmic burst activity of the cardiac ganglion. *J. Neurobiol.* 15: 173–196, 1984.

TAZAKI, K. AND COOKE, I. M. Separation of neuronal sites of driver potential and impulse generation by ligaturing in the cardiac ganglion of the lobster, *Homarus americanus*. *J. Comp. Physiol.* 151: 329–346, 1983.

TAZAKI, K. AND COOKE, I. M. Currents under voltage clamp of burst-forming neurons of the cardiac ganglion of the lobster (*Homarus americanus*). *J. Neurophysiol.* 56: 1739–1762, 1986.

THOMAS, R. C. Intracellular sodium activity and the sodium pump in snail neurones. *J. Physiol. Lond.* 220: 55–71, 1972.

THOMAS, R. C. The role of bicarbonate, chloride, and sodium ions in the regulation of intracellular pH in snail neurons. *J. Physiol. Lond.* 273: 317–338, 1977.

WELSH, J. H. Chemical mediation in crustaceans I. The occurrence of acetylcholine in nervous tissues and its action on the decapod heart. *J. Exp. Biol.* 16: 198–219, 1939.

WIERSMA, C. A. G. AND NOVITSKI, E. The mechanism of nervous regulation of the crayfish heart. *J. Exp. Biol.* 19: 255–265, 1942.

WILSON, W. A., CLARK, M. T., AND PELLMAR, T. C. Tris buffer attenuates acetylcholine responses in *Aplysia* neurons. *Science Wash. DC* 196: 440–441, 1977.

RADIATION RESEARCH 121, 67–70 (1990)

18 S rRNA Degradation Is Not Accompanied by Altered rRNA Transport at Early Times following Irradiation of HeLa Cells

PINHAS FUCHS,* JOHN M. KROLAK,† DAVID MCCLAIN,† AND KENNETH W. MINTON‡[1]

*Israel Institute for Biological Research, Ness-Ziona, Israel; †Armed Forces Radiobiology Research Institute, Bethesda, Maryland 20814-5145; and ‡Uniformed Services University of the Health Sciences, Bethesda, Maryland 20814-4799

FUCHS, P., KROLAK, J. M., MCCLAIN, D., AND MINTON, K. W. 18 S rRNA Degradation Is Not Accompanied by Altered rRNA Transport at Early Times following Irradiation of HeLa Cells. *Radiat Res.* 121, 67–70 (1990).

The effect of ionizing radiation (^{137}Cs) on processing and transport of ribosomal RNA (rRNA) was studied by pulse-labeling HeLa S3 cells with [^{3}H]uridine immediately prior to irradiation. This approach permits kinetic analysis of processing of 45 S rRNA (radiolabeled predominantly prior to irradiation) into its 28 S and 18 S rRNA daughter species following irradiation. By this technique, we have recently demonstrated an increase in the normal 28 S:18 S rRNA stoichiometric ratio of 1:1 to as high as 1.6:1 during the interval 5 to 20 h following irradiation of HeLa cells at ≥7.5 Gy. Alterations in 28 S:18 S ratio were evaluated in greater detail at early times following irradiation, up to 2 h. The 28 S:18 S ratio was found to be maximal at 1 h after radiation, at about 2:1, following 5 or 10 Gy. Using a method for rapid separation of nucleus from cytoplasm, transport of rRNA from nucleus to cytoplasm was also evaluated during this period. Despite an increase in the rate of 45 S rRNA processing, as well as an increased 28 S:18 S ratio, no alterations in transport from nucleus to cytoplasm were detected. This lack of transport alteration suggests that accumulation of excess 28 S rRNA is restricted to the nucleus, where it may represent an early step in the process of radiation-induced cell killing.

INTRODUCTION

In recent investigations on the effects of radiation on rRNA processing in HeLa S3 cells, we pulse-labeled the cells with [^{3}H]uridine immediately prior to irradiation (*1*). The 45 S rRNA precursor, which undergoes nuclear processing to form one each of its major daughter species, 28 S and 18 S rRNA, was separated from the daughter species by gel electrophoresis and the radiolabel in each species determined at various times after irradiation. By pulse-labeling the cells prior to irradiation, superimposed effects caused by radiation-induced alterations of rRNA transcription ((*1*) and Refs. therein) were minimized, permitting selective analysis of the processing of that fraction of 45 S precursor that had been synthesized (radiolabeled) predominantly prior to irradiation. Processing in control cells yielded the normal stoichiometric ratio of 28 S:18 S rRNA of 1:1 (*1–4*). However, irradiated cells showed two effects: (i) an accelerated conversion of radiolabeled 45 S rRNA to 28 S and 18 S species; (ii) an altered stoichiometry of 28 S:18 S rRNA of about 1.6:1 stably maintained from 5 to 20 h following irradiation of 10 or 20 Gy (*1*).

We now report more detailed studies on 45 S rRNA processing within the first 2 h following irradiation in which we have found a maximum 28 S:18 S ratio of 2:1 that is observed about 1 h following irradiation of 5 or 10 Gy. Concurrent studies on nuclear export of the daughter species do not provide evidence of an altered 28 S:18 S ratio in the cytoplasm.

MATERIALS AND METHODS

Cell Culture

HeLa S3 cells were cultured as previously described (*1*). All experiments employed asynchronously growing monolayers at 1–2 × 10^5 cells/cm^2, with a doubling time of 20 h. Cells were seeded 3 days prior to use.

Isotope Labeling of Cells and Exposure to Ionizing Radiation

Cells were labeled in complete conditioned medium containing [5,6-^{3}H]-uridine (50 Ci/mmol; DuPont NEN) at 70 μCi/ml for experiments in which RNA was selectively harvested or 10 μCi/ml for experiments in which acid-insoluble incorporation was measured. Incubation in the presence of label was for 15 min, after which the flasks were washed three times with unlabeled prewarmed medium. After washing, unlabeled prewarmed, complete conditioned, and CO_2-equilibrated medium was added to the flasks which were immediately exposed at 70 Gy/h using a ^{137}Cs source at room temperature (*1*).

Measurement of Radiolabel in rRNA Species

Total RNA was collected and purified using guanidine isothiocyanate (GI), as previously described (*1*). Cytoplasmic RNA was collected using a modification of the technique of Butler (*5*): cells were washed twice with ice-cold culture medium and once with ice-cold phosphate-buffered saline, and then treated for 2 min with reticulocyte sensitizing buffer (RSB; ice-cold Tris–HCl, pH 7.0, 10 m*M*; NaCl, 10 m*M*; $MgCl_2$, 3 m*M*) to induce osmotic swelling of the cells. The RSB was removed, and monolayers in

[1] To whom correspondence should be addressed.

0033-7587/90 $3.00

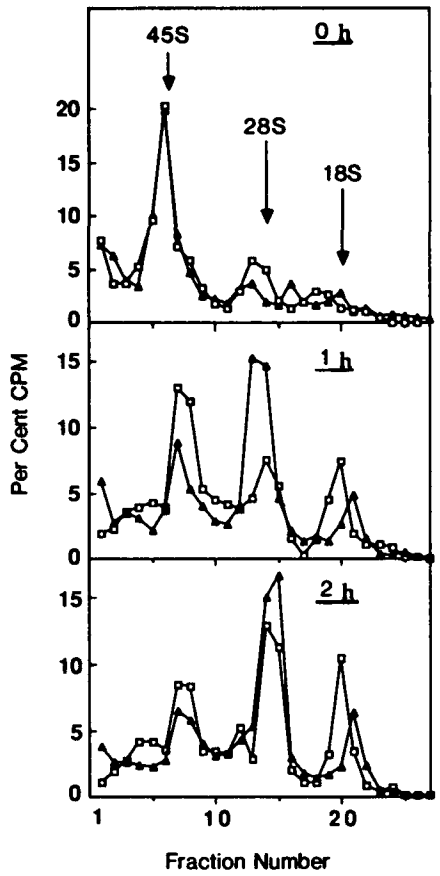

FIG. 1. Gel electrophoresis of whole cell RNA labeled with [^{3}H]uridine. After 15 min of labeling, flasks were washed in prewarmed conditioned full medium and either exposed to 5 Gy or held at room temperature for the same duration (4.3 min). RNA was then harvested immediately or after further incubation of flasks at 37°C for 1 or 2 h. The arrows indicate the location of rRNA species visualized in the ethidium bromide-stained gels. Control (□); 5 Gy (▲).

each flask were then dissolved in 0.8 ml of the following: 5 g ethylhexadecyldimethylammonium bromide plus 3 ml glacial acetic acid brought to 100 ml in water. This solution lyses the plasma membrane but not the nuclei (*5*). Immediately following, 2.3 ml of 10 m*M* Tris–HCl, pH 7.5, containing 10 m*M* EDTA and vanadyl ribonucleoside inhibitor (Sigma), 1:20 dilution, was added to each flask, and the resulting solution was centrifuged at room temperature at 1500*g* for 5 min to pellet the nuclei. The supernatant (cytoplasmic) fraction was ethanol-precipitated twice and the pellet resuspended in GI solution and processed as for whole cells (*1*). A total of 6.5 μg RNA per lane (either whole cell or cytoplasmic RNA) was taken for agarose–formaldehyde gel electrophoresis, as described (*1*). The 45 S, 28 S, and 18 S rRNA bands were visualized by ethidium bromide staining of the gel, as described (*1*). The gels were either sliced into 1-mm fractions and the radioactivity was determined by scintillation counting or blotted onto a nylon membrane; the blot was cut into 2-mm fractions and radioactivity was determined by scintillation counting, as previously described (*1*).

The modified technique of Butler, described above, consistently yielded undegraded cytoplasmic rRNA, with readily identified, clearly separated 28 S and 18 S peaks (e.g., Fig. 4). In control experiments, the nuclear pellet obtained with this technique was dissolved in GI solution, and RNA was purified as for whole cells (*1*) and subjected to gel electrophoresis. Unlike preparations of total or cytoplasmic RNA, the RNA from isolated nuclei using our procedure appeared partially degraded and rRNA species were difficult to identify with confidence.

Measurement of Radiolabel in Acid-Insoluble Fraction

At the desired postirradiation time, monolayers in T-25 flasks were processed into nuclear and cytoplasmic fractions using the modified Butler technique (*5*) described above. Fifty-microliter aliquots of the cytoplasmic fraction were precipitated on Whatman 3MM filters with 5% trichloroacetic acid. The nuclear pellet was washed twice with ice-cold phosphate-buffered saline, resuspended in 1% SDS, and sheared several times with a 22-gauge needle to reduce the viscosity of the resulting solution, and 50-μl aliquots were precipitated on Whatman 3MM filters with 5% trichloroacetic acid.

RESULTS

HeLa S3 cells were pulse-labeled with [^{3}H]uridine for 15 min, followed immediately by washing and irradiation. In prior studies under identical conditions (*1*), we found that (a) the great majority of acid-insoluble incorporation occurred by the end of the 15-min pulse-labeling period; (b) radiation up to 20 Gy did not alter subsequent incorporation of [^{3}H]uridine into the acid-insoluble fraction; and (c) synthesis of 45 S rRNA precursor following irradiation was unaffected by exposures up to 20 Gy.

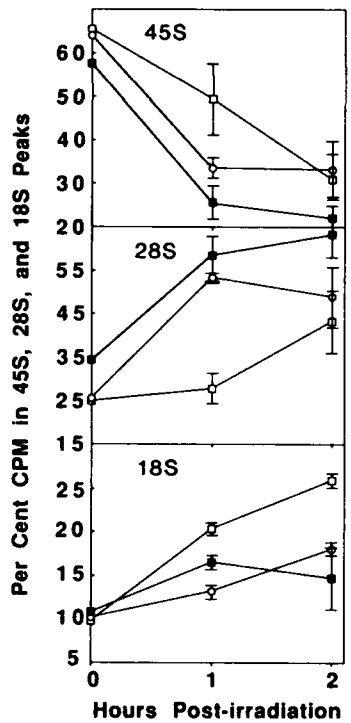

FIG. 2. Relative amounts of 45 S, 28 S, and 18 S rRNA in cells exposed to 5 or 10 Gy. Procedure as in legend to Fig. 1. Two independent experiments on control cells, three on cells receiving 5 Gy, and four on cells receiving 10 Gy were analyzed for the relative areas under the 45 S, 28 S, and 18 S rRNA peaks. Brackets indicate SE. Control (□); 5 Gy (○); 10 Gy (■).

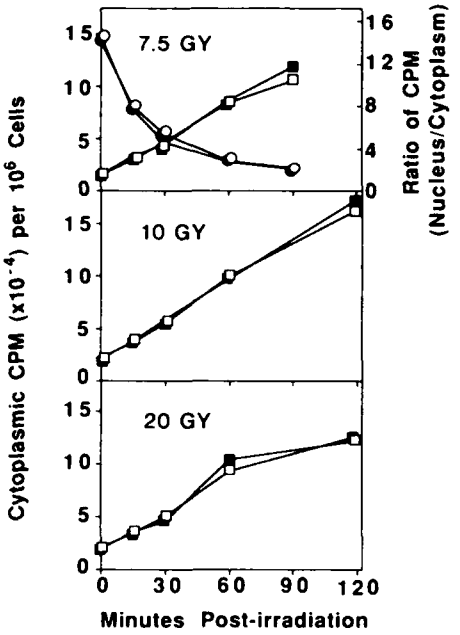

FIG. 3. Transport of acid-insoluble [^{3}H]uridine from nucleus to cytoplasm. Cells were labeled for 15 min with [^{3}H]uridine, followed by washing and incubation for indicated duration. All experiments were accompanied by unirradiated controls processed in parallel. Cytoplasmic fraction was analyzed for TCA-precipitable incorporation (□, control; ■, irradiated), and in the case of 7.5 Gy, the nuclear pellet was also analyzed (○, control; ●, irradiated). Points represent the means of six determinations. In all cases SE was <5.2% of the indicated values.

Figure 1 shows electrophoretic profiles of total RNA, pulse-labeled for 15 min with [^{3}H]uridine prior to an exposure of 5 Gy. RNA was harvested either immediately following irradiation or after further incubation of the flasks for 1 or 2 h at 37°C. Compared to RNA from control cells, at the 1- and 2-h time points there was a decrease in radiolabeled 45 S and 18 S rRNA and an increase in radiolabeled 28 S rRNA. Previous studies (*1*) focused attention on alterations in the 28 S:18 S ratio that remained the same from 5 to 20 h after irradiation, 20 h being the latest time evaluated. However, studies shown here indicate that alterations in 45 S, 28 S, and 18 S rRNA are even more dramatic at shorter times (Fig. 2). From the experimental data summarized in Fig. 2, it can be calculated that the 28 S:18 S stoichiometric ratio is maximal at 1 h, at about 2:1, following either 5 or 10 Gy, and only about 1:1 in control cells, the expected ratio. These calculations take into account the difference in uracil content in the 28 S and 18 S rRNA species, as previously discussed (*1*).

Although rRNA specie content is altered in total RNA preparations, it is not known whether transport from nucleus to cytoplasm reflects this alteration, yielding perturbations in cytoplasmic rRNA content. It might be expected that the accelerated conversion of 45 S rRNA to smaller species results in a higher rate of transfer of [^{3}H]uridine-labeled species to the cytoplasm. However, findings illustrated in Fig. 3 indicate that transfer of acid-soluble label from nucleus to cytoplasm is unaffected following 7.5, 10, or 20 Gy, for up to 2 h. It could be that the increased 28 S:18 S ratio of newly processed rRNA, maximal at 1 h following irradiation, might yield an altered ratio of transport of these daughter species to the cytoplasm without measurably affecting total transport. However, as illustrated in Fig. 4, the content of newly synthesized rRNA in the cytoplasm 60 min following irradiation (approximately 80 min following initiation of 15 min pulse label) is identical to that in control cells. The label in cytoplasmic 18 S rRNA is greater than cytoplasmic 28 S rRNA (Fig. 4); this is consistent with prior findings that the movement of the newly formed 40 S ribosomal subunits from the nuclei in HeLa cells proceeds more swiftly than the movement of the 60 S ribosomal subunit (*6*).

DISCUSSION

We previously measured the stoichiometric ratio of newly processed 28 S:18 S rRNA in whole HeLa S3 cells at times ≥5 h following irradiation (*1*). The 28 S:18 S ratio was altered in a dose-dependent fashion, deviating from the normal of 1:1 in control cells (*1–4*) to a maximum of 1.6:1 following 20 Gy (*1*). The current study extends these observations to earlier times after irradiation, within the first 2 h. We found that the aberrant 28 S:18 S ratio is somewhat larger during the first 2 h (2:1) than at later times (1.6:1), and this difference is detectable following 5 Gy as well as 10 Gy (Fig. 2). At later times (≥5 h) an altered 28 S:18 S ratio

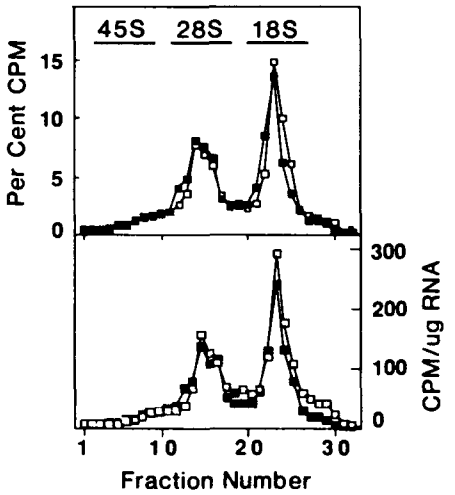

FIG. 4. Labeled rRNA in cytoplasmic fraction 1 h after irradiation. See Materials and Methods for technique and text for further explanation. The location of 28 S and 18 S rRNA species in the ethidium bromide-stained gel are indicated. No 45 S rRNA is present in the cytoplasmic fraction. The location of this species is approximated by comparison to whole cell RNA gels. Control (□); 10 Gy (■).

was not found following 5 Gy (*1*), suggesting a degree of cellular recovery following this lower exposure.

As previously, we suggest that the most likely explanation for the altered 28 S:18 S ratio is degradation of the 18 S portion of the 45 S rRNA precursor during or after processing (*1*). This suggestion is based on the exclusion of three other possible explanations, as follows:

(i) The altered 28 S:18 S ratio is unlikely to be related to alterations in 45 S precursor transcription for two reasons. First, pulse-labeling was completed prior to irradiation, facilitating observation of processing, and minimizing observation of effects caused by postirradiation rRNA synthesis (*1*). Second, even if the measurements were influenced by residual postirradiation incorporation, the opposite result would be expected: since the 18 S portion of the 45 S precursor is upstream from the 28 S portion, postirradiation inhibition of synthesis, yielding partial transcripts, would increase the relative amount of 18 S rRNA, contrary to what was found.

(ii) Effects caused by radiation-induced uridine pool alterations are also an unlikely explanation, for at least two reasons: First, labeling was performed prior to irradiation. Second, since both the 28 S and 18 S rRNA species derive from a single 45 S precursor, any alteration in the specific activity of intracellular pools would affect both daughter species, failing to alter their measured ratio.

(iii) Direct damage of rRNA by ionizing radiation is unlikely to be responsible for the increased 28 S:18 S ratio for two reasons. First, at doses employed in this study direct damage to 45 S rRNA or its daughter species is expected to be slight (*1*). Second, if direct effects were occurring, 28 S rRNA would be expected to present a larger target than 18 S rRNA, decreasing the relative amount of 28 S rRNA, the opposite of what was found.

Cooper observed an increased 28 S:18 S rRNA ratio following pulse-labeling of resting lymphocytes, but not in mitogen-stimulated proliferating lymphocytes, and proposed, as we have, that 18 S rRNA was undergoing degradation in the nondividing cells (*7*). He also proposed that maintenance of cellular integrity would not permit continued accumulation of excess 28 S rRNA in resting lymphocytes, and demonstrated that 28 S rRNA was subsequently degraded, restoring the 28 S:18 S labeling ratio to normal (*8*). This degradation of 18 S and 28 S rRNA may represent an adaptation to cell cycle arrest, reducing the number of newly synthesized ribosomes that would otherwise be required for cellular proliferation (*1*, *7*, *8*). However, we failed to detect any restoration of normal labeling ratio in HeLa cells for durations up to 20 h following irradiation. Perhaps the orderly degradation of excess rRNA in resting cells, first 18 S followed by 28 S rRNA, does not occur in irradiated cells because of abnormal regulation of cellular rRNA content following lethal exposures.

The current studies show that total transport of RNA from the nucleus to the cytoplasm is not affected by the relative overabundance of 28 S rRNA detected in whole cells (Fig. 3). The 28 S:18 S ratio of newly processed rRNA in the cytoplasm was also normal following 10 Gy (Fig. 4). These measurements were carried out within the first 2 h after irradiation when the altered labeling ratio is maximum. Taken together, they suggest that the relative overabundance of 28 S rRNA is limited to the nucleus. However, direct measurement of 28 S:18 S ratio in the nucleus (in contrast to whole cells and the cytoplasmic fraction) was not accomplished because of technical limitations (Materials and Methods). Studies have not yet been carried out to determine whether an altered ratio in the cytoplasm might occur at later times. The apparent accumulation of excess 28 S rRNA in the nucleus, suggested by the current studies, may represent an early step in the process of radiation-induced cell killing.

ACKNOWLEDGMENT

This work was supported by Armed Forces Radiobiology Research Institute MIPR N88015M to K.M.

RECEIVED: April 3, 1989; ACCEPTED: August 14, 1989

REFERENCES

1. J. M. KROLAK, D. MCCLAIN, S. L. SNYDER, P. FUCHS, and K. W. MINTON, 18 S ribosomal RNA is degraded during ribosome maturation in irradiated HeLa cells. *Radiat. Res.* **118**, 234–244 (1989).
2. A. A. HADJIOLOV and N. NIKOLAEV, Maturation of ribosomal ribonucleic acids and the biogenesis of ribosomes. *Prog. Biophys. Mol. Biol.* **31**, 95–134 (1976).
3. R. K. MANDEL, The organization and transcription of eukaryotic ribosomal RNA genes. *Prog. Nucleic Acid Res.* **31**, 115–160 (1984).
4. S. F. WOLF and D. SCHLESSINGER, Nuclear metabolism of ribosomal RNA in growing, methionine-limited, and ethionine-treated HeLa cells. *Biochemistry* **16**, 2783–2791 (1977).
5. W. B. BUTLER, Preparing nuclei from cells in monolayer cultures suitable for counting and for following synchronized cells through the cell cycle. *Anal. Biochem.* **141**, 70–73 (1984).
6. M. GIRARD, H. LATHAM, S. PENMAN, and J. E. DARNELL, Entrance of newly formed messenger RNA and ribosomes into HeLa cell cytoplasm. *J. Mol. Biol.* **11**, 187–201 (1965).
7. H. L. COOPER, Control of synthesis and wastage of ribosomal RNA in lymphocytes. *Nature* **227**, 1105–1107 (1970).
8. H. L. COOPER, Degradation of 28S RNA in ribosomal maturation in nongrowing lymphocytes and its reversal after growth stimulation. *J. Cell Biol.* **59**, 250–254 (1973).

Radiation Protection Dosimetry
Vol. 31 No. 1/4 pp. 85–89 (1990)
Nuclear Technology Publishing

CALCULATIONS OF THE RELATIVE EFFECTIVENESS OF ALANINE FOR NEUTRONS WITH ENERGIES UP TO 17.1 MeV

H. M. Gerstenberg†‡, J. W. Hansen§, J. J. Coyne‡ and J. Zoetelief‡‖
†Armed Forces Radiobiology Research Institute
Bethesda, MD 20814-5145, USA
‡Center for Radiation Research, Nuclear Radiation Division
National Institute of Standards and Technology (formerly National Bureau of Standards)
Gaithersburg, Maryland, USA
§Risø National Laboratory
DK-4000 Roskilde, Denmark
‖Radiobiological Institute TNO
Rijswijk, The Netherlands

Abstract — The relative effectiveness (RE) of alanine has been calculated for neutrons using the RE of alanine for charged particles. The neutrons interact with one or more of the elements (hydrogen, carbon, nitrogen and oxygen) that compose the alanine. These interactions produce spectra of secondary charged particles consisting of ions of H, D, He, Be, B, C, N, and O. From a combination of the calculated secondary charged particle spectra generated by the slowing down neutrons, and the calculated RE of the ions produced, a RE for the neutrons can be obtained. In addition, lineal energy spectra were determined for neutrons with energies up to 17.1 MeV interacting with alanine. An analytical code was used to calculate these spectra for a 1 μm diameter alanine cell surrounded by an alanine medium. For comparison, similar calculations were made for muscle tissue. Finally, the calculated differential RE was folded with dose distributions to obtain RE-weighted distributions for alanine.

INTRODUCTION

The response of a biological system to various kinds of ionising radiation is described by a concept called relative biological effectiveness (RBE). Similarly, the response of a non-biological system, such as a physical or chemical system, is described by a concept called relative effectiveness (RE). Like RBE, RE can be expressed as a function of linear energy transfer (LET).

The RE of high LET radiation is defined as the ratio of doses from the low and high LET radiations (in this work the low LET radiation is ^{60}Co) that produces the same radiation response under identical target conditions. Unlike most biological systems, physical and chemical systems generally display a decrease in RE with increasing LET and have RE values equal to or less than unity.

Values of RE for alanine exposed to various charged particles have been predicted from model calculations and measured[1,2] using the electron spin resonance technique. This technique can be used since radiation-induced stable free radicals are produced in alanine. RE can be calculated over a wide range of LET and particle parameters, and calculated predictions based on the track structure theory of heavy charged particles[3] show agreement with measured data.

Alanine is a particularly interesting material for use as a detector for radiation dosimetry as it has linearity of response over a wide range of dose, good time stability of the induced free radicals, availability of a non-destructive read-out technique and accuracy and repeatability of measurements. Alanine dosimetry is an attractive alternative to the ferrous sulphate, or Fricke, system of dosimetry. In addition, the chemical composition of alanine (CH_3-$CH(NH_2)$–COOH) is quite close to that of tissue, making the amino acid particularly suitable for neutron dosimetry.

OBJECTIVES

Very little information is available concerning the RE of alanine exposed to neutron radiations. When material is irradiated by neutrons, the ionising radiation produced is principally charged particles. Thus it is possible to calculate the neutron RE of alanine if the initial energy spectra of charged particles caused by neutrons are known, and if the RE of each charged particle is known at each energy.

The first objective of this study is to calculate the RE for alanine irradiated with neutrons having energies between 0.1 MeV and 17.1 MeV. The second objective is to calculate the dose distribution for alanine as a function of lineal energy and compare the result with that of tissue. The third

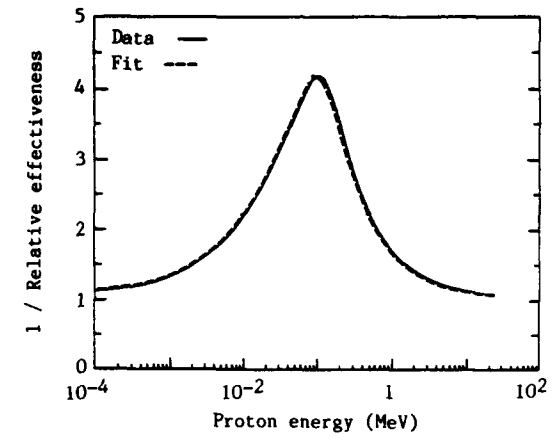

Figure 1. Inverse of the RE of alanine irradiated with protons. These data show the response for completely stopped particles that started with an initial energy given on the abscissa. The solid line is based on calculated and measured data; the dashed line is a modified hyperbolic function fit. A similar hyperbolic function fit was obtained for each of the different charged particles produced by the neutrons.

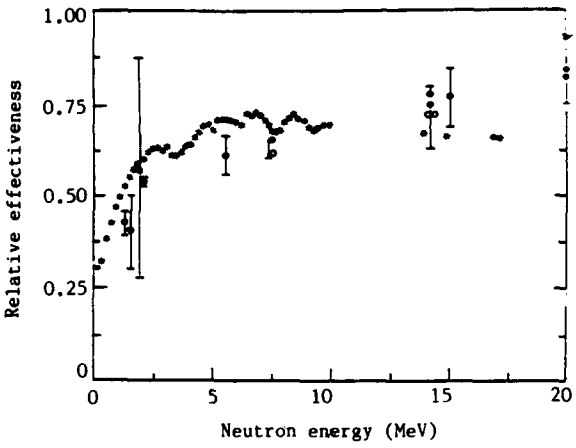

Figure 2. RE for alanine at different neutron energies. The asterisks are the results of our calculations. The solid circles are experimental data and the open circles are calculated data; these data were obtained from the literature on alanine.

objective is to fold the calculated RE with its dose distribution and obtain a RE-weighted dose distribution for alanine.

RELATIVE EFFECTIVENESS

Figure 1 shows the inverse of the RE of alanine exposed to protons. These data show the response for completely stopped particles that started with an initial energy as given on the abscissa. The solid line shows data based on both measurements and calculations. The dashed line is a fit to these data using a modified hyperbolic function. For each charged particle a similar function with different constants was determined. These functions were then folded with the initial energy spectra of charged particles created by monoenergetic neutrons of a given energy. The RE for alanine was then determined at several neutron energies.

RE is calculated according to

$$RE = \frac{\sum_{i=1}^{i=8} \int_0^{E_{max}} n_i(E) \cdot E \cdot RE_i(E).dE}{\sum_{i=1}^{i=8} \int_0^{E_{max}} n_i(E) \cdot E \cdot dE}$$

where $n_i(E)$ is the initial energy distribution of the i-th charged particle, and $RE_i(E)$ is RE as a function of energy for the same particle.

Figure 2 shows the RE for alanine calculated by combining the initial energy spectra of charged particles with their RE. Each of our calculated data points is shown as an asterisk over the neutron energy range between 0.1 MeV and 17.1 MeV. The oscillations of the data points are due to experimental variations in the nuclear cross section data used to calculate the initial spectra of heavy ions. Results of the measurements for the RE, as found in the literature[4], are shown as solid points with indicated error bars. Results of three other calculations are shown as open circles at 7.5 MeV and 14.0 MeV[4].

Relative to the measured data, our calculated data give a higher RE below 6 MeV and a lower RE above 13 MeV. Our calculated data consider neutrons that are nearly monoenergetic; the neutron energy bin width is only 200 keV wide. This contrasts with the measured data in which the neutrons are polyenergetic, with neutron energies in some cases ranging over many MeV of energy. The measurements must also extract the large RE contribution due to photons in the neutron beams.

The primary input for our calculations is the ENDF/B-V nuclear data file[5] of the National Nuclear Data Center at Brookhaven; a more recent evaluated data set[6,7] was used for the carbon cross section. The computer program developed at the National Institute of Standards and Technology[8,9] was used for the calculations.

DOSE DISTRIBUTIONS

Figure 3 shows the calculated dose distribution for a 1 μm cavity as a function of lineal energy (y). The radiation source was monoenergetic neutrons at 1.1 MeV. Figure 4 shows the same except the neutron energy was 16.9 MeV. We assumed that the cavity and surrounding wall were made of the same material. Calculations were then made where

material was either tissue or alanine. The curves in Figures 3 and 4 indicate how the dose distribution varies between the two materials. RE values determined in the previous section were not used in these calculations.

The major contribution to the dose at a neutron energy of 1.1 MeV is due to elastically-scattered protons from hydrogen contained in both tissue and alanine. The dose from the protons shows as a broad peak centred near 50 keV.μm^{-1} in Figure 3. The calculated dose is higher for tissue because tissue has 29% more hydrogen. The dose above the proton cut-off at 150 keV.μm^{-1} is due to a small number of heavy-ion recoils. Table 1 gives percentage by weight of the elemental composition for alanine[10] and tissue. The composition of tissue is given by the International Commission on Radiation Units and Measurements (ICRU)[11].

At 16.9 MeV, the broad peak due to the protons shifts down in lineal energy and is centred near 7 keV.μm^{-1} in Figure 4. The shift occurs because the rate of energy loss in the cavity is less for higher energy protons caused by the 16.9 MeV neutrons than for low energy protons caused by the 1.1 MeV neutrons.

Like the calculation at a neutron energy of 1.1 MeV, the dose distribution from the 16.9 MeV neutrons in the lineal energy region of 7 keV.μm^{-1} is greater for tissue than for alanine. However, in the region above 150 keV.μm^{-1}, the reverse holds true; the dose distribution from alanine is greater than that of tissue because the alanine has a larger fraction of carbon and nitrogen compared with tissue. For these elements at this neutron energy, more reaction channels are open for producing alpha particles and heavy ion recoils; these ions contribute a substantial dose in this lineal energy region.

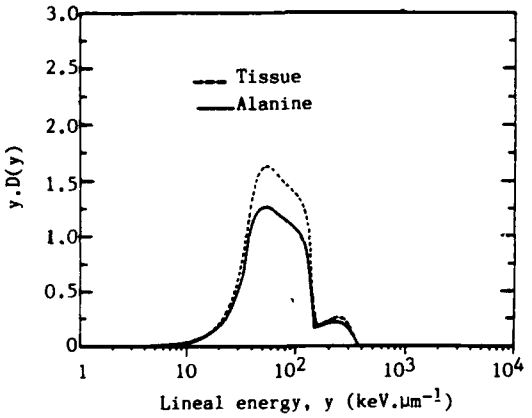

Figure 3. Calculated dose distributions in lineal energy for alanine and tissue at a monoenergetic neutron energy of 1.1 MeV. The solid line is the result for alanine and the dashed line is the result for ICRU tissue. The large peaks are caused by the dose contribution from the protons.

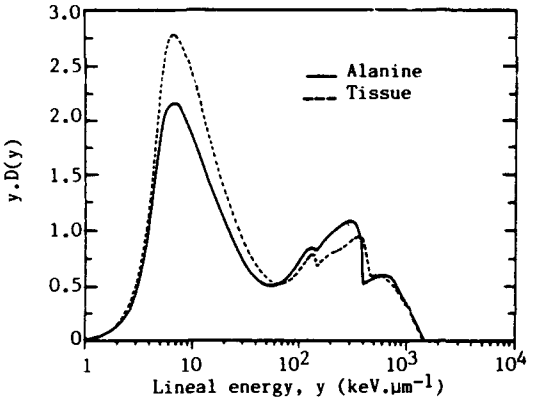

Figure 4. Same as Figure 3 except at a monoenergetic neutron energy of 16.9 MeV. Note that the large peaks have now shifted to a lower lineal energy; this is explained in the text.

Table 1. Elemental composition of alanine and tissue.

Material	H	C	N	O
Alanine	7.92	40.44	15.72	35.92
Tissue	10.20	12.30	3.50	74.00*

* In tissue, the six elements with a Z greater than 8 were considered to be oxygen. The per cent by weight of these few elements was equal to 1.10 and was added to that of oxygen.

Figures 5 and 6 show dose distributions as a function of lineal energy for alanine at neutron energies 1.1 and 16.9 MeV, respectively. The dashed curves show spectra of energy deposited by the charged particles weighted with the differential RE of the ions and normalised to the average RE for that neutron energy. This weighting and normalisation produces some distortion of the y spectra which can be seen by comparing the unmodified y spectra with the modified y spectra shown as solid curves in these figures. For example, for the 1.1 MeV neutrons, the proton edge — normally around 150 keV.μm^{-1} — is reduced to 90 keV.μm^{-1} because, in this region, the protons have a differential response which is lower than the average response for the 1.1 MeV neutrons. The shift is in the opposite direction for the region around 30 keV.μm^{-1}; in this region the protons have an average differential response which is greater than the average response for the neutrons. Although difficult to interpret because more charged particles are involved, similar reasoning explains the distortion for the weighted y spectrum for 16.9 MeV neutrons. The solid curves, shown in these two figures for comparison with the dashed curves, are the same as the solid curves shown in Figures 3 and 4.

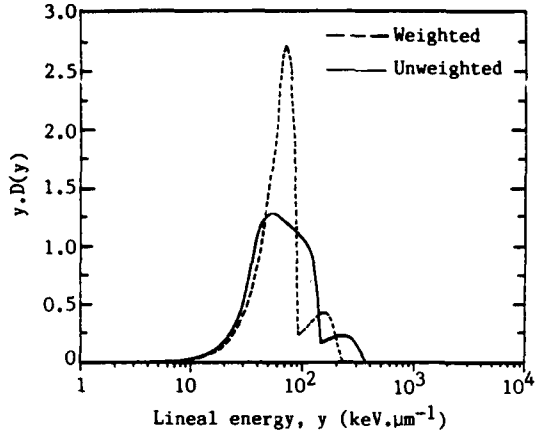

Figure 5. Calculated dose distributions in lineal energy for alanine determined at a neutron energy of 1.1 MeV. The dashed curve shows the spectrum of energy deposited by the charged particles weighted with the differential RE of the ions and normalised to the average RE for that neutron energy. This modification produces a distortion of the y spectrum which can be seen by comparing the modified spectrum with the unmodified spectrum shown as a solid line in this figure. The solid line is the unweighted distribution shown in the previous figure and repeated here for comparison with the weighted result. The reasons for the distortions are explained in the text.

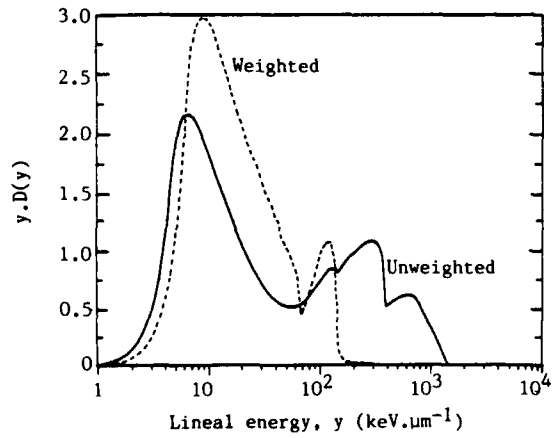

Figure 6. Same as Figure 5 except at a neutron energy of 16.9 MeV.

In general, the effect of the weighted RE on the dose distributions is the same for the results calculated at neutron energies 1.1 MeV and 16.9 MeV. Low y events are emphasised and high y events are de-emphasised because RE decreases with increasing LET. In addition, heavier ions also have a lower RE.

CONCLUSIONS

The RE for alanine has been calculated for monoenergetic neutrons with energies between 0.1 MeV and 17.1 MeV. Comparison of these results with measurements indicates general agreement but shows a somewhat higher calculated RE for lower neutron energies and a lower RE for higher neutron energies. The reason for these differences is being investigated.

The dose distribution as a function of lineal energy has been calculated at several neutron energies for alanine; comparison of these results is made with that of ICRU tissue. Differences observed are readily explained by the relative proportions of hydrogen, carbon, nitrogen, and oxygen found in the two materials.

Dose distributions for alanine, weighted with the differential RE values, were also calculated. The results when compared with the unweighted data show an increase of dose for low y events and a decrease of dose for the high y events. These results are consistent with a decreasing RE for values of high LET.

ACKNOWLEDGEMENTS

We are grateful for the support from the National Institute of Standards and Technology in appointing one of us (H. M. G.) as a guest researcher and one of us (J. Z.) as a visiting scientist. The views presented in this paper are those of the authors. No endorsement by the Defense Nuclear Agency, National Institute of Standards and Technology, Risø National Laboratory, or Radiobiological Institute TNO has been given or should be inferred.

REFERENCES

1. Hansen, J. W., Olsen, K. J. and Wille, M. *The Alanine Radiation Detector for High and Low LET Dosimetry.* Radiat. Prot. Dosim. **19**, 43-47 (1987).
2. Hansen, J. W. *Experimental Investigation of the Suitability of the Track Structure Theory in Describing the Relative Effectiveness of High-LET Radiation of Physical Radiation Detectors.* Risø-R-507, Risø National Laboratory (Roskilde, Denmark) (1984).
3. Katz, R., Sharma, S. C. and Homayoonfar, M. *The Structure of Particle Tracks.* In: Topics of Radiation Dosimetry, Suppl. 1. Ed. F. H. Attix, pp. 317-383 (New York: Academic Press) (1972).
4. Waligórski, M. P. R., Danialy, G., Loh, Kim Sun and Katz, R. *The Response of the Alanine Detector After Charged Particle and Neutron Irradiations.* In: 2nd Int. Symp. on ESR Dosimetry and Applications, Munich/Neuherberg (1988).

5. ENDF/B Summary Documentation. BNL-NCS-17541 (ENDF-201), 3rd edn (ENDF/B-V). Ed. R. Kinsey (National Nuclear Data Center, Brookhaven National Laboratory) (1979).
6. Axton, E. J. (National Institute of Standards and Technology, Gaithersburg, MD 20899 USA) private communication (1988).
7. Gerstenberg, H. M., Caswell, R. S. and Coyne, J. J. *Initial Spectra of Neutron-Induced Secondary Charged Particles.* Radiat. Prot. Dosim. **23**, 41-44 (1988).
8. Caswell, R. S. *Deposition of Energy by Neutrons in Spherical Cavities.* Radiat. Res. **27**, 92-107 (1966).
9. Caswell, R. S. and Coyne, J. J. *Neutron Deposition Spectra Studies.* In: Proc. 4th Symp. on Microdosimetry, EUR 5122, Verbania Pallanza, Italy. pp. 967-982 (Luxembourg: CEC) (1973).
10. Seltzer, S. M. and Berger, M. J. *Evaluation of the Collision Stopping Power of Elements and Compounds for Electrons and Positrons.* Int. J. Appl. Radiat. Isot. **33**, 1189-1218 (1982).
11. International Commission on Radiation Units and Measurements. *Physical Aspects of Irradiation.* Report 10b. (International Commission on Radiation Units and Measurements, Bethesda, Maryland) (1964).

Hypermetabolic priming of canine neutrophils by 7-S nerve growth factor

Dale F. Gruber, PhD; Kevin P. O'Halloran; Michele M. D'Alesandro, PhD; Ann M. Farese, MA

SUMMARY

Canine circulating neutrophils, isolated by a blood lysing technique, were incubated with 7-S nerve growth factor (NGF), at final concentrations between 12.5 and 800 ng/ml, for 30 minutes at 37 C. Neutrophil cytosolic H_2O_2 production, measured by flow cytometry, after 7-S NGF incubation was not significantly different from that produced at 37 C (baseline temperature controls) alone. Phorbol myristate acetate (PMA; 100 ng/ml) stimulation of neutrophils produced cytosolic H_2O_2 concentrations almost 13 times that of baseline temperature control neutrophils. Preincubation of neutrophils with 7-S NGF (100 to 800 ng/ml, 30 minutes, 37 C) and subsequent stimulation by PMA resulted in augmented H_2O_2 production in excess of twice that of neutrophils treated with PMA alone, and almost 30 times that of baseline temperature controls.

It has become apparent that individual cytokines have the capacity to exert multiple biological effects. Examples are platelet-derived growth factor, which is a cellular mitogen[1] and a chemoattractant,[2] and thrombin, which is a blood clotting enzyme, a cellular mitogen,[3] and a chemoattractant.[4] Sources of bioregulatory cytokines may include cells or specialized tissues (eg, glands). Salivary gland secretions have been examined based on observations that, in addition to enzymatic and hydrolytic activities, saliva also promoted healing. Saliva contains many biologically active substances including epidermal growth factor,[5] kallikrein,[6] amylase,[7] lysozyme,[8] immunoglobulins,[7] renin,[9] and nerve growth factor (NGF).[10,11] Despite its descriptive designation, NGF is capable of neuronal and nonneuronal biological activities. In serum and saliva, NGF exists principally in 2 molecular weights, with sedimentation coefficients (S) of 2.5 and 7.[10] The 2.5-S NGF form promotes neuronal outgrowth from embryonic sensory ganglia.[11,12] The 7-S NGF form, topically applied to skin wounds of mice, accelerated wound contraction and healing processes.[13] Because the presence (or absence) of bioregulatory or inflammatory mediator substances may considerably alter the host's ability to respond to tissue damage or initiate wound repair, we examined the metabolic responses of isolated canine neutrophils after incubation with 7-S NGF. Neutrophils were selected because they represent the host's primary cellular elements of nonspecific resistance. The canine model was selected because of its preclinical model status for examination of septic shock[14-16] and cardiac[17] and pulmonary injuries.[18]

Received for publication Oct 31, 1988.

From the Experimental Hematology Department, Armed Forces Radiobiology Research Institute, Bethesda, MD 20814-5145 (Gruber, O'Halloran, Farese), and the Environmental Medicine Department, Naval Medical Research Institute, Bethesda, MD 20814-5050 (D'Alesandro).

Supported by the Armed Forces Radiobiology Research Institute, Defense Nuclear Agency, under work unit 00130. Research was conducted according to the principles enunciated in the "*Guide for the Care and Use of Laboratory Animals*" prepared by the Institute of Laboratory Animal Resources, National Research Council.

The authors thank R. T. Brandenburg, L. Huff, and L. M. Konradi for technical assistance.

Materials and Methods

Reagents—Stock solutions of dichlorofluorescin diacetate (DCFH-DA[a]; 5 m*M*) were stored in absolute ethanol. Phorbol myristate acetate (PMA)[b] was dissolved in dimethylsulfoxide[b] at a concentration of 0.01*M* and stored at 4 C until used. Fetal bovine serum (FBS)[c] was heat-inactivated (56 C, 60 minutes) and filtered (0.45 μm) before use.

Dogs—Beagles (10 to 12 kg, 1 to 2 years old) were used in the study. Dogs were quarantined on arrival and screened for evidence of disease before being released for the study. Dogs were individually kenneled and provided commercial dog chow and tap water ad libitum. Animal holding rooms were maintained at 21 ± 1 C with 50 ± 10% relative humidity, using at least 10 changes of 100% conditioned fresh air/h; the lighting schedule was a 12-hour light/dark full-spectrum cycle with no twilight.

Neutrophil isolation—Blood (5 ml) was drawn from the lateral saphenous vein once weekly into syringes containing preservative-free heparin[d] (10 U/ml). Blood was washed in Hanks balanced salt solution[d] without Ca^{2+} and Mg^{2+} (400 × g, 10 minutes, 21 C). Contaminating RBC were lysed with 0.83% NH_4Cl[e] (10 minutes, 4 C), and the leukocytes were pelleted by centrifugation. The cell pellet was minimally resuspended in phosphate-buffered saline solution (PBSS)[d] supplemented with 0.2% heat-inactivated FBS. Wright-stained blood smears were prepared for differential and morphologic examination. Complete blood cell count was determined by automated analysis.[f]

NGF *incubation*—Commercial 7-S NGF[g] (mol wt 130,000) obtained from mouse submaxillary glands by the method of Varon et al[19] was added to isolated canine neutrophils in PBSS supplemented with 0.2% FBS and 10% 50 μ*M* glucose. Final concentration(s) ranged between 12.5 and 800

[a] Eastman Kodak Co, Rochester, NY.
[b] Sigma Chemical Co, St Louis, Mo.
[c] Hyclone Laboratories, Logan, Utah.
[d] Grand Island Biological Co, Grand Island, NY.
[e] Fischer Scientific, Silver Spring, Md.
[f] Coulter Electronics, Hialeah, Fla.
[g] Collaborative Research Inc, Lexington, Mass.

ng of 7-S NGF/10^6 cells/ml. Cells were incubated with 7-S NGF for 15 to 30 minutes at 37 C.

Measurement of intracellular H_2O_2 production—Hydrogen peroxide production was measured by flow cytometry essentially as described by Bass et al.[20] The DCFH-DA, a nonpolar, nonfluorescent compound diffused through cell membranes, was hydrolyzed by cellular esterases to nonfluorescent, intracellularly trapped 2',7'-dichlorofluorescin. The H_2O_2 produced by activated neutrophils oxidizes 2'7'-dichlorofluorescin to the fluorescent analogue 2',7'-dichlorofluorescein. Neutrophils (10^6 cells/ml) were incubated with 5 μM DCFH-DA in PBSS supplemented with 0.2% FBS and 10% 50-μM glucose for 10 minutes at 37 C, then stimulated with PMA (100 ng/ml) or variable concentrations of 7-S NGF for 15 minutes. Other neutrophil aliquots were primed with 7-S NGF for 30 minutes and subsequently stimulated with PMA. Intracellular fluorescence was measured by flow cytometry on a fluorescence-activated cell sorter analyzer.[h] The percentage change in H_2O_2 production was determined by the formula:

$$\frac{\text{Mean fluorescent intensity (FL), experimental} - \text{FL, control}}{\text{FL, control}}$$

Statistical analysis—All data are expressed as the mean ± SEM. Statistical differences were determined, using the Student *t* test. Probability values < 0.05 were considered statistically significant.

Results

Phorbol myristate acetate has been used to activate the protein kinase C (PKC)-dependent oxidative metabolism of neutrophils.[21] We previously determined that the metabolic effects (ie, H_2O_2 production) of PMA on canine neutrophils were near maximal at 100 ng of PMA/ml.[22] This concentration was used throughout this study as the PMA reference standard. Table 1 indicates the cytosolic H_2O_2 production in neutrophils incubated at 37 C (baseline temperature control) alone, or in the presence of either PMA (100 ng/ml) or 7-S NGF (400 ng/ml). Phorbol myristate acetate-induced neutrophil cytosolic H_2O_2 production was 13 times that of temperature-control neutrophils. There was no difference between H_2O_2 production by baseline temperature-control neutrophils or those incubated with 7-S NGF.

The ability of NGF (50 ng/ml) to stimulate cellular PKC[23] activity prompted examination of the 7-S NGF upregulation of isolated canine neutrophils to secondary stimulation. In neutrophils incubated for 30 minutes in medium containing 7-S NGF (400 ng/ml) and subsequently stimulated with PMA, cytosolic H_2O_2 production was greater than twice that of cells not preincubated, and almost 30 times higher than that of baseline temperature-control cells (Table 1). Figure 1 is a dose-response curve of 7-S NGF priming for secondary stimulation by PMA. Hydrogen peroxide production was significantly ($P < 0.001$) augmented after preincubation with 100 ng of 7-S NGF/ml. Maximal H_2O_2 production was observed after preincubation of cells with 200 to 800 ng of 7-S NGF/ml prior to PMA stimulation.

Discussion

It has become apparent that growth factors biologically affect a wide variety of target cells. In this study, we suggest that in addition to its neurobiologic properties,[24-27] NGF is capable of influencing the oxidative metabolism (ie, H_2O_2 production) of nonspecific inflammatory cells, ie, neutrophils. Although 7-S NGF alone had no direct effect on in vitro neutrophil cytosolic H_2O_2 production, preincubation of neutrophils with 7-S NGF resulted in substantially enhanced production of cytosolic H_2O_2 in response to secondary stimulation with PMA. Neutrophils preincubated with 7-S NGF responded to PMA stimulation at production in excess of twice that of PMA alone.

Despite recognition of NGF as a neurobiologic stimulating factor, concentrations of 7-S NGF in tissues and fluids have remained somewhat uncertain, owing in large part to quantitative differences obtained by application of the chicken embryo dorsal root ganglion bioassay[28] or radioimmunoassay[10,29] techniques. Reported human plasma 7-S NGF concentration has ranged between 3.9[29] and 600[30] ng/ml, and reported mouse plasma concentration ranges between 2[31] and 1,590[29] ng/ml. Organ concentrations likewise have been reported to have wide ranges. Male mouse submaxillary glands, for example, have been reported to have NGF concentrations between 0.85 and 35 mg/g (wet weight).[29,32] Because little information existed on the effects of 7-S NGF on hematopoietic

[h] Becton, Dickinson & Co, Mountain View, Calif

Table 1—Increases* in neutrophil cytosolic H_2O_2 concentrations as a function of treatment

Treatment(s)	Increase H_2O_2 production (± SEM, × 100)
37 C	1.05 ± 0.13
37 C + 7-S NGF	0.97 ± 0.11
37 C + PMA	13.25 ± 1.14†
37 C + 7-S NGF + PMA	39.19 ± 2.64†

* All increases were normalized to a T = 0-minute measure and are expressed in terms of fold increases (± SEM) relative to T = 0 minute. Individual experimental means were calculated from a minimum of 10,000 cellular events
† $P < 0.05$, compared with 37 C treatment

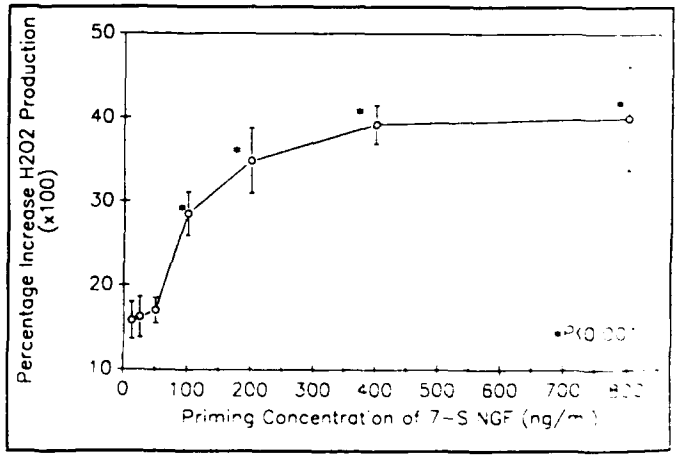

Figure 1—Effect of 7-S nerve growth factor (NGF; 12.5 to 800 ng of 7-S NGF/ml) preincubation on phorbol myristate acetate-induced H_2O_2 production. Results are expressed as the mean (± SEM) increase (× baseline) compared with baseline temperature controls of 6 replicate experiments. Experimental means were calculated from a minimum of 10,000 cellular events.

inflammatory cells, we investigated the cellular metabolic effects of 7-S NGF on neutrophils at concentrations within previously reported maxima.

The cellular mechanisms by which PMA and 7-S NGF operate may indicate some metabolic commonality in the involvement of PKC. The role of PKC in biological signal transduction has been previously described.[33] Phorbol myristate acetate activates cellular PKC and mimics some actions of NGF. Added to serum-free medium, PMA supports neuronal survival and outgrowth in a manner similar to NGF.[34] The PC12 cell cultures treated with 50 ng of NGF/ml responded with four- to fivefold increases in PKC activity within 60 minutes.[23] It was suggested by Hama et al[23] that PC12 cells treated with NGF may have cytosolic cofactors generated for PKC. The cytosolic availability of cofactors, although representing an attractive explanation for the 7-S NGF-induced hypermetabolic results reported here, remains an area that deserves further examination.

We have reported that 7-S NGF significantly influences the cellular oxidative metabolism of neutrophils in vitro by priming them for secondary stimulation. In a clinical scenario, altered in vivo concentrations of NGF, or other cytokines, could exacerbate tissue injury and inflammation via the indiscriminant release of toxic oxygen radicals. The mechanism(s) by which NGF or other cytokines are released or affect cellular function(s) are areas that deserve further investigation.

References

1. Ross R. Platelet-derived growth factor. In: Baserga R, ed. *Tissue growth factors*. New York: Springer-Verlag, 1981;133–159.
2. Deuel TF, Senior RM, Huang SJ, et al. Chemotaxis of monocytes and neutrophils to platelet-derived growth factor. *J Clin Invest* 1982;69:1046–1049.
3. Chen LB, Buchanan JM. Mitogenic activity of blood components: I. thrombin and prothrombin. *Proc Natl Acad Sci USA* 1975;72:131–135.
4. Bar-Shavit R, Kahn A, Fenton JW, et al. Chemotactic response of monocytes to thrombin. *J Cell Biol* 1983;96:282–285.
5. Pasquini F, Petris A, Sbaraglia G, et al. Biological activities in the granules isolated from the mouse submaxillary gland. *Exp Cell Res* 1974;86:233–236.
6. Maranda B, Rodrigues JAA, Schachter M, et al. Studies on kallikrein in the duct systems of the salivary glands of the cat. *J Physiol* 1978;276:321–328.
7. Kraus FW, Mestecky J. Immunohistochemical localization of amylase, lysozyme and immunoglobulins in the human parotid gland. *Arch Oral Biol* 1971;16:781–789.
8. Flemming A. On a remarkable bacteriolytic element found in tissues and secretions. *Proc R Soc Lond [Biol]* 1922;B93:307–317.
9. Cozzari C, Angletti PU, Lazar J, et al. Separation of isorenin activity from nerve growth factor (NGF) activity in mouse submaxillary gland extracts. *Biochem Pharmacol* 1973;22:1321–1327.
10. Thoenen H, Barde YA. Physiology of nerve growth factor. *Physiol Rev* 1980;60:1284–1335.
11. Levi-Montalcini R, Hamburger V. Selective growth stimulating effects of mouse sarcoma on the sensory and sympathetic nervous system of the chicken embryo. *J Exp Zool* 1951;116:321–361.
12. Levi-Montalcini R, Hamburger V. A diffusable agent of mouse sarcoma, producing hyperplasia of sympathetic ganglia and hyperneurotization of viscera in the chick embryo. *J Exp Zool* 1953;123:233–287.
13. Li AKC, Koroly MJ, Schattenkerk ME, et al. Nerve growth factor: acceleration of the rate of wound healing in mice. *Proc Natl Acad Sci USA* 1980;77:4379–4381.
14. Hinshaw LB, Beller BK, Archer LT, et al. Recovery from lethal *E coli* shock in dogs. *Surg Gynecol Obstet* 1979;149:545–553.
15. Wichterman KA, Baue AE, Chaudry IH. Sepsis and septic shock: a review of laboratory models and a proposal. *J Surg Res* 1980;29:189–201.
16. Evans SF, Hinds CJ, Varley JG. A new canine model of endotoxin shock. *Br J Pharmacol* 1984;83:433–442.
17. Shatney CH, MacCarter DJ, Lillehei RC. Temporal factors in the reduction of myocardial infarct volume by methylprednisolone. *Surgery* 1976;80:61–69.
18. Joyce LD, Smith JM, Mauer HG, et al. Zymosan-induced resistance to endotoxin and hemorrhagic shock. *Adv Shock Res* 1979;1:125–147.
19. Varon S, Nomura J, Perez-Polo JR, et al. The isolation and assay of the nerve growth factor proteins. *Methods Neurochem* 1972;3:203–229.
20. Bass DA, Parce JW, Dechatelet LR, et al. Flow cytometric studies of oxidative product formation by neutrophils: a graded response to membrane stimulation. *J Immunol* 1983;130:1910–1917.
21. Hafeman DG, McConnell HM, Gray JW, et al. Neutrophil activation monitored by flow cytometry: stimulation by phorbol diester is an all-or-none event. *Science* 1982;215:673–675.
22. Gruber DF, D'Alesandro MM. Changes in canine neutrophil function(s) following cellular isolation by Percoll gradient centrifugation or isotonic lysis. *Immunopharmacol Immunotoxicol* 1989;10:537–544.
23. Hama T, Huang K, Guroff G. Protein kinase C as a component of a nerve growth factor-sensitive phosphorylation system in PC12 cells. *Proc Natl Acad Sci USA* 1986;83:2353–2357.
24. Liuzzi A, Pocchiari F, Angletti PU. Glucose metabolism in embryonic ganglia: effect of nerve growth factor (NGF) and insulin. *Brain Res* 1968;7:452–454.
25. Angletti PU, Liuzzi A, Levi-Montalcini R. Stimulation of lipid biosynthesis in sympathetic and sensory ganglia by a specific nerve growth factor. *Biochim Biophys Acta* 1964;84:778–781.
26. Levi G, Lattes MG. Effect of nerve growth factor on the transport of amino acids in spinal ganglia from chick embryos. *Life Sci* 1968;7:827–834.
27. Angletti PU, Gandini-Attardi D, Toschi G, et al. Metabolic aspects of the effect of nerve growth factor on sympathetic and sensory ganglia: protein and ribonucleic acid synthesis. *Biochim Biophys Acta* 1965;95:111–120.
28. Levi-Montalcini R, Angeletti PU. Nerve growth factor. *Physiol Rev* 1968;48:534–569.
29. Johnson DG, Gorden P, Kopin IJ. A sensitive radioimmunoassay for 7S nerve growth factor antigens in serum and tissues. *J Neurochem* 1971;18:2355–2362.
30. Fabricant RN, DeLarco JE, Todara GJ. Nerve growth factor receptors on human melanoma cells in culture. *Proc Natl Acad Sci USA* 1977;74:565–569.
31. Lakshmanan J. Nerve growth factor levels in mouse serum: variations due to stress. *Neurochem Res* 1987;12:393–397.
32. Bocchini V, Angeletti PU. The nerve growth factor: purification as a 30,000-molecular-weight protein. *Proc Natl Acad Sci USA* 1969;64:787–794.
33. Tauber AI. Protein kinase C and the activation of the human neutrophil NADPH-oxidase. *Blood* 1987;69:711–720.
34. Wakade AR, Wakade TD, Malhotra RK, et al. Excess K^+ and phorbol ester activate protein kinase C and support the survival of chick sympathetic neurons in culture. *J Neurochem* 1988;51:975–983.

Journal of Immunological Methods, 135 (1990) 95–99
Elsevier

JIM 05772

Effect of anticoagulants and heat on the detection of tumor necrosis factor in murine blood

Patricia A. Holobaugh and Daniel C. McChesney *

Department of Experimental Hematology, Armed Forces Radiobiology Research Institute, Bethesda, MD 20889, U.S.A.

Assays for tumor necrosis factor (TNF) may be inhibited by nonspecific factors present in body fluids. We found that the ability to quantitate TNF is greatly affected by blood processing methods. Mice were anesthetized by inhalation of methoxyflurane before obtaining blood by cardiac puncture. The blood from a group of mice was allowed to clot before recovery of serum. Plasmas were obtained from three other groups of mice after collection of blood into tubes containing EDTA, sodium citrate, or preservative-free heparin. The pooled serum or plasmas were spiked with rhTNF to a final concentration of 1 μg/ml and aliquoted for frozen storage. The serum and plasmas were divided into heated (56°C for 30 min) and unheated portions prior to a standard L929 cytotoxicity assay. Comparison of absorbances at 595 nm after crystal violet staining of cells revealed differences in detection of TNF in plasmas compared to serum and in heated compared to nonheated samples. Citrated plasma clotted in the assay at dilutions at or below 1 : 25. EDTA plasma consistently produced unexplained lysis of L929 cells in both heated and unheated unspiked samples. We conclude that TNF levels should be determined only in heat treated serum samples, and that comparisons be made against both a TNF standard and a TNF standard prepared in normal homologous serum that can be heated and assayed in parallel with the test samples.

Key words: Tumor necrosis factor; Bioassay; Plasma; Serum; (Murine)

Introduction

Tumor necrosis factor (TNF) has both beneficial and adverse effects on the animal host (Beutler et al., 1986). It is the mediator of the toxic effects of endotoxin (Hesse et al., 1988). An increase in circulating TNF is generally considered to be deleterious (Waage et al., 1987). Circulating TNF has been detected in some nonbacterial disease states (Kern et al., 1989), but not in others (Moldawer et al., 1987).

Current methods to assay for TNF in body fluids or culture supernatants depend on immunologic and biologic endpoints (Meager et al., 1989). The presence of serum in culture medium may interfere with the sensitivity of bioassays (Kramer et al., 1986). This does not reconcile the inherent variability present among individual serum or plasma samples to be tested. The manner in which a blood sample is handled greatly alters the levels of detectable TNF; thus, endotoxin-contaminated tubes cause rapid increases in TNF released from blood monocytes (Leroux-Roels et al., 1988).

Our research is focussed on the effects of immunomodulators administered following exposure to radiation in murine models. The results of our

Correspondence to: P.A. Holobaugh, Biomedical Research Monitoring, Center for Biologics Evaluation and Research, Food and Drug Administration, Rockville, MD 20855, U.S.A.
* *Present address:* Division of Animal Feeds, Center for Veterinary Medicine, Food and Drug Administration, Rockville, MD 20857, U.S.A.

initial TNF assays using EDTA plasma were difficult to interpret because we noted the almost total lysis of the indicator cells at the lowest dilution and the apparent absence of a dilution-response relationship. When serum from parallel sets of mice were studied, this phenomenon did not occur. The experiments described here were performed to determine whether anticoagulants affect the detection of recombinant human TNF (rhTNF) added to plasmas. We also examined heat treatment of serum and plasma samples to determine whether TNF detection could be enhanced. We found that detection of TNF is optimal from mouse serum that is heat treated prior to assay.

Materials and methods

JAX: B6D2F1 female mice, 12–15 weeks of age (20–25 g) were quarantined on arrival and screened for evidence of disease before being released for experimental use. They were maintained in an AAALAC-accredited facility in plastic Micro-Isolator cages (Lab Products, Maywood, NJ) containing autoclaved hardwood chip contact bedding. Mice were provided commercial rodent chow and acidified tap water (pH 2.5 with concentrated HCl) ad libitum. Animal holding rooms were maintained at 21°C ± 1°C with 50% ± 10% relative humidity using at least ten air changes/h of 100% conditioned fresh air. The mice were on a 12 h light/dark full-spectrum lighting cycle with no twilight. All research was conducted in accordance with NIH and our Institutional Animal Care and Use Committee guidelines for the care and use of laboratory animals.

Mice were anesthetized by inhalation of methoxyflurane immediately before 1 ml of blood was obtained by cardiac puncture before being killed by cervical dislocation. The serum or plasma obtained from eight mice was pooled. Serum was obtained after allowing blood to clot in sterile microcentrifuge tubes for 1 h at ambient temperature before centrifugation at 4000 rpm for 4 min. Pooled sera were spun again. Citrated plasma was obtained by placing blood from individual mice into a microfuge tube containing 10 µl of 32% sodium citrate. EDTA plasma was obtained by placing blood from individual mice into 2 ml tubes (Starstedt, Princeton, NJ) containing 3 mg EDTA. Heparinized plasma was obtained by depositing blood from individual animals into sterile microfuge tubes containing 100 U preservative-free heparin (Fisher Scientific, Pittsburgh, PA). All plasmas were rocked on a blood mixer (Coulter, Hialeah, FL) prior to centrifugation at 4000 rpm for 4 min at 4°C. The plasma groups were pooled and spun again to remove any debris and aliquoted into sterile microfuge tubes.

The rhTNF-α produced in *Escherichia coli* was purchased from Sigma Chemical Co., St. Louis, MO, and has a biologic activity of 2.2×10^3 U/µg. Dilutions of rhTNF were added to serum and plasma aliquots to yield a final concentration of 1 µg/ml TNF. These spiked aliquots and untreated control samples were stored at −20°C until assayed. Some aliquots were heated to 56°C for 30 min immediately before assay.

TNF activity in serum or plasma was assayed using a modification of the method of Hogan et al. (1988). Briefly, 1.25×10^4 L929 cells were deposited in each well of 96-well tissue culture plates in plate medium (Dulbecco's modified Eagle's medium supplemented with 10% fetal bovine serum (FBS), 2 mM glutamine, 250 U/ml penicillin and 125 µg/ml streptomycin) and allowed to grow overnight at 37°C in a humidified 5% CO_2 incubator.

Samples for assay and the TNF standard were diluted in separate 96-well plates in assay medium (RPMI 1640 supplemented with 5% FBS, 2 mM glutamine, 250 U/ml penicillin, 125 µg/ml streptomycin, 30 mM Hepes, and 3 mg/ml sodium bicarbonate). In some assays, an additional TNF standard was prepared in homologous normal mouse serum and heated to 56°C for 30 min before further dilution in assay medium. Culture medium was removed from the seeded plates, and 100 µl of diluted sample or standard was added. Actinomycin D (Sigma Chemical Co., St. Louis, MO) was diluted to 10 µg/ml in assay medium, and 100 µl was added to the wells. Plates were returned to the incubator for 18 h.

Culture medium was aspirated and wells were washed once with 200 µl saline and aspirated again. Cells were stained with 50 µl of 0.05% crystal violet in 20% ethanol for 20 min; plates

were washed with cool tap water and allowed to dry in air. Absorbances at 595 nm were recorded using a Titertek spectrophotometer (Flow Laboratories, McLean, VA) after the addition of 50 μl methanol/well. Absorbance readings for dilutions of standard TNF were plotted to compare the amount of cytolytic activity present in samples. Student's *t* tests were performed to determine levels of significance.

TNF-dependent cytolytic activity in spiked samples was confirmed by neutralization of this activity by using a modification of the TNF assay described earlier (Meager et al., 1989). Briefly, 50 μl of dilutions of the rhTNF standard were mixed with 50 μl of dilutions of polyclonal rabbit-anti-mouse TNF antibody (Genzyme, Boston, MA) in microtiter wells and incubated for 2 h at 37°C. 100 μl of actinomycin-D treated L929 cells were then added (2×10^4/well) and incubated for an additional 18 h before staining with crystal violet as previously described.

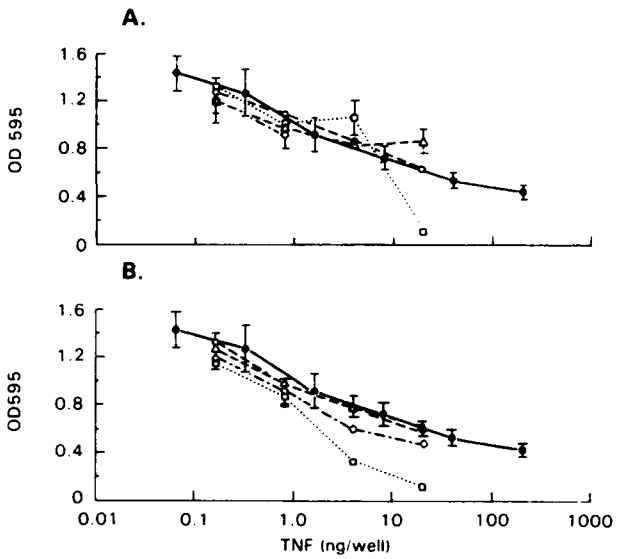

Fig. 1. Absorbances of serum or plasma pools spiked with 1 μg/ml of rhTNF. Five-fold dilutions of mouse serum (○- - - - -○), EDTA plasma (□·····□), citrated plasma (◇·–·–·◇) and heparinized plasma (△- - - - -△) were compared to a rhTNF standard curve (●———●). Curves represent means of absorbances ± standard error. *A*: Spikes serum and plasmas tested for cytolytic activity. *B*: Absorbances following heat treatment of serum and plasma samples. The standard TNF contains approximately 2.2 biological activity U/ng.

Results

The detection of TNF in plasma and serum samples varied according to the method of collection. The results of a typical experiment using spiked serum and plasma samples are presented in Fig. 1*A*. In unheated samples to which TNF had been added, only serum showed a consistent dilutional effect for the entire series tested. The absorbances of spiked serum were similar to the standard curve, while there was greater variability among the spiked plasma samples.

EDTA plasma samples consistently produced extensive lysis in dilutions at or below 1/10 in both spiked and unspiked samples. This non-specific lysis was removed by dialysis against Hanks' balanced salt solution containing Mg^{2+} and Ca^{2+} (data not shown). Citrated plasma consistently clotted in the assay at dilutions at or below 1/25. The absorbances from wells containing clots ranged from that of the control (no lysis) to those of a normal standard TNF curve. Heparinized plasma responded similarly to serum, but was more variable at the higher TNF concentrations; at lower concentrations the absorbances were similar to those of the standard curve.

Heat treatment of spiked samples resulted in improved TNF detection (Fig. 1*B*). This treatment eliminated the problem of clotting found with citrated plasma, although the lytic activity detected in the assay was still above that of the standard curve. Heat treatment of spiked EDTA

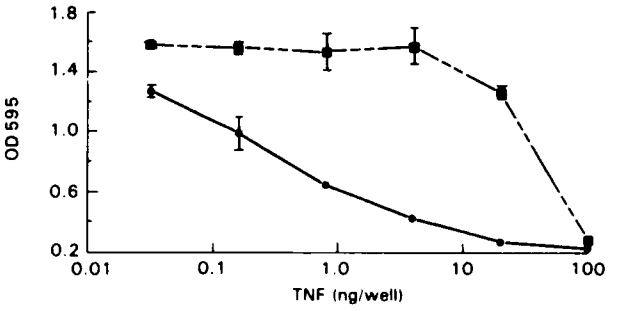

Fig. 2. Absorbances of rhTNF in L929 bioassay with (■) or without (●) the addition of rabbit antibody against mouse TNF. Curves are mean ± standard error. All values except the highest tested were significant at $P < 0.02$.

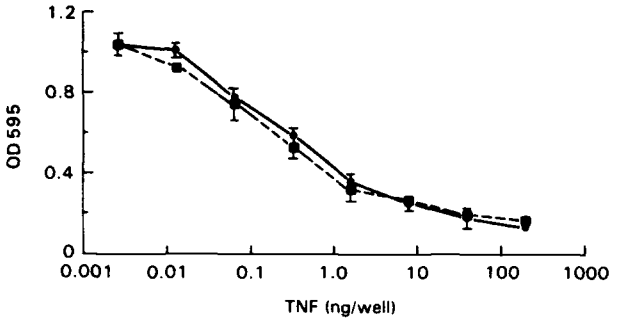

Fig. 3. Absorbances of rhTNF diluted in medium (●) or normal mouse serum (■) heated to 56°C for 30 min before bioassay. Curves are mean ± standard error. There were no significant differences between values ($P > 0.05$).

plasma did not alter the almost total lysis of L929 cells. Both serum and heparinized plasma that were heat treated before assay demonstrated excellent detection of spiked TNF.

The lytic activity in our assay was neutralized by antibody against TNF (Fig. 2). The anti-mouse TNF was able to neutralize rhTNF in all but the highest concentration of rhTNF tested. The anti-mouse TNF antibody was used in these experiments so that our results could be attributable to TNF alone. In addition, we plan to test this anti-mouse TNF antibody in future in vivo experiments.

We also examined whether normal mouse serum might nonspecifically bind spiked TNF. Normal homologous mouse serum heated to 56°C for 30 min before assay was used as the diluent for the first well of a five-fold dilution sequence. Fig. 3 shows that the activity of TNF diluted in pure mouse serum was indistinguishable from the activity of TNF diluted in medium alone, and that heating did not compromise TNF quantitation.

Discussion

We have demonstrated that reagents used in the processing of blood affect the subsequent bioassay for TNF. EDTA plasma was found to be unsuitable for use in a TNF bioassay because of nonspecific lysis of indicator cells. This effect could not be reversed by heat treatment of samples prior to assay. The effects of dilution on EDTA plasma were found to be inconsistent and, therefore, unsuitable for calculating TNF activity.

Citrated plasma clotted in our assay at the lower dilutions, but after heat treatment, cell lysis was found to be more than what was anticipated from the standard curve, and was attributed to a nonspecific mechanism. Citrated plasma, therefore, is not recommended if TNF activity is to be quantitated in a sample.

Heparinized plasma was found to be more suitable for TNF quantitation. Heat treatment of heparinized plasma was shown to optimize the detection of TNF from intentionally spiked samples. However, it has been reported that many commercial blood collection tubes are contaminated with endotoxin and that this can result in TNF release by cells within a blood sample destined for TNF quantitation (Leroux-Roels et al., 1988). In addition, many commercially available heparin preparations contain preservatives that interfere with any bioassay.

TNF was demonstrated from spiked serum samples in a quantitative manner that was consistent within a dilution series. Heat treatment of serum samples resulted in absorbances that were slightly, but insignificantly, lower than those of the unheated serum samples. The detection of TNF that was intentionally added to mouse serum was unaffected by heat treatment, and this simple step has been incorporated as routine in our laboratory. It has been reported (Ruff et al., 1981) that TNF from rabbit and mouse are stable at 56°C. Others have adopted heat treatment in their TNF assays (Kawasaki et al., 1989; Van de Wiel et al., 1989), but have not presented quantitative evidence as shown here.

We, therefore, recommend that circulating TNF should be quantitated from serum collected in sterile pyrogen-free tubes, and heated to 56°C for 30 min prior to assay. In addition, a standard curve prepared in normal homologous serum should be heated and assayed in parallel to assure that nonspecific factors are not present because they could affect the quantitation of TNF in test samples.

Acknowledgements

This work was supported by The Armed Forces Radiobiology Research Institute, Defense Nuclear

Agency, under Research Work Unit 00129. The views presented in this paper are those of the authors. No endorsements by the Defense Nuclear Agency has been given or should be inferred. Research was conducted according to the principles enunciated in the 'Guide for the Care and Use of Laboratory Animals' prepared by the Institute of Laboratory Animal Resources, National Research Council.

References

Beutler, B. (1988) The presence of cachectin/tumor necrosis factor in human disease states. Am. J. Med. 85, 287.

Beutler, B. and Cerami, A. (1986) Cachectin and tumour necrosis factor as two sides of the same biological coin. Nature 320, 584.

Hesse, D.G., Tracey, K.J., Fong, Y., Manogue, K.R., Palladino, Jr., M.A., Cerami, A., Shires, G.T. and Lowry, S.F. (1988) Cytokine appearance in human endotoxemia and primate bacteremia. Surg. Gynecol. Obstet. 166, 147.

Hogan, M.M. and Vogel, S.N. (1988) Production of tumor necrosis factor by rIFN-γ-primed C3H/HeJ (Lps^d) macrophages requires the presence of lipid A-associated proteins. J. Immunol. 141, 4196.

Kawasaki, H., Moriyama, M., Ohtani, Y., Naitoh, M., Tanaka, A. and Nariuchi, H. (1989) Analysis of endotoxin fever in rabbits by using a monoclonal antibody to tumor necrosis factor (cachectin). Infect. Immun. 57, 3131.

Kern, P., Hemmer, C.J., Van Damme, J., Gruss, H.L. and Dietrich, M. (1989) Elevated tumor necrosis factor alpha and interleukin-6 serum levels as markers for complicated *Plasmodium falciparum* malaria. Am. J. Med. 87, 139.

Kramer, S.M. and Carver, M.E. (1986) Serum-free in vitro bioassay for the detection of tumor necrosis factor. J. Immunol. Methods 93, 201.

Leroux-Roels, G., Offner, F., Philippe, J. and Vermeulen, A. (1988) Influence of blood-collecting systems on concentrations of tumor necrosis factor in serum and plasma. Clin. Chem. 34, 2373.

Meager, A., Leung, H. and Woolley, J. (1989) Assays for tumour necrosis factor and related cytokines. J. Immunol. Methods 116, 1.

Moldawer, L.L., Gelin, J., Schersten, T. and Lundholm, K.G. (1987) Circulating interleukin 1 and tumor necrosis factor during inflammation. Am. J. Physiol. 253, R922.

Ruff, M.R. and Gifford, G.E. (1981) Tumor necrosis factor. In: E. Pick (Ed.), Lymphokines: a Forum for Immunoregulatory Cell Products. Academic Press, New York, p. 235.

Sheehan, K.C.F., Ruddle, N.H. and Schreiber, R.D. (1989) Generation and characterization of hamster monoclonal antibodies that neutralize murine tumor necrosis factors. J. Immunol. 142, 3884.

Van de Wiel, P.A., Pieters, R.H.H., Van der Pijl, A. and Bloksma, N. (1989) Synergic action between tumor necrosis factor and endotoxin or poly (A·U) on cultured bovine endothelial cells. Cancer Immunol. Immunother. 29, 23.

Waage, A., Halstensen, A. and Espevik, T. (1987) Association between tumour necrosis factor in serum and fatal outcome in patients with meningococcal disease. Lancet i, 355.

RADIATION RESEARCH 124, 107–109 (1990)

SHORT COMMUNICATION

Enhancement of Topoisomerase I-Mediated Unwinding of Supercoiled DNA by the Radioprotector WR-33278

ERIC A. HOLWITT,[1] ERIK KODA,[2] AND C. E. SWENBERG

Radiation Biochemistry Department, Armed Forces Radiobiology Research Institute, Bethesda, Maryland 20814-5145

HOLWITT, E. A., KODA, E., AND SWENBERG, C. E. Enhancement of Topoisomerase I-Mediated Unwinding of Supercoiled DNA by the Radioprotector WR-33278. *Radiat. Res.* 124, 107–109 (1990).

The radioprotector WR-33278, the disulfide of WR-1065 (*N*-(2-mercaptoethyl)-1,3-diaminopropane), is shown to stimulate eukaryotic topoisomerase I unwinding of negatively supercoiled DNA. This observation suggests the possibility that some protection may be conferred to DNA either by a decrease in its supercoiled state or by altering directly other enzymatic processes. This is the first report of a radioprotective compound stimulating an enzyme involved in DNA structure and synthesis.

INTRODUCTION

Cellular DNA is one of the critical targets for ionizing radiation. To mitigate the effects of ionizing radiation, the U.S. Army Medical Research and Development Command has synthesized several radioprotective drugs, primarily aminothiol compounds. Many mechanisms responsible for their radioprotective action have been proposed, including radical scavenging (*1*), hydrogen atom donation to DNA carbon center radicals (*2*), enhancement of DNA repair processes (*3*), and reduction in the target volume. All of these processes require that the radioprotector or its metabolite be located within molecular distances, less than 50Å, from DNA.

Recent experimental studies of the radioprotector WR-1065 (*N*-(2-mercaptoethyl)-1,3-diaminopropane), the dephosphorylated product of WR-2721 (*S*-2-(3-aminopropylamino)ethylphosphorothioic acid), have shown that it binds with DNA at physiological pH (*4, 5*). However, the rapid rate of WR-1065 autooxidation (*6*) and its strong dependence on trace metal ions strongly suggest that locally the DNA neighborhood contains not only the chemical WR-1065, but also its symmetric disulfide, WR-33278. Prutz (*7*) has recently shown that disulfide radicals, which WR-33278 can form, may be the active form of sulfhydryl radioprotectors. For these reasons we restricted our studies to WR-33278. Furthermore, Holwitt and co-workers (unpublished) have shown that the binding of WR-33278 to calf thymus DNA is cooperative and dependent on salt concentration. WR-33278 binds to DNA with an association constant similar to that reported for WR-1065 (*4*). We expect that the experimental results for WR-1065 will be similar. The study was conducted to determine whether WR-33278 alters eukaryotic topoisomerase I unwinding of supercoiled DNA. WR-33278 was chosen because of the chemical similarity of the polyamine spermidine and WR-33278, the observation that both bind to DNA backbone primarily through electrostatic interactions, and the recently reported observation by Srivenugopal and Morris that calf thymus topoisomerase I unwinding of supercoiled DNA was stimulated by spermidine (*8*).

We first present the experimental protocol, followed by the main experimental results (reported in Figs. 1 and 2). Our results indicate that WR-33278 enhances topoisomerase I unwinding of supercoiled DNA. To our knowledge, this constitutes the first observation of an enzyme process enhanced by a radioprotective agent. The paper concludes with a discussion of the superhelical state of prokaryotic and eukaryotic DNA and possible implications for radioprotector–enzyme interaction.

METHODS

Plasmid pIBI30 was isolated by the alkaline lysis method from *Escherichia coli* (*9*). Calf thymus Type I DNA topoisomerase was purchased from Bethesda Research Laboratory and was used as received. One unit of activity was defined as the amount of enzyme needed to relax 1 μg of supercoiled DNA in 1 h. The radioprotector WR-33278 was obtained from Walter Reed Medical Research Institute and was used as received. Topoisomerase reactions were performed as described by Srivenugopal *et al* (*10*). Stock solutions were as follows: 5× KCl (100 m*M*); spermidine (16.5

[1] Present address: USAF School of Aerospace Medicine, Radiation Sciences Division, Brooks Air Force Base, San Antonio, TX 78235-5301.

[2] Permanent address: United States Air Force Academy, Colorado Springs, CO 80841.

0033-7587/90 $3.00

FIG. 1. Photograph of agarose gel illustrating the stimulation of topoisomerase I unwinding of supercoiled DNA by spermidine and WR-33278. S denotes supercoiled state; NC denotes the nicked circular form and/or the completely relaxed form of DNA. Numbers in parentheses are final concentrations for each gel lane. Controls: Lane 1, pIBI30 DNA alone (33.3 μg/ml); Lane 2, pIBI30 DNA (33.3 μg/ml) and topoisomerase (13.3 units/ml); Lane 3, DNA, topoisomerase, and spermidine (1.65 m*M*); Lanes 4 to 8, DNA, topoisomerase, and varying concentrations of WR-33278 (50, 100, 200, 500, and 1000 μ*M*, respectively).

m*M*), whose pH adjusted to 7.5 with the basic form of Tris; and WR-33278, which required no pH adjustment. pIBI30 DNA (125 μg/ml) and topoisomerase (0.0667 units/μl) were prepared in reaction buffer: 20 m*M* Tris (pH 7.5), 0.5 m*M* DTT, and 6% glycerol. Topoisomerase was assayed by incubating 1 μg (0.101 m*M* in bases) of plasmid DNA with 0.4 units of enzyme in 20 m*M* of KCl. This salt concentration is below the optimum salt concentration of approximately 180 m*M* KCl needed for maximum topoisomerase activity (*11, 12*). It was chosen to enhance the demonstration of any stimulatory effect by polyamines and WR-33278 of topoisomerase I activity. Total sample volume for each tube was 30 μl. Reactions were carried out at 37°C and terminated after 3 h by addition of a Sarkosyl/EDTA mixture to a final concentration of 1% and 20 m*M*, respectively. Conversion of supercoiled DNA to relaxed forms of DNA was determined by gel electrophoresis (1.3% agarose). DNA was subjected to electrophoresis at 60 V in Tris acetate EDTA buffer until the tracking dye (bromphenol blue) was approximately 1 cm from the leading edge; this usually took 3 h. Gels were stained with ethidium bromide.

RESULTS

Figure 1 is a photograph of representative DNA topoisomerase I assay on agarose gel. The relaxed or open circle form of the plasmid is at the top of the gel, and the supercoiled form is at the bottom. When topoisomerase I relaxes DNA, the lower band's density decreases. Lane 1 is pIBI30 alone and shows where the relaxed and supercoiled forms of the plasmid run under our electrophoresis conditions. Under the assay conditions employed (20 m*M* KCl), topoisomerase I has low activity, and lane 2 of Fig. 1 demonstrates this lack of supercoil unwinding by the enzyme during the time allowed for the enzyme assay. Lane 3 of Fig. 1 shows clearly the stimulation of calf thymus type I topoisomerase by spermidine as previously reported by Srivenugopal and Morris (*8*) for native ColE1 DNA. It can be seen in Lanes 4–6 in Fig. 1 that WR-33278 also stimulates the topoisomerase I unwinding of supercoiled DNA and produces a ladder of isomers similar to that produced in the presence of spermidine. Also evident from these lanes is that an increase in the concentration of WR-33278 increases the amount of stimulation. A similar result was observed for spermidine-enhanced stimulation of topoisomerase I (*8*). Lanes 7 and 8 in Fig. 1 show a pattern similar to Lane 1. For these lanes the molar ratios of WR-33278 to DNA bases was above 2:1, and we have demonstrated using spectrophotometry that for these ratios, DNA precipitates; hence the lack of a ladder as shown in Lanes 3 through 6. The DNA appears on the gel because it is resolubilized by the detergent added to stop the reaction. The data in Fig. 2 demonstrate that neither spermidine (Lane 3) nor WR-33278 (Lanes 6–8) in the absence of topoisomerase I relaxes DNA.

DISCUSSION

The superhelical state of intracellular DNA is an important structural determinant of the function of DNA in cells (*13–15*). Superhelicity of DNA is controlled by a class of enzymes called topoisomerases, which are ubiquitous both in prokaryotic and in eukaryotic cells. These enzymes alter the topological conformation of DNA by nicking and resealing the DNA sugar–phosphate backbone. Those that change the DNA linking number by unity are called type I enzymes; type II enzymes change the link number by two. Type I enzymes act by producing transient single-strand breaks in DNA, whereas type II topoisomerases introduce transient double-stranded breaks (*16–18*).

Our experimental observation of the stimulation of calf thymus topoisomerase I action by WR-33278 is similar to

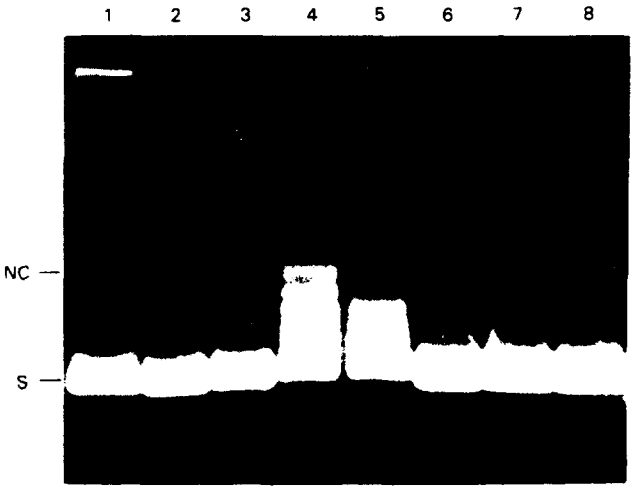

FIG. 2. Photograph of agarose gel demonstrating lack of supercoil unwinding in absence of topoisomerase I. S denotes supercoiled state; NC denotes the nicked circular form and/or the completely relaxed form of DNA. Numbers in parentheses are final concentrations for each gel lane. Lanes 1 and 2, same as in Fig. 1; Lane 3, DNA (33.3 μg/ml) and spermidine (1.65 m*M*); Lanes 4 and 5, DNA and topoisomerase (13.33 units/ml) with 1.65 and 2.75 m*M* spermidine. Lanes 6 to 8, DNA and WR-33278 (50, 100, and 200 μ*M*, respectively).

the enhanced relaxation of supercoils by spermidine reported by Srivenugopal and Morris (*8*). This is a reasonable result in view of the similarity in their structure since WR-33278 may loosely be considered a polyamine containing a disulfide bond. In addition we note that both WR-33278 and spermidine (*19, 20*) bind externally to DNA through electrostatic interactions with the charged phosphate oxygen anions (*21*). Because supercoiled domains exist in both prokaryotic and eukaryotic cells, our observation suggests that radioprotectants may confer some protection to the genome by decreasing the supercoiling of DNA. The decrease in superhelicity could produce a decrease in the initial damage incurred and/or change the functional properties of DNA. If the first process is operative, then the critical DNA damage sites or "hot spots" would correspond to those DNA regions where the superhelicity is large. The second mechanism suggests possible changes in metabolic processes, a virtually unexplored field, although WR-1065 has been reported to enhance DNA repair (*22, 23*).

The molecular mechanism responsible for the stimulation of eukaryotic type I topoisomerase by WR-33278 is unclear. Both compounds bind to DNA but whether a transient tertiary complex is formed is not known and has not been investigated. The binding of WR-33278, even at a DNA site remote from the topoisomerase site of action, may provide a mechanism for stimulation of topoisomerase I action by conferring enhanced stabilization to the DNA backbone. These possibilities are currently under study. Nevertheless, the observation that WR-33278 stimulates topoisomerase I unwinding of the supercoiled state suggests new mechanisms by which radioprotective chemicals induce protection against ionizing radiation.

ACKNOWLEDGMENTS

The authors thank Colleen Loss for the technical support in producing sufficient quantities of pIBI30 plasmid with high superhelical content. We also appreciate the numerous scientific discussions with Steven Knizner.

RECEIVED: October 3, 1989; ACCEPTED: May 1, 1990

REFERENCES

1. T. J. PHILLIPS. Rationale for initial clinical trials and future development of radioprotectants. *Cancer Clin. Trials* **3**, 165–173 (1980).
2. R. F. DURAND. Radioprotection by WR-2721 *in vitro* at low oxygen tensions. Implications for its mechanism of action. *Br. J. Cancer* **47**, 387–392 (1983).
3. F. RIKLIS, R. KOB, M. GREEN, A. PRAGER, R. MARKO, and M. MINTSBERG. Increased radioprotection attained by DNA repair enhancement. *Pharmacol. Ther.* **39**, 311–322 (1988).
4. G. D. SMOLUCK, R. C. FAHEY, and J. F. WARD. Interaction of glutathione and other low-molecular-weight thiols with DNA: Evidence for counterion condensation and cation depletion near DNA. *Radiat. Res.* **114**, 3–10 (1988).
5. S. ZHENG, G. L. NEWTON, G. GONICK, R. C. FAHEY, and J. F. WARD. Radioprotection of DNA by thiols: Relationship between the net charge on a thiol and its ability to protect DNA. *Radiat. Res.* **114**, 11–27 (1988).
6. J. E. BIAGLOW, R. W. ISSELS, L. E. GERWECK, M. E. VARNES, B. JACOBSON, J. B. MITCHELL, and A. RUSSO. Factors influencing the oxidation of cysteamine and other thiols: Implications for hyperthermic sensitization and radioprotection. *Radiat. Res.* **100**, 298–312 (1984).
7. W. A. PRUTZ. Chemical repair in irradiated DNA solutions containing thiols and/or disulphides. Further evidence for disulphide radical anions acting as electron donors. *Int. J. Radiat. Biol.* **56**, 21–33 (1989).
8. K. S. SRIVENUGOPAL and D. R. MORRIS. Differential modulation by spermidine of reactions catalyzed by type I prokaryotic and eukaryotic topoisomerases. *Biochemistry* **24**, 4766–4771 (1985).
9. F. M. AUSUBEL, R. BRENT, R. E. KINGSTON, D. D. MOORE, J. G. SEIDMAN, J. A. SMITH, and K. STRAHL (Eds.). *Current Protocols in Molecular Biology*, pp. 1.71–1.74. Wiley-Interscience, New York, 1989.
10. K. S. SRIVENUGOPAL, D. E. WEMMER, and D. R. MORRIS. Aggregation of DNA by analogs of spermidine: enzymatic and structural studies. *Nucleic Acids Res.* **15**, 2563–2580 (1987).
11. B. L. MCCONAUGHY, L. S. YOUNG, and J. J. CHAMPOUX. The effect of salt on the binding of the eukaryotic DNA nicking-closing enzyme to DNA and chromatin. *Biochim. Biophys. Acta* **655**, 1–8 (1981).
12. J. J. CHAMPOUX. Evidence for an intermediate with a single-strand break in the reaction catalyzed by the DNA untwisting enzyme. *Proc. Natl. Acad. Sci. USA* **73**, 3488–3491 (1976).
13. M. GELLERT. DNA topoisomerase. *Annu. Rev. Biochem.* **50**, 879–910 (1981).
14. K. DRLICA. Biology of bacterial deoxyribonucleic acid topoisomerase. *Microbiol. Rev.* **48**, 273–289 (1984).
15. J. C. WANG. DNA topoisomerases. *Annu. Rev. Biochem.* **54**, 665–697 (1985).
16. F. B. FULLER. Decomposition of linking number of a closed ribbon: A problem from molecular biology. *Proc. Natl. Acad. Sci. USA* **75**, 3557–3561 (1978).
17. P. O. BROWN and N. R. COZZARELLI. A sign inversion mechanism for enzymatic supercoiling of DNA. *Science* **206**, 1081–1083 (1979).
18. K. MIZUUCHI, L. M. FISHER, M. H. O'DEA, and M. GELLERT. DNA gyrase action involves introduction of transient double-stranded breaks into DNA. *Proc. Natl. Acad. Sci. USA* **77**, 1847–1851 (1980).
19. B. C. HOOPES and W. R. MCCLURE. Studies on the selectivity of DNA precipitation by spermine. *Nucleic Acids Res.* **20**, 5413–5422 (1981).
20. I. BAEZA, P. GARIGLIO, L. M. RANGEL, P. CHAVEZ, L. CERVANTES, C. ARGUELLO, J. E. MORGAN, J. W. BLANKENSHIP, and H. R. MATTHEWS. Electron microscopy and biochemical properties of polyamine-compacted DNA. *Biochemistry* **26**, 6387–6392 (1987).
21. M. J. MARTON and D. R. MORRIS. In *Inhibition of Polyamine Metabolism: Biological Significance and Basis for New Therapy*. (P. P. McCann, A. E. Pegg, and A. Sjoerdma, Eds.), pp. 79–105. Academic Press, Orlando, 1987.
22. E. LOWENSTEIN, J. L. GLEESON, E. HECHT, R. FACTOR, C. GOLDFISCHER, A. CAJIGAS, and J. J. STEINBERG. Excision repair is enhanced by WR2721 radioprotection. In *Terrestrial Space Radiation and Its Biological Effects* (P. D. McCormack, C. E. Swenberg, and H. Bucker, Eds), pp. 697–714. Plenum, New York, 1989.
23. C. E. SWENBERG. DNA and radioprotection. In *Terrestrial Space Radiation and Its Biological Effects* (P. D. McCormack, C. E. Swenberg, and H. Bucker, Eds), pp. 675–695. Plenum Press, New York, 1989.

Nuclear Instruments and Methods in Physics Research A299 (1990) 162–165
North-Holland

Development and testing of a new alpha radiac

J.P. Jacobus
Armed Forces Radiobiology Research Institute, Bethesda, MD 20889-5145, USA

J.R. McNaughton
Science Applications International Corporation, San Diego, CA 92121, USA

A new, state-of-the-art alpha radiac has been developed to monitor for alpha contamination in both laboratory and field operations. The detector is a 7.6 cm (3 inch) diameter circular diffused-junction semiconductor with an active detection area of 42.6 cm^2. Its surface is coated with aluminum and a thin layer of epoxy to provide light shielding and protection against abrasion during decontamination. The modular design of the detector-preamplifier, the probe processor unit and the detector interface unit allows for ease in replacement. The electronic components are contained in the probe housing so that only the processed, digitized detector signal is sent to a separate, detached display device. An external computer and IEEE connector are used to set the detector threshold levels and operational parameters, e.g. various calibration factors. Additional enhancements include shock hardening of the detector assembly, shielding from electromagnetic interference, and a removable decontamination shield. Testing and evaluation of prototype units were performed at several military and civilian laboratories to determine the detector's limitations and abilities to monitor alpha radiation, and to determine its capabilities under various operational conditions. These tests indicate that the radiac meets or exceeds the requirements.

1. Introduction

The U.S. military services require portable detection equipment to monitor for alpha contamination in maintenance areas and in field operations that involve the cleanup of Pu-contaminated or nuclear-accident sites. Of specific concern is the ability to survey for the unrestricted release of property and equipment within established or proposed guidelines [1–3]. Currently available radiacs, which use ZnS scintillators with photomultiplier tubes, have several performance limitations that are summarized in table 1. In addition, the units lack reliable accuracy when used for surveying, even in the hands of routine users [4].

A development and procurement program was initiated to obtain a new radiac that would overcome the operational shortcomings of the current devices and meet the new requirements for the unrestricted release of property. The new device would have to (1) measure alpha contamination down to a level of 200 dpm/100 cm^2, (2) be human-factor engineered, (3) be easily decontaminated, and (4) be able to detect a 200 dpm point source with 63% confidence at a distance of 0.5 cm while scanning at 10 cm/s.

The decision to use a solid-state detector system was based on several factors. Solid-state silicon diode detectors have been used for many years in health physics applications. They are shock-resistant, and require low voltages and minimal electronic circuitry. Current manufacturing techniques permit the production of large-surface-area silicon wafers that can be several centimeters across.

Throughout the development phase and initial testing of prototype units, input was solicited from repre-

Table 1
Comparison of ZnS/PM tube and solid-state detector performance factors

	ZnS/Pm tube detector [a]	Silicon wafer detector
Sensitivity (2π)	< 40%	~ 94%
Shock/drop resistance	Limited	Good, with hardened housing
Ruggedness	Poor to fair, Mylar window easily damaged; light leakage damaging PM tube	Good, with hardened coating to resist surface abrasion; maintain light tightness
Power-supply requirements	≥ 1000 V	24 V
Warm-up time	~ 15 min	None
Time needed for calibration	hours	< 0.5 h

[a] Based on present ZnS/PM tube technology used by the military services (AN/PDR-56)

0168-9002/90/$03.50

sentatives of the military services to ensure that the final product met their requirements. In addition, a complete battery of tests evaluated the radiac's radiation detection capabilities, and survivability in harsh environments and rough handling.

2. Detector, electronics and enhanced signal development

The detector used in the new radiac is a 46 cm (3 inch) diameter, 0.508 mm (0.02 in.) thick "p-type" double-diffused-junction silicon wafer diode. Tests show that the detector efficiency is 94.1% for a 2π point source. The detection surface is coated with a 2500 Å (0.25 μm) thick layer of epoxy that is spun onto the surface, and an aluminum coating that is also 2500 Å (0.25 μm) thick. This coating causes a decrease of approximately 400 keV in alpha-particle energy. The detector itself is attached to a shock-absorbing foam backing using a fiber glass/epoxy matrix, and is mounted in a Kovar/Ni ring to provide uniform thermal expansion.

The detector is connected to a low-noise 1 GHz gain-bandwidth amplifier circuit that forms a singular detector subassembly (DET). The DET is connected directly to the detector interface unit (DIU) and probe processor unit (PPU) by a detachable connector. This arrangement allows for easy disassembly of the unit and replacement of component parts within 15 min.

A preamplifier circuit in the DET consisting of a wide-band field-effect transformer (FET) that converts detector charge pulses into voltage pulses. The voltage pulses are shaped by four wide-band operational amplifiers with a nominal time constant of 1.25 μs. The preamplifier also incorporates a test-pulse circuit that routes pulses generated by the microprocessor in the PPU through the system to provide for internal self-testing. A Delrin ring placed between the DET and DIU/PPU assemblies holds the shock ring in place and separates the subassemblies.

The DIU provides voltages to the DET and PPU with three voltage converter systems which allows the external battery voltage to vary without effecting the probe performance. In addition, a dual discriminator in the DIU compares the incoming analog signals from the DET, with two threshold levels provided by the microprocessor in the PPU. The output pulses are stretched into logic level signals that are counted by the microprocessor.

The PPU uses an 80C51FA-based signal microcontroller to monitor the response of the DET and communicate with external devices through a modified serial bus. The microcontroller contains 8 kbytes of electrically erasable read-only memory (EEPROM), 256 kbytes of random-access memory (RAM), pulse-width modulating analog-to-digital converters, and the 8-bit microprocessor. The EEPROM is used to store calibration factors and threshold discrimination levels. No potentiometers are used in the probe which prevents variations of performance over time due to changes in potentiometer values. The microcontroller generates digital signals that are sent to the external meter. The total power consumption of the probe electronics is approximately 183 mW.

The detector and electronic system are designed to provide the following features to a newly designed, stand-alone display unit:

(1) three sampling modes (peak, average, scalar);
(2) dual, variable discrimination thresholds;
(3) selectable sampling times;
(4) multiple tone outputs for headphones:
  (a) clicks proportional to the counting events;
  (b) 1 kHz tone for threshold alarm;
(5) selectable alarm thresholds for each sampling mode;
(6) selectable time interval for back-light illumination;
(7) programmable conversion factor (counts to disintegration);
(8) battery life indicator;

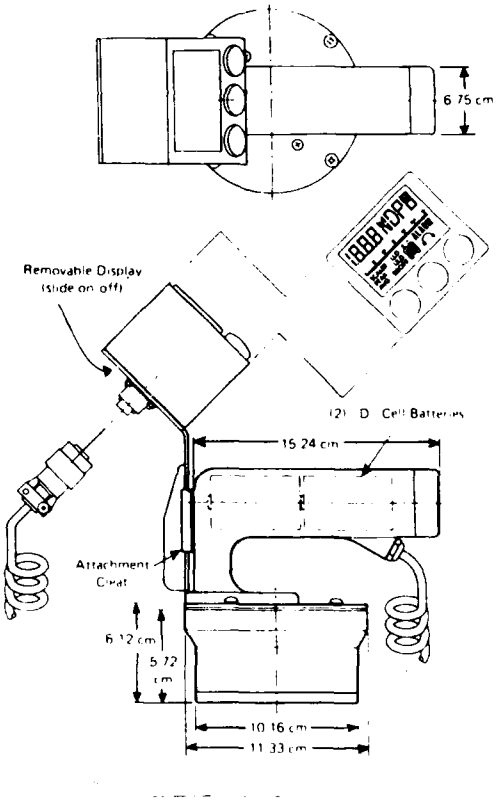

Fig. 1. Alpha radiac with removable stand-alone display unit.

(9) dual operational modes (use with or without removable decontamination shield);
(10) removable external power pack for low-temperature display operations to −40 °C.

In addition, the probe has a twist-on swipe tray for use in the scalar mode for survey operations.

3. Detector housing

The electronic subassemblies are located inside an aluminum housing with an attached handle as shown in fig. 1. The entire radiac weighs approximately 0.9 kg (2 lb). The aluminum handle is designed so that the center of gravity is positioned over the center of the radiac, and can hold two "D" cell batteries that support operations with the stand-alone display unit.

The housing is constructed as a Faraday cage to protect the electronics from electromagnetic interference (EMI). The sensitive preamplifier is further enclosed in another aluminum housing to isolate it from both external EMI and internally generated noise from the DIU and PPU. In addition, a silicon seal between the DET Kevar ring and the housing reduces the unit's susceptibility to moisture.

Covering the silicon detector is a 8.4 cm diameter disposable decontamination shield. The shield is an aluminized Mylar film attached to a honeycomb-patterned aluminum screen that covers only 7.4% of the Mylar film.

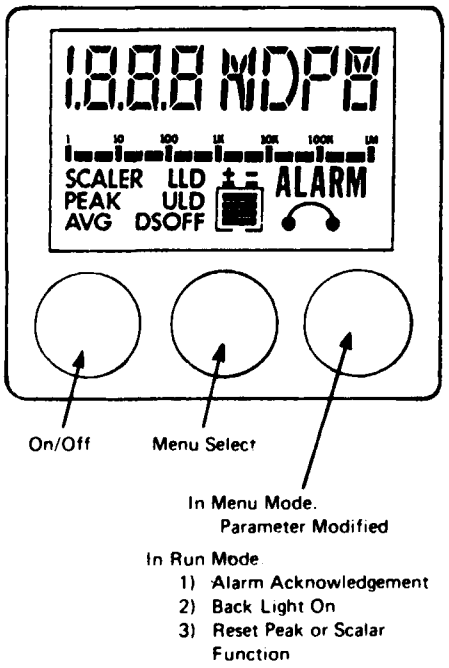

Fig. 2. Stand-alone display unit and function buttons.

Table 2
Stand-alone operational classes

Class 1: functions for field use
– Turn headphone audio on and off
– Adjust headphone volume
– Select either average of peak detection sampling
Class 2: Class 1 functions plus:
– Select display units (CPM, CPS, DPM, DPS)
– Operate the probe with or without decontamination shield
– Use scalar functions
Class 3: Class 2 functions plus:
– Adjust dual discrimination levels

4. Stand-alone display unit

The alpha radiac is designed to operate with either a multifunction radiac power/readout box, or the newly designed, detachable stand-alone display unit shown in fig. 2. This unit supports the functions listed in table 2. When the stand-alone display unit is used, two "D" batteries located in the radiac's handle supply power for both the radiac detector and display. The same cable used to connect the detector unit to the multifunction radiac power/readout box or calibrating computer is used with the stand-alone, back-lighted display unit. This stand-alone display unit can be programmed into one of three classes of operations listed in table 2. This permits the radiac to be used by personnel of differing qualifications and duties.

Table 3
Operational tests and results

Humidity	95% at 22.3 °C for 4 h
Operating temperature range	−40° to +50 °C
Storage temperature range	−65° to +71 °C
Thermal shock	+23° to +50 °C in 5 min
	+23° to −10 °C in 5 min
Pressure/altitude operation	795–525 mm Hg (operational after exposure to 14.6 mm Hg)
Waterproof/splash proof	passed
Mechanical vibration	sinusoidal 5–500 Hz
	10–33 Hz at 2*G* acceleration
	11–2000 Hz randomly
Mechanical shock	18 ms shocks at 50*G* acceleration
Drop limits	1 m to hardwood floor/concrete
EMI tests	
Electric-field susceptibility:	14 kHz to 10 GHz
Magnetic-field susceptibility:	30 Hz to 50 kHz
Broadband EM emissions:	0.01 MHz to 1 GHz
Narrowband EM emissions:	0.01 MHz to 10 GHz

Table 4
Radiation response capabilities

Detector surface uniformity	4 mm increments < 10% variation
Response time	1.5 s
Interfering radiation	gamma-ray, beta, neutron recorded response within 1 standard deviation
Resolution	300 keV FWHM
Count-rate reduction with decontamination shield	25% (point source)
Counting accuracy:	
point source	within 10% for sources > 460 dpm
large-area source	9.1% for 4800 dpm
Scanning rate	~ 63% confidence of detecting 200 dpm point source at 10 cm/s

5. Testing and evaluation

To ensure that the final product met the requirements of the users, testing of prototype alpha radiacs was performed at several military facilities and contracted civilian laboratories using both standard military test for equipment reliability and tests for evaluating radiation detection devices [5,6]. Tables 3 and 4 provide a listing of the tests and ranges of measurements performed [7].

6. Conclusion

The development of new radiation detection devices required (1) a review of current technologies, and (2) a cooperative effort between the developer and user. In developing a new alpha radiac for the U.S. military, user-demanded requirements allowed for the incorporation of many features that enhanced the original design. This approach led to the design of a radiac that meets the needs of a diverse number of operators with different requirements.

Acknowledgement

This work was supported by the Armed Forces Radiobiology Research Institute, Defense Nuclear Agency. Views presented in this paper are those of the authors; no endorsement by the Defense Nuclear Agency has been given or should be inferred.

References

[1] E.T. Bramlitt, Proc. 22nd Midyear Topical Meeting on Instrumentation (South Texas Chapter of the Health Physics Society, San Antonio, TX, USA, 1988) p. 67.
[2] ANSI, N13.12 (draft) (American National Standards Institute, NY, 1978).
[3] NRC, Regulatory Guide 1.83 (1982).
[4] R.H. Olsher, J.S. Haynie and E. Schultz, Los Alamos National Laboratory Report LA-10729 (1986).
[5] ANSI, N42.17A (draft) (American National Standards Institute, NY, 1985).
[6] J.M.R. Hutchinson and S.J. Bright, J. Res. NBS 92 (1987) 311.
[7] Report of test results being prepared by one of us (JPJ).

RADIATION RESEARCH 125, 158–162 (1991)

Reductions in Calcium Uptake Induced in Rat Brain Synaptosomes by Ionizing Radiation

SATHASIVA B. KANDASAMY, THOMAS C. HOWERTON, AND WALTER A. HUNT

Behavioral Sciences Department, Armed Forces Radiobiology Research Institute, Bethesda, Maryland 20889-5145

KANDASAMY, S. B., HOWERTON, T. C., AND HUNT, W. A. Reductions in Calcium Uptake Induced in Rat Brain Synaptosomes by Ionizing Radiation. *Radiat. Res.* 125, 158–162 (1991).

Gamma irradiation (^{60}Co) reduced KCl-stimulated voltage-dependent $^{45}Ca^{2+}$ uptake in whole-brain, cortical, and striatal synaptosomes. The time course (3, 10, 30, and 60 s) of calcium uptake by irradiated (3 Gy) and nonirradiated synaptosomes, as well as the effect of KCl (15–65 m*M*), was measured in whole-brain synaptosomes. The fastest and highest rate of depolarization-dependent calcium uptake occurred at 3 s with 65 m*M* KCl. Irradiation reduced calcium uptake at all incubation times and KCl concentrations. Bay K 8644 enhancement of KCl-stimulated calcium influx was also reduced by radiation exposure. Nimodipine binding to dihydropyridine (DHP) L-type calcium channel receptors was not altered following radiation exposure. These results demonstrate an inhibitory effect of ionizing radiation on the voltage-sensitive calcium channels in rat brain synaptosomes that are not mediated by DHP receptors.

INTRODUCTION

Although the central nervous system (CNS) is generally considered to be relatively resistant to the direct effects of ionizing radiation, exposure to ionizing radiation can have a complex effect on the CNS that is dependent on the dose and time elapsed after radiation exposure (*1–6*). The biochemical basis for radiation-induced behavioral/physiological changes mediated by the CNS is unknown.

Calcium plays several important roles in various electrophysiological and neurochemical processes, and it is generally accepted that extracellular calcium influx can be regulated by calcium channel agonists (i.e., cardiostimulatory drugs), or can be blocked by calcium channel antagonists (*7*). These antagonists are structurally heterogenous and include verapamil, diltiazem, D-600, and the dihydropyridine (DHP) compounds, such as nimodipine and nifedipine (*8*). These drugs exhibit a common locus of action on voltage-sensitive calcium channels (VSCC) (*9, 10*). Several types of VSCC have been identified, of which L, N, and T are most important. The DHP antagonists mentioned above are specific for the L-type VSCC, which is characterized by large conductances of long duration (*7*).

Calcium channel binding sites for DHP compounds have been located in the brain and heart using nimodipine and nifedipine (*11–13*). Nimodipine binding provides a molecular probe by which the kinetics of calcium receptors may be evaluated (*12*). A slight structural modification of DHP calcium antagonists yields Bay K 8644 [methyl-1,4-dihydro-2,6-dimethyl-3-nitro-4-2(trifluoromethylphenyl) pyridine-5-carboxylate], which confers agonist activity for calcium influx in the brain (*13–18*) and smooth and cardiac muscle (*19, 20*). Interestingly, a direct effect of Bay K 8644 on synaptosomal calcium entry in rat brain has not been observed (*21–23*).

The present experiments indicate a reduction in calcium uptake after irradiation in whole-brain, cortical, and striatal synaptosomes. This study characterizes the effect of ionizing radiation on voltage-dependent calcium influx by measuring KCl-stimulated $^{45}Ca^{2+}$ uptake into rat whole-brain, cortical, and striatal synaptosomes. Additionally, calcium channel receptor binding studies were done to determine whether the reductions were due to any alterations in DHP L-type receptors.

MATERIALS AND METHODS

Materials. Bay K 8644 and nimodipine were gifts from Miles Laboratories, Inc. (West Haven, CT) and were dissolved in dimethylsulfoxide (DMSO). Due to the light sensitivity of these compounds, all experiments were done using foil-wrapped test tubes. $CaCl_2$ and [^{3}H]nimodipine were purchased from New England Nuclear (DuPont, Boston, MA), and all other chemicals and reagents used were of the highest analytical grade and were obtained from Sigma (St. Louis, MO).

Experimental animals. Male Sprague-Dawley rats weighing 200–300 g (Charles River Breeding Laboratories, Kingston, NY) were quarantined on arrival and screened for evidence of disease by representative serology and histopathology sampling before being released from quarantine. The rats were housed individually in polycarbonate Micro Isolator cages (Lab Products, Maywood, NJ) on autoclaved hardwood contact bedding (Beta Chip Northeastern Products Corp, Warrenburg, NY) and provided with commerical rodent chow and acidified water (pH = 2.5) *ad libitum*. Animal holding rooms were kept at 21 ± 1°C with 50 ± 10% relative humidity on a 12-h light:dark cycle with no twilight.

Tissue preparation and calcium uptake. Animals were killed by decapitation, and the brain was removed from the skull and placed on ice. Whole brain, cortex, and striatum were dissected using the method of Glowinski and Iversen (*24*), and the synaptosomal pellet (P2) from these regions was, or pellets were, prepared by a modification of the method of Gray and

0033-7587/91 $3.00

Whittaker (25). The final pellet was resuspended in ice-cold incubation medium containing 136 m*M* NaCl, 5 m*M* KCl, 1.3 m*M* $MgCl_2$, 0.12 m*M* $CaCl_2$, 10 m*M* glucose, and 20 m*M* Tris base, with the pH adjusted to 7.65 with 1.0 *M* maleic acid to provide a concentration range of approximately 4–6 mg protein/ml and divided into two equal portions. One portion was irradiated with γ photons while the other was used as a sham-irradiated control.

Aliquots (480 μl) of the synaptosomal preparation were transferred into test tubes and incubated for 14 min at 30°C in a Dubnoff metabolic shaker in the presence or absence of various concentrations of Bay K 8644 as detailed below. The Bay K 8644 or DMSO vehicle was added as a 20-μl volume to make a final incubation volume of 500 μl. Following the incubation period, 500 μl of depolarizing or nondepolarizing solution containing $^{45}Ca^{2+}$ (3 μCi) was added. The depolarizing solution was the same composition as that of the incubation medium, except that a portion of the NaCl was replaced by an osmotically equivalent amount of KCl to provide final KCl concentrations of 15, 30, or 65 m*M*. Calcium uptake was terminated by addition of 5 ml of an ice-cold buffer containing 3 m*M* EGTA (ethylene glycol bisβ-aminoethyl ether) *N*, *N*'-tetraacetic acid), 10 m*M* glucose, and 20 m*M* Tris base, with the pH adjusted to 7.65 with 1.0 *M* maleic acid. Each sample was then immediately filtered under vacuum through a presoaked Whatman GF/B filter. Excess and loosely bound $^{45}Ca^{2+}$ was eliminated with two 5-ml washes of ice-cold incubation medium. The filters were then placed in scintillation vials and radioactivity was determined by liquid scintillation spectrometry.

Net uptake of $^{45}Ca^{2+}$ into synaptosomes was calculated by subtracting the uptake in the absence of depolarization (5 m*M* KCl) from the uptake in the presence of depolarization (15, 30, or 65 m*M*). This value will be referred to as *k* (potassium-induced change) and represents net KCl-induced calcium uptake (*26, 27*).

[^{3}H]Nimodipine binding assays The binding assay was done based on the methods reported by Skattebol and Triggle (*28*). Whole brain, cortex, and striatum were obtained and isolated as described above and pooled according to protein needs for significant binding determined in preliminary experiments (data not shown). The P2 pellet was prepared as described above and resuspended in 50 m*M* Tris base buffer (pH 7.4) and divided into two equal portions, one of which was irradiated with γ photons, while the other was used as a sham-irradiated control. Synaptosomes were irradiated to maintain procedural continuity with the calcium uptake studies. Following irradiation, the synaptosomes were homogenized for a second time (glass/glass) in 3 ml buffer to form membrane fragments, which were aliquoted (200 μl: 100 μg/sample, striata; 400 μg/sample, whole brain; 400 μg/sample, cortex) into black snap-cap polypropylene test tubes. Half of these tubes contained 5 μ*M* unlabeled nimodipine (25 μl/sample) for determination of nonspecific binding. A preliminary displacement experiment indicated that the apparent K_d for this system was approximately 1 n*M* (data not shown).

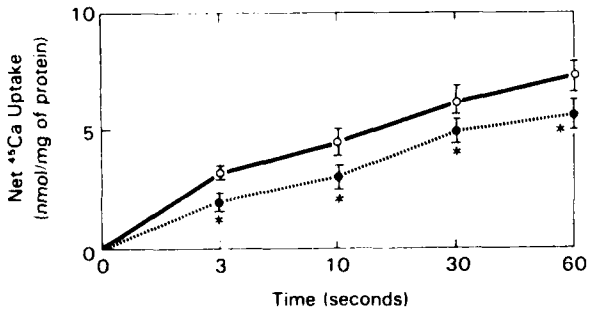

FIG. 1. The time course of 65 m*M* KCl-stimulated calcium uptake in nonirradiated (○) and irradiated (●) rat whole-brain synaptosomes. Points and bars represent means ± SEM values from three separate experiments, each using triplicate samples. A significant effect of ionizing radiation is indicated as follows: $^*P < 0.05$.

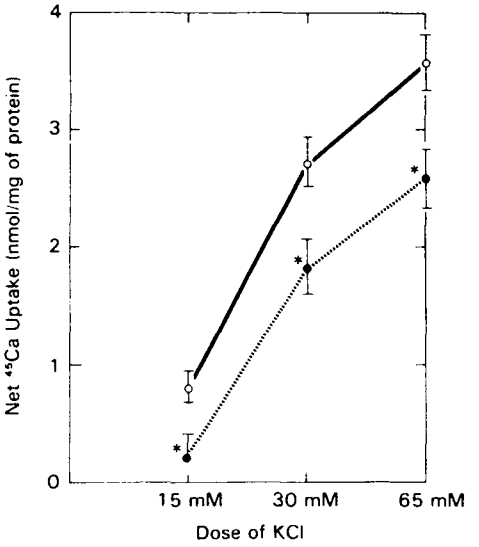

FIG. 2. Effects of 15, 30, and 65 m*M* KCl-stimulated calcium uptake in nonirradiated (○) and irradiated (●) rat whole-brain synaptosomes. Points and bars represent means ± SEM values from three separate experiments, each using triplicate samples. A significant effect of ionizing radiation is indicated as follows: $^*P < 0.05$.

Based on preliminary experiments, maximal binding was obtained in 20 min (data not shown). [^{3}H]Nimodipine (NEN, 123.3 Ci/m*M*, 25 μl/sample) was added to the aliquoted samples (in duplicate, final volume 565 μl) over a concentration range of 50 p*M* to 0.8 n*M* for 1 h at 4°C. The binding experiment was then terminated using a 24-place Brandel Cell Harvester (Gaithersburg, MD), and the membrane fragments were collected on Whatman GFC filters, followed by 3 × 3-ml washes with 50 m*M* Tris base buffer. The filters were then transferred to scintillation vials. After determining radioactivity by liquid scintillation spectrometry, the data were converted to fmol and expressed as fmol/mg protein.

Irradiation procedures It has been reported that no significant oxygen uptake occurs in whole-brain homogenates *in vitro* after irradiation, which suggests that the brain synaptosomes will not consume enough oxygen to affect the results[1] (*29*). To maintain the maximum viability of the synaptosomes, they were placed in glass test tubes in a Plexiglas ice bath and were exposed to radiation using a ^{60}Co source at a dose rate of 1 Gy/min (for the 1-Gy dose only), 10 Gy/min (for the 3-, 5-, and 10-Gy doses), or 20 Gy/min (for the 30-Gy dose). Dosimetry was performed using a 0.05-cm^3 tissue-equivalent ion chamber. The ion chamber was placed in a glass test tube inside the Plexiglas ice bath during dosimetry measurements.

Miscellaneous methods Protein content was determined by the method of Lowry *et al.* (*30*), using bovine serum albumin as the standard. Statistical analysis was performed using Student's *t* test. Multiple comparisons with a control were done by analysis of variance (RS1; BBN Software Products Corp., Cambridge, MA) and Dunnett's test (*31*). Data were identified as significant if $P < 0.05$.

[1] K. S. Kumar, Y. N. Vaishnav, A. M. Sancho, and J. F. Weiss, Iron-catalyzed generation of pentane from irradiated erythrocyte membranes. In *Radiation Research Society Abstracts, 33rd Annual Meeting, Los Angeles, CA*, p. 132, 1985. [Abstract JF-2]

TABLE I

Effect of γ Radiation on 65 m*M* KCl-Stimulated $^{45}Ca^{2+}$ Uptake by Rat Whole-Brain, Cortex, and Striatal Synaptosomes

Dose of radiation (Gy)	Dose rate (Gy/min)	Net uptake of $^{45}Ca^{2+}$ (nmol/mg protein)[a]		
		Whole brain	Cortex	Striatum
Sham	Sham	3.4 ± 0.05	3.3 ± 0.05	3.5 ± 0.10
1	1	3.0 ± 0.10*	3.3 ± 0.10	3.3 ± 0.10
3	10	2.7 ± 0.05*	3.0 ± 0.10	3.0 ± 0.10*
5	10	2.4 ± 0.10*	2.8 ± 0.10*	2.8 ± 0.10*
10	10	2.0 ± 0.05*	2.5 ± 0.05*	2.5 ± 0.05*
30	20	1.7 ± 0.05*	2.2 ± 0.05*	2.4 ± 0.05*

[a] Values are means ± SEM of three separate experiments, each using triplicate samples.

* Significantly different from sham value: $P < 0.05$.

RESULTS

The time course (3, 10, 30, and 60 s) as well as the dose effect of KCl (15–65 m*M*) (Figs. 1 and 2) of calcium uptake was reduced following exposure of the whole brain to 3 Gy of γ photons. The fastest rate of depolarization-dependent calcium uptake occurred at 3 s (Fig. 1). The KCl dose–response curve (Fig. 2) showed that 65 m*M* KCl stimulated calcium uptake most. In the above two studies, irradiation reduced calcium uptake at all incubation times and KCl concentrations. Based on the above data, a time point of 3 s and KCl dose of 65 m*M* were selected for investigation of the radiation dose–response curve (Table I).

Gamma irradiation (1–30 Gy) reduced 65 m*M* KCl-stimulated calcium uptake after 3 s in whole-brain, cortical, and striatal synaptosomes. A comparison between regions showed a significant interaction term. Whole-brain synaptosomes were clearly more sensitive to irradiation than those of the cortex or striatum.

Gamma irradiation (1–30 Gy) also reduced 15 m*M* KCl-stimulated calcium uptake in whole-brain, cortical, and striatal synaptosomes after 3 s (Table II). The enhancement of 15 m*M* KCl-stimulated calcium uptake by Bay K 8644 following γ photon exposure was reduced by irradiation (3 Gy) (Fig. 3). Because the differences in uptake for the whole-brain, cortical, and striatal synaptosomes are very similar, only the whole-brain results are shown in Fig. 3. However, the same concentrations of Bay K 8644 did not enhance 30 or 65 m*M* KCl-stimulated calcium uptake (data not shown).

The effects described above indicate that γ irradiation will reduce KCl-stimulated calcium uptake. Several hypotheses can be advanced to explain these data. The initial hypothesis we investigated concerned calcium channel recognition receptor binding. The data showing that Bay K 8644-stimulated calcium uptake is reduced by γ irradiation justifies the selection of nimodipine, the antagonist for the calcium L-channel, as the appropriate ligand with which to perform binding studies.

Data obtained from whole-brain, cortical, and striatal membranes demonstrate that the specific binding of [^{3}H]-nimodipine is unaffected by γ irradiation at 10 Gy (data not shown). These data indicate that the significance of the reduction in KCl and/or Bay K 8644-stimulated calcium uptake is not due to alteration of the L-type calcium channel recognition receptor.

TABLE II

Effect of γ Radiation on 15 m*M* KCl-Stimulated $^{45}Ca^{2+}$ Uptake by Rat Whole-Brain, Cortex, and Striatal Synaptosomes

Dose of radiation (Gy)	Dose rate (Gy/min)	Net uptake of $^{45}Ca^{2+}$ (nmol/mg proteins)[a]		
		Whole brain	Cortex	Striatum
Sham	Sham	2.6 ± 0.05	2.7 ± 0.10	2.7 ± 0.10
1	1	2.4 ± 0.10	2.6 ± 0.10	2.6 ± 0.10
3	10	2.1 ± 0.05*	2.2 ± 0.05*	2.2 ± 0.10*
10	10	1.3 ± 0.10*	1.5 ± 0.15*	1.5 ± 0.15*
30	20	1.3 ± 0.15*	1.1 ± 0.20*	1.1 ± 0.20*

[a] Values are means ± SEM of three separated experiments, each using triplicate samples.

* Significantly different from sham value: $P < 0.05$.

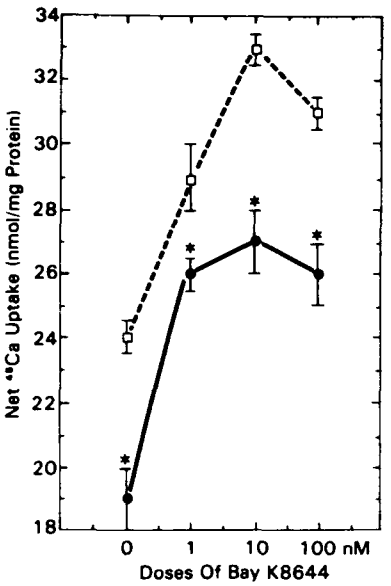

FIG. 3. Effect of γ radiation on Bay K 8644-induced 15 m*M* KCl-stimulated calcium uptake in nonirradiated (□) and irradiated (●) rat whole-brain synaptosomes. Points and bars represent means ± SEM values from three separate experiments, each using triplicate samples. A significant effect of ionizing radiation is indicated as follows: $^{*}P < 0.05$.

DISCUSSION

This study indicates that ionizing radiation decreases KCl-stimulated calcium uptake in the whole brain, cortex, and striatum. These results support electrophysiological studies suggesting reduced neuroexcitability after radiation exposure (*32, 33*) and contradict reports of radiation-induced increases in excitability (*34*). To our knowledge, this is the first report indicating reduction in KCl-stimulated calcium uptake following irradiation.

Bay K 8644 significantly increased the net voltage-dependent entry of calcium stimulated by 15 m*M* KCl in rat whole brain, cortex, and striatum. Our findings are consistent with previous reports about the potentiating action of Bay K 8644 on synaptosomal calcium channel activity, or KCl-stimulated norepinephrine, acetylcholine, and serotonin release from rat brain slices (*14–18*). The effectiveness of Bay K 8644 only at submaximal KCl concentrations agrees with the study by Woodward *et al.* (*35*). These findings are also consistent with reports suggesting that DHP agonists do not potentiate calcium entry into brain synaptosomes at high levels of KCl depolarization[2] (*35*).

The negative data from [^{3}H]nimodipine binding to whole brain, cortex, and striatum indicate that radiation-induced inhibition of Bay K 8644-enhanced KCl-stimulated or KCl-stimulated calcium uptake is not a result of an altered L-type calcium channel recognition receptor. Apparently, radiation does not decrease calcium uptake by a DHP-sensitive mechanism. Further work is in progress to determine the role of N and T calcium channels in mediating radiation-induced decreased calcium uptake.

In conclusion, the present data indicate that ionizing radiation significantly reduces KCl-stimulated calcium uptake.

At the present time we have no data to explain the differences in sensitivity to irradiation of whole brain, cortex, and striatum. Additionally, it is not clear how ionizing radiation causes this dose-dependent decrease in calcium uptake. Preliminary experiments with inositol trisphosphate,[3] prostaglandins (*36*), and phorbol esters (*37*) suggest an impairment in protein kinase C activity that is linked to the opening or closing of ion channels (*38*). Further work is in progress to compare protein kinase C activity of irradiated and nonirradiated synaptosomes, and we are studying G protein receptor binding to determine whether radiation-induced decreases in calcium uptake are due to impairment of protein kinase C, or alterations in G protein receptors, or both.

RECEIVED: February 22, 1990; ACCEPTED: September 6, 1990

REFERENCES

1. J. C. SMITH. Radiation: Its detection and its effects on taste preferences. In *Progress in Physiology Psychology* (E. Stellar and J. M. Sprague, Eds.), Vol. 4, pp. 53–117. Academic Press, New York, 1971.
2. F. ROSENTHAL and P. S. TIMIRAS. Changes in brain excitability after whole-body x-irradiation in the rat. *Radiat. Res.* **15**, 648–657 (1961).
3. T. MINAMISAWA and T. TSUCHIZA. Long-term changes in the averaged evoked potentials of the rabbits after irradiation with moderate x-ray doses. *Electroencephalogr. Clin. Neurophysiol.* **43**, 416–424 (1977).
4. D. J. KIMELDORF and E. L. HUNT. Radiation effects on performance capacity. In *Ionizing Radiation: Neural Function and Behavior* (D. J. Kimeldorf and E. L. Hunt, Eds.), pp. 166–213. Academic Press, New York, 1965.
5. G. A. MICKLEY, K. E. STEVENS, G. A. WHITE, and G. L. GIBBS. Endogenous opiates mediate radiogenic behavioral change. *Science* **220**, 1185–1187 (1983).
6. A. P. CASARETT and C. L. COMAR. Incapacitation and performance decrement in rats following split doses of fission spectrum radiation. *Radiat. Res.* **53**, 455–461 (1973).
7. D. J. TRIGGLE. Drugs active at voltage-dependent calcium channels. *Neurotransmission* **5**, 1–14 (1989).
8. S. VATER, G. KRONEBERG, F. HOFFMEISTER, H. KALLER, K. MENG, A. OBERDORF, W. PUTS, K. SCHLOSSMANN, and K. STOEPEL. On the pharmacology of 4-(2'-nitro-phenyl)-2,6-dimethyl-3,5-dicarbo-

[2] M. M. Murawsky and J. B. Suszkiw, Which type(s) of Ca channels are present in mammalian brain synaptosomes? *Soc. Neurosci. Abstr.* **13**, 103 (1987).

[3] S. B. Kandasamy and W. A. Hunt, Effect of ionizing radiation on calcium channels in rat brain synaptosomes. *Soc. Neurosci. Abstr.* **14**, Part 1, (1988). [Abstract 54.13]

methyl-1,4-dihydropyridine (nifedipine, Bay K 1040). *Arzneim. Forsch.* **22,** 1–14 (1972).

9. S. HAGIWARA and L. BYERLY, Calcium channels. *Annu. Rev. Neurosci.* **4,** 69–125 (1983).
10. R. W. TSIEN, Calcium channels in excitable cell membranes. *Annu. Rev. Physiol.* **45,** 341–358 (1983).
11. P. BELLEMANN, A. SCHADE, and R. TOWART, Dihydropyridine receptor in rat brain labeled with [^{3}H] nimodipine. *Proc. Natl. Acad. Sci. USA* **80,** 2356–2360 (1983).
12. S. A. THAYER, S. N. MURPHY, and R. J. MILLER, Widespread distribution of dihydropyridine-sensitive calcium channels in the central nervous system. *Mol. Pharmacol.* **30,** 505–509 (1986).
13. J. J. WOODWARD and S. W. LESLIE, Bay K 8644 stimulation of calcium entry and endogenous dopamine release in rat striatal synaptosomes antagonized by nimodipine. *Brain Res.* **370,** 397–400 (1986).
14. M. C. NOWYCKY, A. P. FOX, and R. W. TSIEN, Three types of neuronal calcium channel with different calcium agonist sensitivity. *Nature* **316,** 440–443 (1985).
15. T. M. PERNEY, L. D. HIRNING, S. F. LEEMAN, and R. J. MILLER, Multiple calcium channels mediate neurotransmitter release from peripheral neurons. *Proc. Natl. Acad. Sci. USA* **83,** 6656–6659 (1986).
16. S. KONGSAMUT and R. J. MILLER, Nerve growth factor modulates the drug sensitivity of neurotransmitter release from PC-12 cells. *Proc. Natl. Acad. Sci. USA* **83,** 2243–2247 (1986).
17. A. G. GARCIA, F. SALA, J. A. REIF, S. VINNIEGRA, J. FRIAS, R. FONTERIZ, and L. GANDIA, Dihydropyridine Bay K 8644 activates chromaffin cell calcium channels. *Nature* **309,** 69–71 (1984).
18. D. N. MIDDLEMISS and M. SPEDDING, A functional correlate for the dihydropyridine binding site in rat brain. *Nature* **314,** 94–96 (1985).
19. M. SCHRAMM, G. THOMAS, R. TOWART, and G. FRANOWIAK, Novel dihydropyridines with positive inotropic action through activation of Ca^{2+} channels. *Nature* **303,** 535–537 (1983).
20. H. ROGG, L. CRISCIONE, A. TRUOG, and M. MEIER, *In vitro* comparative studies of the calcium-entry activators YC-170, CGP 28392, and Bay K 8644. *J. Cardiovasc. Pharmacol.* **7,** Suppl. 6, 31–37 (1985).
21. D. RAMPE, R. A. JANIS, and D. J. TRIGGLE, Bay K 8644, a 1,4-dihydropyridine Ca^{2+} channel activator: Dissociation in binding and functional effects in brain synaptosomes. *J. Neurochem.* **43,** 1688–1692 (1984).
22. J. A. CREBA and M. KAROBATH, The effect of dihydropyridine calcium agonists and antagonists on neuronal voltage sensitive calcium channels. *Biochem. Biophys. Res. Commun.* **134,** 1038–1047 (1986).
23. I. J. REYNOLDS, J. WAGNER, S. H. SNYDER, S. A. THAYER, B. M. OLIVERA, and R. J. MILLER, Brain voltage-sensitive calcium channel subtypes differentiated by ω-conotoxin fraction GVIA. *Proc. Natl. Acad. Sci. USA* **83,** 8804–8807 (1986).
24. J. GLOWINSKI and L. L. IVERSEN, Regional studies of catecholamines in the rat brain-1. *J. Neurochem.* **13,** 655–669 (1966).
25. E. G. GRAY and V. P. WHITTAKER, The isolation of nerve endings from brain: An electron-microscopic study of cell fragments derived by homogenization and centrifugation. *J. Anat.* **96,** 79–87 (1962).
26. M. P. BLAUSTEIN and S. ECTOR, Barbiturate inhibition of calcium uptake by depolarized nerve terminals *in vitro*. *Mol. Pharmacol.* **11,** 369–378 (1975).
27. S. W. LESLIE, M. B. FRIEDMAN, R. E. WILCOX, and S. Y. ELROD, Acute and chronic effects of barbiturates on depolarization-induced calcium influx into rat synaptosomes. *Brain Res.* **185,** 409–417 (1980).
28. A. SKATTEBOL and D. J. TRIGGLE, Regional distribution of calcium channel ligand (1,4-dihydropyridine) binding sites and $^{45}Ca^{2+}$ uptake processes in rat brain. *Biochem. Pharmacol.* **36,** 4163–4166 (1987).
29. S. B. KANDASAMY, K. S. KUMAR, W. A. HUNT, and J. F. WEISS, Opposite effects of WR-2721 and WR-1065 on radiation-induced hypothermia: Possible correlation with oxygen uptake. *Radiat. Res.* **114,** 240–247 (1988).
30. O. H. LOWRY, N. J. ROSENBROUGH, A. L. FARR, and R. J. RANDALL, Protein measurement with the Folin phenol reagent. *J. Biol. Chem.* **193,** 265–275 (1951).
31. C. W. DUNNETT, New tables of multiple comparisons with a control. *Biometrics* **20,** 482–491 (1964).
32. H. B. GERSTNER and J. S. ORTH, Effects of high intensity of x-ray irradiation on the velocity of nerve conduction. *Am. J. Physiol.* **130,** 232–286 (1950).
33. E. L. GASTEIGER and B. CAMBELL, Alteration of mammalian nerve compound action potentials by beta irradiation. In *Responses of the Nervous System to Ionizing Radiation* (T. J. Haley and R. S. Snider, Eds.), pp. 597–606. Academic Press, New York, 1962.
34. C. S. BACHOFER, Radiation effects on bioelectric activity of nerves. In *Responses of the Nervous System to Ionizing Radiation* (T. J. Haley and R. S. Snider, Eds.), pp. 573–583. Academic Press, New York, 1962.
35. J. J. WOODWARD, M. E. COOK, and S. W. LESLIE, Characterization of dihydropyridine-sensitive calcium channels in rat brain synaptosomes. *Proc. Natl. Acad. Sci. USA* **85,** 7389–7393 (1988).
36. S. B. KANDASAMY and W. A. HUNT, Arachidonic acid and postaglandins enhance potassium-stimulated calcium influx in rat brain synaptosomes. *Neuropharmacol.* **29,** 825–829 (1990).
37. S. B. KANDASAMY and W. A. HUNT, Role of protein kinase C in radiation-induced decreased calcium-uptake in rat brain synaptosomes. *Toxicologist* **10,** 422 (1990).
38. J. L. MARX, Polyphosphoinositide research updated. *Science* **235,** 974–976 (1987).

The International Narcotics Research Conference (INRC) '89, pages 137–140

MORPHINE INDUCES AN INTRACELLULAR ALKALINIZATION IN BOVINE AORTIC ENDOTHELIAL CELLS (BAECs)

Juliann G. Kiang and M. Colden-Stanfield

Department of Physiology, Armed Forces Radiobiology Research Institute, Bethesda Maryland 20814-5145, U. S. A.

The resting intracellular pH (pHi) of BAECs, by using BCECF fluorescence, at 37 °C in Na^+ Hanks' was 7.22±0.03. Cells which had been acid-loaded recovered from the intracellular acidification in Na^+ Hanks' in a $[Na^+]_o$-dependent and amiloride-sensitive manner. Recovery from acidification had an apparent Km for Na^+ of 40 ± 10 mM and Ki for amiloride of 26±4 μM. Morphine (50 μM, 20 min, 37 °C) increased the pHi to 7.55 ± 0.05. Naloxone (50 μM) given 5 min before morphine (50 μM) blocked this effect, indicating that this was an opiate receptor-mediated phenomenon. To determine if morphine activated the Na^+/H^+ exchanger, pHi was monitored in Na^+-free Hanks', acidic Na^+ Hanks' or amiloride-containing Na^+ Hanks'. The alkalinization produced by morphine was not observed under all these circumstances. These data suggest morphine activates the Na^+/H^+ exchanger via opiate receptors.

INTRODUCTION

A monolayer of vascular endothelial cells lines the inner surface of the blood vessels and has broad metabolic functions. The intracellular pH (pHi) must be maintained in a narrow range to provide an environment for various intracellular reactions (Moolenaar, 1986). In many cells, pHi homeostasis is maintained by 3 defined ion transporters: the Na^+/H^+ exchanger, Na^+-dependent and Na^+-independent Cl^-/HCO_3^- exchangers (Grinstein et al., 1989). The presence of the Na^+/H^+ exchanger has been demonstrated in rat brain capillary endothelial cells in vivo and nonadherent bovine aortic endothelial cells in vitro.

Previous studies showed that δ-opiate agonists elicited a cytoplasmic alkalinization in NG108-15 cells which was concentration-dependent and reversed by naloxone (Isom et al., 1987). We report, herein, that morphine can alkalinize adherent BAECs via activation of Na^+/H^+ exchanger.

MATERIALS AND METHODS

BAECs were obtained from bovine aorta by digestion with 0.2% collagenase (Eskin et al., 1978). The cells were cultured in Dulbecco's modified Eagle medium supplemented with 2 mM glutamine, 4.5 g/l glucose, 25 mM HEPES, 10% fetal bovine serum, penicillin (50 μg/ml) and streptomycin (50 U/ml) (Gibco, Grand Island, NY). Typical cobblestone morphology was observed and angiotensin converting enzyme activity was measured. The cells at passage 6-10 were used for experiments. To measure pHi, Confluent monolayers of BAECs were incubated with 5 μM BCECF acetoxymethyl ester in Na^+ Hanks' (in mM, 148 NaCl, 4.6 KCl, 1.2 $MgCl_2$, 1.6 $CaCl_2$, 20 HEPES, pH=7.38) at 37 °C for 15 min. The fluorescence signal was measured at 37 °C on a SLM 8000C spectrofluorometer as the ratio of emission at 529 $\pm$ 4 nm for excitation at 505 $\pm$ 4 and 442 $\pm$ 4 nm. The fluorescence signal was calibrated by using nigericin (3 μM) and valinomycin (3 μM). To determine the recovery rate from acidification in acid-loaded cells, cells were incubated in Hanks' with 40 mM NH_4Cl for 15 min. Then, cells were placed in Na^+-free Hanks' (N-methyl-(+)glucamine substituted for Na^+) for 2 min. Recovery from acidification was measured when cells were placed in Hanks' containing different concentrations of Na^+. The initial rate of recovery was determined.

RESULTS

The resting pHi in adherent BAEC at 37 °C in Na^+ Hanks' is 7.22 $\pm$ 0.03 (n=32). Amiloride (100 μM), a blocker of Na^+/H^+ exchanger, added to the cells did not change the resting pHi indicating the Na^+/H^+ exchanger was inactive in resting cells. Acid-loaded cells had a pHi of 6.76 $\pm$ 0.05 (n=22) in Na^+-free (NMG) Hanks' but recovered their pHi to 7.2 within 2 min after being placed in Na^+ Hanks'. Cells which had been acid-loaded recovered from the intracellular acidification in Na^+ Hanks' in a $[Na^+]_o$-dependent manner (Fig. 1) and had an apparent Km for Na^+ of 40 $\pm$ 10 mM. Amiloride (1 mM) inhibited the initial rate of recovery from acidification in Na^+ Hanks' by 94%; inhibition was concentration-dependent with an apparent Ki for amiloride of 26 $\pm$ 4 μM (data not shown). The results suggest the pHi recovery from an imposed acid-loading is mediated by the Na^+/H^+ exchanger in BAECs.

When morphine (50 μM, 20 min) was added to the cells, an alkalinizaton to 7.55 $\pm$ 0.05 pH units (n=10) was produced (Fig. 2A) and took an hour to return to its resting pHi. Naloxone (50 μM) given 5 min before morphine (50 μM) blocked this effect (naloxone: 7.32 $\pm$ 0.06; naloxone+morphine: 7.29 $\pm$ 0.05, n=5 for both groups), suggesting that this was an opiate receptor-mediated phenomenon. It should be noted that naloxone itself increased pHi by 0.14 $\pm$ 0.05 units (n=5). To determine if morphine activated the Na^+/H^+ exchanger, pHi was monitored in the presence of amiloride by which Na^+/H^+ exchanger was blocked. Morphine

did not induce changes in pHi (Fig. 2A). Experiments were also conducted in Na^+-free Hanks' in which the activity of the Na^+/H^+ exchanger was inhibited by removing extracellular Na^+. Morphine-induced

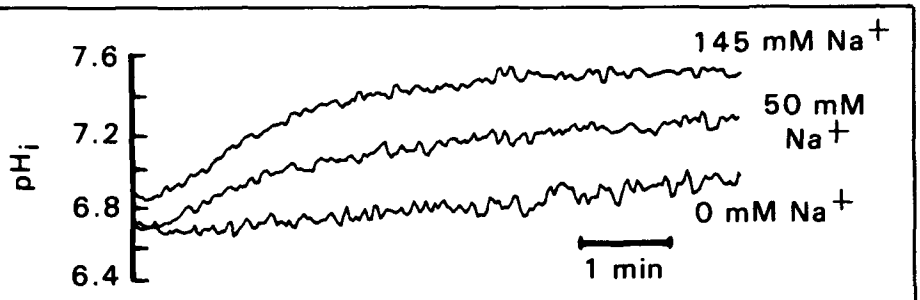

Fig. 1. Evidence for Na^+/H^+ exchanger in adherent BAECs. Cells were loaded with NH_4Cl (40 mM) for 15 min, placed in Na^+-free media for 2 min and, then replaced in buffer containing 0, 50, 145 mM Na^+ Hanks'. No recovery was observed in Na^+-free Hanks'.

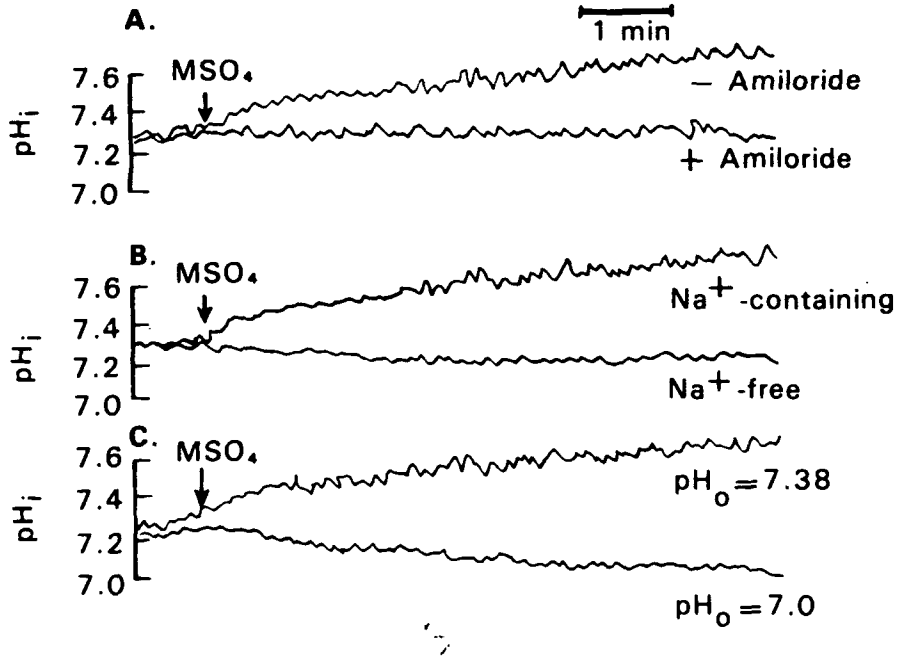

Fig. 2. Effects of morphine on BAECs under conditions which inhibited the Na^+/H^+ exchanger. (A) Amiloride (1 mM) was added 5 min prior to morphine (50 μM). (B) Cells were placed in Na^+-free Hanks'. (C) Cells were placed in Na^+ Hanks' at pH_o = 7.0. The pH_o of normal Na^+ Hanks' was 7.38.

alkalinization was not observed (Fig. 2B). Similarly, an increase in extracellular proton which can block antiporter-dependent H^+ efflux also inhibited morphine-induced alkalinization (Fig. 2C). The lack of an effect of morphine on pHi after the blockade of Na^+/H^+ exchanger suggests that morphine alkalinized BAEC via an activation of Na^+/H^+ exchanger.

DISCUSSION

The resting pHi of adherent BAECs is 7.22 $\pm$ 0.03 which is in agreement with the resting pHi of nonadherent BAECs as shown by Kitazona et al. (1988). Morphine induced an intracellular alkalinization which took 1 hr to return to its resting pHi. The effect was via Na^+/H^+ exchanger since the presence of amiloride prevented the effect. The view was further supported by two other observations. That is, removal of extracellular Na^+ or an increase of extracellular proton inhibited morphine-induced alkalinization. This is not unique to morphine. A similar effect has been reported in many different cells treated with agents such as growth factors, mitogens, tumor-promoting agents (Grinstein and Rothstein, 1986). The underlying mechanism(s) of morphine-induced alkalinization is not understood. It is possible that morphine activates the Na^+/H^+ exchanger either by modifying the apparent affinity for Na^+ or H^+, or by changing the maximal rate of exchange. Our preliminary data have also indicated that opiate receptors are on the cell membrane in BAECs (data not shown). Pretreatment of naloxone prevented the alkalinization suggesting that morphine-activated Na^+/H^+ exchange is coupled to opiate receptors. It will be interesting to study if the alkalinization produced by opiates in BAECs is involved in changing the blood pressure which occurs following administration of opiates in vivo.

REFERENCES

Eskin S C, Sybers H D, Trevino L, Lie J T, Chimoskey J E (1978). Comparison of tissue-cultured bovine endothelial cells from aorta and saphenous vein. In Vitro Cell Deu Biol 14:903-910.

Grinstein S, Rothstein A (1986). Mechanisms of regulation of the Na^+/H^+ exchanger. J Membrane Biol 90:1-12.

Grinstein S, Rotin D, Mason M J (1989). Na^+/H^+ exchange and growth factor-induced cytosolic pH changes. Role in cellular proliferation. Bioch Bioph Acta 988:73-97.

Kitazono T, Takeshige K, Cragoe E J, Minakami S (1988). Intracellular pH changes of bovine aortic endothelial cells in response to ATP addition. Biochem Bioph Res Comm 152:1304-1309.

Isom L L, Cragoe E J, Limbird L E (1987). Multiple receptors linked to inhibition of adenylate cyclase acccelerate Na^+/H^+ exchange in neuroblastoma x glioma cells via a mechanism other than decreased cAMP accumulation. J Biol Chem 262:6750-6757.

Moolenaar W H (1986). Regulation of cytoplasmic pH by Na^+/H^+ exchange. Trends Biochem Sci 11:141-143.

Microecology and Therapy
Mikroökologie und Therapie
Vol. 19, 135 – 139 (1989)
ISSN 0720-0536

Edited by
Institut für Mikroökologie
D 6348 Herborn-Dill
Federal Republic of Germany

COMBINED THERAPY OF SEPTICEMIA WITH OFLOXACIN AND/OR SYNTHETIC TREHALOSE DICORYNOMYCOLATE (S-TDCM)IN IRRADIATED AND WOUNDED MICE

DIE KOMBINIERTE THERAPIE DER SEPTIKÄMIE MIT OFLOXACIN UND/ODER SYNTHETISCHEM TREHALOSE-DICORYNOMYCOLAT (S-TDCM) BEI BESTRAHLTEN UND VERWUNDETEN MÄUSEN

GARY S. MADONNA, MARY M. MOORE, G. DAVID LEDNEY, THOMAS B. ELLIOTT, and ITZHAK BROOK

SUMMARY

Following lethal irradiation, mice usually succumb to sepsis as a result of translocation of intestinal bacteria and impairment of the host defense system. Additional trauma in these immunocompromised mice further increases susceptibility to bacterial infection from either endogenous or exogenous origin. Treatment with ofloxacin or synthetic trehalose dicorynemycolate (S-TDCM) and was evaluated in mice, which were lethally irradiated and wounded, and which died with sepsis within six days. Wounding was performed on C3H/HeN mice anesthetized by inhalation of methoxyfurane. Dorsal skin and muscle equal to 30% total body surface was removed 1 h after 8.0 Gy gamma radiation. S-TDCM, which augments nonspecific resistance to infection in irradiated mice, was given once i.p. immediately after wounding. Ofloxacin was injected s.c. daily from day 0 to day 10. *Staphylococcus aureus, Streptococcus faecium*, and *Escherichia coli* were isolated from both the livers and wound sites of moribund, untreated mice 4 and 5 days postirradiation. Although all mice died, ofloxacin increased the mean survival time from 4.7 days (untreated) to 11.4 days and decreased the number of bacterial species isolated from liver and wound. Combined treatment with ofloxacin and S-TDCM did not increase survival time compared with ofloxacin treatment alone. Although they prolong survival, ofloxacin and S-TDCM alone are inadequate for effective therapy of polymicrobic infections in irradiated/wounded mice.

ZUSAMMENFASSUNG

Im Gefolge letaler Bestrahlung fallen Mäuse normalerweise einer Sepsis zum Opfer, bedingt durch die Translokation intestinaler Bakterien und der Dysfunktion des wirtseigenen Abwehrsystems. Die Empfänglichkeit gegenüber bakteriellen Infektionen wird bei solchermaßen immunkomprimittierten Mäusen durch zusätzliche Wundtraumata entweder endogenen oder exogenen Ursprungs weiter erhöht. Bei letal bestrahlten und verwundeten Mäusen, die innerhalb von 6 Tagen an Sepsis starben, wurde die Behandlung mit Ofloxacin und/oder synthetischem Trehalose-Dicorynomycolat (S-TDCM) überprüft. Das Setzen von Wunden wurde an C3H/HeN-Mäusen vorgenommen, die durch die Inhalation von Methoxyfluran anästhetisiert wurden. Eine Stunde nach 8,0 Gy Gamma-Bestrahlung wurden dorsal Haut- und Muskelgewebe in Entsprechung von 30% der gesamten Körperoberfläche entfernt. Unmittelbar

nach der Wundsetzung wurde S-TDCM, welches die unspezifische Resistenz gegenüber Infektionen bei bestrahlten Mäusen erhöht, in einer einmaligen Dosis intraperitoneal appliziert. Ofloxacin wurde täglich subkutan von Tag 0 bis Tag 10 injiziert. *Staphylococcus aureus, Streptococcus faecium* und *Escherichia coli* wurden sowohl aus den Lebern, als auch von den Wundstellen sterbender, unbehandelter Mäuse im Zeitraum von 4 und 5 Tagen nach der Bestrahlung isoliert. Obwohl alle Mäuse starben, erhöhte Ofloxacin die mittlere Überlebenszeit von 4,7 Tagen (unbehandelt) auf 11,4 Tage und erniedrigte die Anzahl der aus Leber und Wunden isolierten Bakterienspezies. Die kombinierte Behandlung mit Ofloxacin und S-TDCM erhöhte die Überlebenszeit im Vergleich mit alleiniger Ofloxacin-Behandlung nicht. Ofloxacin und S-TDCM alleine sind für die effektive Therapie von Infektionen durch mehrere Mikroben bei bestrahlten und verwundeten Mäusen ungeeignet, obwohl sie die Überlebenszeit verlängern.

INTRODUCTION

One of the many problems that physicians will encounter in the treatment of radiation victims is providing life-sustaining support to individuals who have not only received a lethal dose of radiation but have received physical trauma as well. We previously showed that i.p. injection of synthetic trehalose dicorynemycolate (S-TDCM) 20 h before or 1 h after lethal irradiation significantly increases survival in B6D2F1 or C3H/HeN mice (MADONNA et al., 1989). Further, S-TDCM-enhancement of survival in irradiated mice was shown to be associated with a reduction in sepsis, increase in nonspecific resistance to infection, and stimulation of hematopoesis. Ofloxacin is one of a new generation of fluorinated quinolones with activity against most Gram-negative bacteria, many Gram-positive bacteria and some anaerobes (MONK and CAMPOLI-RICHARDS, 1987).

Our purpose in the present study was to determine whether S-TDCM or ofloxacin would increase survival in irradiated mice that are wounded 1 h after irradiation and which die one week earlier than mice exposed to radiation alone. Results showed that aggressive antibiotic therapy with ofloxacin, but not S-TDCM injection, significantly increased the survival time of combined injured mice. In addition, ofloxacin therapy reduced the number of bacterial species cultured from the wound and liver of irradiated/wounded mice.

METHODS

Radiation

C3H/HeN female mice (8 - 12 weeks) were given a whole body dose of ^{60}Co radiation (MADONNA et al., 1989). Mice received 8.0 Gy at 0.4 Gy/min. This dose results in 85 - 100% mortality in 30 days.

Wounding and S-TDCM Therapy

One hour postirradiation, groups of mice were anesthetized by inhalation of methoxyflurane and treated as follows:

Irradiated Group

Mice were injected with a suspension of S-TDCM (Ribi ImmunoChem Research, Inc., Hamilton, MT) (200 μg/mouse, i.p.) in 0.2% Tween 80/saline, or saline (control) (0.5 ml/mouse, i.p.). The synthesis and preparation of S-TDCM has been described (MADONNA et al., 1989).

Combined-Injury Group

Mice were given a 30% total-body-surface-area wound (LEDNEY et al., 1985) and then injected i.p. with either S-TDCM or saline (control). The time required for the wound trauma procedure is approximately 10 minutes. In brief, the fully anesthetized mouse is subjected to wound trauma by punching out a double layer of dorsal surface skin between the shoulders. The panniculus carnosus muscle and overlying skin is removed by sliding the loose dorsal skin away from the body and by striking a steel punch with a hammer. The procedure is done on a clean teflon covered operation board. Aseptic technique is used throughout the entire procedure. The wound size is 30% of the total skin surface.

Antibiotic Therapy

Ofloxacin (Ortho Pharmaceuticals) was prepared in sterile, pyrogen-free water and was injected into mice (0.1 ml/mouse, s.c.) at a dose of 40 mg/kg/day. Control mice received 0.1 ml of water/day, s.c.

Isolation of Bacteria From Wound Site and Liver

Additional mice were included in each group to assess the degree of bacterial colonization of the wound and/or the presence of sepsis indicated by bacteria in the liver.

Wound Culture

The wound site of injured mice was cultured for bacteria by rolling a sterile, saline-soaked cotton swab over the wound surface. The swab was then inoculated to one plate of 5% defibrinated sheep blood agar (with phenyl ethanol) and one plate of MacConkey Agar. Media were incubated overnight at 35° C. Colonies of bacteria were identified by standard diagnostic procedures (ASM Manual of Clinical Laboratory Microbiology).

Liver culture

Mice were euthanized by cervical dislocation and a portion of each liver was aseptically removed, weighed, and homogenized in cold saline solution. Serial dilutions of each liver homogenate were made in cold saline solution and suspensions were inoculated in duplicate to media by a Spiral plater (Spiral Systems Inc.), enumerated and identified.

RESULTS

Survival and Culture of Irradiated/Wounded Mice

Ofloxacin therapy increased the mean survival time of irradiated/wounded mice from 4.7 days (untreated) to 11.4 days (treated) (Figure 1). Culture of the wounds of untreated, moribund mice on day 4 yielded *Staphylococcus aureus*, *Streptococcus faecium*, *Escherichia coli*, and *Proteus mirabilis*. In contrast, only *S. aureus* and *S. faecium* were recovered from the wounds of ofloxacin-treated mice. In addition, *P. mirabilis* was recovered from the livers of untreated mice on day 4, whereas no bacteria were recovered from the livers of irradiated/wounded mice treated with ofloxacin.

Although S-TDCM increased the survival of irradiated mice, it decreased the mean survival time of irradiated/wounded mice from 4.7 days to 3.8 days. Cultures of the wounds of irradiated/wounded mice yielded *S. aureus*, *S. faecium*, *E. coli*, and *P. mirabilis* as did those of untreated mice. *P. mirabilis* was isolated from the livers of both untreated and treated mice.

Combination therapy with S-TDCM and ofloxacin decreased survival time of irradiated/wounded mice compared with ofloxacin treatment alone by 1.1 days (11.4 days with ofloxacin vs. 10.2 days with ofloxacin and S-TDCM). No bacteria grew in liver cultures from ofloxacin-treated mice 4 days postirradiation. In contrast, cultures of liver from S-TDCM/ofloxacin treated mice yielded *S. faecium* and *S. aureus*.

DISCUSSION

These studies demonstrated that early mortality in combined injured mice is associated with fulminant infection most likely resulting from the unhindered spread of bacteria from the wound site. The usefulness of aggressive antibiotic therapy to suppress the growth and spread of opportunistic bacteria was demonstrated by the increased mean survival time and the reduction in the number of bacterial species isolated from the wound and liver of ofloxacin-treated mice.

Results suggested that therapy with an immunomodulator, such as S-TDCM, can be toxic rather than beneficial. Interestingly, previous studies have shown that combined therapy with natural TDM from *Mycobacterium phlei* and ceftriaxone (a third-generation cephalosporin) synergistically increased survival of mice exposed to a sublethal dose of radiation and challenged with a lethal dose of *Klebsiella pneumoniae* (MADONNA et al., 1989).

These studies illustrated the association and complexity of wound trauma and susceptibility to infection in the immunocompromised host. Further investigations into the mechanisms of early mortality in combined injury will be necessary in order to determine better treatment regimens.

Experiments are in progress to determine whether ceftriaxone is more efficacious than ofloxacin when combined with S-TDCM therapy in irradiated/wounded mice. The spectrum of activity of ceftriaxone includes staphylococci, except methicillin-resistant strains, but not enteric streptococci.

ACKNOWLEDGEMENTS

The authors appreciate the collaborative effort of *J. Terry Ulrich* and *Kent R. Myers*, Ribi ImmunoChem Research, Inc., Hamilton, MT, USA. The testing of S-TDCM at AFRRI would not be possible without their continued support. We are grateful to *William E. Jackson, III*, for analysis of data on survival of mice. This research was supported by Work Unit No. 4420-00129 of the Armed Forces Radiobiology

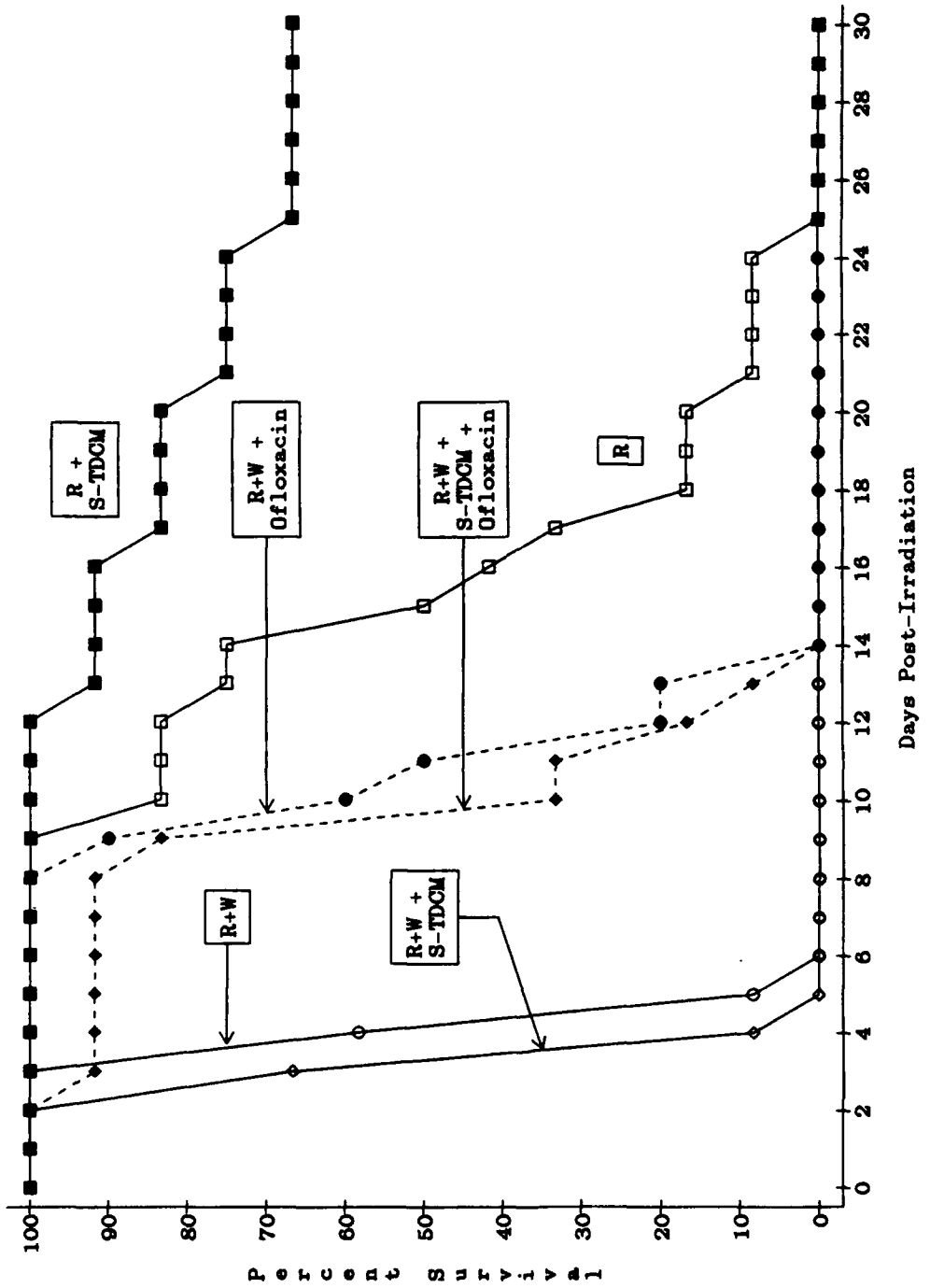

Figure 1: Survival of irradiated/wounded mice given S-TDCM and treated with ofloxacin. Mice (N = 12) were irradiated/wounded (R + W) or irradiated alone (R) on day 0. Mice in each group were injected with S-TDCM (200 μg/mouse, i.p.) or saline solution 1 h post-irradiation. Ofloxacin or water (control) was injected s.c. (40 mg/kg/day) on days 0–10. P values determined by the generalized Savage (Mantel Cox) method were: P = 0.0035 for R + W vs. R + W(S-TDCM), P < 0.001 for R vs. R(S-TDCM), and P > 0.05 for R + W(ofloxacin) vs. R + W(S-TDCM + Ofloxacin).

Research Institute, Defense Nuclear Agency. The views presented in this paper are those of the authors. No endorsements by the Defense Nuclear Agency have been given or should be inferred. Research was conducted according to the principles enunciated in the „Guide for the Care and Use of Laboratory Animals", prepared by the Institute of Laboratory Animal Resources, National Research Council.

Gary S. Madonna, Ph.D., Mary M. Moore, Ph.D., G. David Ledney, Ph.D., Thomas B. Elliott, Ph.D., and Itzhak Brook, Ph.D., Department of Experimental Hematology, Armed Forces Radiobiology Research Institute, Bethesda, MD, 20814-5145, USA.

Paper presented as poster by Dr. Madonna at the XIV. International Symposium on Microbial Ecology and Disease, September 21-23, 1989, San Antonio, Texas, USA.

LITERATURE

LEDNEY, G.D., STEWART, D.A., GRUBER, D.F., GELSTON, H.M., EXUM, E.D., and SHEERY, P.A.: Hematopoietic Colony-Forming Cells from Mice After Wound Trauma. J. Surg. Research. *38*, 55-65 (1985).

MADONNA, G.S., LEDNEY, G.D., ELLIOTT, T.B., BROOK, I., ULRICH, J.T., MYERS, K.R., PATCHEN, M.L., and WALKER, R.I.: Trehalose Dimycolate Enhances Resistance to Infection in Neutropenic Animals. Infect. Immun. *57*, 2495-2501 (1989).

MONK, J.P., and CAMPOLI-RICHARDS, D.M.: Ofloxacin: A Review of its Antibacterial Activity, Pharmacokinetic Properties and Therapeutic Use. Drugs *33*, 346-391(1987).

J. RADIAT RES., 30, 255-265 (1989)

Effect of Electron Radiation on Aggressive Behavior, Activity, and Hemopoiesis in Mice

DONNA M. MAIER, MICHAEL R. LANDAUER, HIRSCH D. DAVIS AND THOMAS L. WALDEN

Departments of Behavioral Sciences and Radiation Biochemistry
Armed Forces Radiobiology Research Institute
Bethesda, MD 20814-5145 U.S.A.

(Received July 3, 1989)
(Accepted July 28, 1989)

Radiation/Hemopoiesis/Aggression/Mice/Locomotor Activity

The behavioral and physiological effects of 10 Gray (Gy) LINAC electrons in male Swiss-Webster mice were followed for 12 days postirradiation (PR). In Experiment 1, aggressive behavior was assessed in irradiated or sham-irradiated resident mice using a resident-intruder paradigm. Aggressive offensive behavior in the irradiated residents was significantly decreased beginning 2 to 5 days PR, and remained suppressed. Defensive behavior in the nonirradiated intruders was decreased significantly by day 5 PR. In Experiment 2, spontaneous locomotor activity was monitored. Ambulation of irradiated mice was significantly depressed from day 5 PR on, while rearing was affected as early as day 2 PR and remained suppressed. Body weights of irradiated animals were significantly decreased by 5 days PR. In Experiment 3, blood parameters were examined. Compared to sham-irradiated controls, leukocytes, erythrocytes, and hematocrit of irradiated mice were reduced significantly beginning on day 1 PR and remained suppressed, while platelets and hemoglobin were decreased beginning day 2 PR. These results demonstrate that 10 Gy of high-energy electrons results in earlier behavioral deficits than has been observed previously with the same dose of gamma photons.

INTRODUCTION

Exposure to electron fluxes in the Earth's radiation belt presents a serious problem for manned space flight and is of special concern for proposed missions to Mars, the establishment of lunar bases, and the use of geostationary orbits[12,17]. Low doses of radiation can exert subtle effects on the nervous system, resulting in possible behavioral decrements that would interfere with the successful completion of a space mission[4,15,29]. Exposure to higher doses of radiation can result in severe early performance decrements, anorexia, nausea, emesis, fever, and diarrhea. These symptoms are followed by anemia, immunosuppression, hemorrhage, and muscular weakness[4,9,14], all of which could present serious threats to astronauts.

Previous research has demonstrated that electron radiation may exert a greater suppressive

effect on behavior than other qualities (types) of radiation, including gamma photon, bremsstrahlung, and neutron radiation. For example, a study measuring performance on an accelerod, a shock-motivated test of motor coordination, revealed that the ED50 (median effective dose) for disruption of motor behavior for electrons, gamma photons, bremsstrahlung, and neutron radiation was 61, 89, 81, and 98 Gy, respectively[3,5]. Similarly, the ED50 for suppressing shock-avoidance behavior on a jump task in rats was 62 Gy for electron radiation and 102 Gy for gamma photons[15]. Moreover, a dose of 100 Gy electrons produced the same degree of radiation-induced catalepsy in rats as 150 Gy gamma photons[16], (Dr. S.B. Kandasamy, personal communication). Whole-body irradiation of rats with 10 Gy electrons produced similar perturbations in calcium channel uptake in synaptosomes as did whole-body irradiation with 20 Gy gamma photons (Dr. S.B. Kandasamy, personal communication).

While electrons may be more effective than other qualities of radiation at suppressing some types of behavior, this is not true of all behavioral measures. In miniature pigs, head-only irradiation with 88 Gy electrons produced the same degree of deficit in shock-avoidance behavior in a shuttlebox as irradiation with 88 Gy mixed gamma-neutrons[10,11]. Development of conditioned taste aversion in rats was affected more severely by high-energy iron particles and neutrons than by electrons: a maximal radiation-induced conditioned taste aversion was produced by irradiation with 0.3 Gy high-energy iron particles, 1 Gy neutrons, 5 Gy gamma photons, or 5 Gy electrons[25].

In the present studies, the effects of high-energy electron radiation on aggressive behavior, locomotor activity, and body weight were assessed. Blood parameters were also monitored to determine if behavioral changes were correlated with radiation-induced hemopoietic alterations.

MATERIALS AND METHODS

Subjects

Male Crl:CFW (SW) BR VAF/Plus Swiss-Webster mice, aged 4 months, were obtained from Charles River Breeding Labs (Raleigh, NC), and served as subjects. All animals were quarantined on arrival, and a random sample of mice were screened for evidence of disease by histopathology and serology. Mice were housed individually in polycarbonate isolator cages on hardwood chip contact bedding in an AAALAC-accredited facility under a reversed 12:12 hr light-dark cycle with lights off at 0700. Temperature was maintained at $21° \pm 1°C$ with $50\% \pm 10\%$ relative humidity. Commercial laboratory rodent chow (Lab Blox, Wayne, OH) and acidified (pH 2.5 using HCl) water[22] were freely available.

Radiation Procedure

The mice were placed in ventilated lucite restraint devices for approximately 20 min during irradiation or sham irradiation. Animals were exposed to 10 Gy of 18.5 MeV electrons from a linear accelerator that provided 4 microsecond pulses (15 pulses/sec). Sham-irradiated animals were placed in the radiation chamber for an equivalent amount of time, but were not exposed to the electrons.

Experiment 1 -Resident-Intruder Test

Social behavior was measured using a resident-intruder paradigm, in which a resident mouse attacks an intruder that has entered its territory[26]. This paradigm has been used widely to measure offensive aggressive behavior (observed in the resident as it attacks the intruder) and defensive behavior (observed in the intruder as it defends itself) and has ethological validity because dominant mice defend their territories in the wild[1,2].

The animals were housed individually for 6 weeks before irradiation because this has been reported to be an effective noninvasive method for inducing offensive aggressive behavior in mice[6,8,19,24]. After 5 weeks of isolation, each animal was brought to the test room and paired with another weight-matched mouse for 5 to 10 min. Subsequently, the animal that dominated in this encounter was designated as the resident and the subordinate mouse became the intruder. Mice remained in the same resident-intruder pairs throughout the study, and all further testing was conducted in the resident's home cage.

On each test day, the mice were habituated to the testing room for 1 hr prior to the aggression test. The intruder was placed in the resident mouse's home cage (25.7 cm × 15.2 cm × 12.1 cm) for 5 min during the dark portion of the light-dark cycle, and the ensuing behavioral interactions were videotaped under infrared light. The following behaviors displayed by the resident mice were analyzed: number of bites, number of lunges and chases, and attack latency[1,2,26]. Bites did not draw blood or leave any discernible mark on the intruder. Behaviors displayed by the intruder mice that were analyzed consisted of number of escapes, number of squeaks, and number of defensive upright postures[1,2,7]. Videotapes were scored by an observer who was unaware of the treatment condition of the animals. Aggressive behavior was measured 2 days before irradiation (baseline); 1 to 3 hr postirradiation (PR); and 1, 2, 5 (N = 8), 7 (N = 7), 9 (N = 5), and 12 days (N = 3) PR in irradiated and sham-irradiated animals (N = 9 on all days). Animals were weighed on each day at the conclusion of testing.

Experiment 2 -Locomotor Activity

In a separate study, a Digiscan Animal Activity Monitor (Omnitech Electronics, Columbus, OH), equipped with an array of infrared photodetectors, was used to record horizontal activity (ambulation) and vertical activity (rearing). Each animal was placed in the open field area (20.0 cm × 20.0 cm × 30.5 cm) during the dark portion of the light-dark cycle. Locomotor activity was recorded for 5 min, the time period corresponding to the length of the resident-intruder encounter in Experiment 1. Activity was monitored 2 days before irradiation (baseline); 30 min PR; and 1, 2, 5, 7 (N = 16), 9 (N = 12), and 12 days (N = 5) PR in irradiated and sham-irradiated animals (N = 16 on all days) Mice were weighed after each activity test.

Experiment 3 -Hemopoietic Parameters

Additional groups of irradiated (10 Gy) and sham-irradiated mice were used in these experiments (N = 9/group/day). The mice were anesthetized by methoxyflurane inhalation and exsanguinated by cardiac puncture. Blood was collected in tubes containing EDTA. The animals were euthanized by cervical dislocation. Hemopoietic parameters (number of leukocytes, platelets, and erythrocytes, the hematocrit, and hemoglobin) were determined by a Baker Instruments System

9000 Automated Cell Counter (Allentown, PA). Blood samples were obtained 2 days before irradiation; 4 hr PR; and 1, 2, 5, 7, and 9 days PR. To control for the possible effect of repeated fighting on hemopoiesis, the mice were paired in their home cages with intruders for 5 min, on every day that the subjects in Experiment 1 were tested, and 4 hr before removal of blood.

Statistical Analysis

Behavioral data from Experiment 1 were nonparametric, and were analyzed by Mann-Whitney U tests (irradiated vs. sham animals on each test day). Activity data and body weight were analyzed

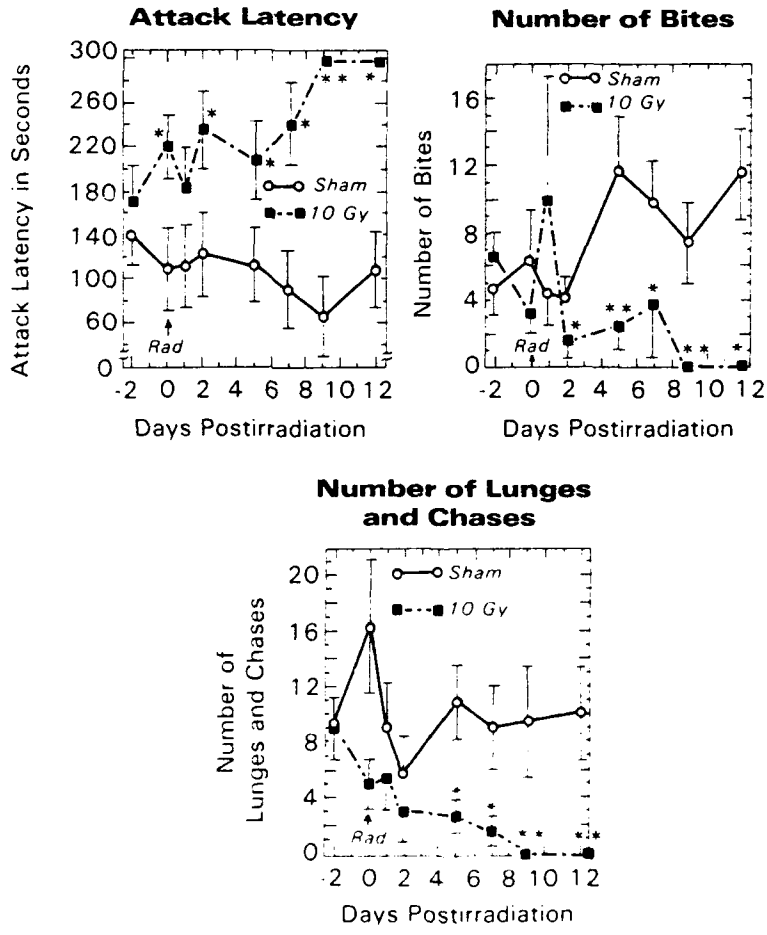

Fig. 1. Effects of 10 Gy electron radiation or sham-irradiation on aggressive offensive behaviors displayed by resident mice. Intruder mice were placed into the residents' home cages for 5 min and social behavior was videotaped 2 days before irradiation, immediately after irradiation, and 1, 2, 5, 7, 9, and 12 days postirradiation. Data are presented as means and S.E.M. (*$p<0.05$, **$p<0.01$).

by t-tests (irradiated vs. sham animals on each test day). Hemopoietic data from Experiment 3 were analyzed by a one-way analysis of variance (radiation was the between groups factor). A one-tailed alpha level of 0.05 was chosen, based upon the results of previous studies[9,14,18,20,21] and was used to evaluate all statistics.

RESULTS

Experiment 1- Aggressive Behavior

Attack latency of irradiated resident mice was significantly greater than that of sham-irradiated

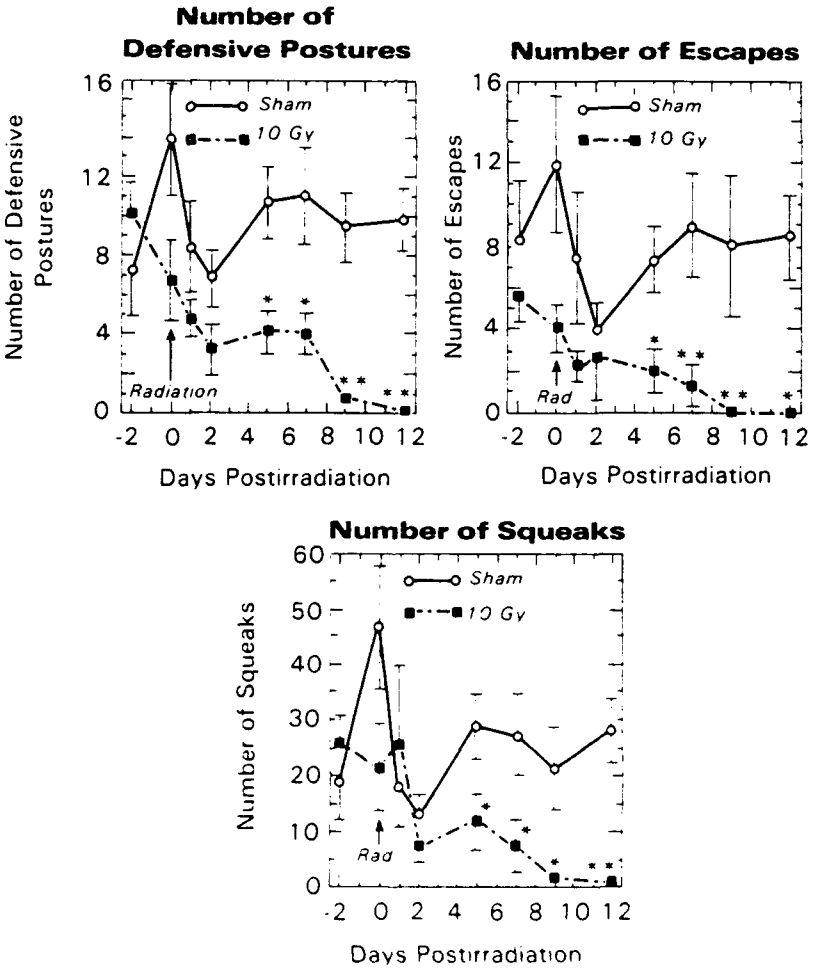

Fig. 2. Defensive behaviors exhibited by nonirradiated intruder mice placed into residents' home cages for 5 min. See Fig. 1 for additional details.

residents on day 0 PR (1 to 3 hr PR) and on days 2, 5, 7, 9, and 12 PR ($p < 0.05$) (Fig. 1). The number of bites exhibited by resident mice was significantly lower in irradiated animals than in sham-irradiated residents on days 2, 5, 7, 9, and 12 PR ($p < 0.05$) (Fig. 1). The number of lunges and chases displayed was significantly lower in irradiated residents than in their controls on days 5, 7, 9, and 12 PR ($p < 0.05$) (Fig. 1). In untreated intruders paired with irradiated resident mice, the number of defensive upright postures, escapes, and squeaks, was significantly lower than in intruders paired with sham-irradiated resident mice on days 5, 7, 9, and 12 PR ($p < 0.05$) (Fig. 2). Body weight of the irradiated mice was significantly decreased from day 5 PR ($p < 0.05$) (Fig. 4A).

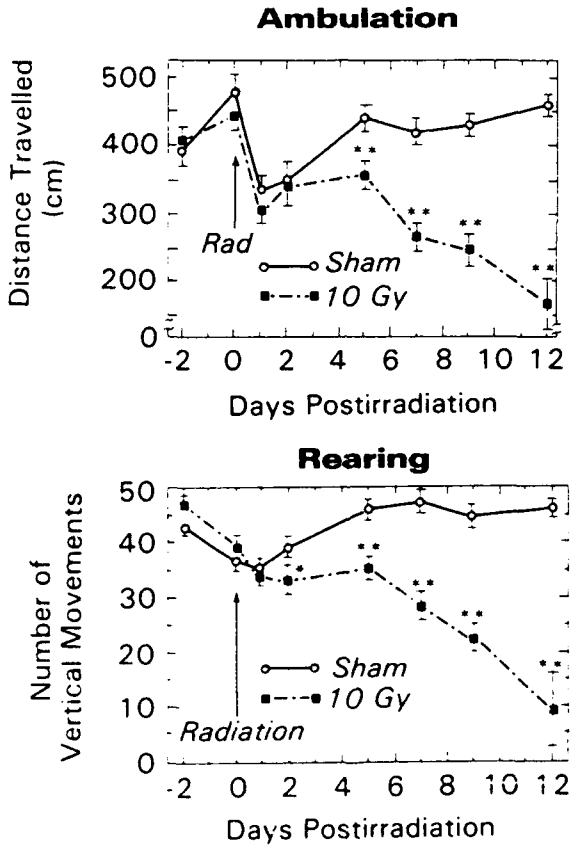

Fig. 3. Locomotor activity in mice as a function of 10 Gy electron radiation or sham-irradiation. Animals were monitored for 5 min for ambulation (horizontal activity) and rearing (vertical activity) 2 days before irradiation, immediately after irradiation, and 1,2,5,7,9, and 12 days postirradiation. Data are presented as means and S.E.M. (*$p < 0.05$, **$p < 0.01$).

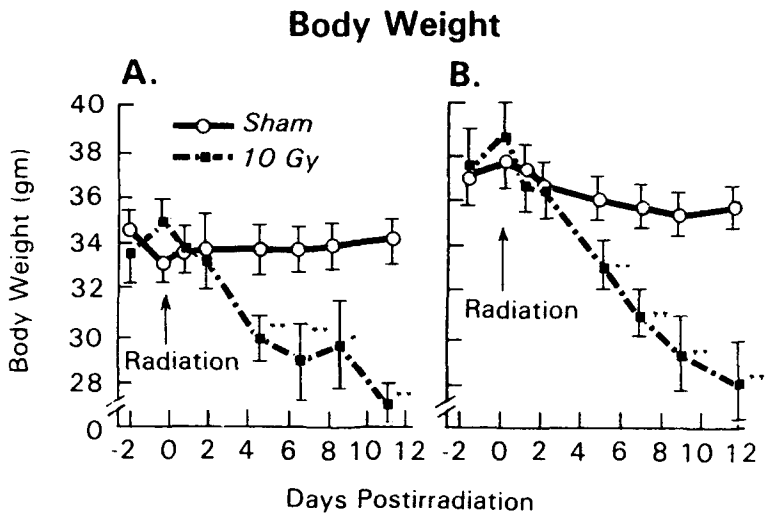

Fig. 4. Body weight in mice as a function of 10 Gy electron radiation or sham-irradiation. Animals were weighed at 2 days before irradiation, on the day of irradiation, and 1, 2, 5, 7, 9, and 12 days postirradiation. A) Resident mice from Exp. 1 (aggressive behavior). B) Mice from Exp. 2 (locomotor activity). Data are presented as means and S.E.M. (*$p<0.05$, **$p<0.01$).

Experiment 2- Locomotor Activity

Rearing was significantly decreased in irradiated mice when compared with their sham-irradiated controls on days 2, 5, 7, 9, and 12 PR ($p<0.05$) (Fig. 3). Ambulation was significantly lower in irradiated mice than in sham-irradiated animals on days 5, 7, 9, and 12 PR ($p<0.05$) (Fig. 3). Electron radiation-induced deficits in rearing appeared earlier postirradiation than deficits in ambulation. Body weight of the irradiated animals was significantly decreased from day 5 PR, replicating the effects of Experiment 1 ($p<0.01$) (Fig. 4B).

Experiment 3- Hemopoietic Parameters

Leukocyte and erythrocyte counts and the hematocrit were decreased significantly in irradiated mice when compared with sham-irradiated mice, on days 1, 2, 5, 7, and 9 PR ($p<0.05$) (Table 1). Platelet count and hemoglobin were decreased significantly in the irradiated mice on days 2, 5, 7, and 9 PR ($p<0.05$) (Table 1).

DISCUSSION

Offensive aggressive behavior, displayed by resident mice towards the intruders, decreased by 2 to 5 days PR in irradiated animals, and remained suppressed through the last test on day 12 PR. In previous studies using 10 Gy gamma photons, irradiated resident mice did not show a deficit in aggressive offensive behavior until day 7 PR[20,21]. With 10 Gy electrons, defensive

Table 1. Hematologic Parameters Over Time as a Function of Irradiation With 10 Gy LINAC Electrons

Measure	Day-2	Day 0	Day 1	Day 2	Day 5	Day 7	Day 9
RBC-RAD	7.35[a]	7.71	7.31*	6.59*	5.99**	4.77**	3.97**
	0.22[b]	0.18	0.13	0.22	0.17	0.34	0.20
RBC-SHAM	7.35	7.42	8.05	7.41	8.07	6.51	6.66
	0.22	0.13	0.19	0.29	0.18	0.13	0.24
WBC-RAD	2.89	2.50	1.36**	0.78*	0.21**	0.47**	0.23**
	0.40	0.22	0.24	0.11	0.02	0.09	0.03
WBC-SHAM	2.89	2.21	4.06	3.44	3.21	2.22	3.47
	0.40	0.23	0.39	0.88	0.32	0.23	0.38
PLT-RAD	1.18	1.17	1.22	1.07*	0.61**	0.06**	0.04**
	0.08	0.03	0.06	0.05	0.04	.006	.003
PLT-SHAM	1.18	1.14	1.33	1.32	1.38	0.89	1.25
	0.08	0.06	0.04	0.11	0.03	0.12	0.04
HGB-RAD	12.8	13.0	12.6	11.2*	9.7**	8.9**	8.3**
	0.4	0.3	0.2	0.4	0.2	0.7	0.7
HGB-SHAM	12.8	12.7	13.3	13.0	13.1	12.8	13.8
	0.4	0.2	0.3	0.5	0.3	0.3	0.3
HCT-RAD	35.8	37.5	35.6*	31.4*	28.0**	25.4**	21.3**
	1.1	1.0	0.6	1.1	0.7	1.7	1.5
HCT-SHAM	35.8	36.0	38.6	35.9	39.0	36.8	38.6
	1.1	0.7	1.0	1.3	0.9	1.2	0.8

a Mean
b SEM
* $p<0.05$ compared to sham controls
** $p<0.005$ compared to sham controls

RBC (erythrocytes) count as 1 × 10 cells/ml
WBC (leukocytes) count as 1 × 10 cells/ml
PLT (platelets) count as 1 × 10 cells/ml
HGB (hemoglobin) in g/dl of whole blood
HCT (hematocrit) as percent of volume

behavior in untreated intruder mice decreased in animals paired with irradiated residents by 5 days PR, and remained suppressed for the duration of the experiment. Decreases in defensive behavior may have appeared later than alterations in offensive behavior because the intruder mouse reflexively assumes defensive postures as soon as it is placed in the resident's cage and may require additional time to learn that its opponent is no longer a threat. In other studies using 10 Gy gamma photons, defensive behavior did not decrease until day 7 PR[20,21]. These data suggest that electron radiation may produce an earlier decrement in aggressive behavior in mice than gamma photons.

Rearing in mice irradiated with 10 Gy electrons decreased significantly by 2 days PR, while ambulation decreased by 5 days PR. In studies with 10 Gy gamma photons, rearing was decreased by 5 to 7 days PR while ambulation was decreased 2 to 5 days PR[20,21]. Thus, for the rearing measure of locomotor behavior, electron radiation appeared to produce an earlier behavioral decrement than gamma photons.

Hemopoietic parameters exhibited significant decreases after irradiation with 10 Gy electrons beginning 1 to 2 days PR, and continuing through 9 days PR (the last day blood was drawn). Mortality within this period generally results from hemopoietic injury leading to hemorrhage and infection[9,14]. The onset and progressive severity of this hemopoietic syndrome following irradiation appears to precede the behavioral deficits observed in the animals. Several important physiological consequences of radiation injury that might influence the ability of the animals to respond normally to social stimuli include a progressive anemia, hemorrhaging, decreased food intake and corresponding weight loss, and alterations in water and electrolyte balance[9,14]. Radiation-induced decreases in body weight appeared by 5 days PR, and reflect the presence of physiological symptoms severe enough to prevent the animal from maintaining its body weight. The decrease in aggressive behavior and locomotor activity following irradiation is more likely related to the onset of the hemopoietic syndrome rather than to direct effects of radiation on the nervous system.

The earlier onset of deficits in aggressive behavior and rearing observed after high-energy electron radiation parallels the more severe effects of this quality of radiation on avoidance responding as reported previously[3-5,15]. Many factors are involved in this effect, including accuracy of dose measurement, dose distribution in the animal, dose rate, pulse timing, linear energy transfer (LET), and energy levels of the radiation field[5]. For many behavioral measures, radiation qualities with low LET (gamma photons, electrons, bremsstrahlung) are often more disruptive than those with high LET (neutrons)[5], although high LET radiation generally has a more rapid effect on mortality[5,30,31]. For example, in shock-avoidance tasks in both pigs and monkeys, irradiation with gamma photons had a more disruptive effect than neutrons[13,28]. Moreover, bremsstrahlung radiation produced greater behavioral incapacitation in monkeys on a shock-avoidance visual-discrimination task than neutrons[30]. In contrast, the intensity of conditioned taste aversions, a model for radiation-induced emesis, has been found to be positively correlated with LET[25]. Similarly, neutron radiation produced a greater frequency of vomiting in monkeys than exposure to gamma photons[23,31]. In addition, mixed radiation (60% gamma and 40% neutron), delivered in a pulse, suppressed performance of a shock-avoidance lever-press task in monkeys more than X-rays[27].

In the present studies, electron radiation was found to exert a suppressive effect on aggressive behavior, locomotor activity, body weight, and hemopoiesis. High-energy electrons appeared to produce behavioral decrements earlier postirradiation than gamma photons[20,21]. Both radiation quality and type of behavioral task are important factors in evaluating the nature of radiation-induced behavioral deficit, and should be considered when extrapolating dose-response effects.

ACKNOWLEDGEMENTS

This research was supported by the Armed Forces Radiobiology Research Institute, under work unit 00159. Views presented in this paper are those of the authors; no endorsement by the Armed Forces Radiobiology Research Institute has been given or should be inferred. Research was conducted according to the principles enunciated in the "Guide for the Care and Use of Laboratory Animals," prepared by the Institute of Laboratory Animal Resources, National Research Council.

Portions of this paper were presented at the 73rd Annual Meeting of the Federation of American Societies for Experimental Biology, New Orleans, LA, March 1989.

REFERENCES

1. Benton, D., Brain, P., Jones, S., Colebrook, E. and Grimm, V. (1983) Behavioural examinations of the anti-aggressive drug fluprazine. Behav. Brain Res. **10:** 325-338.
2. Blanchard, R.J., O'Donnell, V. and Blanchard, D.C. (1979) Attack and defensive behaviors in the albino mouse. Aggress. Behav. **5:** 341-352.
3. Bogo, V. (1984) Effects of bremsstrahlung and electron radiation on rat motor performance. Radiat. Res. **100:** 313-320.
4. Bogo, V. (1988) Radiation: Behavioral implications in space. Toxicology **49:** 299-307.
5. Bogo, V., Zeman, G.H. and Dooley, M.A. (1989) Radiation quality and rat motor performance. Radiat. Res. **118:** 341-352.
6. Brain, P. (1975) What does individual housing mean to a mouse? Life Sci. **16:** 187-200.
7. Brain, P.F., Benton, D., Cole, C. and Prowse, B. (1980) A device for recording submissive vocalizations of laboratory mice. Physiol. Behav. **24:** 1003-1006.
8. Brain, P.F. and Nowell, N.W. (1971) Isolation versus grouping effects on adrenal and gonadal function in albino mice. I. The male. Gen. Comp. Endocrinol. **16:** 149-154.
9. Casarett, A.P. (1968) "Radiation Biology". Prentice-Hall, Englewood Cliffs, NJ.
10. Chaput, R.L. and Berardo, P.A. (1973) Increased brain radio-resistance after supralethal radiation. Armed Forces Radiobiology Research Institute Scientific Report #73-7, Bethesda, MD.
11. Chaput, R.L. and Kovacic, R.T. (1970) Miniature pig performance after fractionated supralethal doses of ionizing radiation. Radiat. Res. **44:** 807-820.
12. Conklin, J.J. and Hagan, M.P. (1987) Research issues for radiation protection for man during prolonged spaceflight. In "Advances in Radiation Biology", vol. 13, Ed. J. Lett, U. Ehmann and A. Cox, pp215-284, Academic Press, New York.
13. George, R.E., Chaput, R.L., Verrelli, D.M. and Barron, E.L. (1971) The relative effectiveness of fission

neutrons for miniature pig performance decrement. Radiat. Res. **48:** 332-345.
14. Hall, E.J. (1984) "Radiation and Life", 2nd ed., Pergamon Press, New York.
15. Hunt, W.A. (1983) Comparative effects of exposure to high-energy electrons and gamma radiation on active avoidance behaviour. Int. J. Radiat. Biol. **44:** 257-260.
16. Joseph, J.A., Kandasamy, S.B., Hunt, W.A., Dalton, T.K. and Stevens, S. (1988) Radiation-induced increases in sensitivity of cataleptic behavior to haloperidol: Possible involvement of prostaglandins. Pharmacol. Biochem. Behav. **29:** 335-341.
17. Kovalev, E.E. (1983) Radiation protection during space flight. Aviat. Space Environ. Med. **54:** S16-S23.
18. Landauer, M.R., Davis, H.D., Dominitz, J.A. and Pierce, S.J. (1987) Effects of acute radiation exposure on locomotor activity in Swiss-Webster mice. Toxicologist **7:** 253.
19. Lister, R.G. and Hilakivi, L.A. (1988) The effects of novelty, isolation, light and ethanol on the social behavior of mice. Psychopharmacology **96:** 181-187.
20. Maier, D.M. and Landauer, M.R. (1988) Radiation-induced alterations in fighting behavior and locomotor activity in mice. In "Multidisciplinary Studies on Aggression". Ed. P. Brain, B. Olivier, J. Mos, D. Benton and P. Bronstein, p.74, International Society for Research on Aggression, Swansea, Wales.
21. Maier, D.M. and Landauer, M.R. Onset of behavioural effects in mice exposed to 10 Gy cobalt-60, submitted.
22. McPherson, C.W. (1963) Reduction in *Pseudomonas aeruginosa* and coliform bacteria in mouse drinking water following treatment with hydrochloric acid or chlorine. Lab. Anim. Care **13:** 737-744.
23. Middleton, G.R. and Young, R.W. (1975) Neutron-gamma ratio and vomiting. Armed Forces Radiobiology Research Institute Scientific Report #75-26, Bethesda, MD.
24. Poshivalov, V.P. (1981) Some characteristics of the aggressive behavior of mice after prolonged isolation: Intraspecific and interspecific aspects. Aggress. Behav. **7:** 195-204.
25. Rabin, B.M., Hunt, W.A. and Joseph, J.A. (1989) An assessment of the behavioral toxicity of high-energy iron particles compared to other qualities of radiation. Radiat. Res. **119:** in press.
26. Rodgers, R.J. (1981) Drugs, aggression and behavioural methods. In "Multidisciplinary Approaches to Aggression Research", Ed. P. Brain and D. Benton, pp.325-340, Elsevier/North Holland Biomedical Press, New York.
27. Sharp, J.C. and Keller, B.K. (1965) A comparison between the effects of exposure to a mixed fission spectrum delivered in a single "pulse" and X-rays delivered at a slower rate upon the conditioned avoidance behavior of primates. Walter Reed Army Institute of Research Technical Report #4, Washington, DC.
28. Thorp, J W. and Young, R.W. (1972) Neutron effectiveness for causing incapacitation in monkeys. Armed Forces Radiobiology Research Institute Scientific Report #72-5, Bethesda, MD.
29. Wixon, H.N. and Hunt, W.A. (1983) Ionizing radiation decreases veratridine-stimulated uptake of sodium into rat brain synaptosomes. Science **220:** 1073-1074.
30. Young, R.W. and Middleton, G.R. (1974) The effectiveness of high-energy neutrons in producing behavioral incapacitation. In "Armed Forces Radiobiology Research Institute Annual Research Report #9", pp.34-35, Bethesda, MD.
31. Zeman, G.H., Jones, S.R., George, R.E. and Levin, S.G. (1972) The relative effectiveness of fission neutrons for gastrointestinal damage in mice: Lethality and jejunal crypt response. Armed Forces Radiobiology Research Institute Scientific Report #72-15, Bethesda, MD.

Original Paper

International Journal of Cell Cloning 8:184-195 (1990)

Further Enrichment and Analysis of Rat CFU-s

Kenneth F. McCarthy, Martha L. Hale

Radiation Biochemistry Department, Armed Forces Radiobiology Research Institute, Bethesda, Maryland, USA

Key Words. Flow cytometry · CFU-s · Indo-1 · DAPI

Abstract. Using the monoclonal antibody W3/13, which recognizes a determinate expressed on a sialoglycoprotein, rat marrow cells with the phenotype Thy-1 antigen upper 20% positive ($Ox7^{20}$) and high molecular weight leukocyte common antigen negative ($Ox22^-$) were separated into W3/13 dim ($W3/13^d$) and W3/13 bright ($W3/13^b$) subpopulations by single-laser cell sorting. The spleen colony-forming unit (CFU-s) was found in the $W3/13^d$ fraction. A 468-fold enrichment of CFU-s was achieved. Only 20% of the $Ox7^{20}$, $Ox22^-$, and $W3/13^d$ cells were in the S phase of the cell cycle as compared to 56% of $Ox7^{20}$, $Ox22^-$, and $W3/13^b$ cells. Using Indo-1, it was not possible to demonstrate increases in cytosolic Ca^{++} levels within the enriched CFU-s population by colony-stimulating factors (CSFs) or interleukins 1, 2, and 3. However, challenge with the Ca^{++} ionophore, ionomycin, demonstrated apparent heterogeneity of intracellular Ca^{++} management within the enriched CFU-s population. The source of this heterogeneity is not known. Only a 12-day CFU-s was detected in the rat, and it was predominantly, but not exclusively, a Rhodamine 123 (Rhl23) dull cell.

Introduction

Previously, sorting rat marrow cells for the Ox7 upper 20% positive ($Ox7^{20}$) and cells other than those expressing high levels of high molecular weight leukocyte common antigen ($Ox22^-$), resulted in a 100-fold enrichment of the rat spleen colony-forming unit (CFU-s) [1], a 350-fold enrichment of cells capable of protecting rats from the lethal effects of ionizing radiation [2] and a 282-fold enrichment of the marrow prothymocyte [3]. The $Ox7^{20}$ and $Ox22^-$ population was found to be phenotypically heterogeneous. It could be separated into two subpopulations by dual laser flow cytometry using the monoclonal antibody W3/13 [2]. The purpose of this study was to characterize the rat CFU-s with respect to the W3/13 dim ($W3/13^d$) and bright ($W3/13^b$) subpopulations of the $Ox7^{20}$ and $Ox22^-$ cell populations.

Correspondence: Dr. Kenneth F. McCarthy, Radiation Biochemistry Department, Armed Forces Radiobiology Research Institute, Bethesda, MD 20814-5145, USA.

Received November 10, 1989; provisionally accepted January 9, 1990; accepted for publication March 3, 1990.

0737-1454/90/$2.00/0 AlphaMed Press

Materials and Methods

Animals

Lewis male rats were obtained from Charles River Laboratory (Kingston, RI) at 4 weeks of age and used at 8 weeks of age in an AAALAC-accredited facility. Rats were euthanized by CO_2 gas inhalation.

Biologicals

Rhodamine 123 (Rh123) and Indo-1/AM were purchased from Molecular Probes (Junction City, OR); pokeweed mitogen (PWM) and 4'6'-diamidino-2-phenylindole dihydrochloride (DAPI) from Sigma Chemical Company (St. Louis, MO); human granulocyte colony-stimulating factor (G-CSF), mouse recombinant interleukin (IL) 1 and 3 from Amgen Biologicals (Thousand Oaks, CA); rat IL-2 from Accurate Chemical and Scientific Corporation (Westburg, NY); ionomycin and trifluoperazine dimaleate (TFP) from CALBIOCHEM Corporation (San Diego, CA). CMRL-1066, RPMI-1640, Opti-1 medium, fetal calf serum (FCS) and Dulbecco's phosphate-buffered saline (PBS) from GIBCO Laboratories (Grand Island, NY).

Flow Cytometry and Sorting

The fluorescence-activated cell sorter (FACS-II; Becton-Dickinson Immunocytometry Systems, Mountain View, CA) was upgraded to a dual laser, six-parameter instrument. A forward light scatter measurement, and 3 immunofluorescence measurements were initiated with the first argon laser (488 nm); fifth and sixth fluorescence measurements were made following excitation with a second ultraviolet argon laser. Filters were purchased from Omega Optical Inc. (Brattleboro, VT). The FACS-II electronics were used to delete the crossover between fluorescence channels. Either the DAPI-DNA fluorescence or Indo-1 violet/blue fluorescence ratio was recorded on the spatially separated delayed channel. The forward light scatter (FWLS) signal was used to trigger the electronics of the FACS-II, but was not recorded on the Consort 40 computer system because of space limitations.

Cell Staining

Single cell preparations and immunofluorescence cell staining with allophycocyanin (APC)-Ox7 Fab', phycoerythrin B (PhyB)-Ox22 Fab', PhyB-W3/13 Fab', and fluorescein isothiocyanate (FITC)-W3/13 IgG were performed as described previously [1, 2]. For DNA staining, the immunofluorescent-tagged cells were suspended in 1 ml PBS containing 200 μg TFP [4] and 3 μg of DAPI for 45 min at 4°C. For either Rh123 or Indo-1/AM staining, cells were incubated at 37°C at a concentration of 1×10^6 cells/ml in 10 ml of 10% FCS-PBS at an Rh123 concentration of 0.1 μg/ml or Indo-1/AM concentration of 0.3 μg/ml for 45 min. The cell suspension was washed twice and tagged with the appropriate immunofluorescent reagents as described above.

CFU-s Assay

A total of 1×10^2 to 3×10^6 cells in 1 ml were injected i.v. into irradiated recipient rats (9 Gy total body radiation at 0.04 Gy per min ^{60}Co). The spleens were removed 12 days later and fixed in Bouin's solution [1].

CFC Assay

Cells were cultured in vitro by a modified version of the double agar technique described by *Bradley et al.* [5]. Pokeweed conditioned medium (PWCM) was prepared by incubating rat spleen cells in RPMI-1640 at 5% CO_2 at 37°C for 7 days. PWCM was mixed in

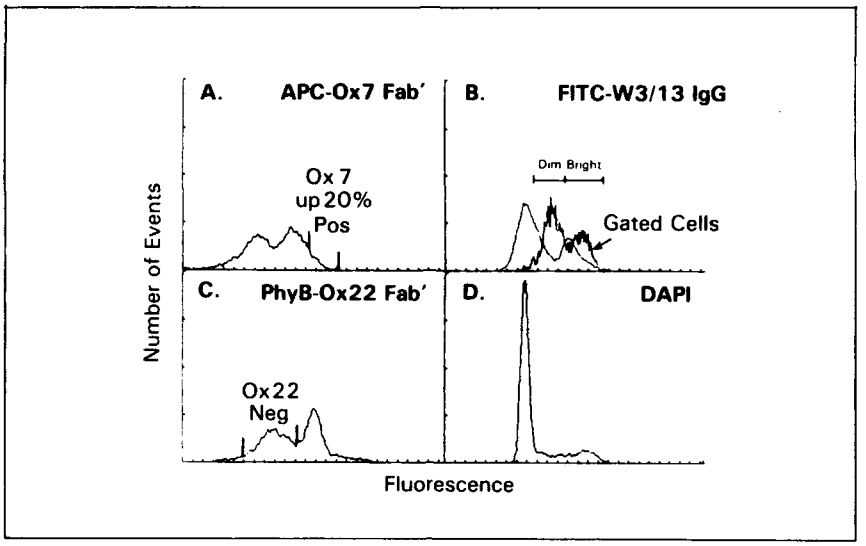

Fig. 1. Five-parameter analysis of rat marrow cells. The primary argon laser was tuned to the 488 nm spectral line and was used to generate the forward light scatter signal and excite the 3 fluorochrome-conjugated monoclonal antibodies. The second argon laser was tuned to the UV and was used to excite the DAPI-DNA complex. By gating on the APC-$Ox7^{20}$ and PhyB-$Ox22^{-}$ cells, a new FITC-W3/13 immunofluorescence histogram was generated and is shown by the line labeled "Gated Cells" in quadrant B.

the bottom layer (equal volumes of 1% BactoAgar and modified 2× CMRL-1066 medium) and layered into a Petri dish. Cells were sorted directly onto the bottom layer. The top layer (equal volumes of 1.5% BactoAgar, 2× CMRL-1066 medium and Opti-1 medium) was immediately added following the sort. Cultures were incubated at 5% CO_2 at 37°C for 5 days at which time the colonies were counted.

Results

Purification

Sorts were performed on either FITC-W3/13 IgG- or PhyB-W3/13 Fab'-labeled rat marrow cells. Sort windows were set to include W3/13 negative, dim, and bright cells. Greater than 96% of CFU-s were recovered in the $W3/13^{d}$ fraction using either immunofluorescent reagent (data not shown). A second series of sorts for CFU-s was performed, gating on all 3 immunofluorescence parameters: APC-$Ox7^{20}$ Fab', FITC-$W3/13^{-}$ IgG, and PhyB-$Ox22^{-}$ Fab' (Fig. 1A-C). Cells were sorted into 1 ml of 2% FCS-PBS and immediately injected i.v. into a single irradiated recipient rat. There was a linear relationship between cells injected and spleen colonies detected (Fig. 2). A 468-fold enrichment of CFU-s was achieved. The sizes of the $Ox7^{20}O$, $Ox22^{-}$, and $W3/13^{d}$ or $W3/13^{h}$ subpopulations were 0.213% ± .019% and 0.115% ± .017% (mean ± SE) of the total marrow cellularity, respectively.

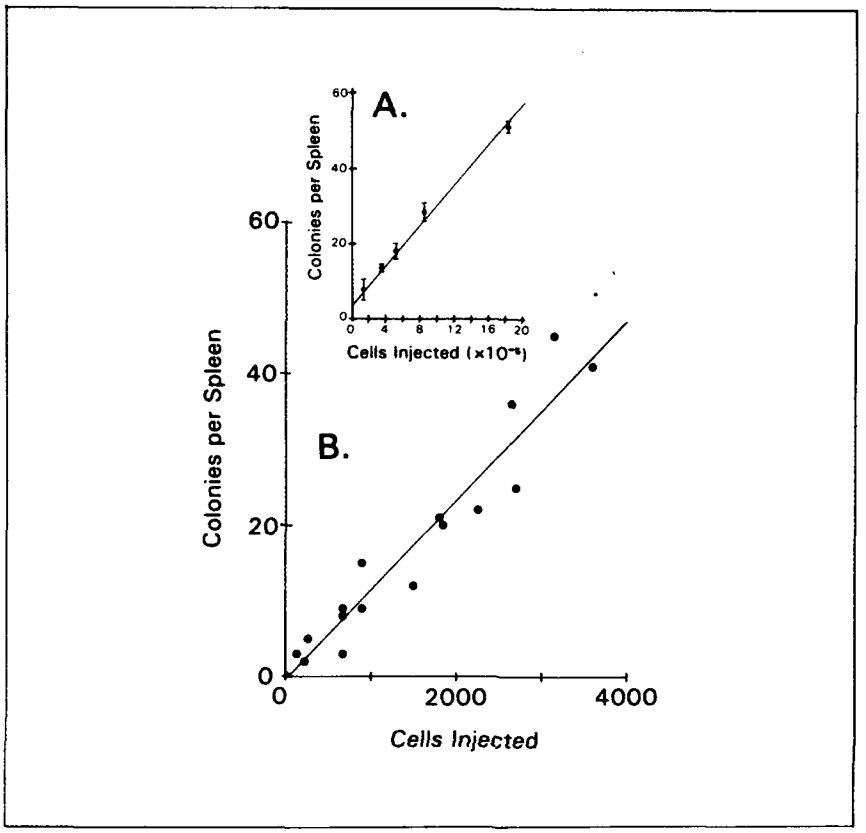

Fig 2. CFU-s dose-response curve for A) normal marrow cells and B) for enriched APC-Ox7^{20}, PhyB-Ox22^{-}, and FITC-W3/13^{d} sorted cells. Based on 25.6 CFU-s per 10^{6} cells for triple-labeled, unsorted marrow cells, a 468-fold purification of CFU-s was realized.

Cells were sorted directly into 35 mm Petri dishes containing the bottom layer, and immediately following the sort, the top layer was added. The number of colonies developing was linear to the number of Ox7^{20}, Ox22^{-} and W3/13^{d} cells sorted and plated. Approximately 1 of 7 cells generated a colony (Fig. 3). Very few of the Ox7^{20}, Ox22^{-} and W3/13^{b} sorted cells developed into colonies (Fig. 3). Theoretically, those colonies that developed were small (less than 50 cells in size) and should have been classified as clusters.

Characterization

The DAPI-DNA histogram for total marrow cells is shown in Figure 1D. The DAPI-DNA histograms for the Ox7^{20}, Ox22^{-}, and W3/13^{d} or W3/13^{b} subpopulations (as shown in Fig. 1B) are presented in Figures 4A and B, respectively. Twenty per cent of the W3/13^{d} population were in the S phase of cell cycle, while the W3/13^{b} population had 56% of its cells in the S phase of cell cycle.

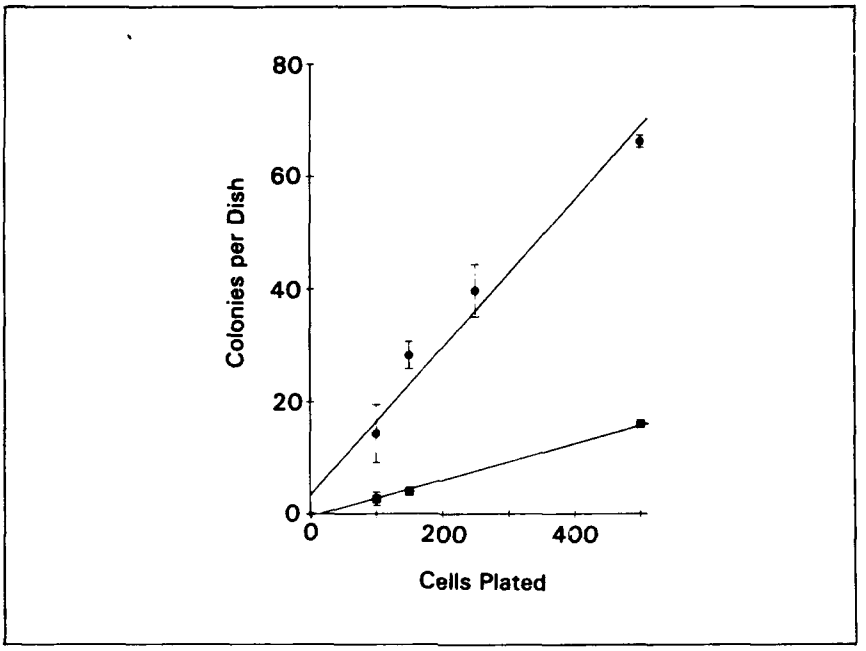

Fig 3. CFC dose-response curves for enriched $Ox7^{20}$, $Ox22^{-}$, and $W3/13^{d}$ (●—●) and $W3/13^{b}$ (■—■) cells.

Figure 5 shows that the $Ox7^{20}$ and $Ox22^{-}$ cells were slightly more Rhl23 positive than most marrow cells. Within this population, CFU-s were predominantly Rhl23 dull.

The Indo-1 violet/blue fluorescence ratio of normal marrow and the $Ox7^{20}$, $Ox22^{-}$, and $W3/13^{d}$ were found to be nearly identical (Figs. 6A and B). Titering Indo-1-loaded marrow cells with increasing amounts of ionomycin at 8°C to a final concentration of 105 μM ionomycin showed that marrow lymphocytes were the most sensitive to ionomycin; myelocytes were less sensitive, and what appeared to be predominantly erythroid precursors were the least sensitive. Intermediate between lymphocytes and myelocytes were the $Ox7^{20}$, $Ox22^{-}$, and $W3/13^{d}$ or $W3/W13^{b}$ cells. At 35 μM ionomycin, the resulting histogram for marrow cells was trimodal (Fig. 6A). As shown in the correlated plot(s) of PhyB-Ox22 Fab' (or APC-Ox7 Fab' or FITC-W3/13 IgG) fluorescence versus Indo-1 violet/blue fluorescence ratio (Fig. 7), the origin of the 3 peaks appeared to be cell lineage specific. In contrast, the $Ox7^{20}$, $Ox22^{-}$ and $W3/13^{d}$ gated population appeared to be heterogeneous (Fig. 6B).

Indo-1 (0.3 μg/ml) and ionomycin (35 μM) were not toxic for CFU-s. These cells were found to be relatively resistant, as compared with marrow lymphocytes, to ionomycin-induced increases in cytosolic Ca^{++} levels (Fig. 6A). Efforts to induce cytosolic Ca^{++} fluxes in the cells found within the $Ox7^{20}$, $Ox22^{-}$, and $W3/13^{d}$

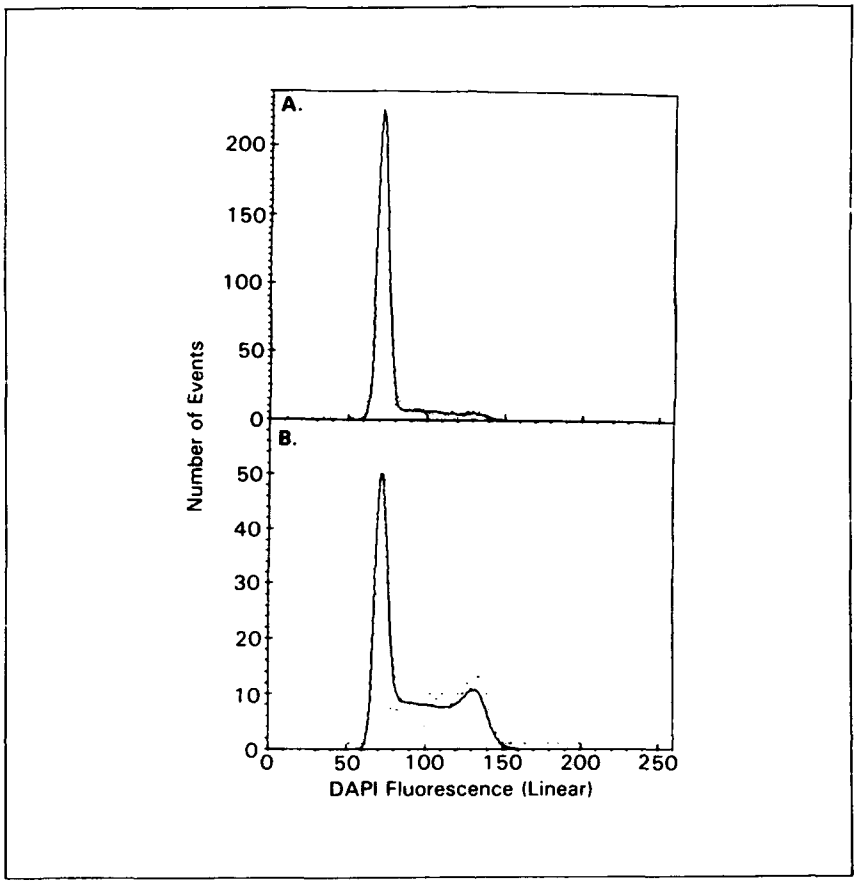

Fig 4. DNA histograms. A) APC-Ox7^{20}, PhyB-Ox22^{-}, and FITC-W3/13^{d} cells. B) APC-Ox7^{20}, PhyB-Ox22^{-}, and FITC-W3/13^{b} cells. Points are actual data points while the solid lines are computer-fitted lines generated by the Cotfit program based on the method of *Fox* [6].

population with recombinant G-CSF, PWCM and IL-1, IL-2, and IL-3 at either 8°C or 37°C were not successful.

Discussion

By single laser excitation of FITC, PhyB, and APC, it was possible to perform three-parameter immunofluorescence sorts for rat CFU-s with an enrichment of 468-fold being achieved. This enrichment is an improvement over the 320-fold purification reported by *Goldschneider et al.* [7] using anti-Thy-1 and light scatter properties of CFU-s from cortisone pre-treated rats. The cortisone treatment diminished marrow lymphocytes and separated them from cortisone-resistant CFU-s. Starting with marrow from normal rats, *Goldschneider et al.*

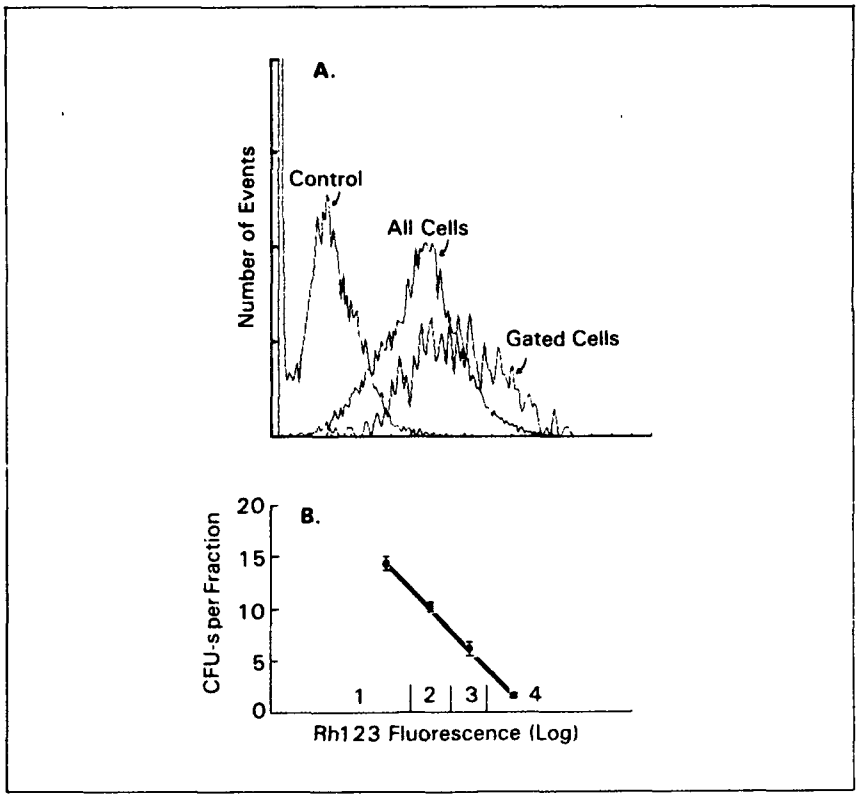

Fig 5. A) Rh123 green fluorescence of APC-Ox7^{20} and PhyB-Ox22^{-} labeled marrow cells. The green fluorescence of double-labeled cells without Rh123, the green fluorescence of double-labeled cells previously incubated with Rh123 and the green fluorescence of gated APC-Ox7^{20} and PhyB-Ox22^{-} cells are illustrated. B) CFU-s content of fractions sorted only on the Rh123 fluorescence. The number of CFU-s is expressed as the number of colonies per fraction from 1 × 10^{6} sorted normal cells.

[7] achieved a CFU-s enrichment of 151-fold. Using the present purification protocol, marrow lymphocytes were gated out of the sort by the Ox22 monoclonal antibody, and the cortisone pretreatment as well as density gradient pre-purification steps [8] could be omitted.

The size of the Ox7^{20}, Ox22^{-} and W3/13^{d} population was determined to be 0.213% of the total marrow population. If all rat CFU-s are characterized by this phenotype, then the maximum enrichment of CFU-s that could be achieved by this sorting protocol would be 469-fold. Depending upon whether normal marrow CFU-s concentration is determined from the CFU-s dose-response curve for normal marrow (Fig. 2A) or from the controls for the results graphed in Figure 2B, the maximum CFU-s concentration of the "purified" CFU-s population would be between 12,006 to 14,070 CFU-s per 1 × 10^{6} cells. The observed purity of the enriched CFU-s population was found to be 11,500 CFU-s per 1 × 10^{6} cells

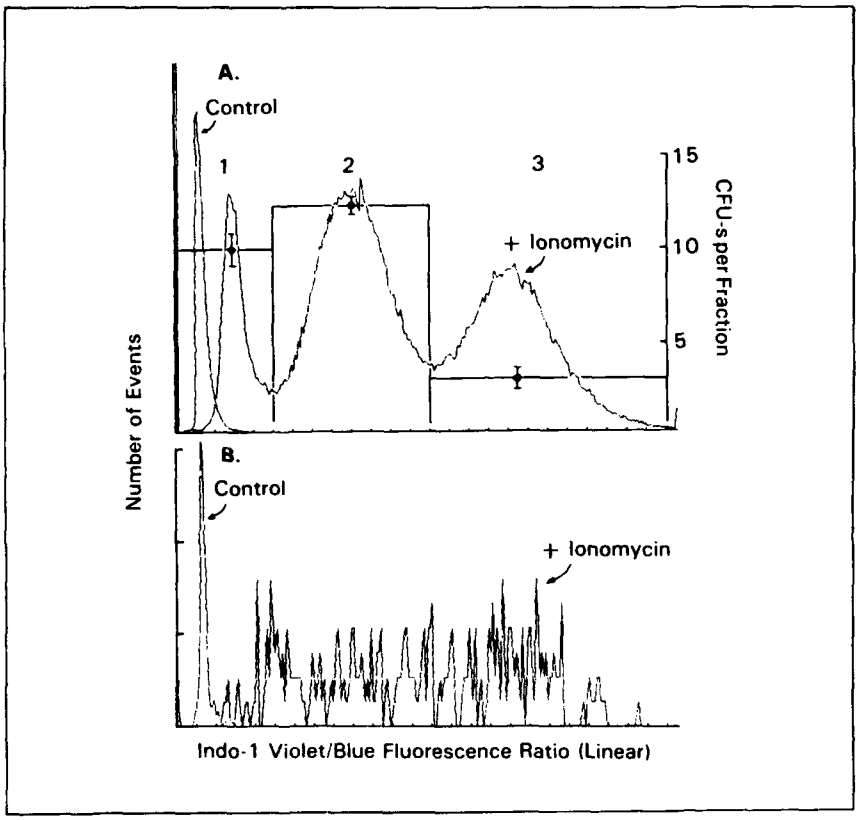

Fig 6. A) Indo-1 violet/blue fluorescence ratio of normal and ionomycin-incubated (35 μM at 8°C) marrow cells. CFU-s content of fractions sorted only on Indo-1 violet/blue fluorescence ratio. Results are expressed as CFU-s per fraction, based on a sort of 1×10^6 cells. B) The Indo-1 violet/blue fluorescence ratio histograms of the APC-Ox7^{20}, PhyB-Ox22$^-$, and FITC-W3/13^d gated cells in the presence and absence of ionomycin are shown for comparison.

indicating that 82 to 96% of all rat CFU-s are defined by this phenotype.

Mouse CFU-s have been enriched 441- to 613-fold by cell sorting [9-11]. The present enrichment of rat CFU-s was 468-fold. In order to calculate the absolute purity of the enriched CFU-s populations, it is necessary to adjust for the number of CFU-s injected i.v. and the number that actually "seed" the spleen and form colonies. This correction factor is commonly referred to as "f." Unfortunately, there are a variety of ways to calculate f; the 2 h, 24 h, 24 h post-irradiated recipient, dip, and extrapolation methods have all been used and generate estimates for f between a high of 30% and a low of 0.2% [12]. The 2 h and 24 h f values are similar in the rat and mouse, and if used, indicate that mouse FACS-enriched CFU-s populations [9-11] are approximately 10-fold more pure than rat-enriched CFU-s population. However, the "extrapolation" method for determining f indicates a

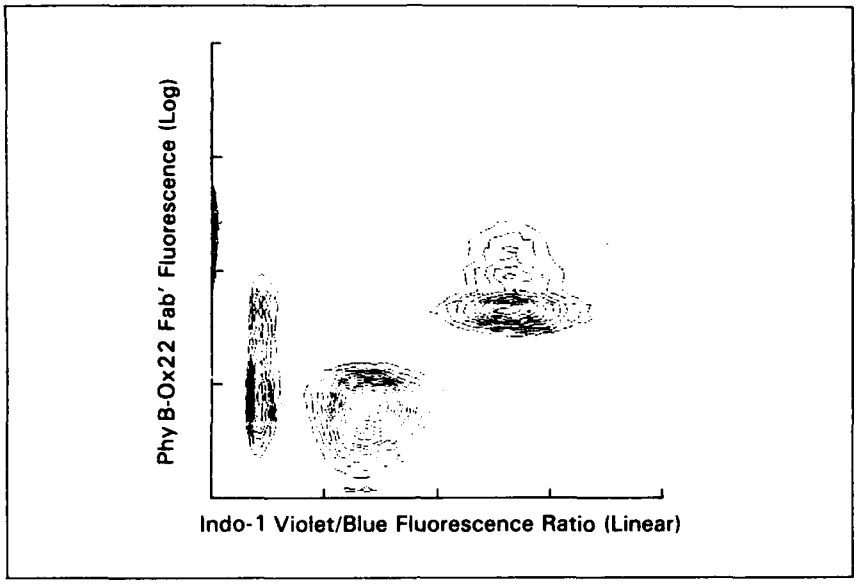

Fig 7. A correlated plot of Indo-1 violet/blue fluorescence ratio versus PhyB-Ox22 fluorescence following incubation with ionomycin (35 μM at 8°C).

5- to 7-fold lower f for rat CFU-s as compared to mouse CFU-s. If the extrapolated f's are used, it can be calculated that the FACS-enriched rat and mouse CFU-s populations are of the same relative purity. The extrapolated f for mouse CFU-s is 5%; for the BN rat CFU-s (uncorrected marrow CFU-s concentration approximately 30 to 50 CFU-s per 1×10^6) it is 0.9% [12, 13]. Using the BN rat CFU-s seeding efficiency for the Lewis rat CFU-s, slightly greater than a 100% (111%) purity of the highly enriched Lewis rat CFU-s was calculated.

Because *van Bekkum's* studies [12] demonstrated different splenic homing characteristics for rat and mouse CFU-s, it is interesting to note that the mouse CFU-s population can be subdivided into 8-day Rh123 bright, 12-day Rh123 bright, and 12-day Rh123 dull CFU-s subpopulations [14-16]. The mouse CFU-s subpopulations are also phenotypically distinct [9, 17]. In the rat CFU-s assay, only 12-day CFU-s is observed [13], and it is primarily, but not exclusively, an Rh123 dull CFU-s (Fig. 5). Efforts to demonstrate phenotypically distinct subpopulations within the rat 12-day CFU-s population have not yet been successful [3]. Therefore, there is the possibility (with the reservations noted in the last paragraph) that the mouse CFU-s seeding efficiency is the average seeding efficiency of several CFU-s subpopulations, some of which are not detected in the rat CFU-s assay. Further, the mouse 12-day Rh123 dull CFU-s is Thy-1 dim [18], wheat germ agglutinin (WGA) very bright [10], while the rat CFU-s is Thy-1 very bright [7], WGA dim [19]. These differences in phenotype may account, in part, for differences in the homing of rat and mouse CFU-s to the spleen.

It might be questioned whether the rat CFU-s develops more slowly than the mouse CFU-s, so that the rat 12-day CFU-s is more representative of the mouse 8-day CFU-s than the mouse 12-day CFU-s. Results to date do not support such a concept. The rat 12-day CFU-s is primarily Rh123 dull, and like the mouse 12-day CFU-s [20], appears to be relatively resistant to the cytotoxic compound 5-fluorouracil (studies in progress).

An alternative hypothesis would be that both the rat and mouse have the same absolute number of CFU-s, but because the amount of rat marrow is ten times greater than that found in the mouse, the concentration of rat marrow CFU-s is tenfold less than that determined for the mouse. Such a hypothesis is contradicted by the facts that A) the concentration of Thy-1-positive, lineage-negative cells (phenotype of both rat and mouse CFU-s) in rat and mouse marrow is approximately the same, i.e., between 0.2 to 0.4% of the total marrow cellularity [1, 2, 9, 21]; B) one of seven of these mouse- or rat-enriched marrow cells are capable of generating an in vitro CFC colony, and C) the amount of normal marrow or Thy-1- positive, lineage-negative marrow required for a successful bone marrow transplantation on a Kg body-weight basis is nearly identical for both rat and mouse [2, 12, 21]. However, our preliminary work using irradiated long-term chimeric rats to assay hematopoietic stem cells by the limiting dilution technique appears to support the alternative hypothesis, as does the observation that the concentration of rat marrow prothymocytes assayed by direct intrathymic injection—seeding efficiency 30 to 100% [22, 23]—is approximately one-tenth of that found for mice [23].

The $Ox7^{20}$, $Ox22^{-}$, and $W3/13^{d}$ population is a slowly proliferating cell population (20% in the S phase of cell cycle) as compared to the $W3/13^{h}$ population, which has 56% of its cells in the S phase of cell cycle. This finding was consistent with CFU-s having been characterized as non-proliferating cells [24]. The hematological function of the $Ox7^{20}$, $Ox22^{-}$, and $W3/13^{h}$ is, at the present time, not known.

The $Ox7^{20}$, $Ox22^{-}$, and $W3/13^{d}$ cells were heterogeneous in their response to elevation of cytosolic Ca^{++} levels by ionomycin. CFU-s found within this limited marrow population also share this trait as shown by sorting for CFU-s based on their ionomycin-perturbed Indo-1 violet/blue fluorescence ratios. Efforts to relate differences in intracellular Ca^{++} management to CFU-s differentiation and/or proliferation by challenge with ILs or CSFs were unsuccessful. This was unexpected, for the cells within the enriched CFU-s population can differentiate in the thymus (unpublished results) into thymocytes and, in the in vitro CFC culture to myelocytes, suggesting these cells are multipotent.

The apparent conflict in the observations of a) a restricted rat CFU-s phenotype limited to less than 0.213% of the cells found within rat marrow and b) the extreme physiological heterogeneity of cells within this subpopulation including CFU-s, as shown by challenge with ionomycin and to a lesser extent by Rh123 uptake, cannot be considered proof of heterogeneity within the rat CFU-s compartment. As has been noted by *Wilson et al.* [25], flow cytometric analysis underestimates intracellular Ca^{++} levels of individual cells if cytosolic Ca^{++} levels are being generated by frequency modulation of the Ca^{++} signaling system.

Although we have no evidence that CFU-s are capable of supporting Ca^{++} spiking and prolonged Ca^{++} oscillations, the postulated heterogeneity within the CFU-s populations based on the results of cell sorting experiments using intracellular fluorescent probes might be questioned. The CFU-s population is certainly an oscillating system with regard to G_0, G_1 transition [26], and ATP production may fluctuate between glycolysis and mitochondrial respiration [27, 28]. The interpretation of flow cytometry, intracellular fluorescent probe studies is critically dependent upon understanding the nature of the probe-cell interaction. One must also consider that analysis of cellular physiology by flow cytometry is a one-time point measurement made on individual cells. If these cells constitute a randomly fluctuating cell population, the results might suggest greater heterogeneity within the CFU-s population than that which actually exists [29].

Acknowledgments

The authors wish to thank *Mr. Philip D. Craw* for excellent technical assistance and *Mr. Michael Yee* for helpful discussions on the upgrade of the FACS-II to a six-parameter instrument.

This research was supported by the Armed Forces Radiobiology Research Institute, Defense Nuclear Agency. Views presented in this paper are those of authors; no endorsement by the Defense Nuclear Agency has been given nor should be inferred.

References

1 McCarthy KF, Hale ML, Fehnel PL. Rat colony forming unit spleen is OX7 positive, W3/13 positive, OX1 positive and OX22 negative. Exp Hematol 1985;13:847-854.
2 McCarthy KF, Hale ML, Fehnel PL. Purification and analysis of rat hematopoietic stem cells by flow cytometry. Cytometry 1987;8:296-305.
3 Hale ML, Greiner DL, McCarthy KF. Characterization of rat prothymocyte with monoclonal antibodies recognizing rat lymphocyte membrane antigenic determinants. Cell Immunol 1987;107:188-200.
4 Krishan A. Effect of drug efflux blockers on vital staining of cellular DNA with Hoechst 33342. Cytometry 1987;8:642-645.
5 Bradley TR, Stanely ER, Sumner MA. Factors from mouse tissues stimulating colony growth of mouse bone marrow cells *in vitro*. Aust J Exp Biol Med Sci 1971;49:595-603.
6 Fox MH. A model for the computer analysis of synchronous DNA distributions obtained by flow cytometry. Cytometry 1980;1:71-77.
7 Goldschneider I, Metcalf D, Battye F, Mandel T. Analysis of rat hemopoietic cells on the fluorescence activated cell sorter. I. Isolation of pluripotent hemopoietic stem cells and granulocyte-macrophage progenitor cells. J Exp Med 1980;152:419-437.
8 Castagnola C, Visser JWM, Boersma W, van Bekkum DW. Purification of rat hemopoietic stem cells. Stem Cells 1981;1:250-260.
9 Spangrude GJ, Heimfeld S, Weissman IL. Purification and characterization of mouse hematopoietic stem cells. Science 1988;241:58-62.
10 Visser JWM, Bauman JGJ, Mulder AH, Eliason JF, DeLeeuw AM. Isolation of murine pluripotent hematopoietic stem cells. J Exp Med 1984;159:1576-1590.

11 Lord BI, Spooncer E. Isolation of haemopoietic spleen colony forming cells. Lymphokine Res 1986;5:59-72.
12 van Bekkum DW. The appearance of the multipotent hemopoietic stem cells. In: Baum SJ, Ledney GD, eds. Experimental Hematology Today 1977. New York: Springer-Verlag, 1977:3-10.
13 Martens ACM, van Bekkum DW, Hagenbeek A. Heterogeneity within the spleen colony-forming cell population in rat bone marrow. Exp Hematol 1986;14:714-718.
14 Ploemacher RE, Brons NHC. Cells with marrow and spleen repopulating ability and forming spleen colonies on day 16, 12, and 8 are sequentially ordered on the basis of increasing Rhodamine 123 retention. J Cell Physiol 1988;136:531-536.
15 Mulder AH, Visser JWM. Separation and functional analysis of bone marrow cells separated by Rhodamine-123 fluorescence. Exp Hematol 1987;15:99-104.
16 Bertoncello I, Hodgson GS, Bradley TR. Multiparameter analysis of transplantable hemopoietic stem cells. II. Stem cell of long-term bone marrow-reconstituted recipients. Exp Hematol 1988;16:245-249.
17 Harris RA, Hogarth PM, Wadeson LJ, Collins P, McKenzie IFC, Penington DG. An antigenic difference between cells forming early and late haematopoietic spleen colonies (CFU-S). Nature 1984;307:635-641.
18 Basch RS, Berman JW. Thy-1 determinates are present on many murine hematopoietic cells other than T cells. Eur J Immunol 1982;12:359-364.
19 McCarthy KF, Hale ML. Flow cytometry techniques in radiation biology. Toxicol Letters 1988;43:219-233.
20 van Zant G. Studies of hematopoietic stem cells spared by 5-fluorouracil. J Exp Med 1984;159:679-690.
21 Müller-Sieburg CE, Townsend K, Wiessman IL, Rennick D. Proliferation and differentiation of highly enriched mouse hematopoietic stem cells and progenitor cells in response to defined growth factors. J Exp Med 1988;167:1825-1840.
22 Katsura Y, Kina T, Amagai T, et al. Limiting dilution analysis of the stem cells for T cell lineage. J Immunol 1986;137:2434-2439.
23 Goldschneider I, Komschlies KL, Greiner DL. Studies of thymocytopoiesis in rats and mice. I. Kinetics of appearance of thymocytes using a direct intrathymic adoptive transfer assay for thymocyte precursors. J Exp Med 1986;163:1-17.
24 Becker AJ, McCulloch EA, Siminovitch L, Till JE. The effect of differing demands for blood cell production on DNA synthesis by hemopoictic colony-forming cells of mice. Blood 1965;26:296-308.
25 Wilson HA, Greenblatt D, Poenie M, Finkelman FD, Tsien RY. Crosslinkage of B lymphocytes surface immunoglobulin by anti-Ig or antigen induces prolonged oscillation of intracellular ionized calcium. J Exp Med 1987;166:601-606.
26 Hagen MP. Cell proliferation kinetics analyzed with BrdU and near-UV light treatment. In: Baum SJ, ed. Current Methodology In Experimental Hematology. Basel: S. Karger, 1984:384-401.
27 Dexter TM, Whetton AD, Bazill GW. Haemopoietic cell growth factor and glucose transport: its role in cell survival and the relevance of this in normal haemopoiesis and leukaemia. Differentiation 1984;27:163-167.
28 Visser JWM, de Vries P. Isolation of spleen-colony forming cells (CFU-s) using wheat germ agglutinin and Rhodamine 123 labeling. Blood Cells 1988;14:369-384.
29 Blackett NM. Haemopoietic spleen colony growth: a versatile, parsimonious, predictive model. Cell Tissue Kinet 1987;20:393-402.

RADIATION RESEARCH 123, 263–267 (1990)

Effect of γ Radiation on Membrane Fluidity of MOLT-4 Nuclei

DAVID E. MCCLAIN, CAROL A. TRYPUS, AND LEOPOLD MAY[1]

Radiation Biochemistry Department, Armed Forces Radiobiology Research Institute, Bethesda, Maryland 20814-5145

MCCLAIN, D. E., TRYPUS, C. A., AND MAY, L., Effect of γ Radiation on Membrane Fluidity of MOLT-4 Nuclei. *Radiat. Res.* 123, 263–267 (1990).

These experiments measured the effect of γ radiation on the nuclear envelope using doxyl-fatty acid spin-label probes. Nuclei were isolated from cultured MOLT-4 cells, a radiation-sensitive human T-cell lymphocyte. Membrane fluidity was measured from the electron paramagnetic resonance spectra of the probes. MOLT-4 cells were grown under standard conditions, and suspensions were exposed to ^{60}Co γ radiation at room temperature. The spectra of 5-doxylstearic acid in the nuclei were those of a strongly immobilized label. A difference in the membrane fluidity was detected in a series of experiments comparing labeled irradiated and nonirradiated nuclei. The change in fluidity was measured by comparing the changes in the order parameter, *S*, of the spin label in irradiated nuclei with those in control nuclei. The change in the *S* ratio is dependent on radiation dose, increasing with doses up to 15 Gy. The maximum change of the order parameter with time after irradiation occurs 16–20 h after radiation exposure. These observations are correlated with changes in cell viabilities.

INTRODUCTION

The nuclear envelope consists of a double-layer membrane perforated by pore complexes and lined on its nucleoplasmic surface by a protein scaffold consisting primarily of the nuclear lamins A, B, and C (*1, 2*). The envelope serves as a semipermeable barrier between the cytoplasmic and the nucleoplasmic spaces, regulating transport of messenger RNA and other macromolecular traffic through the pore complex. Although the function of the lamins is not yet understood, they appear to serve a structural role, supporting the nuclear membrane (*3*) and providing attachment sites for chromatin (*4, 5*). Alteration of the nuclear envelope by radiation could severely affect the metabolic and reproductive viability of the cell.

Many studies indicate that the nuclear envelope is sensitive to radiation. The first morphological change observed in the irradiated lymphocyte is a dilation and invagination of the nuclear envelope (*6*). Sato *et al.* (*7*) detected radiation-induced changes in the negative charge on nuclear membranes by measuring the electrophoretic mobility of isolated nuclei. They showed that there is a good correlation between the mobility of intact nuclei and the surviving fraction of three cell lines.

Damage to the nuclear envelope is related to the survival of the cell. Cole *et al.*, in a series of experiments beginning in the 1970's, showed that limiting radiation exposure to the region of the nuclear envelope in intact cells can lead to division delay and cell death (*8–10*). Schneiderman and Hofer (*11*) found that cells containing DNA labeled with ^{125}IUdR during S phase did not experience enhanced division delay, while cells with DNA labeled during late-S/G_2 phase did. Chromatin is bound to the nuclear envelope during G_2 phase but not during S phase. Therefore, ionizations that occur proximal to the nuclear envelope are more harmful to the cell than those that do not.

The mechanism by which radiation damages the envelope remains unclear, and the specific sites of damage are unknown. In an effort to understand more about the effects of radiation on the nuclear envelope, we used a fatty acid spin-label probe to measure radiation-induced changes in nuclear membrane fluidity. Our results show that γ irradiation results in increased nuclear membrane fluidity in MOLT-4 cells *in vivo*. Nuclei purified from the irradiated cells exhibit changes in the electron paramagnetic resonance (EPR) spectra of the spin-label probe 5-doxylstearic acid that are related to radiation dose and time after irradiation. This damage is correlated with cell viability.

MATERIALS AND METHODS

Cell culture

MOLT-4 is a human leukemic T-lymphocyte cell line originally isolated from a patient with acute lymphoblastic leukemia and previously characterized as radiosensitive (*12*) with a D_0 value of 0.49 Gy for X rays (*13*). Cells (ATCC CRL 1582) were grown in RPMI 1640 medium, supplemented with 10% heat-inactivated fetal calf serum (GIBCO Laboratories, Grand Island, NY), penicillin (100 units/ml, GIBCO), and streptomycin (100 μg/ml, GIBCO) in loosely capped plastic culture flasks at 37°C in an atmosphere of 5% CO_2 in air. Subculturing the cells every 3–4 days maintained them in log-phase growth. Doubling time of the cells was 24–30 h.

Irradiation

Irradiation was performed at room temperature, using the Armed Forces Radiobiology Research Institute's Theratron ^{60}Co source at a dose

[1] Also at the Department of Chemistry, The Catholic University of America, Washington, DC 20064.

0033-7587/90 $3.00

rate of 0.85 Gy/min. Cells were irradiated as a suspension in growth medium at a density of 0.5–1.0 × 10^6 cells/ml.

Nuclei Purification and Spin-Labeling

Cells were removed from medium by centrifugation and washed twice with nuclei buffer [NB: 10 m*M* Tris–HCl, 2 m*M* $MgCl_2$, 140 m*M* NaCl, 1 m*M* phenylmethylsulfonyl fluoride (PMSF), pH 7.4]. The washed pellet was resuspended in hypotonic Hepes buffer (10 m*M* Hepes, 2 m*M* $MgCl_2$, 1 m*M* PMSF) to a concentration of 1–3 × 10^7 cells/ml and allowed to swell for 12 min on ice. Cells were then homogenized by seven strokes in a Dounce homogenizer ("A" pestle). The homogenate was centrifuged (750*g* at 4°C for 7 min) to pellet the nuclear fraction. The pellet was washed twice with NB before labeling with the spin-label probe. Nuclei were labeled by adding 5-doxyl stearic acid (Molecular Probes, Inc., Eugene, OR; 10 μl of 2.3 × 10^{-3} *M* solution in methanol) to 1 ml of the nuclei suspension (0.5–1.0 × 10^8 nuclei). Methanol used to dissolve the spin label had no effect on the EPR spectra of either control or irradiated nuclei. The suspension was incubated for 10 min on ice, then centrifuged (13,000 rpm in an Eppendorf microcentrifuge for 7 s at 4°C) to pellet the nuclei, which were then washed once with NB and stored on ice until analyzed. The single wash reduces handling steps yet is sufficient to remove all detectable levels of free spin label.

Our experience indicated that the MOLT-4 nuclei tend to aggregate during purification unless all steps are done gently, expeditiously, and on ice at all times, using buffers containing PMSF.

Electron Paramagnetic Resonance

Immediately before obtaining a spectrum, the nuclei were resuspended into 50 μl of NB. The suspension was aspirated into a 50-μl disposable micropipet that was then sealed and inserted into an EPR quartz tube (two-thirds filled with ordinary household oil) located in the EPR cavity. All EPR spectra were obtained at room temperature with the operation parameters fixed for any given experiment. Typical settings on the spectrometer were: field set, 3380 G; scan range, 100 G; scan time, 8 min; time constant, 0.128 s; modulation amplitude, 2 G; and microwave power, 16 mW. The order parameter, *S*, of the strongly immobilized probe was calculated from these spectra using the equation: $S = (T_\parallel - T_\perp)/(3(T_{zz} - a')/2)$, where $2T_\parallel$ is the outer hyperfine splitting, $2T_\perp$ is the inner hyperfine splitting, a' is $(T_\parallel + 2T_\perp)/3$, and the tensor $T_{zz} = 32$ G [(*14*), Fig. 1].

Viability Measurements

Cell viability was assayed by trypan blue vital dye exclusion by adding one part of 0.1% trypan blue in deionized water to three parts of the medium containing the cells. After a 5-min equilibration period, cells were counted under an optical microscope. Cells taking up the dye were scored as nonviable and expressed as a fraction of the total number of cells counted.

Biochemical Determinations

The plasma membrane marker enzyme 5'-nucleotidase was determined by colorimetry at 660 nm by monitoring the production of inorganic phosphate resulting from the hydrolysis of adenosine monophosphate (Sigma Diagnostics Procedure No. 675) (*15*).

Protein was determined using the Bio-Rad standard protein assay.

RESULTS

The nuclear isolation procedure used in these experiments produces nuclei devoid of visible cellular debris (as judged by light microscopy). Because of concern that significant contamination of the nuclei preparations by other cellular membranes could affect the interpretation of our data, we analyzed the purity of our nuclei preparations by assaying for the plasma membrane marker, 5'-nucleotidase. Five percent of the activity present in the whole cell remains in the purified nuclei preparation. In addition, nuclei preparations from irradiated cells do not demonstrate any difference in contamination compared to controls. Two other isolation techniques tested, using sucrose gradients, result in somewhat less contamination of the nuclei, but produce a greater tendency for the nuclei to aggregate despite the use of different buffers designed to inhibit this phenomenon. All isolation procedures tested, however, produced identical EPR spectra.

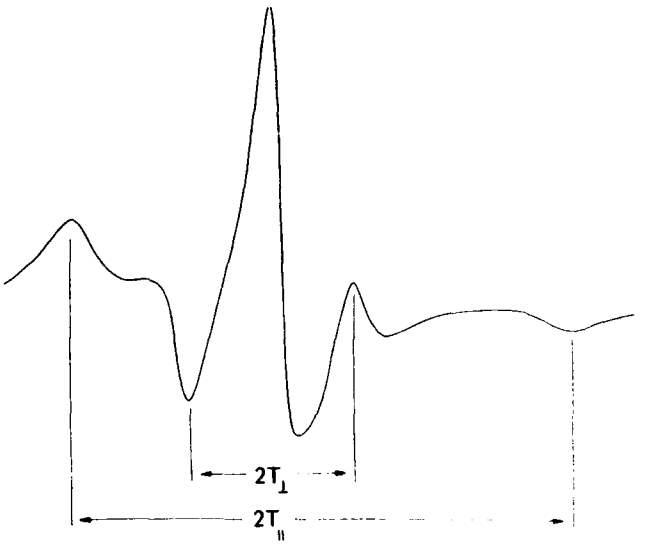

FIG. 1. EPR spectrum of nuclei incubated with 5-doxylstearic acid. The spectrum is typical of that of a membrane-bound spin-probe. $S = (T_\parallel - T_\perp)/(3(T_{zz} - a')/2)$, where $2T_\parallel$ is the outer hyperfine splitting, $2T_\perp$ is the inner hyperfine splitting, a' is $(T_\parallel + 2T_\perp)/3$, and the tensor $T_{zz} = 32$ G (*14*). An increase in *S* indicates an increase in the fluidity of the membrane.

Figure 1 shows the first-derivative EPR spectra obtained with the spin-label probe, 5-doxyl stearic acid, in nuclei from nonirradiated MOLT-4 cells. The probe incorporates into the lipid portion of the nuclear membrane and produces a spectrum typical of a membrane-immobilized spin-label probe. The order parameter, *S*, is an empirical indicator of the spin-label mobility in the membrane. An increase in *S* implies a more fluid nuclear membrane lipid environment. In these experiments *S* was remarkably consistent in control cells from preparation to preparation. Sixty independent measurements of nuclei from nonirradiated cells produced a value of 1.001 ± 0.002 (mean ± SEM). Greater variability was observed in nuclei from irradiated cells (Figs. 2 and 3).

The data in Fig. 2 demonstrate that fluidity of the nuclear membrane increases with time after irradiation. No significant change is observed until 15 h postirradiation; after that

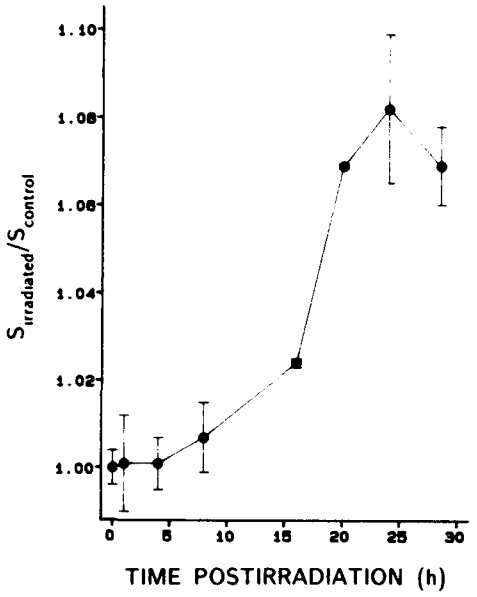

FIG. 2. Ratio of $S_{irradiated}/S_{control}$ varies with time postirradiation. MOLT-4 cells were exposed to 7.5 Gy ^{60}Co γ radiation and their nuclei extracted and labeled. Values represent the means ± SEM from nine determinations of S (three independent experiments) from control and irradiated nuclei, respectively.

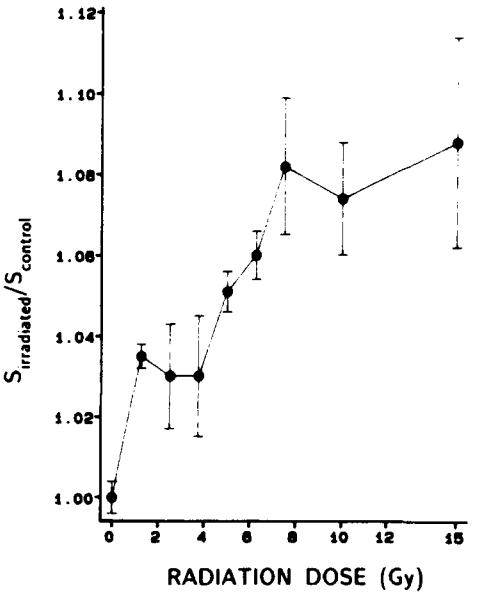

FIG. 3. Ratio of $S_{irradiated}/S_{control}$ varies with radiation dose. MOLT-4 cells were exposed to various doses of ^{60}Co γ radiation and their nuclei extracted and labeled 24 h postirradiation. Values represent the means ± SEM from nine determinations of S (three independent experiments) from control and irradiated nuclei, respectively.

the membrane fluidity increases to the maximum observed at 20–24 h.

Radiation dose also influences membrane fluidity (Fig. 3). Exposures as low as 1.25 Gy produce a significant increase in the membrane fluidity compared with controls. Increases in nuclear membrane fluidity are roughly proportional to dose up to 7.5 Gy, with larger doses producing smaller increases.

Measurements of the viability of irradiated cells indicate that the number of cells scored as viable by their ability to exclude trypan blue decreases with both radiation dose and time after irradiation. Figure 4 shows that radiation doses greater than 5 Gy reduce the number of viable cells measured 24 h postirradiation to a minimum. Figure 5 shows that 5-7 h after exposure to 7.5 Gy, viability decreases steadily until a minimum is observed at 24–30 h postirradiation. Comparison of these viability curves with the increase in membrane fluidity (Figs. 2 and 3) indicates an inverse relationship between viability and fluidity.

DISCUSSION

Although many studies have provided indirect evidence that the nuclear envelope is sensitive to radiation, few studies have identified specific alterations in the envelope that occur as the result of radiation exposure. Sato *et al.* (7) reported that radiation induces a net loss of negative surface charge on nuclei from three cell lines. This change was shown to correlate with the ability of the cells to survive radiation exposure.

Our experiments are the first to measure a change in the membrane fluidity of the nuclear envelope of nuclei iso-

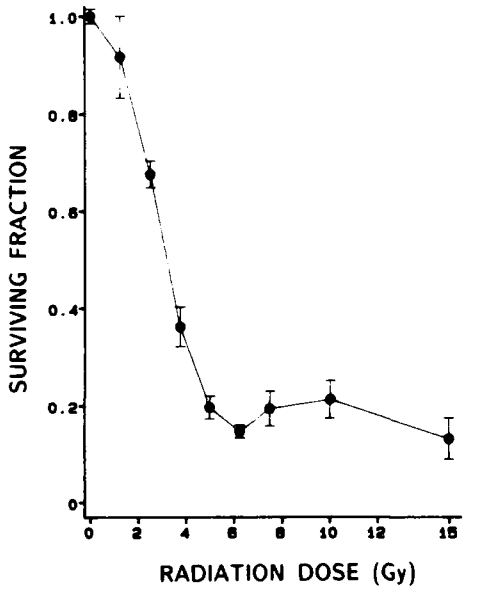

FIG. 4. Viability of MOLT-4 cells assayed by trypan blue exclusion after exposure to various radiation doses. Viability is expressed as the mean ± SEM (three determinations) of the normalized fraction of irradiated cells/control cells that exclude trypan blue.

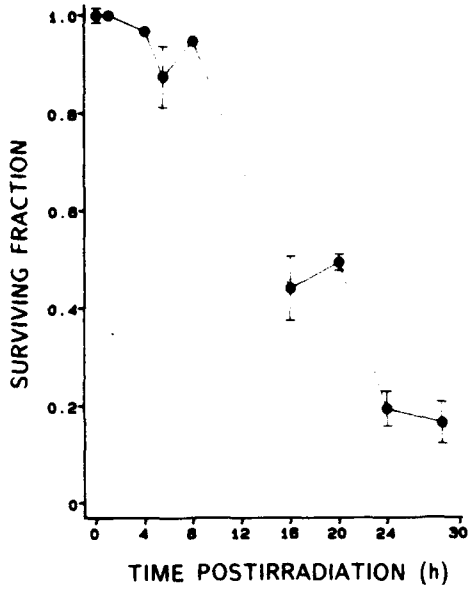

FIG. 5. Viability of MOLT-4 cells measured by trypan blue exclusion at various times after radiation exposure. Viability is expressed as the mean ± SEM (three determinations) of the normalized fraction of irradiated cells/control cells that exclude trypan blue.

lated from irradiated cells compared with that from nonirradiated cells. The change in fluidity increases with radiation dose and time after irradiation, and is related to the viability of the cells. The radiation doses required to produce the change in nuclear membrane fluidity and the time course of the changes observed are similar to those reported by Sato *et al.* Our qualitative observation that nuclei from irradiated cells tend to aggregate in relation to radiation dose also suggests that exposure to radiation produces changes in the nuclear surface. The protease inhibitor PMSF and cold temperatures greatly inhibit this effect, suggesting that protease substrates that are not exposed in nuclear envelopes of nonirradiated cells are exposed by radiation.

Fluidity changes in the plasma membrane have been shown to be associated with lipid peroxidation (*16, 17*) and alterations in the properties of membrane proteins (*18–20*). The role of either in radiation injury to the cell is still unclear [for reviews see (*21, 22*)]. Also, the radiation doses used to produce detectable radiolytic effects on the molecular components of membranes are often in the 10- to 1000-Gy range, far higher than the doses required to alter fluidity in our experiments. This may imply that low levels of lipid peroxidation or protein damage induce fluidity changes in the nuclear envelope or that the irradiated nuclear membrane is altered by another mechanism.

The changes in nuclear membrane fluidity we observed may arise from either alteration of the lipids themselves or alterations to sulfhydryl groups or other amino acid residues, leading to conformational changes in membrane proteins that influence membrane lipid structure. Any such fluidity changes could affect the viability of the cell. For example, a radiation effect that changes the lipid environment of pore complex proteins or alters the pore proteins themselves could disrupt the bidirectional, transmembrane traffic of proteins and mRNA. Radiation-induced alteration of membrane lipids could affect the binding of nuclear membrane-bound proteins such as lamin B, which is thought to mediate the attachment of chromatin to the nuclear envelope through lamins A and C (*23*).

Further study of radiation effects on nuclear membrane fluidity could determine the primary site of radiation damage. A more detailed characterization of the changes in lipid fluidity in our system might use lipid spin probes with the doxyl group located at different positions along the hydrocarbon chain, which would allow measurement of membrane fluidity at various depths within the lipid bilayer. The effect of radiation on membrane proteins could be studied by measuring changes in the mobility of probes bound to those proteins.

Much evidence suggests that the nuclear envelope is a target of radiation in the cell, the impairment of which affects cell viability. We have demonstrated a radiation-induced change in nuclear membrane lipid fluidity not previously reported. The specific membrane alterations producing this change remain unknown. Whether this is a primary effect of radiation or a secondary expression of damage awaits further study.

RECEIVED: January 16, 1990; ACCEPTED: April 4, 1990

REFERENCES

1. L. GERACE, C. COMEAU, and M. BENSON, Organization and modulation of nuclear lamina structure. *J. Cell Sci. Suppl.* **1**, 137–150 (1984).
2. W. FRANKE, U. SCHEER, G. KROHNE, and F. JARASCH, The nuclear envelope and the architecture of the nuclear periphery. *J. Cell Biol* **91**, 39s–50s (1981).
3. L. GERACE and G. BLOBEL, Nuclear lamina and the structural organization of the nuclear envelope. *Cold Spring Harbor Symp. Quant. Biol.* **46**, 967–978 (1982).
4. R. HANCOCK and M. HUGHES, Organization of DNA in the interphase nucleus. *Biol. Cell* **44**, 201–212 (1982).
5. J. LEBKOWSKI and U. LAEMMLI, Non-histone proteins and long-range organization of HeLa interphase DNA. *J. Mol. Biol.* **156**, 325–344 (1982).
6. T. AOYAMA, Y. KAWAMOTO, I. FURATA, and T. KONDO, Early morphological changes in cortical medullary thymocytes of the rat after whole-body irradiation. *Int. J. Radiat. Biol.* **21**, 545–558 (1972).
7. C. SATO, K. KOJIMA, T. MATSUZAWA, and Y. HINUMA, Relationship between loss of negative charge on nuclear membrane and loss of colony-forming ability in X-irradiated cells. *Radiat. Res.* **62**, 250–257 (1975).
8. W. T. TOBLEMAN and A. COLE, Repair of sublethal damage and oxygen enhancement ratio for low-voltage electron beam irradiation. *Radiat. Res.* **60**, 355–360 (1974).

9 R. DATTA, A. COLE, and S. ROBINSON, Use of track-end alpha particles from Am-231 to study radiation-sensitive sites in CHO cells. *Radiat. Res.* **65**, 139–151 (1976).

10 A. COLE, W. G. COOPER, F. SHONKA, P. M. CORRY, R. M. HUMPHREY, and A. T. ANSEVIN, DNA scission in hampster cells and isolated nuclei studied by low-voltage electron beam irradiation. *Radiat. Res.* **60**, 1–33 (1974).

11 M. H. SCHNEIDERMAN and K. HOFER, The target for radiation-induced division delay. *Radiat. Res.* **84**, 462–476 (1980).

12 T. HAN, J. L. PAULY, and J. MINOWADA, *In vitro* preferential effect of radiation on cultured T lymphoid cell line. *Clin. Exp. Immunol.* **17**, 455–462 (1974).

13 J. G. SZEKELY and A. U. LOBREAU, High radiosensitivity of the MOLT-4 leukaemic cell line. *Int. J. Radiat. Biol.* **48**, 277–284 (1985).

14 J. SEELIG, Spin label studies of oriented smectic liquid crystals (a model system for bilayer membranes). *J. Am. Chem. Soc.* **92**, 3881–3887 (1970).

15 T. F. DIXON and M. PURDOM, Serum 5'-nucleotidase. *J. Clin. Pathol.* **7**, 341–352 (1954).

16 D. J. W. BARBER and J. K. THOMAS, Reaction of radicals with lecithin bilayers. *Radiat. Res.* **74**, 51–65 (1978).

17 E. GRZELINSKA, G. BARTOSZ, K. GWOZDZINSKI, and W. LEYKO, A spin-label study of the effect of gamma radiation on the erythrocyte membrane. Influence of lipid peroxidation on membrane structure. *Int. J. Radiat. Biol.* **36**, 325–334 (1979).

18 S. YONEI, T. TODO, and M. KATO, Radiation effects on erythrocyte membrane structure studied by intrinsic fluorescence. *Int. J. Radiat. Biol.* **35**, 161–170 (1979).

19 L. KWOCK, P.-S. LIN, K. HEFTER, and D. F. H. WALLACH, Impairment of Na^+-dependent amino acid transport in a cultured human T-cell line by hyperthermia and radiation. *Cancer Res.* **38**, 83–87 (1978).

20 T. TODO, S. YONEI, and M. KATO, Radiation-induced structural changes in human erythrocyte membrane proteins revealed by sodium dodecyl sulfate/polyacrylamide gel electrophoresis. *Radiat. Res.* **89**, 408–419 (1978).

21 W. LEYKO and G. BARTOSZ, Membrane effects of ionizing radiation and hyperthermia. *Int. J. Radiat. Biol.* **49**, 743–770 (1986).

22 J. C. EDWARDS, D. CHAPMAN, W. A. CRAMP, and M. B. YATVIN, The effects of ionizing radiation on biomembrane structure and function. *Prog. Biophys. Mol. Biol.* **43**, 71–93 (1984).

23 J. NEWPORT, Nuclear reconstitution *in vivo*: Stages of assembly around protein-free DNA. *Cell* **48**, 205–217 (1987).

J. Membrane Biol. 116, 47–56 (1990)

The Journal of
Membrane Biology

Effect of Adherence, Cell Morphology, and Lipopolysaccharide on Potassium Conductance and Passive Membrane Properties of Murine Macrophage J774.1 Cells

Leslie C. McKinney and Elaine K. Gallin
Department of Physiology, Armed Forces Radiobiology Research Institute, Bethesda, Maryland 20814

Summary. The effects of adherence, cell morphology, and lipopolysaccharide on electrical membrane properties and on the expression of the inwardly rectifying K conductance in J774.1 cells were investigated. Whole-cell inwardly rectifying K currents (K_i), membrane capacitance (C_m), and membrane potential (V_m) were measured using the patch-clamp technique. Specific K_i conductance (G_K, whole-cell K_i conductance corrected for leak and normalized to membrane capacitance) was measured as a function of time after adherence, and was found to increase almost twofold one day after plating. Membrane potential (V_m) also increased from -42 ± 4 mV ($n = 32$) to -58 ± 2 mV ($n = 47$) over the same time period. G_K and V_m were correlated with each other; G_l (leak conductance normalized to membrane capacitance) and V_m were not. The magnitudes of G_K and V_m 15 min to 2 hr after adherence were unaffected by the presence of 100 μM cycloheximide, but the increase in G_K and V_m that normally occurred between 2 and 8 hr after adherence was abolished by cycloheximide treatment. Membrane properties were analyzed as a function of cell morphology, by dividing cells into three categories ranging from small round cells to large, extremely spread cells. The capacitance of spread cells increased more than twofold within one day after adherence, which indicates that spread cells inserted new membrane. Spread cells had more negative resting membrane potentials than round cells, but G_K and G_l were not significantly different. Lipopolysaccharide (LPS; 1 or 10 μg ml) treated cells showed increased C_m compared to control cells plated for comparable times. In contrast to the effect of adherence, LPS-treated cells exhibited a significantly lower G_K than control cells, indicating that the additional membrane did not have as high a density of functional G_K channels. We conclude that both adherence and LPS treatment increase the total surface membrane area of J774 cells and change the density of K_i channels. In addition, this study demonstrates that membrane area and density of K_i channels can vary independently of one another.

Key Words potassium channel · macrophage · J774.1 cells · lipopolysaccharide · adherence · ion transport

Introduction

A number of different K currents have been described in macrophages or macrophage-like cell lines (for review *see* Gallin & McKinney, 1989). Several of these studies have shown that ionic currents change with the functional state of the cell. In human peripheral blood monocytes, large conductance Ca-activated K channels appear in the plasma membrane over a time course of 4–5 days as the cells mature from monocytes into macrophages (Gallin & McKinney, 1988), while different, smaller conductance Ca-activated K channels are present both shortly after isolation and after 4–5 days in culture (Gallin, 1989). In addition, exposure of human monocytes to lipopolysaccharide (LPS), an 'activating' or 'priming' stimulus, increases the percentage of cells expressing a transient outward K current (K_o) from 0 to approximately 30% (Jow & Nelson, 1989). In the murine macrophage-like cell line J774.1, a K_o current is briefly expressed immediately after cells become adherent, while an inwardly rectifying K current (K_i) increases in magnitude over a time course of approximately one day (Gallin & Sheehy, 1985). Adherent mouse peritoneal macrophages also express a K_i current after five days in culture (Randriamampita & Trautmann, 1987), but do not appear to express this conductance before that time (Ypey & Clapham, 1984).

These studies demonstrate that the state of maturation of the macrophage, as well as adherent culture conditions or exposure to LPS, can affect the expression of K channels in macrophages. It is well known that adherence induces functional changes in macrophages that are associated with cell activation. (For a general discussion of macrophage activation *see* Cohn (1978) or Karnovsky and Lazdins (1978).) These include increased synthesis or secretion of various lymphokines (Fuhlbrigge et al., 1987; Haskill et al., 1988), and an increase in the oxidative burst induced by phorbol myristate acetate (PMA; Berton & Gordon, 1983; Kunkel & Duque, 1983). Other adherence-induced changes include an increase in resting membrane potential (Sung et al., 1985), increased amino acid transport

(Pofit & Strauss, 1977), transiently increased levels of IP_3 (Zabrenetzky & Gallin, 1988), development of peroxidase activity within 2 hr post-adherence (Bodel, Nichols, & Bainton, 1977), and expression of several surface antigens that are not expressed in cells in suspension (Triglia, Burns & Werkmeister, 1985; Midoux et al., 1989).

Exposure to LPS also induces a variety of changes in macrophages and macrophage cell lines, including increased spreading (Pabst & Johnston, 1980) and membrane ruffling of adherent cells (Morland & Kaplan, 1977), and stimulation of lymphokine synthesis and secretion (Zacharchuk et al., 1983; Fuhlbrigge et al., 1987). Most importantly, LPS 'primes' the cell to respond to other stimuli (Gordon, Unkeless & Cohn, 1974; Pabst, Hedegaard & Johnston, 1982). In J774.1 cells, LPS inhibits cell division (Ralph & Nakoinz, 1977; Kurland & Bockman, 1978; Okada et al., 1978) and induces secretion of prostaglandin E (Kurland & Bockman, 1978) and T-cell activating factors (Okada et al., 1978).

The purpose of this study was to determine the effects of both adherence and LPS on the expression of the inwardly rectifying K conductance and on the electrical membrane properties (membrane potential, V_m; leak resistance, R_L; and capacitance, C_m) of the murine macrophage-like cell line J774.1. While Gallin and Sheehy (1985) noted that the magnitude of K_i in J774.1 cells increased with time after adherence, they did not determine whether the increased current magnitude was due to an increase in cell size, or whether current density (current/unit membrane area) increased. This question was resolved in the present study by directly measuring whole-cell inwardly rectifying K conductance and normalizing this value to C_m to obtain specific K_i conductance (G_{K_i}). Since membrane capacitance is directly proportional to membrane area, these measurements also yielded information about the effect of adherence and LPS on the insertion of new membrane by the cell. We also examined the effect of cycloheximide, a protein synthesis inhibitor, on the expression of G_{K_i} following adherence, since protein synthesis inhibitors have been shown to interfere with the expression of other surface antigens in the macrophage (Smith & Ault, 1981; Triglia et al., 1985). Finally, the expression of G_{K_i} as a function of cell shape was characterized, to determine if G_{K_i} was differentially expressed in very spread *versus* nonspread cells.

Materials and Methods

Cell Culture

J774.1 (J774A.1) cells were obtained from American Type Tissue Culture (Rockville, MD) and maintained in suspension at 37°C for not more than 40 days. Cells were fed at least 12 hr prior to plating for electrophysiological experiments. J774.1 cells have a doubling time of <24 hr and were not synchronized with respect to cell cycle. Whittaker RPMI 1640 culture medium (Bioproducts, Walkersville, MD) was supplemented with 5% fetal calf serum, 4 mM glutamine, and 100 U/ml penicillin-streptomycin (DIFCO). For recording, cells were placed on glass coverslips and maintained in culture medium for varying times (minutes to days). Prior to patch-clamp recordings, coverslips were mounted in a plexiglass chamber in 300–400 μl of Na Hanks', maintained at room temperature (23 to 26°C), and the recording media changed every 20 to 30 min. Coverslips were recorded from for no more than 1 hr.

Recording Methods

Recording methods were the same as those previously described (McKinney & Gallin, 1988). Briefly, whole-cell current records were obtained using a List (Darmstadt, FRG) EPC-7 patch clamp. Voltage pulses were generated by computer and currents were digitized, displayed, and analyzed using an Indec Laboratory Display System (Sunnyvale, CA). Patch electrodes of 3–5 MΩ resistance were made from hematocrit glass (#02-668-68, Fisher Scientific, Pittsburgh, PA). Zero current potentials were measured in current clamp mode immediately after attainment of the whole-cell configuration, and cells were held within 5 mV of this value.

Analytical Methods

Whole-cell records were corrected for leak and capacity currents. Electrode capacitance was compensated while in the cell-attached mode. Total membrane capacitance (C_m) was measured in the whole-cell mode by integrating the capacity transient and was then compensated electronically. Series resistance (R_s) was measured either directly from the EPC-7 after capacity transient cancellation or by fitting a capacitance record with a mono-exponential function to find τ and calculating R_s from the relationship $R_s = \tau/C$. The average series resistance for 95 cells was 6.9 ± 0.6 MΩ. Leak current was measured in one of two ways: by measuring the current in the voltage range −45 to −32 mV where no time-dependent current was present, or by measuring the current at negative voltages in the presence of 2 mM barium, which blocks all inwardly rectifying current and results in a linear I–V relationship. Leak resistances (R_l) obtained using either method were not significantly different from one another: R_L = 2.7 ± 0.3 GΩ (n = 89) in the absence of barium and R_L = 3.0 ± 0.3 GΩ (n = 39) in the presence of barium. For purposes of comparison to inwardly rectifying K conductance measurements, leak resistance values were converted to units of conductance [R_l (GΩ) = 1/G (nS)]. Specific leak conductance (G_l) was determined by dividing the leak conductance by total membrane capacitance. As in our previous study (McKinney & Gallin, 1988), for calculations of channel density (# channels/μm^2 of membrane), the specific capacitance of the cell membrane was assumed to be 1 μF/cm^2. Values of surface area calculated using this value compare well with values reported for mouse peritoneal macrophages obtained by stereologic analysis (Steinman, Brodie & Cohn, 1976). Values of surface area obtained using either capacitance measurements or stereologic techniques are two- to three-fold larger than surface area measurements calculated from values of cell diameter (assuming a spherical cell shape). This is because macrophages are irregularly shaped and can have considerable membrane ruffling and infolding.

Whole-cell conductance for inward current (K_i) was measured in the following way. Peak current amplitude was measured at the beginning of a hyperpolarizing voltage step by eye using a cursor. Current *vs.* voltage (*I–V*) curves were constructed and a straight line fitted to the data for steps between −90 to −160 mV to yield a conductance value. After subtraction of leak conductance, values were normalized to membrane capacitance to yield a value for specific K, conductance G_{K_i}.

In order to get an accurate sampling of whole-cell conductance values from the population of J774.1 cells, cells were not excluded on the basis of low resting membrane potentials or small inward current amplitudes. After verifying increased capacitance after rupture of the patch (the lowest value accepted was 11 pF) and an acceptable series resistance value (not greater than 20 MΩ) for a particular recording, we included virtually all cells that had stable membrane properties in the study.

^{3}H-Leucine Incorporation

The effect of cycloheximide on protein synthesis was assayed by measuring incorporation of ^{3}H-leucine into protein in the presence of varying concentrations of the protein synthesis inhibitor cycloheximide (Sigma Chemical, St. Louis, MO). An IC_{50} of approximately 1 μM was observed; 100 μM cycloheximide inhibited greater than 90% of ^{3}H-leucine incorporation in these cells.

Solutions

Cells were bathed in a Na Hanks' solution consisting of (in mM): 145 NaCl, 4.5 KCl, 1.6 $CaCl_2$, 1.1 $MgCl_2$, 10 HEPES/NaOH buffer, pH 7.3. The pipette contained (in mM): 145 KCl, 1 $MgCl_2$, 1.1 EGTA, 0.1 $CaCl_2$, and 10 HEPES/KOH, pH 7.3. Free Ca in this solution was less than 10^{-8} M. *Escherichia coli* derived lipopolysaccharide (LPS) was obtained from DIFCO Laboratories (Detroit, MI).

Statistical Methods

Unless otherwise stated, mean values were considered to be significantly different from one another if $P < 0.05$ using a Student's *t* test. Linear regression analysis was carried out on a VAX 11/750 using the RS1 statistical package (BBN Software Products, Cambridge, MA). Two values were said to be correlated if the *R* value of the slope of the line relating the two variables was significantly different from zero ($P < 0.05$). In some cases, in order to analyze upward or downward trends in the data with time, biweight regressions were done and slopes were compared to zero. Slopes of control *vs.* test data were compared to each other using a *t* test.

Results

Membrane Capacitance, Specific K_i Conductance, and Membrane Potential Increase with Time After Adherence

Figure 1*A* shows an example of inwardly rectifying K_i currents recorded from J774.1 cells bathed in Na Hanks, with the corresponding *I–V* relationship shown in Fig. 1*B*. The K_i current activates at −50 mV, and shows time-dependent inactivation below about −120 mV that is partially due to block by Na, and partially due to inactivation of the current (McKinney & Gallin, 1988). Properties of both the whole-cell current and the single-channel events underlying them have been described in detail elsewhere (McKinney & Gallin, 1988). The K_i current is completely blocked by 1 mM barium and in >95% of the recordings was the only time-dependent current observable under these recording conditions. Therefore, the leak-subtracted whole-cell conductance measured over negative voltages appears to be due solely to the conductance of the K_i current. An inactivating outward K current (K_o) was observed in about 5% of cells, but it activated at potentials above −40 mV (Gallin & Sheehy, 1985), and did not interfere with measurements of the inwardly rectifying current. Randriamampita and Trautmann (1987) have reported the existence of a linear Ca-dependent K current in J774 cells which is apparent only when intracellular calcium is buffered at 1 μM. In our experiments, $[Ca]_i$ was buffered at 10^{-8} M and so this current was not observed.

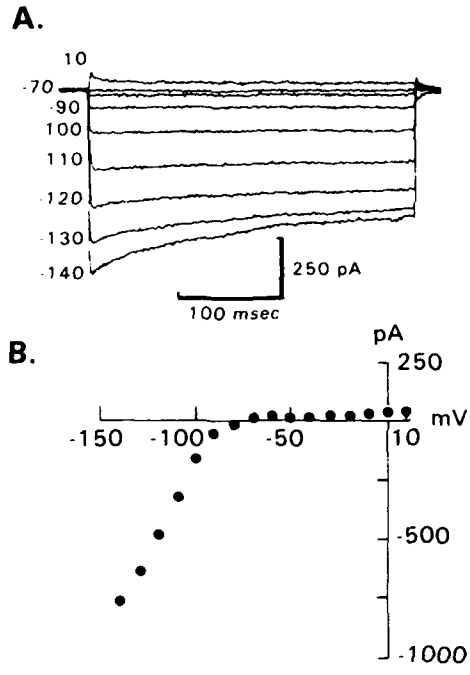

Fig. 1. (*A*) Inwardly rectifying K current. Cell was held at −70 mV and 440 msec voltage pulses applied in 10-mV increments. Records have not been leak subtracted to show total current. (*B*) Peak current-voltage plot for experiment shown in *A*

In order to study how the K_i conductance and other membrane properties change after adherence, whole-cell recordings were obtained at varying times after plating. Values for C_m, G_{K_i}, V_m, and G_L are plotted in the form of bar graphs showing the mean ± SEM as a function of time after adherence

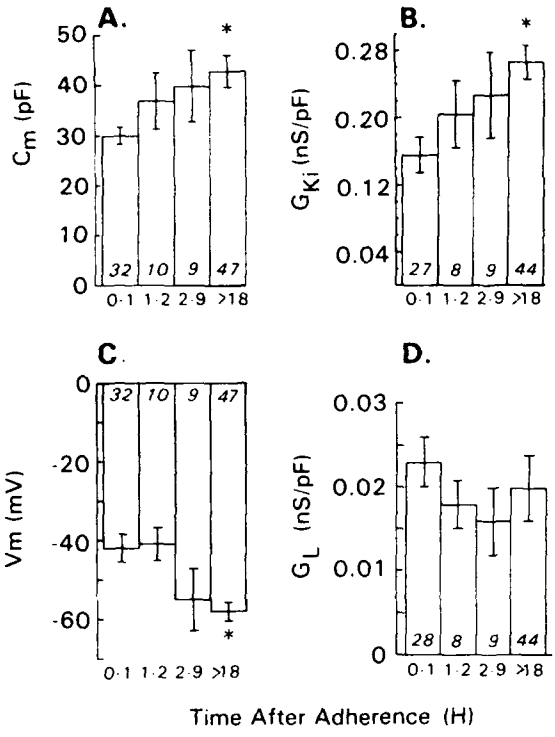

Fig. 2. Plots of (*A*) C_m (*B*) G_{K_i}, (*C*) V_m, and (*D*) G_L *vs.* time after adherence. Values plotted are means ± SEM. Asterisk (*) indicates values which are significantly different from values at 0–1 hr. Numbers within the bar, for these and all subsequent graphs, indicate number of cells studied

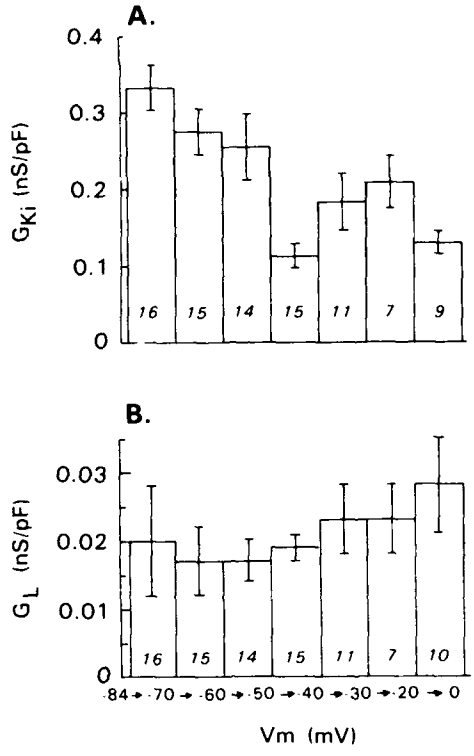

Fig. 3. (*A*) Plot of G_{K_i} *vs.* resting V_m. (*B*) Plot of G_L *vs.* V_m. Conductance values given are mean ± SEM. V_m values (in mV) were grouped as follows: −84 to −70, −69 to −60, −59 to −50, −49 to −40, −39 to −30, −29 to −20, −19 to 0

(Fig. 2). Cells were grouped into four time periods: 0–1 hr (to follow changes in membrane properties at early times after adherence), 1–2, 2–9, and >18 hr. It should be noted that the earliest time point at which recordings were made was approximately 15 min after adherence, and no recordings were made at times longer than about 36 hr after adherence.

Significant changes in membrane properties were noted following adherence. Membrane capacitance increased significantly with time after plating (Fig. 2*A*) from 30 ± 2 pF to 43 ± 3 pF. Assuming that 1 cm^2 of membrane has a capacitance of 1 μF, the average membrane area of the cells increased by about 40%. Thus, the morphological changes which J774.1 cells undergo after adherence do not merely represent shape changes but reflect a net insertion of additional membrane. G_{K_i} increased almost twofold over 18 hr (Fig. 2*B*), from 0.16 ± 0.02 nS/pF to 0.27 ± 0.02 nS/pF. Since this value is normalized to membrane area, the increase in G_{K_i} was not due to the increased membrane area of the cells. Our single-channel data indicate that the conductance of single inwardly rectifying channels does not change after adherence (*data not shown*). Therefore, the increase in G_{K_i} represents an increase in the density of K_i channels in the membrane over this time period from 44 channels/pF (0.44 channels/μm^2) to 75 channels/pF (0.75 channels/μm^2). These data were supported by direct observations of K_i channel activity in cell-attached patches (McKinney & Gallin, 1988). Membrane patches from freshly plated cells usually contained few (0–3) channels, while membrane patches from cells adherent for one day usually contained many (2–6) channels. Since both channel density and membrane area increased with time after adherence, the average number of channels per cell increased from 1,320 to 3,225 over 18 hr.

During the 18-hr period following adherence, the average V_m of the cells increased from −42 ± 4 mV to −58 ± 2 mV (Fig. 2*C*). The increase in membrane potential could be due to an increase in G_{K_i} or could also be due to a concomitant decrease in G_L. However, as shown in Fig. 2*D*, G_L did not change significantly with time after adherence, indicating that the cells maintained a rather constant leak conductance over the time that C_m, V_m, and G_{K_i} were increasing.

Specific K_i Conductance and Membrane Potential Are Correlated

Figure 3 shows the relationship between G_{K_i} and resting V_m. (Note: resting V_m is actually determined

Table 1. Effect of cycloheximide on membrane properties of J774.1 cells

	Time after adherence (hr)	G_{K_i} (nS/pF)	G_L (nS/pF)	V_m (mV)	C_m (pF)
Control	0–2	0.16 ± 0.02 (35)	0.02 ± 0.003 (36)	−42 ± 3 (42)	31 ± 2 (42)
Cycloheximide-treated	0–2	0.25 ± 0.04 (7)	0.03 ± 0.006 (8)	−51 ± 6 (10)	35 ± 4 (10)
Control	2–9	0.23 ± 0.05 (9)	0.02 ± 0.004 (9)	−55 ± 8 (9)	40 ± 7 (9)
Cycloheximide-treated	2–8	0.14 ± 0.04 (14)	0.03 ± 0.006 (15)	−54 ± 5 (15)	30 ± 2 (15)

Note that cells were exposed to cycloheximide for 1 hr prior to plating, as well as during plating.

by steady state, not peak K conductance. However, over the voltage range of −50 to −110 mV, peak and steady-state conductance are equivalent.) Data are from cells plated at all times. Between −84 and −40 mV there was a positive correlation between G_{K_i} and resting V_m. That is, over the range at which the inwardly rectifying K conductance is activated, cells which had higher conductance to K_i also had a more negative resting membrane potential. In contrast, there was no correlation between G_{K_i} and V_m for voltages positive to −40 mV. In addition, there was no correlation between V_m and G_L over any voltage range. This result indicates that cells which had low resting membrane potentials were not depolarized merely because they were 'leakier'. Likewise, there was no correlation between G_{K_i} and G_L; cells with a low specific K_i conductance were not necessarily those with a large leak conductance. Thus, it is likely that the increase in resting V_m observed over the first 24 hr of adherence is a function of the increased conductance to K_i, and not a function of a change in G_L.

Initial Expression of G_{K_i} Is Not Inhibited by Cycloheximide

To determine (*i*) whether the observed increase in the density of K_i channels after adherence depended on protein synthesis and (*ii*) whether inhibition of protein synthesis before cells were allowed to become adherent would interrupt the initial expression of K_i, G_{K_i} was measured in cells treated with the protein synthesis inhibitor cycloheximide, which was shown to inhibit ^{3}H-leucine incorporation in these cells (*see* Materials and Methods). Cells were exposed to cycloheximide (100 μM) for 1 hr prior to plating, plated in the presence of cycloheximide, and G_{K_i} was measured at various times after plating. Cells treated with cycloheximide were able to adhere and spread similar to untreated cells, and the general morphology appeared normal. However, Gigaohm seals were considerably less stable, which made recording from the cells for an extended period of time difficult. Values for G_{K_i}, G_L, V_m and C_m are given in Table 1, grouped into two time periods: 0–2 and 2–8 hr after adherence. Because prolonged incubation in cycloheximide may affect cell viability, the conductance of cells which had been plated in cycloheximide for more than 8 hr was not measured. Cycloheximide did not inhibit the initial expression of inward current. Average G_{K_i} 0–2 hr after adherence was not significantly different from the average G_{K_i} value for untreated cells plated for the same amount of time. Values for G_L, V_m and C_m were also not different from controls. However, with time after adherence, cycloheximide did inhibit the increase in G_{K_i} and V_m normally observed in control cells. While control cells increased their mean G_{K_i} from 0.16 to 0.23 nS/pF 2–9 hr after adherence, the mean G_{K_i} of cycloheximide-treated cells decreased from 0.25 to 0.14 nS/pF. When G_{K_i} values were plotted *vs.* time for cycloheximide-treated cells, the slope of the line was found to decline significantly (Fig. 4). Cycloheximide-treated cells did not show a significant trend to more negative resting membrane potentials with time after adherence, nor was there a significant trend toward increased membrane capacitance as was shown by control cells. G_L of cycloheximide-treated cells was unchanged after adherence. These data indicate that cycloheximide does not interfere with the initial expression of the inwardly rectifying K conductance, but does inhibit the upregulation of K channels and the insertion of new membrane which occurs following adherence.

Different Morphological Groups Have Different Membrane Properties

Adherent J774.1 cells exist in a variety of shapes and sizes that may reflect different functional states. For instance, cells undergoing cell division become rounded while migrating cells have a polarized appearance, with a leading and trailing edge. Other cells exhibit a very flattened appearance almost immediately after adherence. In order to de-

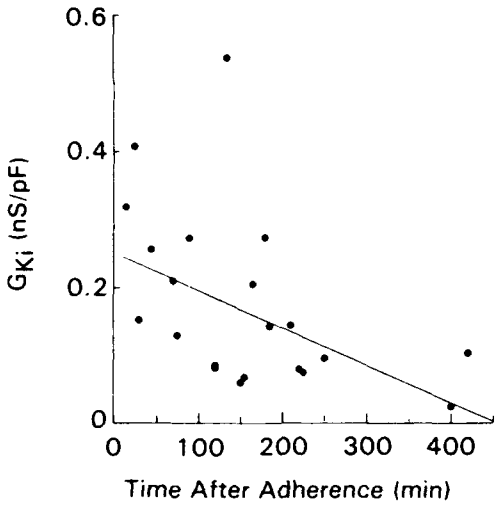

Fig. 4. Plot of G_{K_i} *vs.* time after adherence for cycloheximide-treated cells. Solid line is a linear biweight fit to the data. Its slope is significantly different from zero. Note that cells were exposed to cycloheximide 1 hr prior to plating, as well as during plating

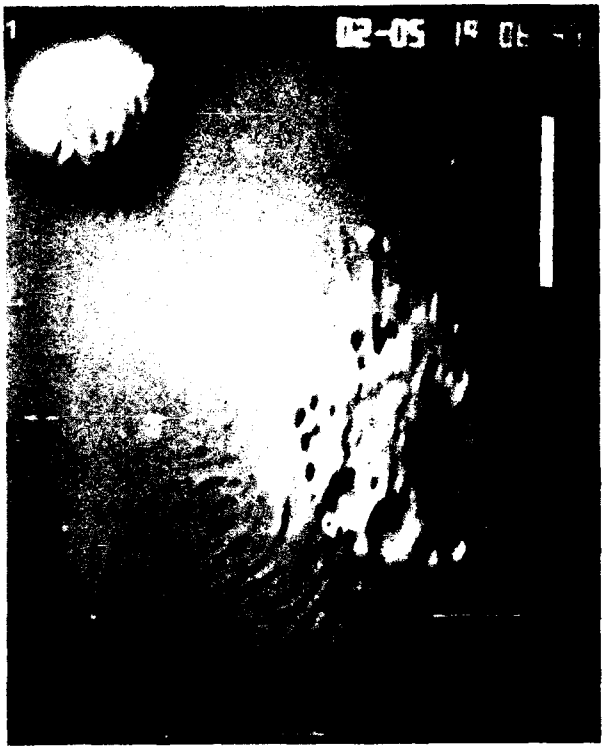

Fig. 5. Photograph of adherent J774.1 cells showing different morphological categories. Bar: 20 μm

termine whether cells of different morphologies had different membrane properties, cells were divided into three groups according to shape (*see* photograph, Fig. 5): group *#1*, small round cells without visible processes, mean capacitance 27 ± 3 pF (n = 20), average diameter 22 μm; group *#2*: somewhat spread or polarized cells, some with visible processes, mean capacitance 36 ± 2 pF (n = 40), average dimensions 37 × 28 μm; and group *#3*: extremely spread cells, mean capacitance 45 ± 4 pF (n = 36), average dimensions 50 × 42 μM. V_m, C_m, G_{K_i}, and G_L for each morphological category were determined for two time periods: 0–2 and >18 hr after adherence (Fig. 6). Examining the data in this way revealed some interesting differences between cell types that were not apparent when the data from all cells were pooled (as in Fig. 2).

Values for V_m, C_m, G_{K_i} and G_L were not significantly different between groups *1* and *2* at either 0–2 hr or >18 after adherence. Thus, for clarity, only data from groups *1* and *3* are shown in Fig. 6. Very spread cells were different from round cells in several respects. They were significantly more hyperpolarized than round cells at either 0–2 or > 18 hr following adherence (Fig. 6*A*). Also, one day after adherence, spread cells had much larger membrane capacitance than round cells (Fig. 6*B*). Both round and spread cells still showed a positive correlation between V_m and G_{K_i}. However, G_{K_i} (Fig. 6*C*) and G_L (Fig. 6*D*) were not significantly different between groups *1* and *3* compared at the same time period (0–2 or >18 hr).

We also examined how membrane properties changed with time after adherence for each group. First, only the very spread cells showed a significant (almost twofold) increase in membrane capacitance over 18 hr (Fig. 6*B*). Thus, most of the previously observed increase in membrane area which occurs after adherence (*see* Fig. 2*A*) can be attributed to the increased membrane area of very spread cells. Second, membrane potential significantly increased with time after adherence for both groups of cells (Fig. 6*A*). Round cells showed the largest increase in V_m, and also showed the largest increase in G_{K_i} 18 hr after adherence (Fig. 6*C*). Spread cells showed a smaller increase in V_m, and a correspondingly smaller increase in G_{K_i}. G_L values did not change after adherence for either round or spread cells (Fig. 6*D*). We conclude that very spread cells behave differently from round cells after adherence; they insert more membrane but do not significantly increase K_i current density after adherence.

LPS-Treated Cells have Different Membrane Properties

The effect of LPS on membrane properties of J774.1 cells was examined by incubating cells in suspen-

Table 2. Effect of LPS on membrane properties of J774.1 cells

	Time after adherence (hr)	G_{K_i} (nS/pF)	G_L (nS/pF)	V_m (mV)	C_m (pF)
Control	0–2	0.16 ± 0.02 (35)	0.02 ± 0.003 (36)	−42 ± 3 (42)	31 ± 2 (42)
LPS-treated	0–2	[a]0.09 ± 0.02 (13)	0.02 ± 0.007 (14)	−37 ± 5 (16)	[a]42 ± 5 (17)
Control	>18	[b]0.27 ± 0.02 (44)	0.02 ± 0.004 (44)	[b]−58 ± 2 (47)	[b]43 ± 3 (47)
LPS-treated	>18	[a,b]0.15 ± 0.02 (8)	0.02 ± 0.006 (9)	[b]−62 ± 4 (10)	[a,b]68 ± 10 (10)

[a] Significantly different from control cells at the same time period.
[b] Significantly different from the value at 0–2 hr.
Note that cells were exposed to LPS one day prior to plating, as well as during plating.

sion with 1 or 10 μg/ml of LPS overnight and then plating cells for various times in the presence of LPS. Values for G_{K_i}, G_L, V_m and capacitance are given in Table 2, grouped into two time periods, 0–2 and 18 hr after adherence. Data were not separated into different morphological categories; LPS-treated cells were of all three groups but primarily of group #2. For a given time period after adherence, V_m and G_L values were comparable to those of control cells, but G_{K_i} values were significantly lower. However, G_{K_i} and V_m were still correlated; G_L and V_m were not. Membrane capacitance was larger, indicating that LPS-treated cells have a larger membrane surface area. Thus, activation of cells by LPS resulted in the insertion of new membrane, but did not result in increased density of K channels. Membrane properties of LPS-treated cells showed changes with time after adherence in a manner similar to control cells. G_{K_i}, V_m and C_m all increased significantly one day after adherence, as they did for untreated cells, while G_L was unchanged.

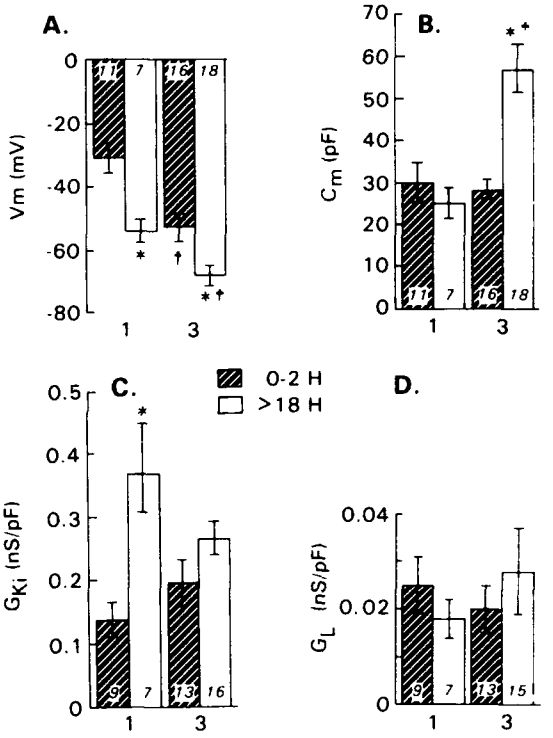

Fig. 6. *(A)* V_m, *(B)* C_m, *(C)* G_{K_i}, and *(D)* G_L with time after adherence for round (group *1*) and spread (group 3) cells. Mean values were compared at 0–2 and >18 hr for each group. *Indicates values that are significantly different from values from the same group at 0–2 hr. †Indicates values that are significantly different from values of group *1* at the same time period

Discussion

This study demonstrates that membrane properties of J774. cells vary with time after adherence, cell morphology, and after exposure to LPS. Values for membrane capacitance (C_m), membrane potential (V_m), and specific K conductance (G_{K_i}) were significantly increased 18 hr after adherence. As shown in Fig. 1, these trends were evident at times earlier than 18 hr post-adherence, even though statistically significant differences between mean values were not yet demonstrable. As a point of comparison, previous studies in T cells demonstrated that stimulation with the mitogens phorbol myristate acetate or concanavalin A caused an increase in K channel density over a time course of about one day (Deutsch, Krause & Lee, 1986; DeCoursey et al., 1987). The increase in channel density occurred over the same time course as the increase in protein synthesis induced by mitogen.

The observed increase in membrane capacitance after plating provides the first evidence that J774.1 cells actively increase their membrane area following adherence. We found that very spread cells showed the largest increase in membrane area following adherence (>twofold), while small round

cells showed very little change. This does not imply that the membrane of smaller cells is unchanging, however. It has been shown that mouse peritoneal macrophages can pinocytose their plasma membrane at high rates (3.1%/min; Steinman, Brodie & Cohn, 1976). Membrane area is undoubtedly regulated by a balance between insertion and retrieval processes, either of which could be altered following adherence. It should also be noted that small and large cells do not necessarily represent two different subpopulations of cells. The J774 cell line is continuously dividing, and morphology may vary with cell cycle. For example, it is generally known that cells 'round up' during mitosis. The variability of membrane properties with cell cycle was not addressed here, although it is an interesting question that bears further study.

Membrane potential also increased with time after adherence, from −42 to −58 mV. Our results are consistent with those of Sung et al. (1985) who used ^{3}H-tetraphenylphosphonium to measure the membrane potential of J774 cells and found that it increased from about −35 to −70 mV between 1 and 8 hr after plating. It is unclear whether there is a significant increase in membrane potential between 0 and 1 hr after plating. Membrane potential values of suspended J774 cells, acquired using indirect probes, have been reported to be −15 mV (Sung et al., 1985), −25 mV (J774.2 cells; Ehrenberg et al., 1988), and −36 mV (J774.2 cells; McCaig & Berlin, 1983), and represent the average V_m of a large population of cells. The latter value is not very different from the average V_m determined in this paper for adherent cells (−42 mV) shortly after plating. Given the variability in the V_m values reported for suspended cells, and the unavoidable delays in measuring V_m after adherence, this study could not resolve whether or not there is a significant hyperpolarization of J774 cells immediately after plating. However, it does demonstrate that membrane potential was positively correlated with $G_{K,}$, that is, cells with larger $G_{K,}$ were more negative. $G_{K,}$ increased significantly with time after adherence, while G_L did not. We have no evidence that any other conductance was modulated following adherence. Thus, it is likely that the increase in $G_{K,}$ accounts for the observed increase in V_m. We cannot exclude the possibility that part of the hyperpolarization following adherence is due to an increase in the activity of an electrogenic Na^+/K^+ pump, which is known to contribute −7 and −11 mV to the resting membrane potential of mouse spleen macrophages (Gallin & Livengood, 1983) and human monocytes (Ince et al., 1987), respectively. Increased pump activity might also lead to changes in $[K]_i$ and thus E_K. Our value of E_K is derived from measurements of $[K]_i$ in suspended J774 cells (Melmed, Karanian & Berlin, 1981; Sung et al., 1985), and is approximately −90 mV. However, even if resting V_m was determined solely by E_K, $[K]_i$ would have to double to shift E_K sufficiently to account for the observed increase in V_m.

It is important to note that, although $G_{K,}$ and V_m are positively correlated in J774 cells under a wide variety of conditions, the fact that resting V_m is considerably more positive than our assumed valued for E_K indicates the presence of a depolarizing conductance, such as sodium (E_{Na} = +70 mV, Sung et al., 1985) or chloride (E_{Cl} = −23 mV, Melmed et al., 1981). In our previous studies of J774 cells (Gallin & Sheehy, 1985; Gallin & McKinney, 1988), where more negative resting V_m values were reported (−70 to −80 mV), the contribution of other conductances to resting V_m was probably underestimated. This was because we tended to record from larger, more spread cells, and to assume that more positive resting V_m values were due to cell damage. Although we do not know what the ionic composition of the leak conductance is at this time, further dissection of this current may explain why the resting V_m is more positive than E_K.

Protein synthesis inhibitors have been shown to block the adherence-induced expression of the surface antigen FMC17 (recently classified as CD14; Triglia et al., 1985) and the transient increase in the surface expression of Ia-antigen in human monocytes that occurs during the first 12 hr in culture (Smith & Ault, 1981). In our studies, the protein synthesis inhibitor cycloheximide did not block the initial (0 to 2 hr) expression of $G_{K,}$ in adherent cells, but did inhibit the subsequent increase in channel density that occurred 2 to 8 hr after adherence. Increases in V_m and C_m were also inhibited. Because we did not record from cells which had been plated in cycloheximide for >8 hr, it was not possible to evaluate whether or not the increase in $G_{K,}$ which had occurred by one day after adherence requires further protein synthesis. In addition, because the time course of expression of $G_{K,}$ in J774.1 cells was similar to the time course of expression of the FMC17 antigen in human monocytes, we tested the effect of an antibody to the FMC17 antigen on $G_{K,}$. However, no effects on whole-cell or single-channel K_i currents were observed.

Since 'primed' or 'activated' macrophages often exhibit increased spreading on surfaces (Pabst & Johnson, 1980) and since the degree of spreading in adherent J774.1 cells varied tremendously, it was also relevant to determine whether the membrane properties of very spread cells were different from those of nonspread cells. Spread cells had more negative resting membrane potentials than round

cells, both initially and one day after plating. Differences were also noted for the two groups of cells in their patterns of change after adherence. Only rounded cells increased G_K after adherence, and only spread cells increased capacitance. Thus, very spread cells inserted additional membrane area with time after adherence, but the increase in membrane area was not associated with a large increase in K_i channel density. The fact that G_K and capacitance varied independently of one another indicates that the increase in membrane area and expression of inwardly rectifying K channels were not necessarily linked. Final K_i channel density is determined by a balance between channel insertion or activation and channel internalization or inactivation. Our data do not differentiate between any of these processes.

The finding that spread cells did not show an increased density of K_i channels after adherence was consistent with the observation that exposing cells to LPS (which also increases cell spreading) did not increase the density of K_i channels. In fact, LPS-treated cells had significantly lower G_K values than control cells plated for comparable times. This is due in part to the increased capacitance of LPS-treated cells compared to controls, a result of the fact that LPS-treated cells are still growing, even though cell division has ceased.

Although the density of K_i channels in LPS-treated cells was lower than in control cells, resting V_m values were comparable. Clearly, there must be other differences between the two groups of cells to account for this result. Possible explanations are that LPS-treated cells have (*i*) a higher K permeability ratio (*ii*) a more negative E_K and/or (*iii*) increased electrogenic pump activity. However, like control cells, there was still a clear correlation between G_K and V_m in LPS-treated cells. Also, LPS-treated cells exhibited the same *increase* in K_i channel density, resting V_m, and capacitance following adherence as control cells did. Finally, in human monocytes, LPS has been reported to increase the percentage of cells expressing the transient outward K current (Jow & Nelson, 1989). In our studies, the K_{to} current was present in about 5% of the cells, but its expression was not increased by LPS.

In summary, the membrane properties of J774.1 cells change significantly after adherence, after exposure to LPS, and with cell morphology. Adherence is specifically correlated with increased K_i channel density, but only for rounded and not for spread cells. Spread cells rapidly increased their membrane area after adherence, but did not concomitantly increase K_i channel density. J774.1 cells treated for 24 hr with LPS were similar to spread cells in that they had increased capacitance but not increased K_i channel density compared to controls. G_K was positively correlated with V_m in both control and LPS-treated cells. Thus, the increase in G_K after adherence can account for the hyperpolarization which J774.1 cells undergo after plating, and an increase in surface membrane area is not necessarily linked to an increase in K_i channel density.

We thank Spencer Green for carrying out functional assays, Mr. William E. Jackson for advice on statistical analyses, and Ms. Jeanine Faw for maintaining cell cultures. Drs. Margaret Colden-Stanfield, David Livengood, and Joel Lowy critically reviewed the manuscript. Dr. Heddy Zola, Flinders Medical Center, Bedford Park, S. Australia, generously provided a sample of antibody to FMC17.

This work was supported by the Armed Forces Radiobiology Research Institute, Defense Nuclear Agency, under work unit 00020. Views presented in this paper are those of the authors; no endorsement by the Defense Nuclear Agency has been given or should be inferred.

References

Berton, G., Gordon, S. 1983. Superoxide release by peritoneal and bone marrow-derived mouse macrophages. Modulation by adherence and cell activation. *Immunology* **49**:693–704

Bodel, P.T., Nichols, B.A., Bainton, D.F. 1977. Appearance of peroxidase reactivity within the rough endoplasmic reticulum of blood monocytes after surface adherence. *J. Exp. Med.* **145**:264–274

Cohn, Z.A. 1978. The activation of mononuclear phagocytes: Fact, fancy, and future. *J. Immunol.* **121**:813–816

DeCoursey, T.E., Chandy, K.G., Gupta, S., Cahalan, M.D. 1987. Mitogen induction of ion channels in murine T lymphocytes. *J. Gen. Physiol.* **89**:405–420

Deutsch, C., Krause, D., Lee, S.C. 1986. Voltage-gated potassium conductance in human T lymphocytes stimulated with phorbol ester. *J. Physiol. (London)* **372**:405–423

Ehrenberg, G., Montana, V., Wei, M.D., Wuskell, J.P., Leow, L.M. 1988. Membrane potential can be determined in individual cells from the Nernstian distribution of cationic dyes. *Biophys. J.* **53**:785–794

Fuhlbrigge, R.C., Chaplin, D.D., Kiely, J.M., Unanue, E.R. 1987. Regulation of interleukin-1 gene expression by adherence and lipopolysaccharide. *J. Immunol.* **138**:3799–3802

Gallin, E.K. 1989. Evidence for a Ca-activated inwardly rectifying K channel in human macrophages. *Am. J. Physiol.* **257**:C77–C85

Gallin, E.K., Livengood, D.R. 1983. Demonstration of an electrogenic Na^+/K^+ pump in mouse spleen macrophages. *Am. J. Physiol.* **241**:C184–C188

Gallin, E.K., McKinney, L.C. 1988. Patch-clamp studies in human macrophages: Single-channel and whole-cell characterization of two K^+ conductances. *J. Membrane Biol.* **103**:55–66

Gallin, E.K., McKinney, L.C. 1989. Ion transport in phagocytes. *In:* Neutrophil Physiology. M.B. Hallett, editor. CRC Press, Boca Raton (FL)

Gallin, E.K., Sheehy, P.A. 1985. Differential expression of inward and outward potassium currents in the macrophage-like cell line J774.1. *J. Physiol. (London)* **369**:475–499

Gordon, S., Unkeless, J.C., Cohn, Z.A. 1974. Induction of macrophage plasminogen activator by endotoxin stimulation and phagocytosis. *J. Exp. Med.* **140**:995–1010

Haskill, S., Johnson, C., Eierman, D., Becker, S., Warren, K. 1988. Adherence induces selective mRNA expression of monocyte mediators and proto-oncogenes. *J. Immunol.* **140**:1690–1694

Ince, C., Thio, B., van Duijn, B., van Dissel, J.T., Ypey, D.L., Leijh, P.C.L. 1987. Intracellular K^+, Na^+, and Cl^- concentrations and membrane potential in human monocytes. *Biochim. Biophys. Acta* **905**:195–204

Jow, B., Nelson, D.J. 1989. Outwardly rectifying K^+ current as a marker of cellular activation in human macrophages. *Biophys. J.* **55**:539*a*

Karnovsky, M.L., Lazdins, J.K. 1978. Biochemical criteria for activated macrophages. *J. Immunol.* **121**:809–813

Kunkel, S.L., Duque, R.E. 1983. The macrophage adherence phenomenon: Its relationship to prostaglandin E_2 and superoxide anion production and changes in transmembrane potential. *Prostaglandins* **26**:893–901

Kurland, J.I., Bockman, R. 1978. Prostaglandin E production by human blood monocytes and mouse peritoneal macrophages. *J. Exp. Med.* **147**:952–957

McCaig, D.J., Berlin, R.B. 1983. Transmembrane potential of J774.2 mouse macrophage cells measured by microelectrode and ion distribution methods. *Experientia* **39**:906–907

McKinney, L.C., Gallin, E.K. 1988. Inwardly rectifying whole-cell and single-channel K currents in the murine macrophage cell line J774.1. *J. Membrane Biol.* **103**:41–53

Melmed, R.N., Karanian, P.J., Berlin, R.D. 1981. Control of cell volume in the J774 macrophage by microtubule disassembly and cyclic AMP. *J. Cell. Biol.* **90**:761–768

Midoux, P., Petit, C., Pellen, P., Toujas, L., Monsigny, M., Roche, A.-C. 1989. Macrophage antigens associated with adhesion: Identification by a monoclonal antibody specific for Lewis lung carcinoma cells. *Exp. Cell Res.* **183**:168–178

Morland, B., Kaplan, G. 1977. Macrophage activation in vivo and in vitro. *Exp. Cell Res.* **108**:279–288

Okada, M., Kishimoto, T., Igarashi, T., Teranishi, T., Yamamura, Y. 1978. LPS-or 8Br-cyclic AMP-induced production of T cell-activating factor(s) in macrophage tumor cell line J774.1. *J. Immunol.* **120**:1097–1101

Pabst, M.J., Hedegaard, H.B., Johnston, R.B., Jr. 1982. Cultured human monocytes require exposure to bacterial products to maintain an optimal oxygen radical response. *J. Immunol.* **128**:123–128

Pabst, M.J., Johnston, R.B. 1980. Increased production of superoxide anion by macrophages exposed to in vitro muramyl dipeptide or lipopolysaccharide. *J. Exp. Med.* **151**:101–114

Pofit, J.F., Strauss, P.R. 1977. Membrane transport by macrophages in suspension and adherent to glass. *J. Cell. Physiol.* **92**:249–256

Ralph, P., Nakoinz, I. 1977. Direct toxic effects of immunopotentiators on monocytic, myelomonocytic, and histiocytic or macrophage tumor cells in culture. *Cancer Res.* **37**:546–550.

Randriamampita, C., Trautmann, A. 1987. Ionic channels in murine macrophages. *J. Cell Biol.* **105**:761–769

Smith, B.R., Ault, K.A. 1981. Increase of surface Ia-like antigen expression on human monocytes independent of antigenic expression. *J. Immunol.* **127**:2020–2027

Steinman, R.M., Brodie, S.E., Cohn, Z.A. 1976. Membrane flow during pinocytosis. A stereologic analysis. *J. Cell Biol.* **68**:665–687

Sung, S.S., Young, J.D.E., Origlio, A.M., Heiple, J.M., Kaback, H.R., Silverstein, S.C. 1985. Extracellular ATP perturbs transmembrane ion fluxes, elevates cytosolic $[Ca^{2+}]$, and inhibits phagocytosis in mouse macrophages. *J. Biol. Chem.* **260**:13442–13449

Triglia, T., Burns, G.F., Werkmeister, J.A. 1985. Rapid changes in surface antigen expression by blood monocytes cultured in suspension of adherent to plastic. *Blood* **65**:921–928

Ypey, D.L., Clapham, D.E. 1984. Development of a delayed outward-rectifying K^+ conductance in cultured mouse peritoneal macrophages. *Proc. Natl. Acad. Sci. USA* **81**:3083–3087

Zabrenetzky, V., Gallin, E.K. 1988. Inositol 1,4,5-trisphosphate concentrations increase after adherence in the macrophage-like cell line J774.1. *Biochem J.* **255**:1037–1043

Zacharchuk, C.M., Drysdale, B.-E., Mayer, M.M., Shin, H.S. 1983. Macrophage-mediated cytotoxicity: Role of a soluble macrophage cyctotoxic factor similar to lymphotoxin and tumor necrosis factor. *Proc. Natl. Acad. Sci. USA* **80**:6341–6345

Received 28 August 1989; revised 2 January 1990

Volume 261, number 2, 353–357 FEBS 06170 February 1990

The formyl peptide chemoattractant receptor is encoded by a 2 kilobase messenger RNA

Expression in *Xenopus* oocytes

Philip M. Murphy, Elaine K. Gallin*, H. Lee Tiffany and Harry L. Malech

Bacterial Diseases Section, Laboratory of Clinical Investigation, National Institute of Allergy and Infectious Diseases, National Institutes of Health and **Department of Physiology, Armed Forces Radiobiology Research Institute, Bethesda, MD 20892, USA*

Received 19 December 1989; revised version received 8 January 1990

Activation of the formyl peptide chemoattractant receptor (FPCR) of phagocytic cells mobilizes intracellular calcium stores and affects the plasma membrane potential. Affinity crosslinking of FPCR has demonstrated a 60–80 kDa glycoprotein, with core peptide of 32 kDa. It is not known whether functional FPCR is this single peptide or requires multiple subunits. We used *Xenopus* oocyte expression system to determine the size of mRNA required for synthesis of functional FPCR. Injection of oocytes with poly(A)$^+$ RNA from HL60 cells differentiated to the granulocyte phenotype resulted in acquisition of formyl peptide-specific responses (inward transmembrane current with a reversal potential consistent with a chloride conductance, and calcium efflux). FPCR activity expressed in oocytes had a ligand concentration dependence, ligand structure dependence and pertussis toxin sensitivity similar to those reported in phagocytic cells. When RNA was size fractionated, a single peak of FPCR activity at 2 kilobases was observed after injection of mRNA into oocytes. Our data strongly suggest that FPCR is composed of a single-sized polypeptide.

Signal transduction; Chemoattractant receptor; *Xenopus* oocytes; Messenger ribonucleic acid; (HL60 cell)

1. INTRODUCTION

The migration of phagocytic cells from the blood to sites of infection is an essential component of host defense. This response is mediated by a number of chemoattractants including the bacterially derived formyl peptides which activate cell surface receptors that are functionally coupled to a guanine nucleotide binding regulatory protein (G-protein) [1]. Affinity labelling of the formyl peptide chemoattractant receptor (FPCR) yields a single-sized glycoprotein with relative molecular mass of 60–80 kDa. The unglycosylated core peptide is 32 kDa [2]. It is not known whether functional FPCR consists of this single affinity labelled peptide or requires additional subunits for activity.

The *Xenopus* oocyte protein expression system can be used to study heterologous G-protein coupled receptors [3,4]. We show that a phagocytic cell chemoattractant receptor, the FPCR, can be expressed in a functionally active form in *Xenopus* oocytes following injection of human myeloid cell RNA. Analysis of size fractionated RNA shows that the FPCR is encoded by a single 2 kb size class of mRNA, indicating that functional receptor likely is composed of only a single polypeptide chain.

Correspondence address: P.M. Murphy, Bldg 10, Room 11N 110, NIH, Bethesda, MD 20892, USA

Abbreviations: cpm, counts per minute; kb, kilobases or 1000 base pairs; kDa, kilodaltons; mRNA, messenger ribonucleic acid; rpm, revolutions per minute

2. MATERIALS AND METHODS

2.1. *Reagents*

Dibutyryl cyclic AMP, *N*-formyl methionyl-leucyl-phenylalanine (fMLP), *N*-formyl norleucyl-leucyl-phenylalanyl-norleucyl-tyrosyl-lysine (f-Nle-Leu-Phe-Nle-Tyr-Lys), methionyl-leucyl-phenylalanine (MLP), *t*-butoxycarbonyl-phenylalanine-leucine-phenylalanine-leucine-phenylalanine (t-Boc-Phe-Leu-Phe-Leu-Phe) and phenylalanine-leucine-glutamic acid-glutamic acid-valine (Phe-Leu-Glu-Glu-Val) were from Sigma, St. Louis, MO. $^{45}CaCl_2$ was from New England Nuclear, Boston, MA. Pertussis toxin was a gift from Dr Munoz of the Rocky Mountain Research Laboratories of NIAID.

2.2. *Preparation of polyadenylated RNA*

HL60 cells were expanded and differentiated with 0.5 mM dibutyryl cyclic AMP and tested for expression of FPCR as described [2]. Differentiated but not undifferentiated HL60 cell membranes contained FPCR. Polyadenylated RNA was prepared by published methods [5].

2.3. *Fractionation of mRNA*

Poly(A)$^+$ RNA (500 μg) from differentiated HL60 cells was centrifuged on a 5–30% sucrose gradient formed in STE buffer (STE = 10 mM Tris, 10 mM NaCl, 1 mM EDTA, pH 7.4) in an SW41 rotor (Beckman, Fullerton, CA) at 25000 rpm for 14 h at 4°C. Fractions 1–7 and 26–34 were 400 μl each; fractions 8–25 were 250 μl each. The RNA concentration was measured on an ethidium bromide-impregnated agarose plate containing serial dilutions of a standard RNA solution. RNA was then precipitated with ethanol and dissolved

Published by Elsevier Science Publishers B.V. (Biomedical Division)
00145793/90/$3.50

in water at 1 ng/nl. Blot hybridization of 200 ng of RNA from each fraction was performed using ^{32}P-labelled cDNA probes that recognize single transcripts from differentiated HL60 cells: PM1 is a 1.2 kb cDNA that recognizes a 1.2 kb transcript (Murphy and Malech, manuscript submitted). H64 (provided by Stuart Orkin) is a 2.5 kb restriction fragment of the cytochrome b_{558} large subunit cDNA that recognizes a 4.5 kb transcript [6].

2.4. *Whole cell current measurements*

The maintenance of *Xenopus laevis* (Nasco, Fort Atkinson, WI) and the harvesting and microinjection of oocytes were as previously described [4]. Oocytes were injected 1 day after harvesting. Individual oocytes were voltage clamped with an Axoclamp-2 amplifier (Axon, Burlingame, CA) using a standard two-electrode voltage clamp configuration. Electrodes were filled with 3 M KCl and had resistances of 5–15 MΩ. Unless otherwise noted, oocytes were clamped at the resting membrane potential, which ranged from −55 to −75 mV. Current-voltage (I–V) relationships were obtained using 3 s voltage steps to varying potentials.

2.5. *Calcium efflux assay*

This assay was performed essentially as described [4]. Preliminary studies indicated that >90% of stimulated $^{45}Ca^{2+}$ efflux occurred within 15 min of exposure to ligand. The ligand dependent response is reported as the mean ± SE of either the net $^{45}Ca^{2+}$ efflux, calculated as the difference between the cpm detected in the 15 min stimulated extracellular fluid and the cpm detected in the final wash before addition of ligand, or as % of control, calculated as 100 × (*15 min stimulated fluid cpm* ÷ *final wash cpm*). Both treatments of the data gave similar results in all cases. Residual $^{45}Ca^{2+}$ was counted in oocyte lysates after the stimulated extracellular fluid had been removed.

3. RESULTS

Fig.1 shows a representative voltage clamp analysis of oocytes injected with RNA or water, and stimulated with fMLP, control peptides or stock diluent DMSO.

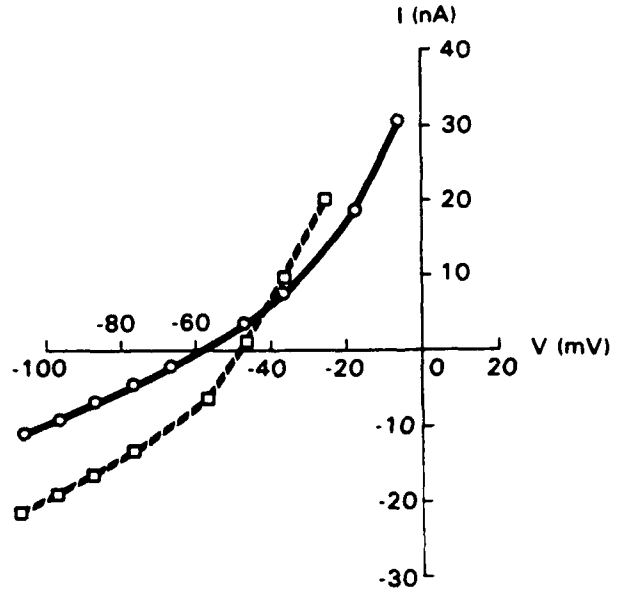

Fig.2. Current-voltage relationships obtained before (open circle, solid line) and during (open square, broken line) exposure to 10^{-6} M fMLP from an oocyte injected with differentiated HL60 cell RNA. Data are from the oocyte in fig.1C and are representative of 5 separate experiments.

When stimulated with fMLP, 15 of 16 oocytes injected with 50 ng of differentiated HL60 cell RNA 4 or more days prior to recording displayed an inward current response that oscillated initially and returned to baseline levels after washing the oocyte with media. The magnitude of the response for oocytes injected with 50 ng of poly(A)$^+$ RNA and stimulated with 10^{-7}

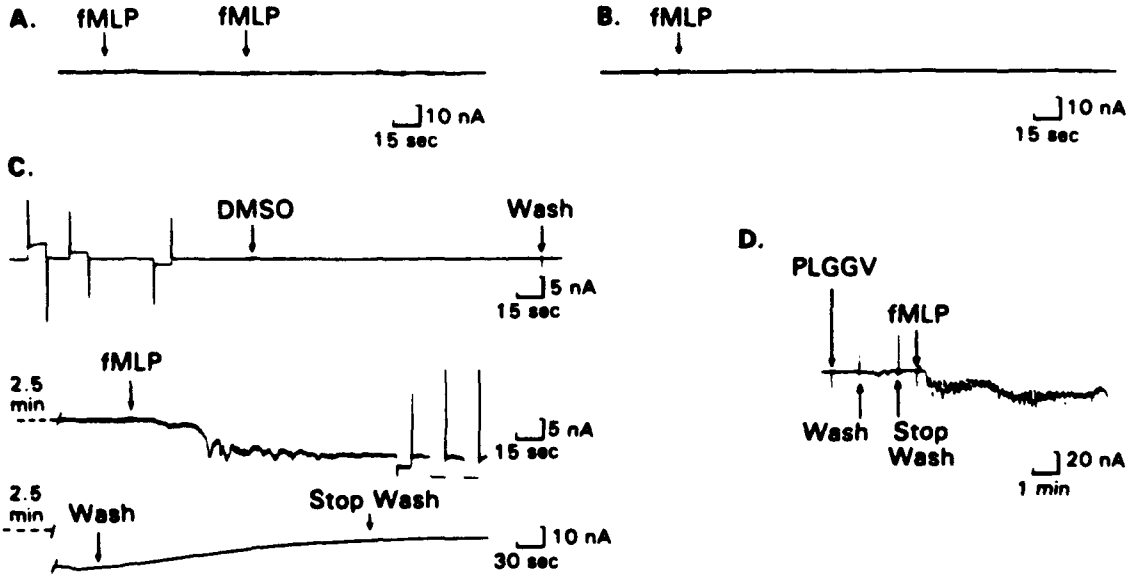

Fig.1. Acquired FPCR induced whole cell currents in *Xenopus* oocytes. Oocytes were injected with: (A) 50 nl of water (holding potential (V_h) = −75 mV). Arrows indicate the times of addition of 10^{-6} M fMLP; (B) 50 ng of poly(A)$^+$ RNA from undifferentiated HL60 cells (V_h = −56 mV). 10^{-6} M fMLP was added at arrow; (C) 50 ng of poly(A)$^+$ RNA from differentiated HL60 cells (V_h = −65 mV). DMSO 0.01% and 10^{-6} M fMLP were added where indicated. Current responses to voltage steps used to measure I–V relationships before and after addition of fMLP are shown; (D) 50 ng of fraction 12 (see fig.3) poly(A)$^+$ RNA from differentiated HL60 cells (V_h = −60 mV). Phe-Leu-Glu-Glu-Val (PLGGV) and fMLP were added at 3 × 10^{-7} M. Downward deflection indicates inward current.

or 10^{-6} M fMLP ranged from 5 to 50 nA. This response was not present in oocytes injected with water or with 50 ng of undifferentiated HL60 cell RNA, nor was it present with DMSO or with non-formylated peptides as stimuli. *N*-formylation of peptides is a structural requirement for activation of the FPCR [7].

The I–V relationship of the fMLP-stimulated response in an oocyte injected with differentiated HL60 poly(A)$^+$ RNA is shown in fig.2. The point of intersection of the two I–V curves generated before and during stimulation is the reversal potential (E_R) for the fMLP-induced current response. The average E_R for 5 different oocytes was -35 ± 4 mV, similar to the Nernst potential for chloride and is therefore most consistent with the activation of a chloride conductance [8].

Differentiated HL60 cell poly(A)$^+$ RNA was fractionated by size on a 5–30% sucrose gradient. The average size of RNA in these fractions increased progressively in each fraction indicating that it was structurally intact (fig.3A). Moreover, the RNA could be translated by reticulocyte lysate (not shown). Fig.3B shows that peak FPCR activity measured electrophysiologically in oocytes injected with RNA was confined to a single peak at fraction 11. The peak positions in the gradient fractionated RNA of HL60 cell transcripts of known size were established by blot hybridization with 2 cDNA probes described in section 2. Based on the position of FPCR activity peak relative to the physically defined size standards, we estimate the size of the RNA encoding FPCR activity to be 2 kb.

Because the FPCR is able to mobilize intracellularly sequestered calcium in phagocytic cells, we tested RNA-injected oocytes for acquired fMLP-dependent calcium mobilization by measuring the accelerated efflux of intracellular $^{45}Ca^{2+}$. FPCR activity appears 2 days after injection of active RNA, peaks at 4 days and is still detectable at least 7 days after injection of RNA.

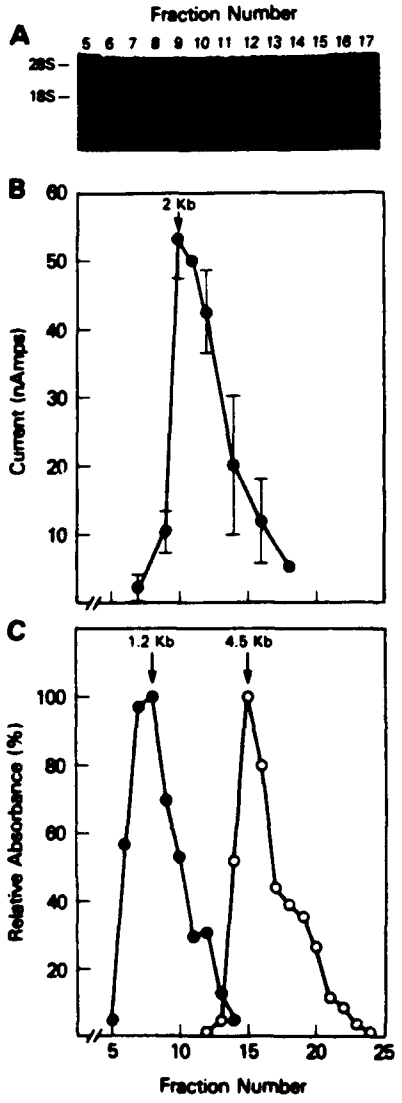

Fig.3. Size estimation of the mRNA encoding the FPCR electrogenic activity. (A) Structural integrity of sucrose gradient fractionated RNA. Poly(A)$^+$ RNA was electrophoresed on an ethidium bromide stained denaturing agarose gel. (B) FPCR activity of RNA fractions. Oocytes were injected with 50 ng of RNA from the indicated fractions and 4 days later were voltage clamped at -60 mV and tested with 10^{-6} M fMLP. Data are representative of 2 separate experiments and are expressed as the mean maximal current ± SE of 3–4 oocytes except for fractions 11 and 18 which were the mean of 2 oocytes. Fractions 5, 6, 21–31 contained no activity. (C) Sucrose gradient resolution of RNA by size. The abundance in each fraction of 2 defined transcripts from HL60 cells was determined by blot hybridization. Densitometric analysis of the autoradiographs is indicated in relative absorbance units.

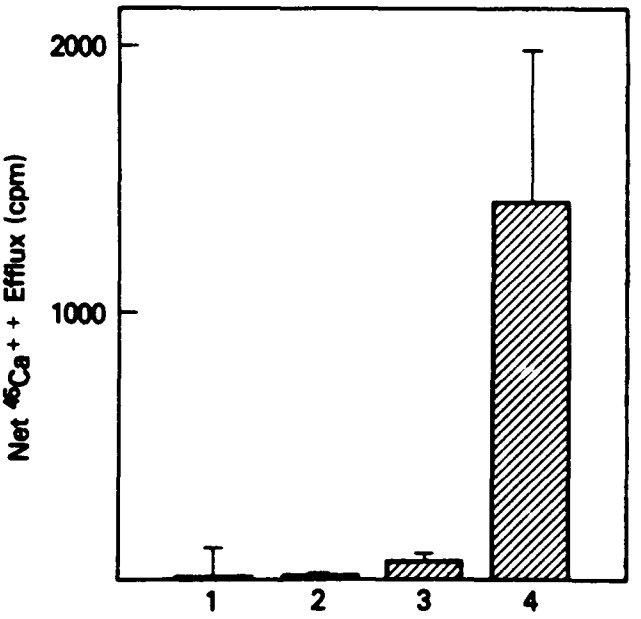

Fig.4. Enrichment of fMLP-dependent $^{45}Ca^{2+}$ efflux activity in size fractionated HL60 cell RNA. Oocytes received 50 nl of water (lane 1), 50 ng of unfractionated RNA from undifferentiated HL60 cells (lane 2) or differentiated HL60 cells (lane 3), or 50 ng of RNA from fraction 11 of sucrose gradient fractionated RNA from differentiated HL60 cells (lane 4) and were tested with 10^{-6} M fMLP 5 days later. Data are representative of 3 separate experiments and are from triplicate groups, 4 oocytes in each group.

The calcium response was linear for amounts of RNA injected from 3 to 50 ng (not shown). Oocytes injected with RNA from the same size fractions as those mediating the electrophysiologic responses to fMLP exhibit a greatly augmented calcium efflux response as compared to unfractionated RNA (fig.4).

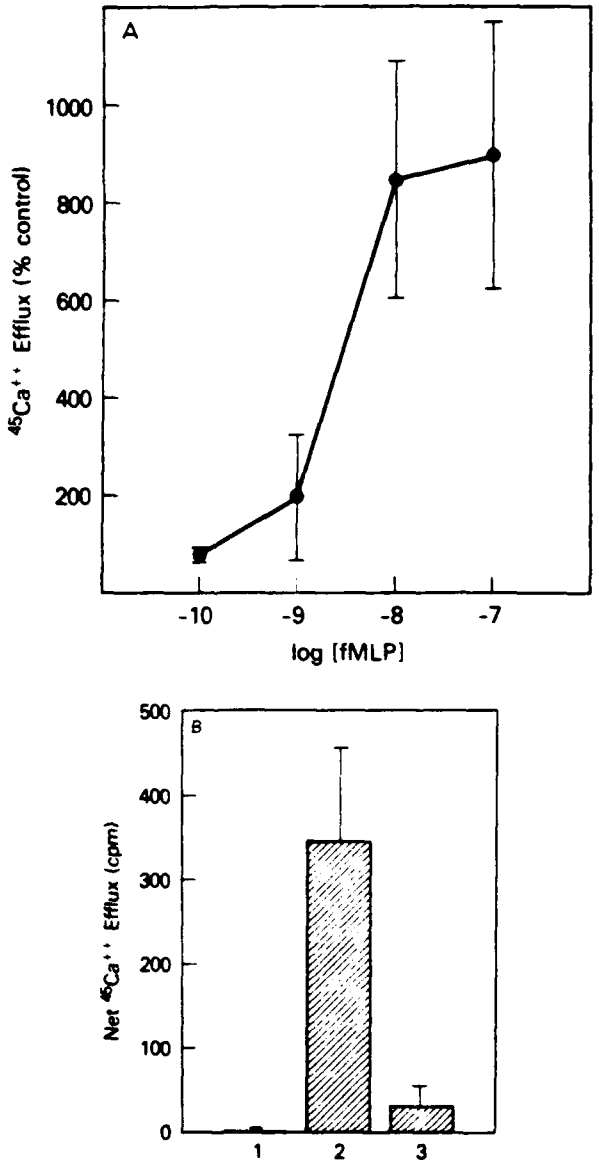

Fig.5. The FPCR calcium mobilizing activity is expressed in *Xenopus* oocytes in a physiologically faithful form. (A) Ligand concentration dependence. Oocytes were injected with 25 ng of fraction 11 RNA and were stimulated 4 days later. Data are representative of 2 separate experiments performed in triplicate, 3 oocytes per replicate. (B) Inhibition by pertussis toxin. Oocytes were injected with 50 nl of water (lane 1) or 25 ng of fraction 13 RNA (lanes 2 and 3). Five days after injection, pertussis toxin (2 μg/ml) was added to the media of half of the RNA injected oocytes (lane 3). One day later, oocytes were tested with 10^{-6} M fMLP. Data are representative of 4 separate experiments and are from 5 (lanes 2 and 3) or 3 (lane 1) replicates, 1 oocyte per replicate. Baseline $^{45}Ca^{2+}$ efflux between conditions differed by <2%.

We have used the calcium response to show that the physiologic properties of the heterologously expressed receptor are similar to those observed in phagocytic cells. Specifically, the ligand structure dependence is identical: non-formylated peptides such as Met-Leu-Phe, Phe-Leu-Glu-Glu-Val and t-BOC-Phe-Leu-Phe-Leu-Phe are inactive whereas fMLP and f-Nle-Leu-Phe-Nle-Tyr-Lys are active (not shown); the fMLP concentration dependence is similar to that previously reported for fMLP-stimulated calcium fluxes in human neutrophils (fig.5A) [9]; and the response is abolished by preincubation of oocytes with pertussis toxin (fig.5B). Pertussis toxin sensitivity could be partially reversed by incubating the toxin-treated oocytes in toxin-free media for an additional 24 h (data not shown).

4. DISCUSSION

These data demonstrate that FPCR can be expressed in a physiologically faithful form in *Xenopus* oocytes. All of the properties of active receptor are expressed after injection with RNA confined to a single sucrose gradient peak corresponding to a transcript size of 2 kb. Although it is possible that RNA encoding other signalling elements is contained in the 2 kb fraction, it has been demonstrated that the oocyte possesses native G-proteins and other more distal effector elements capable of transducing signals from heterologously expressed mammalian receptors [10]. Based on a 32 kDa unglycosylated form of the receptor that is seen by affinity crosslinking methods, a transcript containing a coding region of approximately 1 kb would be required. The data would therefore predict a combined length of 3′- and 5′-untranslated sequences of approximately 1 kb.

Our data also provide evidence that acquired FPCR transmembrane current activity in oocytes is due to activation of a chloride conductance. This raises the possibility that changes in the membrane potential of phagocytic cells stimulated with fMLP may also involve chloride conductance changes [11].

An additional implication of our study is that the oocyte expression system is a valid system for cloning cDNA encoding FPCR by the sib selection strategy, as has been done with other G-protein coupled receptors such as the serotonin-1c receptor [10]. We have recently extended this approach to examine the expression of other G-protein coupled chemoattractant receptors (manuscript in preparation). Our results suggest that this cloning strategy may also be feasible for receptors for C5a and platelet activating factor.

Acknowledgements: We thank Drs Tristram Bahnson and Daniel Rotrosen for helpful discussions. We especially thank Dr Rotrosen for performing the affinity labeling studies of HL60 cell membranes.

REFERENCES

[1] Snyderman, R., Smith, C.D. and Verghese, M.W. (1986) J. Leuk. Biol. 40, 785–800.

[2] Malech, H.L., Gardner, J.P., Heiman, D.F. and Rosenzweig, S.A. (1985) J. Biol. Chem. 260, 2509–2514.

[3] Kubo, T., Fukuda, K., Mikami, A., Maeda, A., Takahashi, H., Mishina, M., Haga, T., Haga, K., Ichiyama, A., Kangawa, K., Kojima, M., Matsuo, H., Hirose, T. and Numa, S. (1986) Nature 323, 411–416

[4] Williams, J.A., McChesney, D.J., Calayag, M.C., Lingappa, V.R. and Logsdon, C.D. (1988) Proc. Natl. Acad. Sci. USA 85, 4939–4943.

[5] Davis, L.G., Dibner, M.D. and Battey, J.F. (1986) Basic Methods in Molecular Biology, pp.129–139, Elsevier, Amsterdam.

[6] Royer-Pokora, B., Kunkel, L.M., Monaco, A.P., Goff, S.C., Newburger, P.E., Baehner, R.L., Cole, F.S., Curnutte, J.T. and Orkin, S.H. (1986) Nature 322, 32–38.

[7] Showell, H.J., Freer, R.J., Zigmond, S.H., Schiffmann, E., Aswanikumar, S., Corcoran, B.A. and Becker, E.L. (1976) J. Exp. Med. 143, 1154–1169.

[8] Kusano, K., Miledi, R. and Stinnakre, J. (1982) J. Physiol. 328, 143–170.

[9] Goldman, D.W., Gifford, L.A., Olson, D.M. and Goetzl, E.J. (1985) J. Immunol. 135, 525–530.

[10] Julius, D., MacDermott, A.B., Axel, R. and Jessell, T.M. (1988) Science 241, 558–564.

[11] Seligmann, B.E., Gallin, E.K., Martin, D.L., Shain, W. and Gallin, J.I. (1980) J. Membr. Biol. 52, 257–272.

Journal of Neuroscience Research 24:437–444 (1989)

Free Radicals Mediate Peroxidative Damage in Guinea Pig Hippocampus In Vitro

T.C. Pellmar, K.L. Neel, and K.H. Lee
Physiology Department, Armed Forces Radiobiology Research Institute, Bethesda, Maryland

Previous studies have shown that peroxide caused electrophysiological damage. The present study investigates the action of agents that interfere with a free radical process in an effort to define the mechanism of peroxide damage. Deferoxamine chelates iron, making it unavailable for the Fenton reaction and thereby preventing the formation of hydroxyl free radicals from peroxide. Dimethylsulfoxide (DMSO) scavenges hydroxyl free radicals. Trolox-C, a water soluble Vitamin E analog, is an antioxidant that can scavenge peroxy radicals. Slices of hippocampus were removed from brains of euthanized guinea pigs. Electrical stimulation of an orthodromic pathway to CA1 region evoked a synaptic response and a population spike. Input-output curves were generated to evaluate the protection by deferoxamine, Trolox-C, and DMSO on the synaptic damage and impaired spike generation caused by peroxide. Lipid peroxidation was measured by the thiobarbituric acid test. Peroxide was found to increase lipid peroxidation. Deferoxamine and Trolox-C protected against the peroxide-induced synaptic damage, impaired spike generation, and lipid peroxidation. DMSO was ineffective synaptically but reduced peroxide damage to spike generating mechanisms and further lipid peroxidation. The data support the hypothesis that peroxide causes damage through a free radical mechanism.

Key words: hydroxyl free radicals, hydrogen peroxide, lipid peroxidation, deferoxamine, Trolox-C, DMSO

INTRODUCTION

Hydrogen peroxide has been used as a model for free radical damage in a number of systems (Ward et al., 1985, Pellmar, 1986, 1987; Mello Filho et al., 1984; van der Zee et al., 1985). Using the hippocampal brain slice from guinea pigs, previous studies (Pellmar, 1986, 1987) revealed that peroxide decreases the synaptic field potential and the intracellularly recorded excitatory and inhibitory postsynaptic potentials. In addition, peroxide impairs the ability of the synaptic response to generate an action potential (Pellmar, 1986) and the ability of the cell to produce a train of action potentials (spike frequency potentiation) (Pellmar, 1987).

Hydrogen peroxide reacts with transition metals such as copper and iron to produce the very reactive hydroxyl free radical through the Fenton reaction. It is likely that generation of this oxygen radical is responsible for at least some of the damage caused by peroxide. The hydroxyl radical is a strong oxidant and an initiator of lipid peroxidation. The present study was designed to evaluate the free radical involvement in peroxidative damage to the hippocampus in vitro. The reagents we used were chosen to interfere with different steps in free radical damage: a) deferoxamine to chelate iron and render it inaccessible for the Fenton reaction (Graf et al., 1984); b) DMSO and thiourea to scavenge hydroxyl free radicals (Littlefield et al., 1988; Halliwell and Gutteridge, 1985; Reuvers et al., 1973; Chapman et al., 1973); and c) Trolox-C, an antioxidant, to provide protection, in part, by scavenging the peroxy radical (Doba et al., 1985; Niki, 1987; Halliwell and Gutteridge, 1985; Burton et al., 1985). The effectiveness of these protectants was evaluated on lipid peroxidation and on the electrophysiological deficits produced by hydrogen peroxide in hippocampal slices.

MATERIALS AND METHODS

Slices of hippocampus were prepared from brains of male Hartley guinea pigs as previously described (Pellmar, 1986, 1987). Animals were anesthetized with halothane and euthanized by cervical dislocation. The brain was quickly removed from the animal and chilled in iced artificial cerebrospinal fluid (aCSF) with the fol-

Received January 20, 1989; revised May 24, 1989; accepted May 25, 1989.

Address reprint requests to Dr. Terry C. Pellmar, Physiology Department, AFRRI, Bethesda, MD 20814-5145.

This paper was presented in part at the 18th Annual Meeting of the Society for Neuroscience, Toronto, November 13–18, 1988.

lowing composition (in mM): NaCl, 124; KCl, 3.0; $CaCl_2$, 2.4; $MgSO_4$, 1.3; KH_2PO_4, 1.24; glucose, 10; and $NaHCO_3$, 26; equilibrated with 95% O_2/5% CO_2. The hippocampus was then dissected bilaterally. Slices 400–450 μm thick were cut on a McIlwain tissue chopper and incubated at room temperature for at least an hour for both electrophysiology and lipid peroxidation experiments.

Deferoxamine (desferal, deferoxamine mesylate) was provided by CIBA Pharmaceutical Company. Trolox-C (Ro20-9747) was a gift from Hoffmann-La-Roche, Inc. Thiourea, dimethylsulfoxide (DMSO), trichloracetic acid, 2-thiobarbituric acid, and ethylenediaminetetraacetic acid (EDTA) were purchased from Sigma Chemical Co., St. Louis, MO. Malonaldehyde bis(dimethyl acetal) (MDA) was obtained from Aldrich Chemical Co., Milwaukee, WI. Hydrogen peroxide was diluted daily from a 50% stock solution from Fisher Scientific Co., Pittsburgh, PA.

Electrophysiology

A single hippocampal slice was placed in a submerged slice chamber for electrophysiological recordings. Artificial CSF (aCSF) at 30° ± 1°C and saturated with 95% O_2/5% CO_2 was continually perfused through the chamber at about 1 ml/min.

A bipolar stainless steel stimulating electrode (DKI) was positioned in the stratum radiatum to stimulate afferents to CA1 region of hippocampus. A glass recording electrode filled with 2 M NaCl was positioned in the stratum pyramidale of CA1 to record the population spike (somatic response). A second recording electrode was placed in the stratum radiatum to record the population postsynaptic potential (dendritic response, population PSP) and the afferent volley, the reflection of the number of afferent fibers firing. The PSP was quantitated by the initial slope of the potential since the evoked population spike frequently prevented measurement of the full amplitude. Constant current stimuli (0.1–1 mA, 200 μs) were applied to the stimulating electrode at 0.2 Hz. The resultant field potentials were recorded with high gain DC amplifiers and were digitized, stored, and analyzed on a PDP 11 computer.

Following placement of electrodes, field potentials were recorded for at least 30 min to ensure a stable preparation. Stimulus intensity was set to a level that produced approximately a half-maximal response and responses (at 0.2 Hz) were continually recorded to monitor the viability of the tissue. Input-output (I/O) curves were generated by varying the stimulus intensity from 0 to 1.0 mA. Curves were obtained first in aCSF. The protectant was then perfused through the chamber. Following a 30 min exposure, another I/O curve was generated. Hydrogen peroxide (0.005%) plus the protectant was then applied for another 30 min and a third I/O curve obtained.

The input-output curves consist of three relationships: 1) afferent volley vs. population PSP, 2) population PSP vs. population spike, and 3) afferent volley vs. population spike. A plot of the afferent volley vs. the population PSP reveals any change in the ability to produce a synaptic potential (synaptic damage). A plot of the population PSP vs. the amplitude of the population spike reveals any change in the ability of the synaptic potential to generate an action potential (spike generation damage). The plot of afferent volley vs. population spike reflects the composite of synaptic and postsynaptic damage.

The input-output curves were analyzed as described previously (Tolliver and Pellmar, 1987; Pellmar and Neel, 1989). In short, the response amplitudes recorded at each stimulus intensity were averaged for all experiments under each experimental condition. The average responses and their standard errors were used to construct the curves in Figures 1 and 2. A sigmoid curve was computer fit to the points. Differences between curves with and without peroxide were tested for significance by comparing the residual sum of squares for the individual curves with the residual sum of squares for the curve fit to all the points under both experimental conditions. Significance was accepted at $P<0.05$.

Lipid Peroxidation

Lipid peroxidation was evaluated through the thiobarbituric acid test as described by Kovachich and Mishra (1980). Slices from one hippocampus were divided into three groups: a) incubated in aCSF for 1 hr b) treated with protectant for 1 hr, and c) treated with protectant for 30 min followed by a 30 min exposure to 0.01% hydrogen peroxide in the presence of the protectant. These 1 hr incubations were done at 30° ± 1°C. At least three slices of hippocampus in each group were necessary to provide sufficient tissue for assay. Each experimental condition was tested at least ten times. After treatment, slices were blotted dry and weighed. Tissue was then homogenized in 1 ml of 20% trichloracetic acid with 0.5 mM EDTA. Thiobarbituric acid (0.67%) in 20 mM NaOH (2 ml) was added, the solution boiled for 10–15 min and then centrifuged for 10 min at 2,400 rpm. The absorbance was measured at 530 nm. Standards of 0.0 to 15 nmoles of malonaldehyde in 500 μl of aCSF containing 0.5 mM EDTA were treated as was the tissue.

To ensure that the protectants did not influence the measured MDA, standard curves were constructed in the presence of 20 μl of the reagents. This volume was the estimated maximum residual volume of aCSF in the tissue after blotting dry, based on wet weight vs. dry weight measurements for sample slices. Two to three

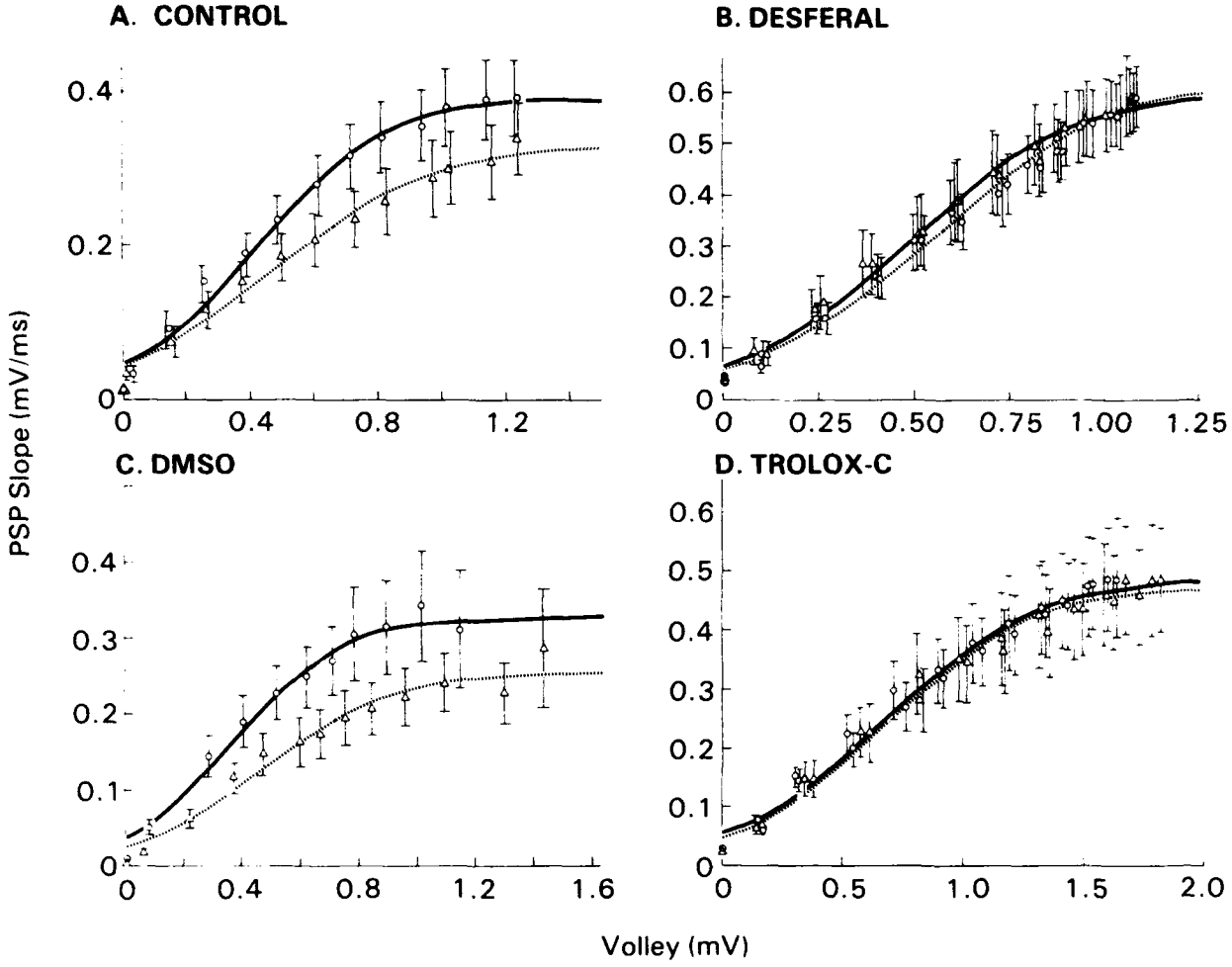

Fig. 1. Input/Output curves showing the effect of peroxide (0.005%) on the relationship of the afferent volley and the size of the synaptic potential (**A**) in the absence of any protectant (Control) and in the presence of (**B**) deferoxamine (1 mM), (**C**) DMSO (50 mM) or (**D**) Trolox-C (100 μM). Hydrogen peroxide severely decreases the ability of the afferent stimulation to evoke a synaptic potential. Deferoxamine and Trolox-C significantly protect against this damage. DMSO does not provide significant protection. None of the three protectants by themselves shifted these curves (not shown). In all graphs, solid lines (circles) show relationship before application of peroxide, with protectant present in B, C, and D. Dotted lines (triangles) show relationship following a 30 min exposure to 0.005% peroxide.

standard curves were constructed for each protectant and for each protectant plus peroxide. There was no significant influence of any of these agents on the standard curves.

RESULTS

Protectants on Electrophysiological Damage

Figure 1 illustrates the effects of deferoxamine, Trolox-C, and DMSO on the damage caused by 0.005% peroxide at the synaptic site. At the doses used these agents had no direct effects on this relationship. In the absence of any protectants (Control), peroxide reduced the ability of orthodromically stimulated afferent fibers to evoke a synaptic potential in the stratum radiatum. In Figure 1A, data from nine hippocampal slices were combined to produce the curves relating the afferent volley amplitude to the population PSP. A statistically significant change in the curve resulted from exposure to peroxide. In contrast, when peroxide was applied in the presence of 1 mM deferoxamine (desferal) (Fig. 1B), no significant shift in the control curve resulted ($n = 5$); deferoxamine protected against peroxide-induced synaptic damage. Similarly Trolox-C (100 μM), a water soluble analog of vitamin E, was very effective in preventing peroxide-induced synaptic damage ($n = 6$) (Fig. 1D). With Trolox-C present, the relationship of afferent volley to synaptic potential was not significantly shifted by per-

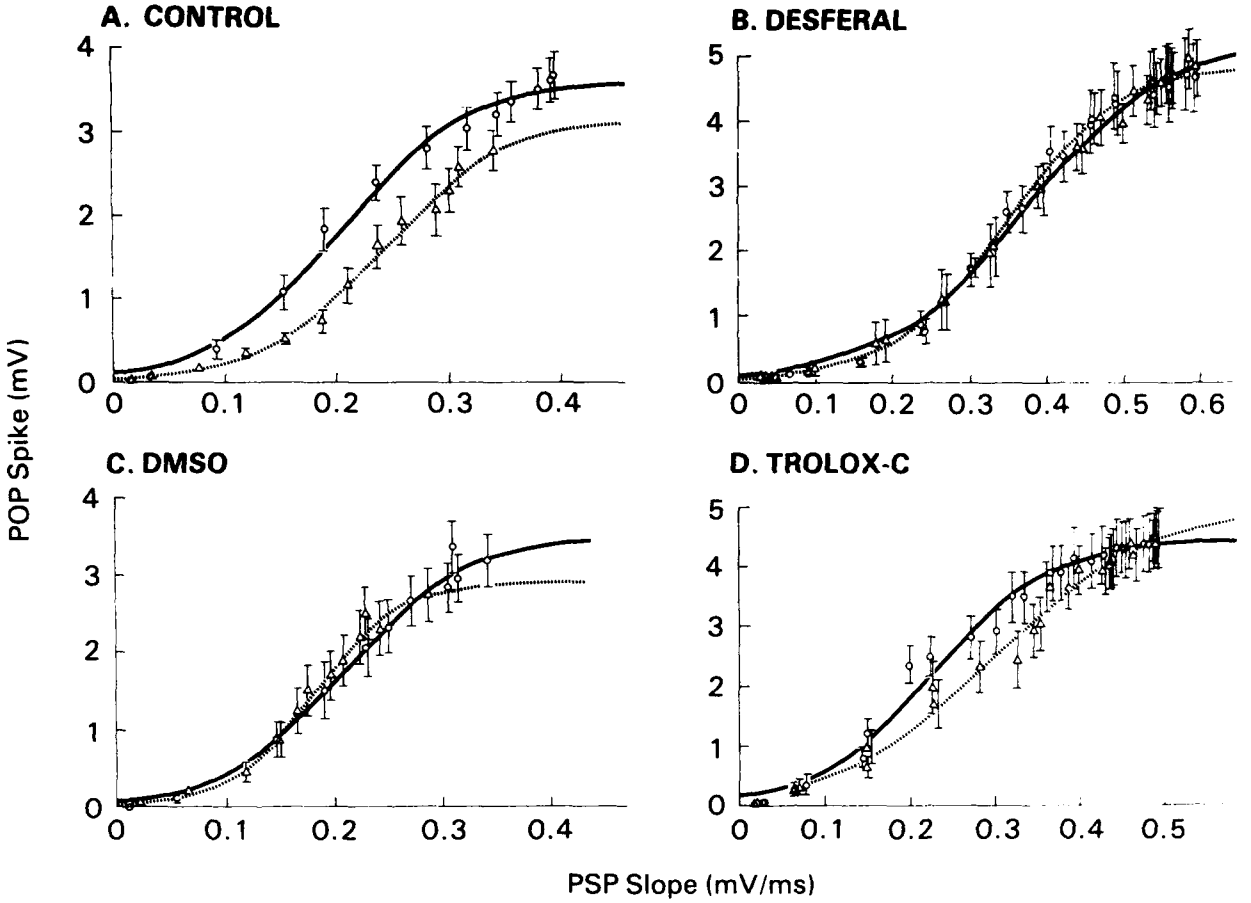

Fig. 2. Input-output curves showing the effect of peroxide (0.005%) on the relationship of the synaptic potential size to the amplitude of the population spike (**A**) in the absence of any protectant and in the presence of (**B**) deferoxamine (1 mM), (**C**) DMSO (50 mM) or (**D**) Trolox-C (100 μM). Hydrogen peroxide significantly reduced the ability of a synaptic potential to evoke a spike. All three protectants provided some protection from this damage. None of the three protectants by themselves shifted these curves (not shown). In all graphs solid lines (circles) show relationship before application of peroxide, with protectant present in B, C and D. Dotted lines (triangles) show relationship following a 30 min exposure to 0.005% peroxide.

oxide. In DMSO (0.36%, 50 mM) (Fig. 1C), however, peroxide produced at least as much synaptic damage as in the absence of any protectants (n = 7). Despite the presence of DMSO the curve was significantly shifted by addition of peroxide.

In addition to synaptic damage, peroxide has been previously shown to decrease the ability of the synaptic potential to evoke an action potential. This action can be seen in Figure 2A. Addition of peroxide produced a significant shift in the relationship between population PSP size and population spike amplitude. All three protectants afforded some degree of protection against this decrement, with no direct effect of their own on the I/O curve. Deferoxamine (n = 5) and DMSO (n = 7) prevented any significant shift in the ability of the synaptic potential to evoke a population spike with exposure to peroxide. In Trolox-C (n = 6) a reduction in population spike generation was still present but was substantially reduced compared to peroxide alone.

The ability of Trolox-C to protect against peroxide damage is illustrated in Figure 3. Five traces from the somatic and dendritic fields were computer averaged. Stimulus intensity was set to a level that produced approximately half-maximal amplitude of the population spike in the control recordings. It is clear that both the population spike (somatic) and the population synaptic potential (dendritic) are little changed by the presence of peroxide. This is in marked contrast to the decreases that occur in both responses in peroxide alone (see Fig. 5B and Pellmar, 1986).

A synopsis of the protective actions of the agents tested is shown in Figure 4. Differences between two

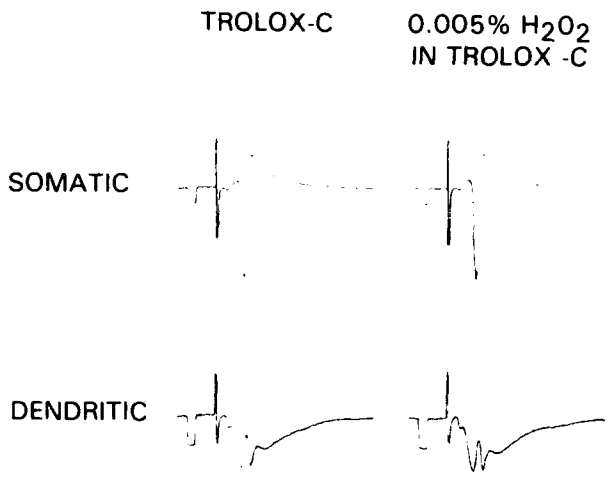

Fig. 3. Electrophysiological records (average of five traces) from stratum pyramidale (somatic) and from stratum radiatum (dendritic) of the CA1 region of hippocampus. Following treatment with 100 μM Trolox-C 0.005% peroxide had minimal effect on both the dendritic response (the population PSP) and the somatic response (population spike). Calibration pulse: 1 mV, 2 ms.

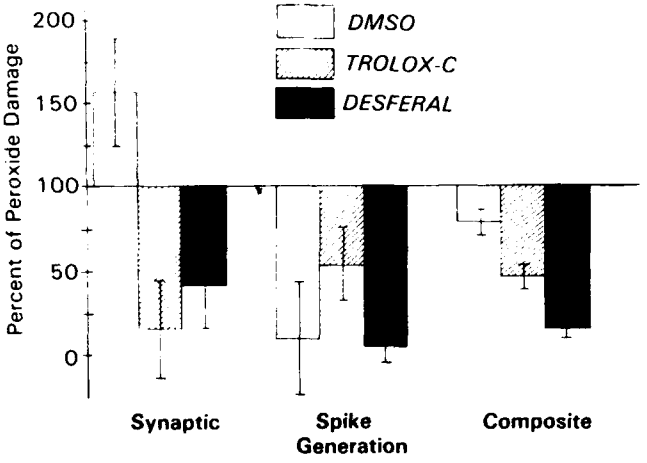

Fig. 4. Relative effects of DMSO, Trolox-C, and deferoxamine on the peroxide-induced decrease in the Population PSP (SYNAPTIC), reduction in the ability to generate an postsynaptic spike (SPIKE GENERATION), and the decreased orthodromic activation of a population spike (COMPOSITE), which combines both synaptic and spike generating deficits. Damage by peroxide in the absence of any protectant is considered to be 100%. Lower values suggest that there is less damage than with peroxide alone while higher values suggest a greater degree of damage. All three protectants were effective on the composite damage and on spike generation. DMSO was not protective against peroxide damage on the synaptic response.

computer-fitted curves can be estimated by comparing the ratio of parameters describing the curves (maximum y value/ x value at half-maximal y value) before and during exposure to peroxide, as described previously (Tolliver and Pellmar, 1987). The change in the curves in the absence of any protectant was set to 100%; the change in the curves in the presence of protectant would be less than that if the peroxide-induced damage was reduced. It can be clearly seen in Figure 4 that all three of the protectants reduce the composite damage produced by peroxide. Deferoxamine was the most effective, allowing only 16% of the damage produced by peroxide alone. DMSO was the least effective, allowing 79% of the unprotected damage. The relative ineffectiveness of DMSO results from its inability to protect at the synaptic site. If anything, the synaptic damage was greater in the presence of DMSO than in its absence, although this was not statistically significant. All three agents improved spike generation damage from peroxide. Trolox-C was least effective. In Trolox-C, peroxide damage was 54% of the unprotected damage while in DMSO and deferoxamine damage was only 5–10% of peroxide control.

Neither deferoxamine, Trolox-C nor DMSO affected the electrophysiological responses in the absence of peroxide (data not shown). In contrast, thiourea did have direct effects on the orthodromically evoked responses. This prevented a comprehensive study of thiourea using input-output curves. Instead, the amplitude of the half-maximal response was monitored for 30 min in thiourea followed by another 30 min in thiourea plus peroxide.

Thiourea (0.5 mM) also afforded some protection from peroxide damage although exposure to this dose of the scavenger caused the population spike to gradually increase with time (Fig. 5A) ($n = 12$). If an estimate is made by extrapolation of the size the population spike would be 30 min after initiation of application of peroxide, one can observe that the decrement with hydrogen peroxide is less than that seen without the scavenger ($n = 10$). Since the protection was incomplete, 5 mM thiourea was tested ($n = 6$). This dose, however, directly decreased the population spike and was not tested in combination with peroxide. Figure 5B illustrates sample traces of the population spike (average of four) with and without thiourea. In the presence of thiourea (0.5 mM) the amplitude of the population spike is about the same 30 min after exposure to peroxide as it was in the control period. This is somewhat misleading since thiourea was, by itself, increasing the population spike amplitude. In contrast, however, peroxide in the absence of any protectant caused a significant reduction in the population spike ($n = 10$).

Protectants on Lipid Peroxidation

Peroxide has been hypothesized to exert its action on hippocampal neurons, at least in part, through peroxidation of the cell's lipid membranes [Pellmar, 1986,

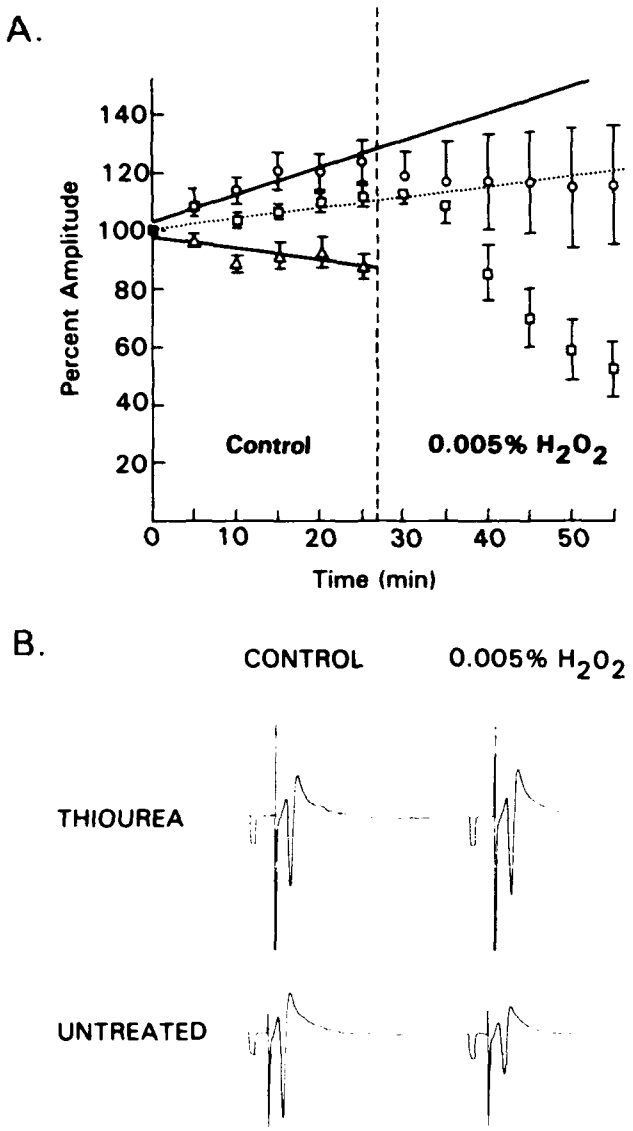

Fig. 5. Thiourea at a dose of 0.5 mM provided some protection from peroxide damage. Orthodromic pathway in CA1 region of hippocampus was stimulated at a frequency of 0.5 Hz, using a stimulus strength that evoked a half-maximal amplitude population spike. Population spike was recorded in stratum pyramidale. Four traces were averaged every 5 min throughout the experiment. **A**. The amplitude relative to the size of the response at time zero is plotted here. Data were collected for 30 min either with thiourea at the doses indicated (circles and triangles, solid lines) or in the absence of any protectant (squares, dotted line). Peroxide (0.005%) was added at the time point indicated by the vertical dashed line. 0.5 mM thiourea (circles) caused a gradual increase in the amplitude of the population spike while higher doses such as 5 mM (triangles) caused a gradual decrease in the amplitude of the population spike. The reduction in the population spike produced by peroxide in the absence of thiourea was greater than the decrease seen in the presence of 0.5 mM thiourea even when the gradual growth of the response is taken into account (extrapolated lines). **B**. Sample electrophysiological records. The population spike was minimally affected when 0.005% peroxide was applied in the presence of thiourea but was substantially decreased when thiourea was not present (untreated). Calibration pulse: 1 mV, 2 ms.

1987]. Using the thiobarbituric acid test for MDA, we found evidence for lipid peroxidation with 0.01% hydrogen peroxide (Table I). Resting level of MDA was 119.43 ± 6.66 nmoles/mg wet weight. Following a 30 min incubation with peroxide the levels increased to 145.04 ± 7.81 nmoles/mg. The actions of DMSO, Trolox-C, and deferoxamine were evaluated on peroxide-induced lipid peroxidation. Tissue was pretreated with protectants for 30 min followed by a 30 min exposure to peroxide. As a control, tissue was also exposed to the protectants for 1 hr to evaluate any direct effects of the protectant on the tissue. Deferoxamine and Trolox-C were capable of preventing the peroxide-induced change in MDA without causing any direct effects (Table I). DMSO also effectively prevented any peroxide-induced changes but itself increased the measured MDA.

DISCUSSION

The data indicate that free radical scavengers can provide protection from peroxidative damage. Both deferoxamine, the iron chelator, and the antioxidant Trolox-C were effective electrophysiologically at the synaptic and spike generating sites and prevented lipid peroxidation. The hydroxyl radical scavenger DMSO effectively prevented both the reduction in spike generation and the increased lipid peroxidation but not the synaptic damage. While the free radical scavenger thiourea was protective, its effects were difficult to interpret due to its direct actions.

Deferoxamine is a very effective iron chelator that can make the metal completely inaccessible for Fenton chemistry (Graf et al., 1984). The nearly complete protection from peroxide damage with deferoxamine strongly suggests iron involvement. This implies that the Fenton reaction is required and therefore it is reasonable to postulate that hydroxyl radicals are mediating the damage. The source of the iron is unclear. While no iron was added to the solution, it is a common contaminant of commercially available compounds [Halliwell and Gutteridge, 1985; Wong et al., 1981]. Free cellular iron is likely to be present in negligible concentrations, but iron chelates of citrate and ATP are available for reaction with peroxide. Several iron binding proteins are also likely to be present in the tissue: hemoglobin and transferrin from residual blood and ferritin intracellularly. These proteins can, under certain conditions, release

TABLE I. Effect of Protectants on Malonaldehyde Levels in Hippocampus[†]

Treatment	N	Untreated	Drug alone	Drug + peroxide
Control	12	119.43 ± 6.66		145.04 ± 7.81*
Desferal	10	127.69 ± 5.36	129.51 ± 9.47	121.93 ± 8.94
Trolox-C	10	118.46 ± 5.34	119.18 ± 5.83	99.72 ± 6.59
DMSO	10	129.12 ± 4.87	145.02 ± 5.43*	139.54 ± 3.17*

[†]Malonaldehyde was measured by the thiobarbituric acid test and standardized by tissue wet weight (nmoles MDA/mg wet weight). Values are the average of N preparations ± SEM. Slices from one animal were divided into three groups: untreated incubated for 1 hr (untreated), treated with the test drug alone for 1 hr (drug alone), and treated with the test drug for 30 min followed by treatment with the test drug and 0.01% peroxide for 30 min (drug + peroxide).

*Statistically significant difference from paired, untreated tissue; paired t test, $P<0.05$.

their iron and promote free radical reactions (Halliwell and Gutteridge, 1984, 1985; Aust, 1988).

Although DMSO is an effective hydroxyl radical scavenger (Reuvers et al., 1973; Chapman et al., 1973; Littlefield et al., 1988), it only protected spike generation but not synaptic potentials from peroxide damage. Yet the results with desferal suggest that hydroxyl radicals are involved in both mechanisms. Since hydroxyl radicals are so reactive, they do not diffuse far. Therefore, interaction of peroxide with iron is likely to cause damage near the metal binding site. Although distribution of DMSO may be fairly uniform throughout the cell, hydroxyl radical production is more likely to be site specific (Chevion, 1988). As a consequence, DMSO might be available in a sufficient concentration to scavenge all the hydroxyl radicals at one site while at another site, the concentration may be inadequate. In addition, steric limitations may prevent access by the scavenger more at one location than another (Chevion, 1988). A differential effect of DMSO on synaptic and spike generating mechanisms therefore may be the result of the nonuniform distribution of iron.

Trolox-C, a vitamin E analog, prevented both the decrease in the synaptic potential and the generation of action potentials caused by peroxide. It is well established that vitamin E scavenges the peroxy radical in the lipid membrane that occurs with the initiation of lipid peroxidation (Doba et al., 1985; Halliwell and Gutteridge, 1985; Burton et al., 1985; Niki, 1987). Doba et al. (1985) suggest that Trolox-C, despite its water solubility, is sufficiently lipophilic to penetrate and traverse lipid bilayers and to scavenge the lipid soluble peroxy radical. Other mechanisms of action for Vitamin E have also been hypothesized. For example, Pascoe et al. (1987) suggested that Vitamin E is effective in chemical toxicity by maintaining levels of cellular protein thiols such as glutathione. It is possible that Trolox-C provides protection against impaired spike generation and synaptic damage through two distinct mechanisms.

Peroxide impairs spike generation and synaptic transmission through a free radical mechanism. The actions of the iron chelator deferoxamine suggest that hydroxyl radicals are likely to be the initiator for both sites of damage. Yet the mechanisms of action of the radicals at the two sites are likely to be distinct. ^{60}Cobalt radiation, like peroxide, produces both spike generation and synaptic damage (Tolliver and Pellmar, 1987). Spike generation damage did not show dose-rate dependence which is consistent with a lipid peroxidation mechanism. The observation that DMSO prevents impairment of spike generation and lipid peroxidation, but not synaptic damage, strengthens this correlation. Synaptic damage from gamma radiation was sensitive to dose-rate suggesting a distinct mechanism. Synaptic damage from peroxide and radiation might be due to an oxidation of membrane proteins. Protein oxidizing agents, chloramine-T and n-chlorosuccinimide, produced only synaptic damage, and did not impair the spike generation (Pellmar and Neel, 1989) nor induce lipid peroxidation (Pellmar and Lee, unpublished data). In conclusion, the data suggest that peroxide reduces synaptic potentials and impairs postsynaptic generation of action potentials through two distinct free radical mechanisms.

ACKNOWLEDGMENTS

This work was supported by the Armed Forces Radiobiology Research Institute, Defense Nuclear Agency, under work unit 00105. Views presented in this paper are those of the authors; no endorsement by the Defense Nuclear Agency has been given or should be inferred. Research was conducted according to the principles enunciated in the "Guide for the Care and Use of Laboratory Animals" prepared by the Institute of Laboratory Animal Resources, National Research Council.

REFERENCES

Aust SD (1988): Sources of iron for lipid peroxidation in biological systems. In "Oxygen Radicals and Tissue Injury," Proceedings of Upjohn Symposium, FASEB, Bethesda, pp 27–33.

Burton GW, Foster DO, Perly B, Slater TF, Smith ICP, Ingold KU

(1985): Biological antioxidants. Phil Trans R Soc Lond B 311: 565–578.

Chapman JD, Reuvers AP, Borsa J, Greenstock DL (1973): Chemical radioprotection and radiosensitization of mammalian cells growing in vitro. Radiation Res 56:291–306.

Chevion M (1988): A site specific mechanism for free radical induced biological damage: the essential role of redox-active transition metals. Free Radical Biol Med 5:27–37.

Doba T, Burton GW, Ingold KU (1985): Antioxidant and co-antioxidant activity of vitamin C. The effect of vitamin C, either alone or in the presence of vitamin E or a water-soluble vitamin E analogue, upon the peroxidation of aqueous multilamellar phospholipid liposomes. Biochim Biophys Acta 835:298–303.

Graf E, Mahoney JR, Bryant RG, Eaton JW (1984): Iron-catalyzed hydroxyl radical formation. Stringent requirement for free iron coordination site. J Biol Chem 259:3620–3624.

Halliwell B, Gutteridge JMC (1985): "Free Radicals in Biology and Medicine." Oxford: Clarendon Press.

Halliwell B, Gutteridge JMC (1984): Oxygen toxicity, oxygen radicals, transition metals and disease. Biochem J 219:1–14.

Kovachich GB, Mishra OP (1980): Lipid peroxidation in rat brain cortical slices as measured by the thiobarbituric acid test. J Neurochem 35:1449–1452.

Littlefield LG, Joiner EE, Colyer SP, Sayer AM, Fromes EL (1988): Modulation of radiation-induced chromosome aberrations by DMSO, an OH radical scavenger. 1: Dose-response studies in human lymphocytes exposed to 220 kV X-rays. Int J Radiat Biol 53:875–890.

Mello Filho AC, Hoffmann ME, Meneghini R (1984): Cell killing and DNA damage by hydrogen peroxide are mediated by intracellular iron. Biochem J 218:273–275.

Niki E (1987): Antioxidants in relation to lipid peroxidation. Chem Physics Lipids 44:227–253.

Pascoe GA, Olafsdotter K, Reed DJ (1987): Vitamin E protection against chemical-induced cell injury I. Maintenance of cellular protein thiols as a cytoprotective mechanism. Arch Biochem Biophys 256:150–158.

Pellmar T (1986): Electrophysiological correlates of peroxide damage in guinea pig hippocampus in vitro. Brain Res 364:377–381.

Pellmar TC (1987): Peroxide alters neuronal excitability in the CA1 region of guinea-pig hippocampus in vitro. Neuroscience 23: 447–456.

Pellmar TC, Neel KL (1989): Oxidative damage in the guinea pig hippocampal slice. Free Rad Biol Med 6:467–472.

Reuvers AP, Greenstock CL, Borsa J, Chapman JD (1973): Studies on the mechanism of chemical radioprotection by dimethyl sulphoxide. Int J Rad Biol 24:533–536.

Tolliver JM, Pellmar TC (1987): Ionizing radiation alters neuronal excitability in hippocampal slices of the guinea pig. Radiation Res 112:555–563.

Van der Zee J, Dubbleman TMAR, van Steveninck J (1985): Peroxide-induced membrane damage in human erythrocytes. Biochim Biophys Acta 818:38–44.

Ward J, Blakely W, Joner E (1985): Mammalian cells are not killed by DNA strand breaks caused by hydroxyl radicals from hydrogen peroxide. Radiation Res 103:383–392.

Wong SF, Halliwell B, Richmond R, Skowroneck WR (1981): The role of superoxide and hydroxyl radicals in the degradation of hyaluronic acid induced by metal ions and by ascorbic acid. J Inorg Biochem 14:127–134.

RADIATION RESEARCH 121, 220–226 (1990)

Radioprotection of Mice with Interleukin-1: Relationship to the Number of Erythroid and Granulocyte-Macrophage Colony-Forming Cells[1]

GRETCHEN N. SCHWARTZ,*[,2] MYRA L. PATCHEN,† RUTH NETA,† AND THOMAS J. MACVITTIE†

*Transplantation Laboratory, American Red Cross, Rockville, Maryland 20855; and †Experimental Hematology Department, Armed Forces Radiobiology Research Institute, Navy Medical Command, National Capital Region, Bethesda, Maryland 20814

SCHWARTZ, G. N., PATCHEN, M. L., NETA, R., AND MACVITTIE, T. J. Radioprotection of Mice with Interleukin-1: Relationship to the Number of Erythroid and Granulocyte-Macrophage Colony-Forming Cells. *Radiat. Res.* 121, 220–226 (1990).

This report presents the results of an investigation of changes in the number of erythroid and granulocyte-macrophage colony-forming cells (GM-CFC) that had occurred in tissues of normal B6D2F1 mice 20 h after administration of a radioprotective dose (150 ng) of human recombinant interleukin-1 (rIL-1). Neutrophilia in the peripheral blood and changes in the tissue distribution of GM-CFC demonstrated that cells were mobilized from the bone marrow in response to rIL-1 injection. For example, 20 h after rIL-1 injection marrow GM-CFC numbers were 80% of the numbers in bone marrow from saline-injected mice. Associated with this decrease there was a twofold increase in the number of peripheral blood and splenic GM-CFC. Also, as determined by hydroxyurea injection, there was an increase in the number of GM-CFC in S phase of the cell cycle in the spleen, but not in the bone marrow. Data in this report suggest that when compared to the spleen, stimulation of granulopoiesis after rIL-1 injection is delayed in the bone marrow. Also, the earlier recovery of GM-CFC in the bone marrow of irradiated mice is not dependent upon an increase in the number of GM-CFC at the time of irradiation.

INTRODUCTION

An increase in the number of mice surviving lethal doses of radiation was observed when mice had been administered a single injection of recombinant interleukin-1 (rIL-1)[3] 18–24 h prior to their irradiation (*1*). Also, there was an earlier recovery of hematopoietic colony-forming cells (CFC) in the bone marrow and spleens from mice exposed to sublethal doses of radiation after rIL-1 injection (*2–6*). The physiological mechanisms promoting the earlier hematopoietic recovery in mice injected with rIL-1 are not well understood. Previous studies demonstrated that the earlier recovery of CFC was not dependent upon an increase in the number of spleen colony-forming units (CFU-S) or in the percentage of CFU-S in S phase of the cell cycle at the time of irradiation (*3–5, 7*).

An increase in colony-stimulating activity (CSA) for granulocyte-macrophage colony-forming cells (GM-CFC), erythroid burst-forming units (BFU-E), and multipotential colony-forming units has been observed in cultures of fibroblasts, endothelial cells, bone marrow stromal cells, or fetal liver stromal cell lines after stimulation with rIL-1 (*8–12*). The increased levels of CSA were partially due to an rIL-1 dose-dependent increase in the production of granulocyte-macrophage and granulocyte colony-forming factors and interleukin-6 (*10–12*). Elevated levels of CSA for GM-CFC also occurred *in vivo* after administration of rIL-1 (*13–14*). Several studies demonstrated that shortly after inducing the production of CSA, rIL-1 injection stimulated granulopoiesis in the bone marrow of normal mice (*13–16*). Neta *et al.* (*16*) suggested that the radioprotective effects of rIL-1 injection may be associated with an increase in the number of cycling CFC at the time of irradiation.

In previous studies it was found that in mice irradiated after rIL-1 injection there was an earlier recovery of GM-CFC in the bone marrow (*3, 4*). Studies in the present report were performed to investigate rIL-1-induced changes in CFC numbers in tissues of mice prior to their irradiation that might further delineate possible mechanisms for the observed earlier hematopoietic recovery. Specifically, the numbers of GM-CFC, erythroid colony-forming units

[1] Views presented in this paper are those of the authors; no endorsement by the Defense Nuclear Agency has been given or should be inferred. This research was supported by the Armed Forces Radiobiology Research Institute, Defense Nuclear Agency under Research Units 00132 and 03147 and NIH Grant No. BSRG 2 S07 RR05737.

[2] To whom correspondence and reprint requests should be addressed at Transplantation Laboratory, Biomedical Research and Development, The Jerome H. Holland Laboratory, 15601 Crabbs Branch Way, Rockville, MD 20855.

[3] Abbreviations used: rIL-1, recombinant interleukin-1; CFC, colony-forming cells; CFU-S, spleen colony-forming units; CSA, colony-stimulating activity; GM-CFC, granulocyte-macrophage colony-forming cells; BFU-E, erythroid burst-forming units; CFU-E, erythroid colony-forming units.

0033-7587/90 $3.00

(CFU-E), and BFU-E in bone marrow or spleen were determined in mice 20 h after saline or rIL-1 injection. The decrease in GM-CFC, CFU-E, and BFU-E after hydroxyurea injection was used to measure the proportion of CFC in S phase of the cell cycle.

MATERIALS AND METHODS

Mice

B6D2F1, or (C57B1/6J × DBA/2)F1, female mice were purchased from Jackson Laboratories (Bar Harbor, ME). Upon arrival, mice were maintained in an AAALAC-accredited facility. They were housed 10 per cage in plastic microisolator cages on hardwood-chip contact bedding, and were allowed food (Wayne Rodent Blox) and HCl-acidified water (pH 2.4) *ad libitum*. Animal holding rooms were maintained at 70 ± 2°F and 50 ± 10% relative humidity using at least 10 air changes per hour of 100% conditioned fresh air and exposed to full-spectrum light from 6:00 AM to 6:00 PM. Upon arrival, mice were tested for *Pseudomonas* contamination and quarantined until test results were obtained. Only healthy mice were released for experimentation. Twelve to 16-week-old mice were used for these studies. Research was conducted according to the principles enunciated in the "Guide for the Care and Use of Laboratory Animals" prepared by the Institute of Laboratory Animal Resources, National Research Council.

Irradiation

Twenty hours after saline or rIL-1 injection, mice were placed in ventilated Plexiglas boxes and exposed bilaterally to γ radiation from a ^{60}Co radiation source. In radiation studies, mice were exposed to 6.5, 1.0, or 0.5 Gy total-body irradiation at a dose rate of 0.40 Gy/min 20 h after saline or rIL-1 injection.

Treatment with Interleukin-1

Purified human rIL-1 alpha, a generous gift from Dr. Steve Gillis of Immunex (Seattle, WA), was used in these studies. The rIL-1 was supplied in a solution of phosphate-buffered saline at pH 7.2 with a specific activity of 7.5 × 10^6 U IL-1/mg protein, and aliquots were maintained at −70°C. Immediately before use, stock solutions of rIL-1 were diluted with pyrogen-free saline (McGaw), and 150 ng/0.5 ml was administered to normal mice by intraperitoneal (i.p.) injection. Mean body weight of mice used in these studies was 27 ± 2 g so that the average dose of rIL-1 was approximately 5.6 μg/kg body weight. Control animals were given 0.5 ml saline at the same time. Endotoxin (LPS) contamination in rIL-1 stock solutions was measured by the *Limulus* lysate assay. Based on these results less than 0.2 ng of LPS was administered per injection. The number of mice surviving >30 days after 10.5 Gy irradiation was similar for noninjected mice (1/10), saline-injected mice (1/10), and mice injected with 150 ng heat-inactivated rIL-1 (1/10). Also, data in an earlier report demonstrated that 150 ng rIL-1 from the same stock solutions as used in the present studies increased the number of B6D2F1 mice that survived after 10.5-Gy irradiation from 7 ± 13% to 85 ± 7% (*4*).

Preparation of Cell Suspensions

Peripheral blood for cell differential determinations was obtained from the orbital sinus of nonanesthetized mice using a 75-μl heparinized microhematocrit capillary tube (Curtin Matheson). Smears were made and stained for differential determinations with Hema 3 (Curtin Matheson), and 200 cells per mouse were counted. Different mice were used for each time point.

Mice were sacrificed by cervical dislocation, and the femurs and spleens were excised. Cells were flushed from the tissues with Hanks' balanced salt solution (HBSS) (GIBCO) and dispersed through a 25-gauge needle until a single cell suspension was obtained. All cell concentrations were determined by hemacytometer counts. When blood was collected for colony-forming assays, mice were anesthetized with ether, and blood was obtained from the vena cava with an 18-gauge needle attached to 1 ml heparinized syringe. The blood was diluted with an equal volume of HBSS and layered over Lympholyte-M (Cedarlane Labs) a Ficol-Hypaque solution with a density of 1.09 g/cm^3 to remove red blood cells and granulocytes (*17*). Cells at the interface were removed, washed two times with HBSS, and counted.

Assay for Granulocyte-Macrophage Colony-Forming Cells

The GM-CFC were assayed using the double-layer agar technique basically as described by Hagan *et al.* (*18*). The culture medium was double strength CMRL-1066 culture medium (Connaught Medical Research Laboratory) containing 10% (v/v) fetal calf serum, 5% (v/v) horse serum, 5% trypticase soy broth, 0.02 g/ml L-asparagine, and penicillin–streptomycin. In the bottom layer of 35-mm plastic petri dishes was 1 ml of a 1:1 mixture of culture medium and 1.0% agar (Bactoagar, Difco) containing 10% (v/v) L-929 cell-conditioned medium as a source of colony-stimulating activity. The top layer contained 1 ml of a 1:1 mixture of culture medium and 0.66% agar containing 5 × 10^4 bone marrow cells, 1 × 10^6 separated blood cells, or 1 × 10^6 spleen cells for assay. Cultures were incubated at 37°C in 5% humidified CO_2 in air. After 10 days of culture colonies greater than 50 cells were scored as GM-CFC.

Assays for Erythroid Colony-Forming Cells

Determinations of CFU-E and BFU-E were made using a plasma clot culture system basically as described by Weinberg *et al.* (*19*). Iscove's modified Dulbecco's medium (GIBCO) was substituted for α medium. Cells were plated with 0.25 U/ml (for CFU-E) or 3.0 U/ml (for BFU-E) anemic sheep plasma, step III erythropoietin (Connaught Labs, Inc., Lot No. 3092-2) as 0.4-ml plasma clots in 4-well Nunclone culture dishes (Nunc). Cultures of CFU-E and BFU-E were placed into a humidified 37°C incubator with 5% CO_2 for 2.5 and 8 days, respectively. Cultures were then harvested, fixed with 5% glutaraldehyde, stained with benzidine, and evaluated as described by McLeod *et al.* (*20*).

Determination of Colony-Forming Cells in S Phase of the Cell Cycle

The percentage of CFC in S phase of the cell cycle was determined basically as described by Rickard *et al.* (*21*). Mice were administered 900 mg/kg body wt hydroxyurea (Sigma) in Dulbecco's PBS (GIBCO) by i.p. injection. Control groups of mice were administered DPBS without hydroxyurea at the same time. Two and a half to 3 h later, tissues were assayed for surviving CFC. The number of CFC in tissues from hydroxyurea injected mice was compared to the number in tissues from DPBS-injected mice, and the percentage decrease in CFC after hyroxyurea injection was calculated as the percentage of CFC that were in S phase of the cell cycle.

Statistics

The two-tailed Student's *t* test was used to test for significant differences in cellularity and CFC per tissue between groups of mice.

RESULTS

Effect of rIL-1 on Recovery of Colony-Forming Cells after Irradiation

Two days after exposure to 0.5- or 1.0-Gy doses of radiation, rIL-1-injected mice had more BFU-E/femur and CFU-E/femur and spleen than saline-injected mice (Table

TABLE I
Recovery of Erythroid Colony-Forming Cells from Tissues of Saline or rIL-1-Injected Mice 2 Days after Irradiation[a]

Assay[b]	Recovery after 0.5-Gy injection		Recovery after 1.0-Gy injection	
	Saline	rIL-1	Saline	rIL-1
No./femur				
CFU-E ($\times 10^4$)[c]	1.1 ± 0.3	1.3 ± 0.2	1.2 ± 0.1	1.2 ± 0.1
BFU-E ($\times 10^2$)[c]	1.3 ± 0.0	3.6 ± 0.8	0 ± 0	0.7 ± 0.3
No./spleen				
CFU-E ($\times 10^4$)[c]	1.4 ± 0.4	6.5 ± 1.0	0.8 ± 0.2	4.7 ± 0.6
BFU-E[c]	0 ± 0	0 ± 0	0 ± 0	0 ± 0

[a] Female B6D2F1 mice (16 weeks old) were administered 0.5 ml saline or 150 ng rIL-1 by i.p. injection 20 h prior to their exposure to 0.5 or 1.0 Gy ^{60}Co radiation.

[b] Cells were pooled from both femurs and the spleens of two mice per group.

[c] Mean number ± SD of two plasma clots each.

I). When compared to the number of GM-CFC/femur for nonirradiated control mice, the percentage of GM-CFC surviving 24 h after 6.5-Gy radiation was 1.0 ± 0.3% for saline-injected mice and 1.2 ± 0.6% for rIL-1-injected mice (n = two studies). However, previous studies demonstrated that 4 and 8 days after exposure of mice to 6.5 Gy radiation, the number of GM-CFC in the bone marrow of rIL-1-injected mice was approximately 1.7 greater than the number in the bone marrow from saline-injected mice (*4*). These studies demonstrate that administration of rIL-1 to mice 20 h prior to their irradiation induced an earlier recovery of CFC. The following studies were performed to compare tissue cellularity and CFC content in saline-injected mice and rIL-1-injected mice prior to their irradiation.

Changes in Peripheral Blood Cellularity after rIL-1 Injection

The number of nucleated cells/mm^3 whole blood was similar for noninjected mice (10,423 ± 2815 for 13 mice) and for mice 2, 6, 24, and 48 h after saline injection (8420 ± 2618 for 15 mice) or rIL-1 injection (9143 ± 1775 for 14 mice). However, compared to noninjected mice, a significant neutrophilia (Fig. 1) and lymphopenia (Fig. 2) were observed within 2 h after saline or rIL-1 injection. The percentage of neutrophils had increased to almost 80% of the nucleated cells in the blood with a significant increase in nonsegmented neutrophils from 12 ± 5% in saline-injected mice to 56 ± 15% in rIL-1-injected mice. By 6 h, the levels of more immature neutrophils had returned to normal values, but a twofold increase in the more mature segmented cells was still evident 48 h after rIL-1 injection. These results demonstrate that soon after injection of a radioprotective dose of rIL-1, mature and immature neutrophils were mobilized from the bone marrow to the blood.

Effect of rIL-1 Injection on the Number of GM-CFC

Twenty hours after saline or rIL-1 injection, there was no significant difference in splenic cellularity from saline and rIL-1-injected mice (Table II). However, total cellularity per

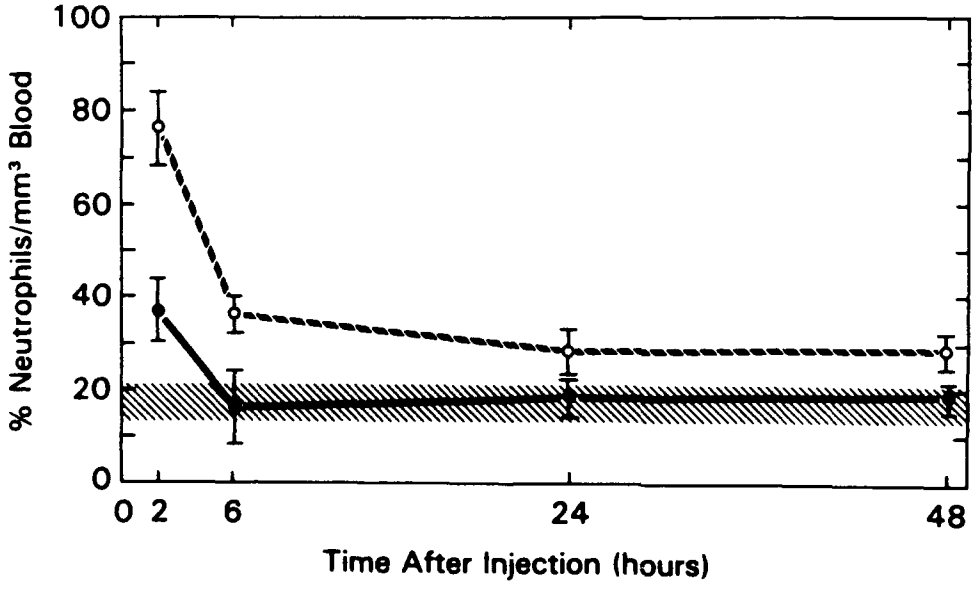

FIG. 1. Effect of rIL-1 injection on neutrophils in peripheral blood. Nucleated cell number and cell differentials were measured in peripheral blood from mice various times after injection of 150 ng rIL-1 or 0.5 ml pyrogen-free saline. Values represent the mean ± SD of numbers from three to five mice (n = two studies). Separate mice were used at each time point. The number of neutrophils/mm^3 blood from noninjected mice was 1625 ± 573 (n = 10). (●) saline injection; (○) rIL-1 injection; (\) no injection.

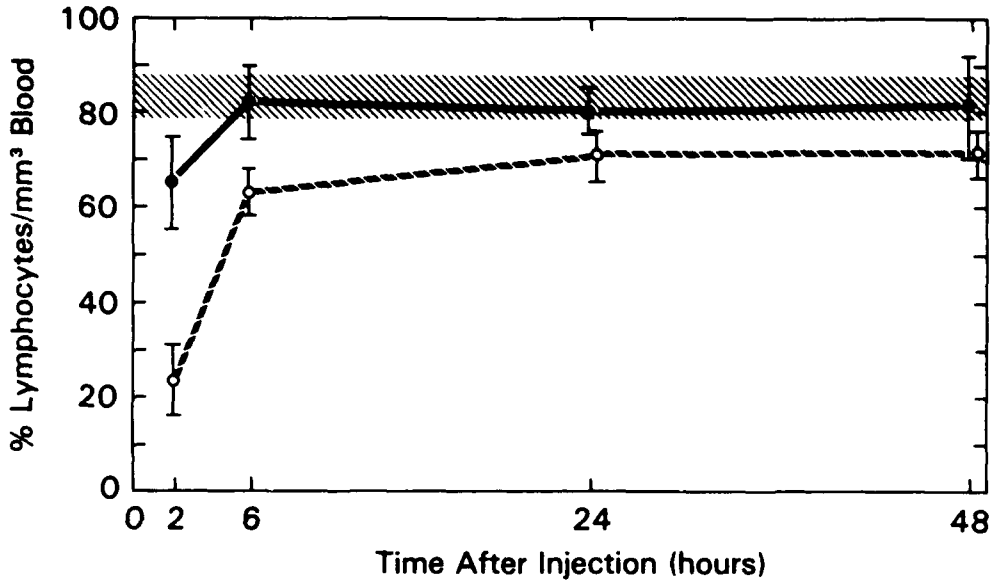

FIG. 2. Effect of rIL-1 injection on lymphocytes in peripheral blood. Nucleated cell number and cell differentials were determined in peripheral blood from mice various times after injection of 150 ng rIL-1 or 0.5 ml pyrogen-free saline. Values represent the mean ± SD of number from three to five mice (n = two studies). Separate mice were used at each time point, and the values were determined from the same samples represented in Fig. 1. Lymphocytes/mm^3 blood from noninjected mice were 7870 ± 1705 (n = 10). (●) saline injection; (○) rIL-1 injection; (\) no injection.

femur of rIL-1-injected mice was approximately 79% of bone marrow cellularity from saline-injected mice. Similar to the decrease in marrow cellularity, there were approximately 20% fewer GM-CFC per femur of mice 20 h after rIL-1 injection (Table II). Associated with the reduction in the number of marrow GM-CFC from rIL-1-injected mice, there was an increased number of GM-CFC in the blood and spleen. In both blood and spleen, the number of GM-CFC was approximately twofold greater than the number in these tissues from saline-injected mice. These data suggest that, in addition to neutrophils, rIL-1 injection induced the mobilization of GM-CFC from the bone marrow.

Sensitivity of Granulocyte-Macrophage Colony-Forming Cells to Hydroxyurea

The decrease in the number of GM-CFC after hydroxyurea injection was used to determine the percentage of GM-CFC in S phase of the cell cycle 20 h after saline or rIL-1 injection. The percentage decrease in the number of GM-CFC in the bone marrow and spleen was similar ($P > 0.05$) for saline-injected mice and rIL-1-injected mice (Table III). Due to the increase in total number of GM-CFC per spleen induced by rIL-1 injection, this represented an increase from 0.3 ± 0.1 ($\times 10^3$) GM-CFC/spleen from saline-injected mice to 0.7 ± 0.04 ($\times 10^3$) GM-CFC/spleen from rIL-1 injected mice in S phase of the cell cycle. However, there was not a similar increase in the number of GM-CFC in S phase of the cell cycle in the bone marrow of rIL-1-injected mice. These results suggest that, compared to the spleen, stimulation of granulopoiesis after rIL-1 injection was delayed in the bone marrow.

Effect of rIL-1 Injection on Number of CFU-E and BFU-E

Twenty hours after rIL-1 injection, the number of CFU-E per femur was reduced to 69 ± 8% (n = 7) of the number in bone marrow from saline-injected mice. The number of CFU-E per spleen from rIL-1-injected mice was 101 ± 35% (n = 4) of the number from saline-injected mice. The number of BFU-E per femur was similar (P = 0.5) for noninjected mice [1.3 ± 0.6 ($\times 10^3$) n = 9 studies], mice 20 h after saline injection [1.3 ± 0.4 ($\times 10^3$) n = 6 studies], and mice 20 h after rIL-1 injection [1.1 ± 0.3 ($\times 10^3$) n = 6 studies]. A decrease in the percentage of CFU-E in S phase of the cell cycle was observed in bone marrow of mice 20 h after saline injection (Table III). There was no significant difference in the percentage of BFU-E in S phase of the cell cycle for saline or rIL-1-injected mice. These results demonstrate that rIL-1 injection did not induce an increase in the number of CFU-E or BFU-E in the bone marrow of mice prior to their irradiation.

DISCUSSION

Data in the present report confirm that, similar to previous studies with C57Bl/6J and B6D2F1 mice, rIL-1 injection induced an earlier hematopoietic recovery in mice after their exposure to sublethal doses of radiation (*3–4*). Also, in nonirradiated mice, marrow CFU-E levels 20–24 h after rIL-1 injection were decreased without an apparent compensatory increase in the spleen (*3*). Results in the present report further demonstrate that injection of a radioprotective dose (150 ng) of rIL-1 induced changes in the tissue

TABLE II

Cellularity and Number of GM-CFC in Tissues of Mice 20 h after Saline or rIL-1 Injection[a]

	Treatment		
No./tissue[b]	Saline injection (n)[c]	rIL-1 injection (n)[c]	% rIL-1/saline[d]
Cellularity			
No./femur ($\times 10^7$)	1.4 ± 0.2 (10)	1.1 ± 0.1 (11)[e]	79 ± 11
No./spleen ($\times 10^8$)	1.3 ± 0.2 (9)	1.2 ± 0.2 (10)	95 ± 16
GM-CFC[f]			
No./femur ($\times 10^4$)	1.6 ± 0.5 (10)	1.2 ± 0.4 (10)[e]	77 ± 12
No./spleen ($\times 10^3$)	0.5 ± 0.3 (8)	1.3 ± 0.3 (8)[e]	231 ± 74
No./10^6 blood	14 ± 5 (2)	33 ± 7 (3)[e]	252 ± 163

[a] Female B6D2F1 mice (12–15 weeks old) were administered 0.5 ml saline or 150 ng rIL-1 by i.p. injection 20 h before assay.

[b] Cells were pooled from both femurs and the spleens of three mice per group in each study.

[c] Number of studies.

[d] Mean ± SD calculated from the percentage of the number from rIL-1-injected mice/saline-injected mice of individual studies.

[e] Significantly different from saline-injected mice at $P < 0.05$.

[f] Values represent the mean ± SD of mean values from three plates per group.

distribution of mature hematopoietic cells and GM-CFC. Neutrophilia and a lymphopenia were observed within 2 h after rIL-1 injection. After 24 h, peripheral blood values were returning to normal. Twenty hours after rIL-1 injection, bone marrow GM-CFC content was 77% of values from saline-injected mice. Also, there was approximately a twofold increase in the number of GM-CFC in the blood and spleens from rIL-1-injected mice. An increase in the number of GM-CFC in S phase of the cell cycle as determined by *in vivo* hydroxyurea treatment was observed in the spleen, but not in the bone marrow of mice 20 h after rIL-1 injection.

Stork *et al.* (*13*) observed a twofold increase in the white blood cell count in mice 6 h after rIL-1 injection. This increase was associated with an increase in the number of neutrophils. Similarly, in the present report, neutrophil counts in the blood were increased in mice after rIL-1 injection. However, there was no increase in total white blood cells due to a comparable decrease in the number of lymphocytes. A lymphopenia has also been observed in rats after rIL-1 injection (*22*).

Others demonstrated that there was a comparable decrease of neutrophils in the bone marrow associated with the increase in the number of neutrophils in the blood after rIL-1 or endotoxin injection (*22–23*). Data in the present report and in an earlier report (*3*) demonstrated that rIL-1 injection induced a decrease in bone marrow cellularity. Neta *et al.* (*16*) observed a 25% increase in the proportion of large or blast cells in the bone marrow of mice 20 h after injection of a radioprotective dose of rIL-1. Metcalf and Wilson (*24*) reported a similar increase in the proportion of large cells such as blasts and myelocytes in the bone marrow of mice after endotoxin injection. In their studies, this was consistent with the capacity of endotoxin to induce mobilization of more mature granulocytes from the bone marrow (*24*).

In the present studies there was a reduction in the number of GM-CFC associated with the decrease in marrow cellularity observed in mice 20 h after rIL-1 injection. Castelli *et al.* (*15*) also observed a decrease in the number of GM-CFC in the bone marrow of mice after rIL-1 injection. In those studies, 6 h after intravenous administration of 0.5 μg/kg body weight, the number of GM-CFC per femur had decreased to 50% of normal values. By 24 h, the number of marrow GM-CFC was still only 75% of normal values. In the present studies and those by Castelli *et al.* (*15*) there was an increase in GM-CFC in blood and spleen associated with the decreased numbers in the bone marrow. Castelli *et al.* (*15*) also observed an early return of GM-CFC levels in peripheral blood to normal. These studies suggest that in addition to neutrophils a radioprotective dose of rIL-1 induced mobilization of GM-CFC from the bone marrow that was still evident 20 h after injection.

Earlier studies suggested that the decrease in marrow GM-CFC content after endotoxin injection is the result of mobilization of GM-CFC from the bone marrow into circulation, as well as differentiation of GM-CFC to replace the decrease in bone marrow neutrophils (*25, 26*). Several reports demonstrated that it is primarily a noncycling population of GM-CFC that is mobilized from the bone marrow

TABLE III

Decrease in the Percentage of Colony-Forming Cells after Administration of Hydroxyurea to Mice 20 h after Saline or rIL-1 Injection

	Treatment[a]	
Assay[b]	Saline injection (n)[c]	rIL-1 injection (n)[c]
% Decrease after hydroxyurea[d]		
GM-CFC/femur	43 ± 13 (4)	47 ± 14 (4)
GM-CFC/spleen	41 ± 14 (3)	56 ± 16 (3)
CFU-E/femur	76 ± 17 (4)	44 ± 15 (5)[e]
BFU-E/femur	46 ± 13 (3)	29 ± 3 (3)

[a] Female B6D2F1 mice (12–16 weeks old) were administered 0.5 ml saline or 150 ng rIL-1 by i.p. injection.

[b] Cells were pooled from both femurs and the spleens of three mice per group in each study.

[c] Number of studies.

[d] Mice were administered DPBS or 900 mg hydroxyurea/kg body weight 20 h after saline or rIL-1 injection, and 2.5–3 h later animals were euthanized for assay.

[e] Significantly different from saline-injected mice ($P < 0.05$).

after endotoxin or dextran injection or extended leukopheresis (*27–29*). Thus an increase in the percentage of GM-CFC in S phase of the cell cycle would be expected. However, in three studies of the present report, as determined by the number of GM-CFC surviving after hydroxyurea treatment, there was no significant increase in the percentage of marrow GM-CFC in S phase of the cell cycle. These studies suggest that the decrease in GM-CFC in bone marrow was a result of rIL-1 injection inducing an early mobilization of GM-CFC from the bone marrow and a differentiation of GM-CFC to replace the decreased marrow neutrophil levels.

Studies in the present report demonstrated that the earlier recovery of GM-CFC in the marrow of mice irradiated 20 h after rIL-1 injection was not dependent upon an increase in GM-CFC in the marrow or stimulation of granulopoiesis at the time of irradiation. However, other studies demonstrated that rIL-1 stimulates granulopoiesis in nonirradiated mice. For example, in studies in which the number of GM-CFC in the marrow from rIL-1-injected mice had returned to values found in saline-injected mice, there was an increase in percentage of GM-CFC in S phase of the cell cycle (*3*). Also, others demonstrated that marrow GM-CFC content increased 1.5- to 2.5-fold above normal values within 48–72 h after rIL-1 injection (*13, 15*). In preliminary studies, 3–5 days after injection of 150 ng rIL-1 (Hoffman La Roche) numbers of GM-CFC in the bone marrow were 2.0 ± 0.7 times greater ($n = 3$ studies) than in marrow from saline-injected mice (data not shown). Thus an increase in marrow GM-CFC content occurred after the optimal time for radioprotection. In a previous report (*3*) and studies by Stork *et al.* (*13*), GM-CFC content of the marrow was similar for mice 24 h after saline or IL-1 injection. Differences in dose of rIL-1 administered per kilogram body weight, timing of assays, batch of rIL-1, and mouse strain are possible reasons for variations in bone marrow GM-CFC content. Other studies demonstrated that the amplitude and timing of IL-1-induced changes in the cellularity of peripheral blood and bone marrow in mice and rats were dependent upon the source and dose of IL-1 (*6, 13, 15, 22*).

Previous reports demonstrated that the serum CSA levels, which increased after rIL-1 injection, returned to normal within 24 h (*13, 14*). Studies by Francis *et al.* (*28*) also demonstrated that human blood CSA levels did not correlate with granulopoietic activity *in vivo*. However, their studies suggested that CSA produced by bone marrow cells regulated marrow granulopoiesis (*28*). Interleukin-1 has been shown to induce the production of CSA and CSF from a variety of cell types that include cells derived from bone marrow (*8–12*). Also earlier reports demonstrated that the radiosensitivity of GM-CFC could be decreased by an increasing CSA concentration or by changing the source of CSA (*29* and *30*). Thus one possible mechanism for the earlier recovery of GM-CFC in tissues of mice irradiated after rIL-1 injection is the production of hematopoietic growth and synergistic factors from cells that are part of the hematopoietic microenvironment.

ACKNOWLEDGMENTS

We are grateful to Mr. Michael White, Ms. Rita Hardy, Mr. Richard Brandenburg, and Ms. Kristina Palomba for their excellent technical assistance.

RECEIVED: July 17, 1989; ACCEPTED: September 5, 1989

REFERENCES

1. R. NETA, S. DOUCHES, and J. J. OPPENHEIM, Interleukin-1 is a radioprotector. *J. Immunol.* **136**, 2483–2485 (1986).
2. V. S. GALLICCHIO, Accelerated recovery of hematopoiesis following sub-lethal whole body irradiation with recombinant murine interleukin-1 (IL-1). *J. Leukocyte Biol.* **43**, 211–215 (1988).
3. G. N. SCHWARTZ, T. J. MACVITTIE, R. M. VIGNEULLE, M. L. PATCHEN, S. D. DOUCHES, J. J. OPPENHEIM, and R. NETA, Enhanced hematopoietic recovery in irradiated mice pretreated with interleukin-1 (IL-1). *Immunpharm. Immunotox.* **9**, 371–389 (1987).
4. G. N. SCHWARTZ, R. NETA, R. M. VIGNEULLE, M. L. PATCHEN, and T. J. MACVITTIE, Recovery of hematopoietic colony-forming cells in irradiated mice pretreated with interleukin-1 (IL-1). *Exp. Hematol.* **16**, 752–757 (1988).
5. G. N. SCHWARTZ, M. L. PATCHEN, R. NETA, and T. J. MACVITTIE, Radioprotection of mice with interleukin-1: Relationship to the number of spleen colony-forming units. *Radiat. Res.* **119**, 101–112 (1989).
6. G. N. SCHWARTZ, M. L. PATCHEN, and T. J. MACVITTIE, Effects of interleukin-1 (IL-1) on granulocyte and macrophage progenitor cells in normal and irradiated mice. *J. Leukocyte Biol.* **44**, 279(86a) (1988). [Abstract]
7. M. G. CHEN, L. A. LEONARD, and G. C. UDEAJA, Mechanism of interleukin-1 (IL-1) radioprotection in lethally irradiated mice. *Int. J. Radiat. Oncol. Biol. Phys.* **15**, 148 (64a) (1988). [Abstract]
8. J. R. ZUCALI, H. E. BROXMEYER, C. A. DINARELLO, M. A. GROSS, and R. S. WEINER, Regulation of early hematopoietic (BFU-E and CFU-GEMM) progenitor cells *in vitro* by interleukin-1-induced fibroblast conditioned medium. *Blood* **69**, 33–37 (1987).
9. M. LEE, G. M. SEGAL, and G. C. BAGBY, Interleukin-1 induces bone marrow derived fibroblasts to produce multilineage hematopoietic growth factors. *Exp. Hematol.* **15**, 983–988 (1987).
10. K. D. RENNICK, G. YANG, L. GEMMELL, and L. LEE, Control of hemopoiesis by a bone marrow stromal cell clone: Lipopolysaccharide- and interleukin-1-inducible production of colony-stimulating factors. *Blood* **69**, 682–691 (1987).
11. Y. YANG, T. SHICKWANN, G. G. WONG, and S. C. CLARK, Interleukin-1 regulation of hematopoietic growth factor production by human stromal fibroblasts. *J. Cell. Physiol.* **134**, 292–296 (1988).
12. K. KAUSHANSKY, N. LIN, and J. W. ADAMSON, Interleukin-1 stimulates fibroblasts to synthesize granulocyte-macrophage and granulocyte colony-stimulating factors: Mechanism for the hematopoietic response to inflammation. *J. Clin. Invest.* **81**, 92–97 (1988).
13. L. C. STORK, V. M. PETERSON, C. H. RUNDUS, and W. A. ROBINSON, Interleukin-1 enhances murine granulopoiesis in vivo. *Exp. Hematol.* **16**, 163–167 (1988).

14. S. N. VOGEL, S. D. DOUCHES, E. M. KAUTMAN, and R. NETA, Induction of colony stimulating factor in vivo by recombinant interleukin-1 alpha and recombinant tumor necrosis factor-alpha. *J. Immunol.* **138**, 2143–2148 (1987).

15. M. P. CASTELLI, P. L. BLACK, M. SCHNEIDER, R. PENNINGTON, F. ABE, and J. E. TALMADGE, Protective, restorative, and therapeutic properties of recombinant human IL-1 in rodent models. *J. Immunol.* **140**, 3830–3837 (1988).

16. R. NETA, M. R. SZTEIN, J. J. OPPENHEIM, S. GILLIS, and S. D. DOUCHES, The *in vivo* effects of interleukin-1. I. Bone marrow cells are induced to cycle after administration of interleukin-1. *J. Immunol.* **139**, 1861–1866 (1987).

17. J. NORTH, Size and Density. In *Selected Methods in Cellular Immunology* (B. B. Mishell and S. M. Shiigi, Eds.), p. 187. Freeman, San Francisco, 1980.

18. M. P. HAGAN, T. J. MACVITTIE, and D. P. DODGEN, Cell kinetics of GM-CFC in steady state. *Exp. Hematol.* **13**, 532–538 (1985).

19. S. R. WEINBERG, E. G. MCCARTHY, T. J. MACVITTIE, and S. J. BAUM, Effect of low-dose irradiation on pregnant mouse haemopoiesis. *Br. J. Hematol.* **48**, 127–135 (1981).

20. D. L. MCLEOD, M. M. SHREEVE, and A. A. AXELRAD, Improved plasma system for production of erythrocytic colonies in vitro: Quantitative assay for CFU-E. *Blood* **44**, 517–534 (1974).

21. K. A. RICKARD, R. K. SHADDUCK, D. E. HOWARD, and F. STOHLMAN, JR., A differential effect of hydroxyurea on hemopoietic stem cell colonies in vitro. *Proc. Soc. Exp. Biol. Med.* **134**, 152–156 (1970).

22. T. R. ULICH, J. CASTILLO, M. KEYS, G. A. GRANGER, and R. NI, Kinetics and mechanisms of recombinant human interleukin 1 and tumor necrosis factor-alpha-induced changes in circulating numbers of neutrophils and lymphocytes. *J. Immunol.* **139**, 3406–3415 (1987).

23. S. S. BOGGS, D. R. BOGGS, and R. A. JOYCE, Response to endotoxin of endotoxin-"resistant" C3H/HeJ mice: A model for study of hematopoietic control. *Blood* **55**, 444–452 (1980).

24. D. METCALF and J. W. WILSON, Endotoxin-induced size change in bone marrow progenitors of granulocytes and macrophages. *J. Cell. Physiol.* **89**, 381–391 (1976).

25. P. J. QUESENBERRY, A. MORLEY, M. RYAN, D. HOWARD, and F. STOHLMAN, JR., The effect of endotoxin on murine stem cells. *J. Cell. Physiol.* **82**, 239–244 (1973).

26. P. QUESENBERRY, A. MORLEY, M. MILLER, K. RICKARD, D. HOWARD, and F. STOHLMAN, JR., Effect of endotoxin on granulopoiesis and the in vivo colony-forming cell. *Blood* **41**, 391–397 (1973).

27. H. H. GERHARTZ and T. M. FLIEDNER, Velocity sedimentation and cell cycle characteristics of granulopoietic progenitor cells (CFUc) in canine blood and bone marrow: Influence of mobilization and CFUc depletion. *Exp. Hematol.* **8**, 209–218 (1980).

28. G. E. FRANCIS, E. G. H. RHODES, J. J. BERNEY, M. A. WING, and A. V. HOFFBRAND, Bone marrow endogenous colony stimulating factor(s): Relation to granulopoiesis in vivo. *Exp. Hematol.* **9**, 332–345 (1981).

29. H. E. BROXMEYER, P. R. GALBRAITH, and F. L. BAKER, Relationship of colony-stimulating activity to apparent kill of human colony-forming cells by irradiation and hydroxyurea. *Blood* **47**, 403–411 (1976).

30. S. SUGAVARA, K. TSUNEOKA, and M. SHIKITA, Colony-stimulating factor and the proliferation of X-irradiated myeloid stem cells. *Biochem. Biophys. Res. Commun.* **96**, 1488–1493 (1980).

DISTRIBUTION LIST

DEPARTMENT OF DEFENSE

ARMED FORCES INSTITUTE OF PATHOLOGY
ATTN: RADIOLOGIC PATHOLOGY DEPARTMENT

ARMED FORCES RADIOBIOLOGY RESEARCH INSTITUTE
ATTN: PUBLICATIONS DIVISION

ARMY/AIR FORCE JOINT MEDICAL LIBRARY
ATTN: DASG-AAFJML

ASSISTANT TO SECRETARY OF DEFENSE
ATTN: AE
ATTN: HA(IA)

DEFENSE NUCLEAR AGENCY
ATTN: TITL
ATTN: DDIR

DEFENSE TECHNICAL INFORMATION CENTER
ATTN: DTIC-DDAC
ATTN: DTIC-FDAC

FIELD COMMAND DEFENSE NUCLEAR AGENCY
ATTN: FCFS

INTERSERVICE NUCLEAR WEAPONS SCHOOL
ATTN: RH

LAWRENCE LIVERMORE NATIONAL LABORATORY
ATTN: LIBRARY

UNDER SECRETARY OF DEFENSE (ACQUISITION)
ATTN: OUSD(A)/R&AT

DEPARTMENT OF THE ARMY

HARRY DIAMOND LABORATORIES
ATTN: SLCHD-NW
ATTN: SLCSM-SE

LETTERMAN ARMY INSTITUTE OF RESEARCH
ATTN: SGRD-UL-B1-R

SURGEON GENERAL OF THE ARMY
ATTN: MEDDH-N

U.S. ARMY AEROMEDICAL RESEARCH LABORATORY
ATTN: SCIENTIFIC INFORMATION CENTER

U.S. ARMY ACADEMY OF HEALTH SCIENCES
ATTN: HSHA-CDF

U.S. ARMY CHEMICAL RESEARCH, DEVELOPMENT, AND ENGINEERING CENTER
ATTN: DIRECTOR OF RESEARCH

U.S. ARMY INSTITUTE OF SURGICAL RESEARCH
ATTN: DIRECTOR OF RESEARCH

U.S. ARMY MEDICAL RESEARCH INSTITUTE OF CHEMICAL DEFENSE
ATTN: SGRD-UV-R

U.S. ARMY NUCLEAR AND CHEMICAL AGENCY
ATTN: MONA-NU

U.S. ARMY RESEARCH INSTITUTE OF ENVIRONMENTAL MEDICINE
ATTN: DIRECTOR OF RESEARCH

U.S. ARMY RESEARCH OFFICE
ATTN: BIOLOGICAL SCIENCES PROGRAM

WALTER REED ARMY INSTITUTE OF RESEARCH
ATTN: DIVISION OF EXPERIMENTAL THERAPEUTICS

DEPARTMENT OF THE NAVY

NAVAL AEROSPACE MEDICAL RESEARCH LABORATORY
ATTN: COMMANDING OFFICER

NAVAL MEDICAL COMMAND
ATTN: MEDCOM-21

NAVAL MEDICAL RESEARCH AND DEVELOPMENT COMMAND
ATTN: CODE 40C

OFFICE OF NAVAL RESEARCH
ATTN: BIOLOGICAL SCIENCES DIVISION

DEPARTMENT OF THE AIR FORCE

BOLLING AIR FORCE BASE
ATTN: AFOSR

BROOKS AIR FORCE BASE
ATTN: USAFOEHL/RZ
ATTN: USAFSAM/RZ
ATTN: USAFSAM/RZB

NUCLEAR CRITERIA GROUP, SECRETARIAT
ATTN: WL/NTN

SURGEON GENERAL OF THE AIR FORCE
ATTN: HQ USAF/SGPT
ATTN: HQ USAF/SGES

U.S. AIR FORCE ACADEMY
ATTN: HQ USAFA/DFBL

OTHER FEDERAL GOVERNMENT

BROOKHAVEN NATIONAL LABORATORY
ATTN: RESEARCH LIBRARY, REPORTS SECTION

CENTER FOR DEVICES AND RADIOLOGICAL HEALTH
ATTN: HFZ-110

DEPARTMENT OF ENERGY
ATTN: ER-72 GTN

GOVERNMENT PRINTING OFFICE
ATTN: DEPOSITORY RECEIVING SECTION
ATTN: CONSIGNED BRANCH

LIBRARY OF CONGRESS
ATTN: UNIT X

LOS ALAMOS NATIONAL LABORATORY
ATTN: REPORT LIBRARY/P364

NATIONAL AERONAUTICS AND SPACE ADMINISTRATION
ATTN: RADLAB

NATIONAL AERONAUTICS AND SPACE ADMINISTRATION,
GODDARD SPACE FLIGHT CENTER
ATTN: LIBRARY

NATIONAL CANCER INSTITUTE
ATTN: RADIATION RESEARCH PROGRAM

NATIONAL LIBRARY OF MEDICINE
ATTN: OPI

U.S. ATOMIC ENERGY COMMISSION
ATTN: BETHESDA TECHNICAL LIBRARY

U.S. FOOD AND DRUG ADMINISTRATION
ATTN: WINCHESTER ENGINEERING AND
ANALYTICAL CENTER

U.S. NUCLEAR REGULATORY COMMISSION
ATTN: LIBRARY

RESEARCH AND OTHER ORGANIZATIONS

BRITISH LIBRARY (SERIAL ACQUISITIONS)
ATTN: DOCUMENT SUPPLY CENTRE

CENTRE DE RECHERCHES DU SERVICE DE SANTE DES
ARMEES
ATTN: DIRECTOR

INHALATION TOXICOLOGY RESEARCH INSTITUTE
ATTN: LIBRARY

INSTITUT FUR RADIOBIOLOGIE
ACADEMIE DES SANITATS UND GESUNHEITSWESESNS DER
BW (WEST GERMANY)
ATTN: DIRECTOR

KAMAN TEMPO
ATTN: DASIAC

NBC DEFENSE RESEARCH AND DEVELOPMENT CENTER OF
THE FEDERAL ARMED FORCES (WEST GERMANY)
ATTN: WWDBW ABC-SCHUTZ

NCTR-ASSOCIATED UNIVERSITIES
ATTN: EXECUTIVE DIRECTOR

RUTGERS UNIVERSITY
ATTN: LIBRARY OF SCIENCE AND MEDICINE

UNIVERSITY OF CALIFORNIA
ATTN: LABORATORY FOR ENERGY-RELATED
HEALTH RESEARCH
ATTN: LAWRENCE BERKELEY LABORATORY

UNIVERSITY OF CINCINNATI
ATTN: UNIVERSITY HOSPITAL, RADIOISOTOPE
LABORATORY